



UNIVERSITY  
OF  
JOHANNESBURG

## COPYRIGHT AND CITATION CONSIDERATIONS FOR THIS THESIS/ DISSERTATION



- Attribution — You must give appropriate credit, provide a link to the license, and indicate if changes were made. You may do so in any reasonable manner, but not in any way that suggests the licensor endorses you or your use.
- NonCommercial — You may not use the material for commercial purposes.
- ShareAlike — If you remix, transform, or build upon the material, you must distribute your contributions under the same license as the original.

### How to cite this thesis

Surname, Initial(s). (2012) Title of the thesis or dissertation. PhD. (Chemistry)/ M.Sc. (Physics)/ M.A. (Philosophy)/M.Com. (Finance) etc. [Unpublished]: [University of Johannesburg](https://ujdigispace.uj.ac.za). Retrieved from: <https://ujdigispace.uj.ac.za> (Accessed: Date).

**A Geometallurgical Examination of Gold, Uranium and  
Thorium in the Black Reef Quartzite Formation, Gold  
One International LTD, Springs**

By:

**Andrew Craig McLoughlin**

DISSERTATION

Submitted in fulfillment of the requirements for the degree

**Magister Scientiae**



In the:

**Faculty of Science**

At the:

**University of Johannesburg**

**Supervisor: Professor K.S. Viljoen**

**Co-Supervisor: Mrs. L. Blignaut**



## DECLARATION

I Mr. Andrew Craig McLoughlin hereby declare that this dissertation submitted for the degree Magister Scientiae in Geology at the University of Johannesburg is my own work. Apart from the help recognised, this research is my own work and has not been formerly submitted to another university for a qualification. I recognize the help I have received from my supervisors, Prof K.S. Viljoen and Ms. Lauren Blignaut. I further state that wherever I have made use of other people's ideas in the dissertation, I have acknowledged and suitably referenced them.

22 April 2015

.....  
Signature

.....  
Date:

## ACKNOWLEDGEMENTS

I would like to extend a sincere word of thanks to the following individuals and organisations for their continued assistance throughout my Masters dissertation:

- Prof Fanus Viljoen, my supervisor, who has continually helped with constructive criticism whenever it has been asked for. You have helped me to better understand the geometallurgy industry as well as furthered my knowledge in many other fields.
- Lauren Blignaut, my co-supervisor, who has given a lot of time to helping me write and complete my dissertation with encouraging words and a helping hand where ever she could in addition to valuable contributions to the work itself.
- Funding for this project was provided through the department of Science and Technology Research chair initiative as administered by the National Research Foundation (Geometallurgy Chair to Prof. K.S Viljoen) as well as an extension provided by the NRF in 2015.(The financial assistance of the National Research Foundation (NRF) towards this research is hereby acknowledged. Opinions expressed and conclusions arrived at, are those of the author and are not necessarily to be attributed to the NRF.)
- Thank you to the staff at the Faculty of Science at the University of Johannesburg for administrative assistance, and granting me the opportunity to complete this study.
- I would like to extend a word of thanks to fellow students and staff who helped with sample preparation and other aspects of the project; Nick Vafeas, Derek Rose, Thomas Dzvinamurungu and Diana Khosa who all played a part in helping to complete this thesis.
- To the staff members at SPECTRAU, particularly Magezi Saky (Baldwin) Maluleke and Lisbon Mangwane, for assistance with the sample preparation.
- Thanks must also be extended to Evan Cooke at Gold One International's Modder East operations who assisted in the sample collection and visit to the underground stope face.
- I would like to extend thanks to Maria Klaas at SGS
- I would like to thank Vincent Simumba, and Billy Blake who assisted with the analysis at the Intertek Laboratories.
- Finally I would like to thank my Family and friends who were always supporting me throughout the duration of my studies. Particularly Gail and Barry McLoughlin.

# TABLE OF CONTENTS

<b>DECLARATION</b>	i
<b>ACKNOWLEDGEMENTS</b>	ii
<b>TABLE OF CONTENTS</b>	iii
<b>LIST OF ABBREVIATIONS</b>	vii
<b>LIST OF FIGURES</b>	ix
<b>LIST OF TABLES</b>	xiv
<b>ABSTRACT</b>	xvii
<b>Chapter 1: Introduction and Purpose of Study</b>	1
1.1 Introduction	1
1.2 Present Study	2
1.2.1 Geographical Location	2
1.2.2 Review of the Modder East Mine	3
1.3 Motivation for the Present Study	5
1.4 Aims of the Present Study	6
<b>Chapter 2: Geology of Study Area</b>	8
2.1. Introduction	8
2.2. The Kaapvaal Craton	8
2.3. The Transvaal Supergroup	9
<b>Chapter 3: The Black Reef Formation</b>	14
3.1 Introduction	14
3.2 The Black Reef Formation	14

3.3 Theories on Enrichment of gold and uranium within the Black Reef	17
<b>Chapter 4: Sampling at Modder East</b>	<b>19</b>
4.1 Introduction	19
4.2 Sample Collection	19
4.3 Underground Locality of Black Reef Samples	20
<b>Chapter 5: Methodology</b>	<b>22</b>
5.1 Introduction	22
5.2 Sample Preparation for Mineralogical Analysis	22
5.2.1 Thin Section Preparation	22
5.2.2 Crushed Material Mounts	24
5.2.3 Minerals Standard File	25
5.3 Mill Tests	25
5.4 Major and Trace Element Chemistry	28
5.5 Grading Analysis	28
5.6 Density Separation	29
5.7 Uranium and Gold Dissolution	29
5.7.1 Uranium dissolution	30
5.7.2 Gold Dissolution	30
5.8 Flotation	31
<b>Chapter 6: Petrographic Description of Samples</b>	<b>34</b>
6.1 Introduction	34
6.2 Macroscopic Description of the Black Reef	34
6.3 Microscopic Description	38
6.4 Discussion	42

<b>Chapter 7: Detailed Mineralogy</b>	44
7.1 Introduction	44
7.2 MLA Standard File	44
7.3 Modal Mineralogy	44
7.4 Gold Mineralogy	47
7.4.1 Gold Occurrence	48
7.4.2 Gold Grain size Distribution	49
7.4.3 Gold Associations	53
7.5 Mineralogy of Uranium Bearing Phases	60
7.5.1 Uraninite and Brannerite Occurrence	62
7.5.2 Uraninite and Brannerite Grain size Distribution	63
7.5.3 Uraninite and Brannerite Associations	68
7.6 Comparison of the Gold and Uranium bearing phases within the BSPL Reef	73
<b>Chapter 8: Major and Trace element Chemistry, Grading Analysis and Density Separation</b>	75
8.1 Introduction	75
8.2 Major and Trace Element Chemistry	76
8.3 Grading Analysis	77
8.3.1 Grade Reporting by Size Fraction	78
8.3.2 Upgrading and Downgrading Through Sieving	81
8.4 Density Separation: Heavy Liquid Separation	82
8.5 Results Summary	84
<b>Chapter 9: Leaching of Gold and Uranium</b>	85
9.1 Introduction	85
9.2 Gold Leach	85
9.3 Uranium Leach	86
9.4 Discussion	88



<b>Chapter 10: Flotation</b>	89
10.1 Introduction	89
10.2 Flotation Results for Au, U, Th and S	89
10.3 Discussion	92
<b>Chapter 11: Discussion and Conclusions</b>	93
11.1 Introduction	93
11.2 Mineralogy of the Ore	93
11.2.1 Gold Mineralogy	94
11.2.2 Uraninite and Brannerite Mineralogy	95
11.3 Major and Trace Element Chemistry, Size Distribution and HLS	96
11.3.1 Gold Grade, Size Department and HLS performance	96
11.3.2 Uranium and Thorium Grade, Size Department and HLS performance	97
11.4 Geometallurgical Testing	98
11.4.1 Gold Metallurgical Performance	99
11.4.2 Uranium Metallurgical Performance	100
11.4.3 Implications for Recovery based on Metallurgical Performance	101
11.5 Conclusions and Recommendations	102
<b>References</b>	106
<b>Appendix 1: Sample Preparation</b>	110
<b>Appendix 2: Mill test Data</b>	117
<b>Appendix 3: Grain Size Distribution and Mineral Association data</b>	119
<b>Appendix 4: Chemical Assay Data</b>	124
<b>Appendix 5: Grading Analysis, Density Separation data</b>	129
<b>Appendix 6: Flotation Data</b>	134
<b>Appendix 7: Published Conference Abstract</b>	139



## LIST OF ABBREVIATIONS

<b>ASX</b>	Australian Stock Exchange
<b>A\$</b>	Australian dollars
<b>BIF</b>	Banded Iron Formation
<b>BPLZ</b>	Buckshot Pyrite Leader Zone
<b>Brn</b>	Brannerite
<b>BRQ</b>	Black Reef Quartzite
<b>BSE</b>	Back Scatter Electron
<b>BSPL</b>	Buckshot Pyrite Leader
<b>Chl</b>	Chlorite
<b>CIL</b>	Carbon in Leach
<b>Ga</b>	Billion years ago
<b>HLS</b>	Heavy Liquid Separation
<b>ICP-MS</b>	Inductively Coupled Plasma Mass Spectrometry
<b>ICP-OES</b>	Inductively Coupled Plasma Optical (atomic) Emission Spectrometry
<b>JSE</b>	Johannesburg Stock Exchange
<b>LOI</b>	Loss on Ignition
<b>LST</b>	Lithium Heteropolytungstates
<b>Ma</b>	Million years Ago
<b>MLA</b>	Mineral Liberation Analyser
<b>Ms</b>	Muscovite
<b>ppb</b>	Parts Per Billion
<b>ppm</b>	Parts Per Million



<b>Py</b>	Pyrite
<b>Qtz</b>	Quartz
<b>Rpm</b>	Rotations Per minute
<b>SEM</b>	Scanning Electron Microscope
<b>Sp</b>	Sphalerite
<b>SPL</b>	Sparse Phase liberation
<b>SPL_DD_Lt</b>	Sparse Phase Liberation Double Dwell Lite
<b>UK9a</b>	Upper Kimberly Reef
<b>Urn</b>	Uraninite
<b>Wt%</b>	Weight percentage
<b>XBSE</b>	Extended BSE liberation analysis
<b>XPL</b>	Cross polarized Light



## LIST OF FIGURES

<b>Figure 1.1</b>	Geographical location of Modder East operation (modified from Eriksson et al., 2001)	2
<b>Figure 1.2</b>	Google earth image of the Modder East operations.	3
<b>Figure 1.3</b>	Modder East metallurgical plant.	4
<b>Figure 2.1</b>	Map indicating the outline of the Kaapvaal Craton (modified after Poujol et al., 2003)	9
<b>Figure 2.2</b>	Transvaal basin of the Transvaal Supergroup (modified after Eriksson et al., 2001)	10
<b>Figure 2.3</b>	Current correlations between subdivisions of the Transvaal Supergroup in the Griqualand West and Transvaal basins (modified after, Moore et al., 2001).	12
<b>Figure 2.4</b>	Schematic summary figure of stratigraphy, inferred depositional palaeoenvironments, tectonic settings and interpreted sequence stratigraphy for the Transvaal Supergroup within the Transvaal preservational basin (modified after Bose et al., 2012).	13
<b>Figure 3.1</b>	Gold One's gold assets indicating the location of the Modder East mine in the study (www.gold1.co.za obtained; 1. 11. 2013)	15
<b>Figure 3.2</b>	Simplified diagram of the Black Reef channel facies (modified after Barton and Hallbauer, 1996).	16
<b>Figure 4.1</b>	Black Reef underground sampling locality at Modder East	21
<b>Figure 5.1</b>	Photograph of the slice taken from the S1, slice 3(sl3) and reverse of sl 3 indicating where the thin sections were taken. This was sample taken at the location illustrated in figure 4.1. Also see figure 6.1.	23
<b>Figure 5.2</b>	Mill curves for samples Sc1, Sc2 and Sc3.(Polynomial curves)	26
<b>Figure 5.3</b>	Average mill curve for BSPL bulk samples, with a desired mill size indicated by the red line.(Polynomial Curve)	27
<b>Figure 5.4</b>	Denver flotation cell.	33
<b>Figure 6.1</b>	BSPL S1, indicating the three layers that make up the Black Reef.	35
<b>Figure 6.2</b>	BSPL S2, indicating the main composition of the three layers of the Black Reef	33

<b>Figure 6.3</b>	BSPL S1, SL (Slice) 6, indicating the pyrite textures and the imbrication and elongation of the quartzite pebbles	37
<b>Figure 6.4</b>	Thin section scan: cut from above the BSPL Reef; indicating quartz pebbles, quartz groundmass, fine grained pyrite, shale clasts and carbon rich material. (Thin section cut from S1 figure 6.1 BSPL PT 1).	38
<b>Figure 6.5</b>	PPL(L) and XPL(R) image indicating the mono-crystalline quartz and the fine grained shale clast that occur above the Buckshot reef.(BSPL PR 1 cut from S1)	39
<b>Figure 6.6</b>	XPL(bottom), PPL(top left) and reflected light(top right) images showing the occurrence of the carbon rich material as well as the fin grained rounded pyrite that occur above the buckshot pyrite layer.(BSPL PT 2 cut from S1).	39
<b>Figure 6.7</b>	Thin section scan using transmitted light: cut from within the buckshot pyrite layer indicating rounded detrital pyrite as well as quartz pebbles, shale clasts and kerogen globules.(BSPL PR 5 cut from S1)	40
<b>Figure 6.8</b>	XPL image: showing muscovite and quartz ground mass. (BSPL PR 4 cut from S1)	40
<b>Figure 6.9</b>	Reflected light images indicating the gold particles found within the buckshot pyrite layer.(BSPL PR cut 5from S1).	41
<b>Figure 6.10</b>	Photograph (A)(reflected light) and scanned image (B)(Transmitted light) of the same thin section indicating the higher abundances of carbon rich and clay material below the buckshot layer as well as the pyrite and quartz still present.(BSPL PB 7 cut from S1).	42
<b>Figure 7.1</b>	Gold EDS peaks from BSPL samples	48
<b>Figure 7.2</b>	BSE images indicating the discrete gold particles found across the BSPL Reef.	50
<b>Figure 7.3</b>	BSE images A-C. They show gold occurring within veins usually within pyrite minerals. D-F indicates mineral agglomerations occurring with the gold providing evidence for remobilization of the gold.	51
<b>Figure 7.4</b>	Gold grain size distribution for all gold particles found above, below and within the buckshot reef	52
<b>Figure 7.5</b>	Gold size distribution indicating the variation of the gold grain sizes above, below and within the buckshot reef.	52
<b>Figure 7.6</b>	Gold associations across the BSPL reef.	54

<b>Figure 7.7</b>	BSE image (R), mineral map (L) indicating the associations of the gold with quartz.	55
<b>Figure 7.8</b>	BSE image (R), mineral map (L) indicating the associations of the gold with pyrite and sphalerite.	55
<b>Figure 7.9</b>	BSE image (R), mineral map (L) indicating the associations of the gold with the edges of pyrite grains, as well as muscovite, pyrophyllite and uraninite	56
<b>Figure 7.10</b>	BSE image (R), mineral map (L) indicating the associations of the gold with edges of the pyrite grains as well as quartz, muscovite, chalcopyrite and chlorite.	56
<b>Figure 7.11</b>	BSE image (R), mineral map (L) indicating the associations of the gold with muscovite.	57
<b>Figure 7.12</b>	BSE image (R), mineral map (L) indicating the associations of the gold with pyrophyllite.	57
<b>Figure 7.13</b>	BSE image (R), mineral map (L) indicating the associations of the gold with chlorite	57
<b>Figure 7.14</b>	BSE image (R), mineral map (L) indicating the more complex associations of the gold within the BSPL Reef.	58
<b>Figure 7.15:</b>	BSE image (R), mineral map (L) indicating the more complex associations of the gold within the BSPL Reef.	58
<b>Figure 7.16</b>	BSE image (R), mineral map (L) indicating the association between the kerogen and gold within the BSPL Reef.	59
<b>Figure 7.17</b>	Uraninite EDS peaks from BSPL samples	61
<b>Figure 7.18</b>	Brannerite EDS peaks from BSPL samples	62
<b>Figure 7.19</b>	BSE images A-F, showing the first type of the uraninite (Urn) and brannerite (Brn) occurrence, where it is completely enclosed by kerogen	64
<b>Figure 7.20</b>	BSE Images A-D showing the second type of uraninite and brannerite occurrence, where the uraninite is found within the replacement minerals with the remnant textures of the kerogen can be seen Images E and F, indicating where the uraninite occurs along the pyrite grain boundaries.	65
<b>Figure 7.21</b>	Uraninite grain size distribution for all uraninite found above, below and within the buckshot pyrite reef.	66

<b>Figure 7.22</b>	Uraninite size distribution indicating the variation of the uraninite grain sizes above, below and within the buckshot pyrite reef.	66
<b>Figure 7.23</b>	Brannerite grain size distribution for all brannerite found above, below and within the buckshot pyrite reef.	67
<b>Figure 7.24</b>	Brannerite size distribution indicating the variation of the brannerite grain sizes above, below and within the buckshot pyrite reef.	67
<b>Figure 7.25</b>	Uraninite association across the BSPL Reef.	68
<b>Figure 7.26</b>	Brannerite association across the BSPL Reef	69
<b>Figure 7.27</b>	BSE image (R), mineral map (L), indicating the uraninite association with kerogen.	70
<b>Figure 7.28</b>	BSE image (R), mineral map (L), indicating the uraninite and brannerite association with kerogen, as well as some association with muscovite	70
<b>Figure 7.29</b>	BSE image (R), mineral map (L), indicating the uraninite association with kerogen, as well as some association with quartz, muscovite and brannerite.	70
<b>Figure 7.30</b>	BSE image (R), and mineral map (L), indicating the uraninite association with muscovite which appears to have formed within the remnant kerogen structure.	71
<b>Figure 7.31</b>	BSE image (R), and mineral map (L), indicating the uraninite and brannerite association with muscovite which appears to form within the kerogen remnant structure along with an association with sphalerite	71
<b>Figure 7.32</b>	BSE image (R), and mineral map (L), indicating the uraninite association with the edge of a pyrite grain	72
<b>Figure 7.33</b>	BSE image (R), and mineral map (L), indicting the uraninite association with kerogen as well as the occurrence of brannerite within the kerogen.	72
<b>Figure 7.34</b>	Comparison of grain size for gold, uraninite and brannerite	74
<b>Figure 8.1</b>	Grading analysis For Sc1 (Sample Collection 1), showing the grade distribution of gold, uranium, thorium and sulphur by size fraction.	79
<b>Figure 8.2</b>	Grading analysis For Sc2 (Sample Collection 2), showing the grade distribution of gold, uranium, thorium and sulphur by size fraction.	80
<b>Figure 8.3</b>	Grading analysis For Sc3 (Sample Collection 3), showing the grade distribution of gold, uranium, thorium and sulphur by size fraction.	80

<b>Figure 8.4</b>	Upgrade - Downgrade of the grading analysis of Au, U, Th and S (Coetzee et al. 2011).	81
<b>Figure 8.5</b>	Results for HLS for run of mine bulk sample SC1	82
<b>Figure 8.6</b>	Results for HLS for run of mine bulk sample SC2	83
<b>Figure 8.7</b>	Results for HLS for run of mine bulk sample SC2	83
<b>Figure 8.8</b>	Comparison of results of the HLS for Sc1, Sc2, Sc3	84
<b>Figure 10.1</b>	Flotation concentrates mass percentages. (Appendix A6 a-g)	90
<b>Figure 10.2</b>	Cumulative mass percentage over time for Au, S, U and Th. (Appendix A6 a-g)	90
<b>Figure 10.3</b>	Average recovery curves for Au, S, Th and U (Appendix A6 a-g).	91
<b>Figure 10.4</b>	Mass pull for samples Sc1, Sc2 and Sc3 (Appendix A6 a-g)	91
<b>Figure A1 a</b>	Splitters used in the preparation of the bulk samples. Splitter A (Jones riffler) was used to create the 10 kg splits. Splitter B (Rotary riffler, 10 sections) was used to create the 1 kg splits. The next two splitters C and D (rotary riffler and micro rotary micro riffler 8 sections) where used to create the smaller splits that were used to create the mounts. Picture curtsey of Derek Rose PhD Candidate at university of Johannesburg, 2013	111
<b>Figure A1 b</b>	Photographs of BSPL s1, sl 1(A) and the reverse (B)	112
<b>Figure A1 c</b>	Photographs of BSPL s1, sl2-3(A-C) and the reverse (B-D)	113
<b>Figure A1 d</b>	Photographs of BSPL s1, sl4-5(A-C) and the reverse (B-D)	114
<b>Figure A1 e</b>	Photographs of BSPL s1, sl7-8 (A-C) and the reverse (B-D)	115
<b>Figure A1 f</b>	Photographs of BSPL s1, sl9(A) and the reverse (B)	116
<b>Figure A2 a</b>	A: Rotary mill, B: Sieve shaker, C: Filter press, D: Oven used to dry samples. In each photograph a 30 cm ruler is used for scale.	118

## LIST OF TABLES

<b>Table 5.1</b>	SPL_DD_Lt setup.	24
<b>Table 5.2</b>	XBSE Setup	25
<b>Table 5.3</b>	Major and trace element chemistry, methods employed for analysis (* indicates elements reported as an oxide)	28
<b>Table 7.1</b>	MLA Standard file (XBSE_STD)	45
<b>Table 7.2</b>	Modal mineralogy of the bulk sample Sc1	45
<b>Table 7.3</b>	Modal mineralogy of the bulk sample Sc2	46
<b>Table 7.4</b>	Modal mineralogy of the bulk sample Sc3	46
<b>Table 7.5</b>	Association per modal mineralogy for the associations of gold.	60
<b>Table 7.6</b>	Chemistry of important ore grade uranium minerals (Bowell et.al. 2012)	61
<b>Table 7.7</b>	Association per modal mineralogy for the associations of uraninite.	73
<b>Table 8.1</b>	Major element chemistry of the run of mine bulk samples (Sc1, Sc2 and Sc3).	76
<b>Table 8.2</b>	Trace element chemistry of the run of mine bulk samples (Sc1, Sc2, Sc3).	77
<b>Table 8.3</b>	Assay details for the size fractions used in the grading analysis	78
<b>Table 8.4</b>	Gold mass percent per size fraction	78
<b>Table 8.5</b>	Uranium mass percent per size fraction	79
<b>Table 8.6</b>	Thorium mass percent per size fraction	79
<b>Table 9.1</b>	Gold dissolution	87
<b>Table 9.2</b>	Uranium dissolution	87
<b>Table A1 a</b>	Thin section names with reference to previous photographs indicating location within the slices.	116
<b>Table A2 a</b>	Data used to plot mill curves obtained during mill testing.	117



<b>Table A2 b</b>	Percentage passing 75 $\mu\text{m}$ , loss during the mill testing process percentage, grams	117
<b>Table A3 a</b>	Gold grain size distribution	119
<b>Table A3 b</b>	Uraninite grain size distribution	120
<b>Table A3 c</b>	Brannerite grain size distribution	121
<b>Table A3 d</b>	Association matrix BSPL Reef	122
<b>Table A3 e</b>	Association matrix below BSPL reef	122
<b>Table A3 f</b>	Association matrix above BSPL reef	123
<b>Table A4 a</b>	Major element chemistry assay for run of mine bulk samples	125
<b>Table A4 b</b>	Trace element chemistry assay for run of mine bulk samples	125
<b>Table A4 c</b>	Grading analysis assay	126
<b>Table A4 d</b>	Assay for heavy liquid separation testing	127
<b>Table A4 e</b>	Flotation assay	128
<b>Table A5 a</b>	Gold data, grading analysis	129
<b>Table A5 b</b>	Uranium Data, grading analysis	130
<b>Table A5 c</b>	Thorium data, grading analysis	130
<b>Table A5 d</b>	Sulphur data, grading analysis	131
<b>Table A5 e</b>	Au data for HLS including mass % calculation	131
<b>Table A5 f</b>	S data for HLS	132
<b>Table A5 g</b>	TH data for HLS	132
<b>Table A5 h</b>	U data for HLS	133
<b>Table A6 a</b>	Flotation calculations for Au	134
<b>Table A6 b</b>	Flotation calculations for S	135
<b>Table A6 c</b>	Flotation calculations for Th	136
<b>Table A6 d</b>	Flotation calculations for U	137

<b>Table A6 e</b>	Flotation combine calculations	137
<b>Table A6 f</b>	Flotation recovery vs. time	138
<b>Table A6 g:</b>	Average Flotation recovery vs. time	138



## ABSTRACT

Within the Black Reef Formation, which forms the basal unit of the Transvaal Supergroup, an auriferous and uraniferous reef occurs. This is known as the Buckshot Pyrite Leader reef. This reef is a conglomerate-hosted gold and uranium deposit, which is similar to the Witwatersrand reefs as they both contain significant amounts of pyrite and have similar depositional environments. This study seeks to identify the geometallurgical characteristics of the gold uranium and thorium that are hosted in the Black Reef at the Modder East operation in Springs. In terms of methodology, a detailed petrographic study was completed on the samples taken from underground and the surface run of mine samples. Mineralogy was conducted on these samples using SEM-based automated technology, namely the FEI Mineral liberation analyser (MLA). Using this, I could further characterise the gold and uranium bearing phases found across the Black Reef. Additionally, mill testing, grading analysis, major and trace element chemistry, density separation, gold and uranium dissolution as well as flotation testing was conducted on the ore in order to determine its geometallurgical characteristics. Through the combination of these methods, this study aims to evaluate the Au, U and Th within the Black Reef with regards to: the metallurgy; the extraction process in relation to the mineralogy of the samples; and the possible implications that these factors could have on the overall recovery of the economic minerals.

The sampling at the Modder East operation took three months to complete, as time needed to be allowed for variability in the mining product to be accommodated and included in the sample collection. Three run of mine bulk samples were taken at the base of the primary crusher at the processing plant over three months at one month intervals. Two large, intact, stope face samples were taken from the uppermost minable location within the Buckshot pyrite leader reef (S1 roughly 30 x 45 cm and S2 30 x 35 cm).

Initially, a petrographic study of the samples indicated that the buckshot pyrite leader reef could be divided into three distinct layers. The first of these was the massive quartzite that was the overlying layer for the buckshot pyrite reef. This layer contains some fine grained pyrite as well as some shale clasts and some carbon rich areas which give it the black color. Largely this layer is made up of mono-crystalline quartz with some large, rounded and elongated quartz pebbles towards the basal contact with the buckshot pyrite layer. The

buckshot pyrite layer contains mostly well-rounded detrital pyrite as well as visible kerogen globules and shale clasts with a largely mono-crystalline quartz matrix. Quartz pebbles are again present throughout this layer. Gold is present in thin section as discrete particles within the matrix of the buckshot pyrite conglomerate. The basal layer below the buck shot pyrite layer contains more clay and carbon rich material than the overlying layers as well some finer grained rounded detrital pyrite that forms in layers giving the appearance of pyrite stringers. This layer again contains significant amounts of quartz as well as smaller rounded elongated quartz pebbles.

The detailed mineralogy was conducted on thin sections cut from one of the large samples taken from the stope face (S1). These thin sections were analysed on the MLA using the Sparse Phase Liberation search. The purpose of this was to obtain and characterise the bright phases, which are the gold, and the uranium and thorium bearing minerals uraninite and brannerite. Polished mounts are created to provide the modal mineralogy of the bulk samples. An X-ray Backscatter Electron search was conducted on these mounts and the data obtained from these analyses yielded information about the occurrence, size distribution, and mineral associations of the Au, U and Th.

The gold occurs as native gold and the U and Th are hosted within uraninite and brannerite. The gold is found to be in association with five main minerals, namely quartz, pyrite, chlorite, muscovite and pyrophyllite. This is expected as these minerals make up the conglomeratic matrix in which the gold is hosted. The U and Th, however, occur predominately in association with carbonaceous globules found within the reef as a process of radiolytic polymerisation trapped the carbon around the U and Th-bearing minerals. Data from the Sparse Phase Liberation search confirmed that the gold is fairly coarse-grained and the uranium and thorium bearing minerals are finer grained.

The head chemistry assay indicated that the samples have a slightly variable gold content, ranging between 7.4 and 12.4 g/ton, and uranium and thorium content between 29.6 and 56.4 g/ton, and 3.6 and 5.2 g/ton respectively. The assay showed that this reef is silica rich with SiO<sub>2</sub> reporting between 76 and 83 wt% and the Fe and S content was also high with 8-13wt% Fe<sub>2</sub>O<sub>3</sub> and between 10 and 5wt% total S. This was confirmed with the MLA modal mineralogy, as the quartz and pyrite content in the bulk samples is dominant.

The grading analysis for these samples indicated that the gold is upgraded into the coarser size fractions (+106µm+75µm) and is significantly downgraded into the finer size fractions

(>75  $\mu\text{m}$ ), whereas the uranium and thorium has the opposite trend as they are downgraded into the coarser size fractions and upgraded significantly into the finer size fractions (<53  $\mu\text{m}$ ). Heavy liquid separation successfully upgraded the ore with regards to the Au and S but the U and Th were largely lost to the slimes and floats fractions. This therefore indicates that the gold can be effectively concentrated using gravity methods whereas the uranium and thorium could be concentrated by using screening to target the finer size fractions.

Cyanide and acid leach testing was conducted on these samples for gold and uranium respectively. It was found that the gold responded very well with above 94% recoveries, whereas the uranium performed relatively poorly with between 60 and 75% recovery. This may be due to the fact that the U found within the brannerite was refractory and could not be recovered during the leaching process.

Flotation testing also proved an effective method in recovering the gold from the samples, as the gold was successfully concentrated during this process. The U and Th bearing phases also showed notable recoveries during this process, which may be due to a strong association with carbon in the sample. Carbon, like gold, is known to be naturally hydrophobic, and so will report to the flotation concentrates. Uraninite, which hosts U and Th, is known to effectively activate with the addition of a xanthate collector which was employed within the flotation testing of this study. This, too, can possibly account for the uranium and thorium that report to the concentrates.

Finally, it can be concluded from this study that the gold within the Black Reef is effectively recovered using conventional methods of extraction. The uranium and thorium may not be viable economic minerals within the Black Reef as their grade and recovery performance indicates that they could be difficult and expensive metals to extract.

# Chapter 1

## Introduction and Purpose of Study

### 1.1 Introduction

The metal extraction industry is a large factor in the twenty-first century South African economy. Metals like gold (Au), Uranium (U) and Thorium (Th) form part of this industry and are essential in the South African economy, as well as in many economies throughout the world. Of the numerous studies that have been conducted on the mineralogical properties of gold, the important are those that focus on the gold resources of the Witwatersrand. This is because these gold resources are extremely large and have been a source of gold for decades. The Witwatersrand has produced over 46 000 t of gold since its discovery in 1886 (Johnson et al., 2009) and over 150 mines have exploited gold from the Witwatersrand Supergroup. There is, however, a lack of published research with regards to gold and uranium bearing phases within the Black Reef Formation particularly. This study seeks to address this gap by providing valuable information regarding the Black Reef Formation's minable metals. The Black Reef is the youngest formation to contain significant concentrations of mineable gold in South Africa (De Bever, 1997).

The mineralisation within the Black Reef can be studied with the aid of a Mineral Liberation Analyser (MLA) as well through studies which aim to determine the location of the gold and uranium-bearing phases and thereafter to describe them (Coetzee et al., 2011). Such analyses help to determine the grain size, mineralogy, mineral associations and the general characteristics of the ore within the Black Reef Quartzite Formation (Coetzee et al., 2011). Samples for this study were taken from Gold One International's gold mine that operates in Modder East, Springs. These samples primarily consist of Buck Shot Pyrite Leader reef, which is the upper most mineable reef of the Black Reef Quartzite Formation. In order to create a representative data set, three Surface bulk samples were taken (each a month apart from each other). Samples of the reef were collected underground from the Buck Shot Pyrite Leader reef and were used to determine the in-situ location of the mineralisation within the reef.

Two functions of the MLA will be used to aid in describing the mineralogy. Firstly, the Sparse Phase Liberation (SPL) SPL\_DD\_Lt, will be conducted on thin sections that will be cut from a large reef sample. This will be conducted in order to observe the bright phases that usually contain the gold and the uranium bearing minerals. Secondly, the XBSE function will be used on polished and mounted 30mm blocks in order to help determine the modal mineralogy and to observe other characteristics of the gold and uranium that occur within the reef (Fandrich et al., 2007).

Further research will also be conducted using metallurgical methods such as leaching and flotation. This is done in order to gain a further understanding of the ore in question and how it reacts to conventional extraction methods (Coetzee et al., 2011).

## 1.2 Present Study

### 1.2.1 Geographical Location

Gold One's Modder East operation, from which the samples for this study were taken, is situated in the gold-rich East Rand region of Gauteng, South Africa. It is approximately 30 kilometres South East of Johannesburg, in Springs (Gold One International, 2013). As indicated in Figure 1.1 the Mine is situated in the Black Reef Formation of the Transvaal Supergroup, South East of the Johannesburg granitic dome. Figure 1.2 provides a google image of the operations at Modder East.

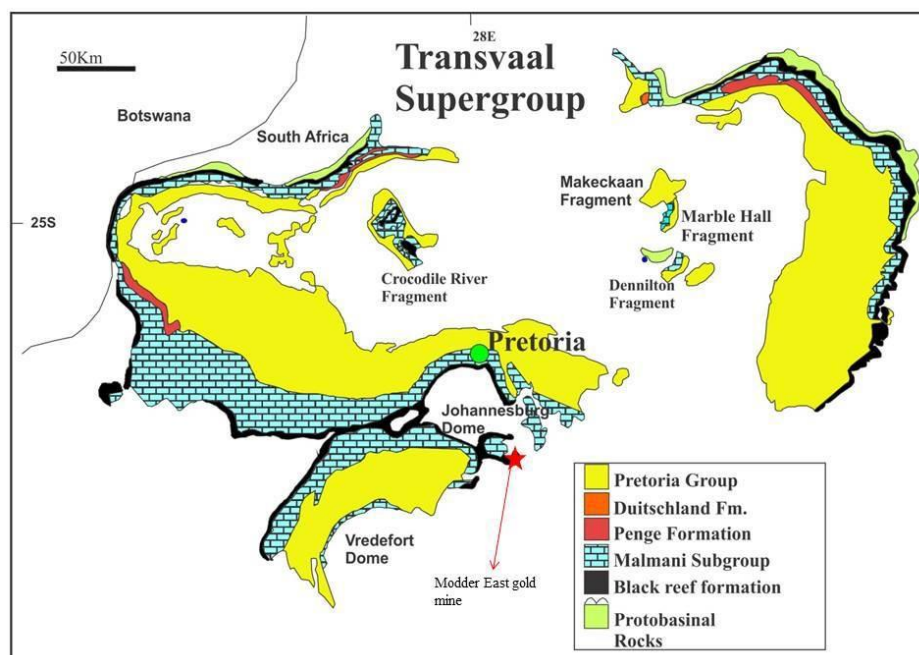


Figure 1.1: Geographical location of Modder East operation (modified from Eriksson et al., 2001)



**Figure 1.2: Google earth image of the Modder East operations.**

## 1.2.2 Review of the Modder East Mine

Modder East is Gold One International's flag ship mine and is the first new mine to be built in the gold rich East Rand region of Gauteng in 28 years. The target reefs of this operation are no more than 500m below surface to allow for trackless mining. The decline provides access to the ore body (Gold One International LTD, 2012). The target reefs are known as the Buckshot Pyrite Leader Zone (BPLZ) and the upper Kimberly reef, UK9a (Gold One International, 2012). Vehicles and other equipment are taken down into the mine via the decline while personnel are taken down in a vertical shaft (Gold One International, 2013).

The first gold pour conducted by this operation took place in July 2009. The first tonne of gold followed in May 2010, only 10 months after the mine was commissioned. By the end of



the first year of operations, which also marked the end of the financial year, the mine had recorded a profit of A\$(Australian dollars) 19.35 million before taxation. This was also the first year that Modder East declared continuous and commercial production (Gold One International, 2013).

The onsite metallurgical treatment plant, which has a capacity of 100 000 tons per month, employs a carbon in leach treatment plan to retrieve the gold from the milled material. In 2012, the plant had a 95% recovery rate (Gold One International, 2013, Figure 1.3).

This project was started in 2012 when Gold One was still listed however in 2014 Gold One was bought out by BCX gold investment holdings and Gold One shares have been delisted. Please consider this throughout the thesis when Gold One is mentioned. Gold One International was dual-listed on the JSE and the ASX and is a mid-tier mining company with gold operations and projects aimed at gold and uranium in Southern Africa. At the beginning of 2012, Gold One expanded with its acquisition of Rand Uranium Proprietary Limited, which comprised the Cooke 1, 2 and 3 underground operations and the Cooke surface assets (known as the Randfontein Surface Operations in the West Rand region of Johannesburg). Through this acquisition, Gold One was able to attain some of its more advanced uranium projects. These projects aim to extract valuable materials from the surface within the tailings dumps. Although this is a large project, the Modder East operations still remains the flag ship operation (Gold One International, 2013).



**Figure 1.3: Modder East metallurgical plant.**

### **1.3 Motivation for the Present Study**

Analyses of the Black Reef will yield useful insights into the chemical and physical properties of the gold and uranium within this formation, which ultimately affects the ease of extraction. This study will allow for improved understanding of the metallurgical properties of the gold and uranium-bearing phases within the Black Reef, and will also outline detailed mineralogical characteristics of the ore bodies and the host rock.

The geological details and metallurgical properties of the ore horizon within the Black Reef Formation are currently poorly understood as little research has been published on the reef with respect to its metallurgical properties. There have been, however, studies conducted with relation to gold and uranium bearing phases within other rock types like the Witwatersrand Supergroup, which is similar to the reef within the Black Reef quartzite Formation. This study will therefore facilitate a greater understanding of the Au, U and Th bearing phases with respect to the metallurgical properties. Metallurgical processing of the ore in the Black Reef is also poorly understood, and this study will aid in the understanding of this important process within the ore horizon. This will be achieved through conducting a classical element and mineral department study with specific relation to the Au, U and Th bearing mineralisation within the Black Reef Quartzite Formation.

This study will also emphasize the importance of modern Scanning Electron Microscopy (SEM) based Mineral Liberation Analysis. The MLA helps to easily, quickly and accurately characterise the ore with respect to metallurgical extraction properties (Fandrich et al., 2007). This approach is aided by the FEI 600F MLA at the University of Johannesburg. The FEI 600F MLA in combination with samples from the Modder East operation will allow for a developed understanding of the resources of the Black Reef Quartzite Formation's ore horizons.

## 1.4 Aims of the Present Study

The main aim of this study is to analyse the properties of the Au, U and Th mineralisation that occur within the BRQ Formation at Gold One International's Modder East operation, keeping in mind extraction and metallurgical properties. This will ultimately improve the knowledge of the reefs within the BQR Formation, as well as increase the number of skilled persons that are able to operate and work on an MLA.

Using the results that are attained from the MLA, as well as the data that is recorded in the metallurgical testing, I will characterise the gold, uranium and thorium bearing mineralisation within the Black Reef Quartzite Formation. The mineralogy of important and relevant minerals will be investigated with the aim to improve recovery and the understanding of the important metal bearing phases. This will include physical and chemical properties of the minerals that will affect the recovery.

The above aims will be achieved in the following ways:

- In-situ, as well as surface run of mine bulk samples from Modder East gold mine will be collected.
- Samples will be described on the macroscopic and microscopic scale.
- Mineralogical analysis will be conducted using the FEI 600F MLA at the University of Johannesburg in order to determine the size distribution, mineralogical characteristics and associations of the gold and uranium bearing phases that occur within the reef.
- Metallurgical processing of the samples will be conducted by using a combination of major and trace elements chemistry, grading analysis, gravity separation, leaching and flotation.

In the following chapters, I will outline the geology of the study area through brief reviews of the Kaapvaal craton and the Transvaal Supergroup. Firstly, a review of the Black Reef Formation will be conducted. This will be followed by an explanation of the sampling that was conducted for this study. Thirdly, the methodology for the study and all associated testing will be discussed. Thereafter, a petrographic description of the macroscopic and microscopic samples will be included before a detailed account of the mineralogy obtained

using the MLA. The major and trace element chemistry, grading analysis and density separation testing will then be discussed and followed by a discussion of the gold and uranium dissolution testing conducted at SGS. Lastly, the testing process of flotation will be discussed. The final chapter involves discussions and conclusions regarding all the test work done throughout this thesis.




## Chapter 2

### Geology of Study Area

#### 2.1 Introduction

The reef in this study forms part of the Black Reef Formation, which is the basal unit of the Transvaal Supergroup. This Formation is only present within the Transvaal basin of this Supergroup, and is absent in the Griqualand West basin. This chapter addresses the geology of the Transvaal basin and provides a brief description of the underlying Kaapvaal craton.

#### 2.2 The Kaapvaal Craton

The logo of the University of Johannesburg, featuring two stylized birds facing each other with a sunburst above them, and the text 'UNIVERSITY OF JOHANNESBURG' in a light grey font.

The Kaapvaal craton is one of the oldest pieces of Archean crust preserved in the geological record (Poujol et al., 2003). The Kaapvaal craton was formed by the accretion of several Archean terrains over a period of  $\pm 1000$  million years between 3500 Ma and 2500 Ma (de Wit et al., 1992). Each of these terrains consists of granitic material, green stone belts and later sedimentary and volcanic cover that occurred after the formation of the craton itself.

The Kaapvaal Craton is divided into four separate domains: the Western, Northern, Eastern and Central domains (Poujol et al., 2003). The oldest rocks of the Kaapvaal craton can be found in the Eastern domain while the youngest can be found within the Northern domain of the craton (Poujol et al., 2003). The Transvaal Supergroup is situated on this craton in a fairly central location with the Transvaal basin occurring near the Johannesburg dome (Figure 2.1, 2.2).

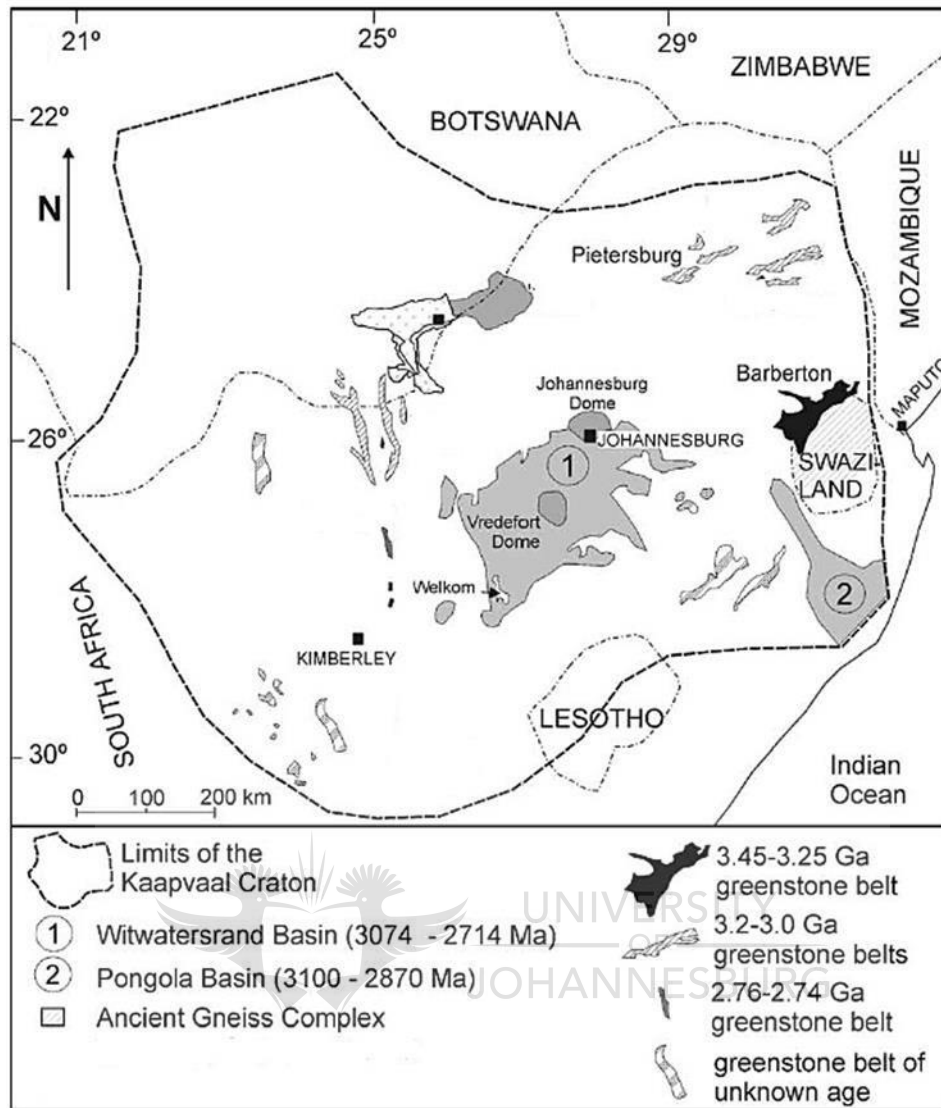


Figure 2. 1: Map indicating the outline of the Kaapvaal Craton (modified after Poujol et al., 2003)

### 2.3 The Transvaal Supergroup

The Transvaal Supergroup is a large sedimentary succession that is present in three structural basins on the Kaapvaal Craton – the Transvaal and Griqualand West basins in South Africa and the Kanye basin in Botswana. This study took place in the rocks of the Transvaal basin where the Black Reef Formation occurs.

This sedimentary sequence is presumed to be late Archaean to early Proterozoic in age. The rocks of the Transvaal basin were intruded by the Bushveld Complex at approximately 2060 Ma (Johnson et al., 2009, Henry et al., 1990). The presence of inliers of Transvaal rocks

surrounded by Bushveld Complex rocks suggests that the floor/basement rocks of the Bushveld are predominately composed of Transvaal Supergroup rocks that have subsided beneath the intruding Bushveld Complex. These inliers include the Rooiberg, Crocodile River, Makeckaan, Marble hall and Dennilton (Figure 2.2). The Transvaal Supergroup overlies more than one succession: it overlies the Witwatersrand and Ventersdorp Supergroups as well as the Archaean basement, with the Black Reef usually being the lower most unit in the succession. This means that the Black Reef is in contact with all the aforementioned formations (Johnson et al, 2009). The Transvaal succession has preserved extensive stromatolites and consists of one of the best preserved carbonate platforms. It also has an excellent record of cyanobacteria and bacteria evolution in the early part of Earth's long history. This is then overlain by large banded iron formations (BIF), which are large iron and asbestos deposits (Johnson et al, 2009).

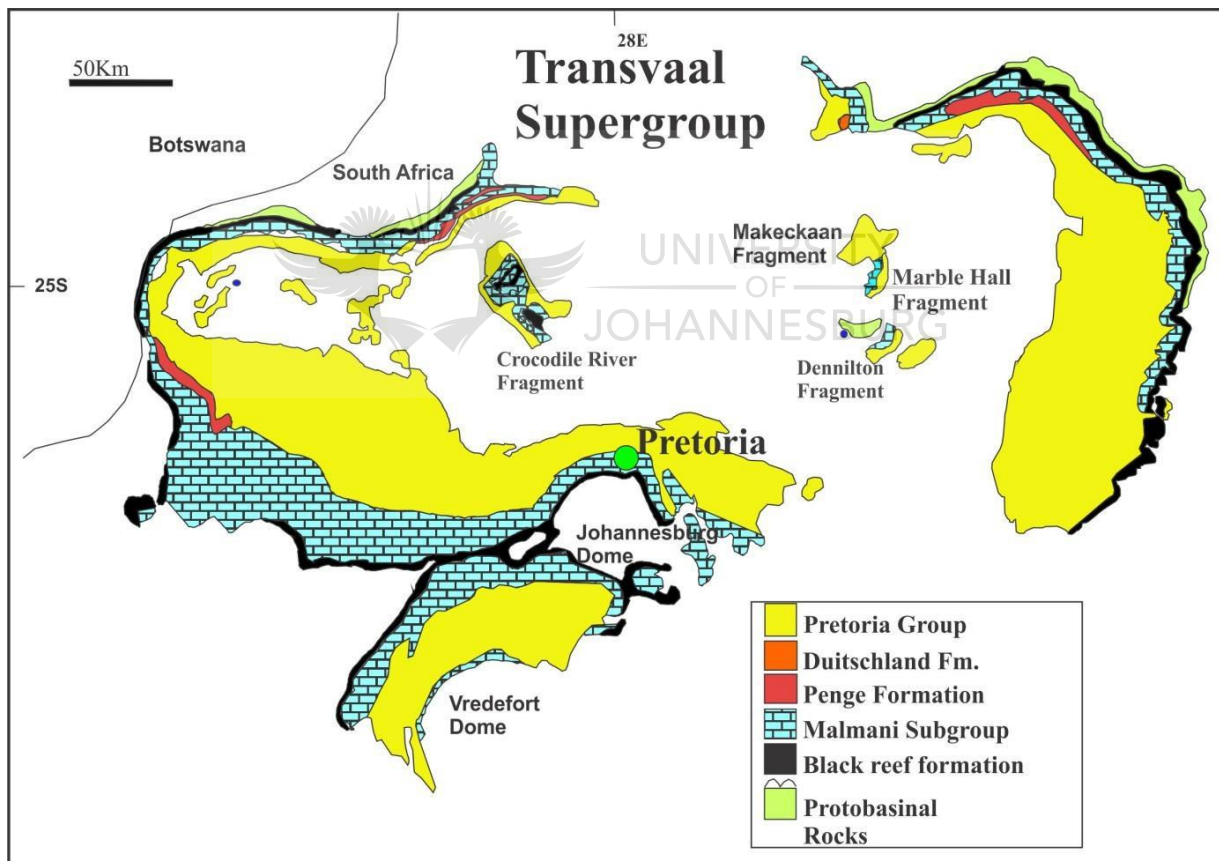


Figure 2.2: Transvaal basin of the Transvaal Supergroup (modified after Eriksson et al., 2001)

The sediments of the Griqualand West and Transvaal basins correlate as seen in Figure 2.3. This figure also displays the ages of these correlations which indicate that the Black Reef Formation is likely to be older than 2.5Ga (Moore et al, 2001).

The basement rocks of the Transvaal Supergroup are then overlain by the sediments of the Black Reef which are largely quartz rich arenites with basal conglomerates. The Malmani sub-group comprises the Oaktree, Monte Cristo, Lyttelton, Eccles and Frisco Formations, which are predominately dolomites and limestone. This suggests a carbonate platform within a marine environment that is tectonically stable (Bose et al., 2012). Overlying the Malmani is the Penge iron formation that also formed in a marine environment, likely at a greater depth. This and the lacustrine sediments of the Duitsland Formation make up the Chuniespoort Group, which in turn overlies the Black Reef Formation (Bose et al., 2012). Next in the succession (Figure 2.3, 2.4) of the Transvaal basin is the Pretoria Group, which is separated from the Chuniespoort Group by a time gap of  $\pm 80$  Ma (Bose et al., 2012). This group consists of the lower Pretoria Group, which is assumed to be a period of base level fall and pre-rift uplift, as there is a change in the tectonic setting (Moore et al., 2001). The Rooihooft Formation of the lower Pretoria Group is an alluvial fan sedimentary package and which suggests deposition in a syn-rift tectonic environment. This is due to the abundance of alluvial fan environments that are commonly seen within the rift tectonic setting. The next formation, the Timeball Hill Formation, suggests a more open rift given the shallow to deep marine environment. Both of these formations have glacial influences seen within the sediments (Bose et al., 2012).

Another base level change is evident in the braided and alluvial sediments of the Boshhoek Formation of the lower Pretoria Group. This formation is capped by basaltic andesites that make up the Hekpoort Formation (Figure 2.3, 2.4). These in turn separate the Dwaalheuwel from the Boshhoek Formation, as they both comprise similar alluvial and braided sediments. The Dwaalheuwel is overlain by the shallow, lacustrine sediments of the Strubenkop Formation. This all leads to the theory that the tectonic setting for this deposit was syn-rift subsidence, which created the basin for these sediments (Bose et al., 2012).

Following this was a period of stable tectonic activity which allowed for the formation of an intracratonic sag basin where the first formation, the Daspoort Formation (Figure 2.4), was deposited. This formation consists of distal fans and alluvial braid plain sediments. This is overlain by a shallow to deep marine environment where the sediments that make up the



Silverton formation are deposited. A regressive shore line grades into fluvial sediments of the Magaliesberg Formation. The Daspoort, Silverton and Magaliesberg make up the remaining formations of the lower Pretoria Group (Bose et al., 2012). Overlying the lower Pretoria Group are the alluvial fans and shallow basin sediments of the Vermont, Lakenvlei, Nederhorst, Steenkampsberg and Houtenbek Formations of the Pretoria Group. These environments show another change in base level, suggesting the pre-rift doming may have occurred during the time of sedimentation of these formations. Finally, the intrusion of the Bushveld Complex at 2050Ma represents the end of the deposition of the Transvaal basin sediments (Figure 2.4, Bose et al., 2012).

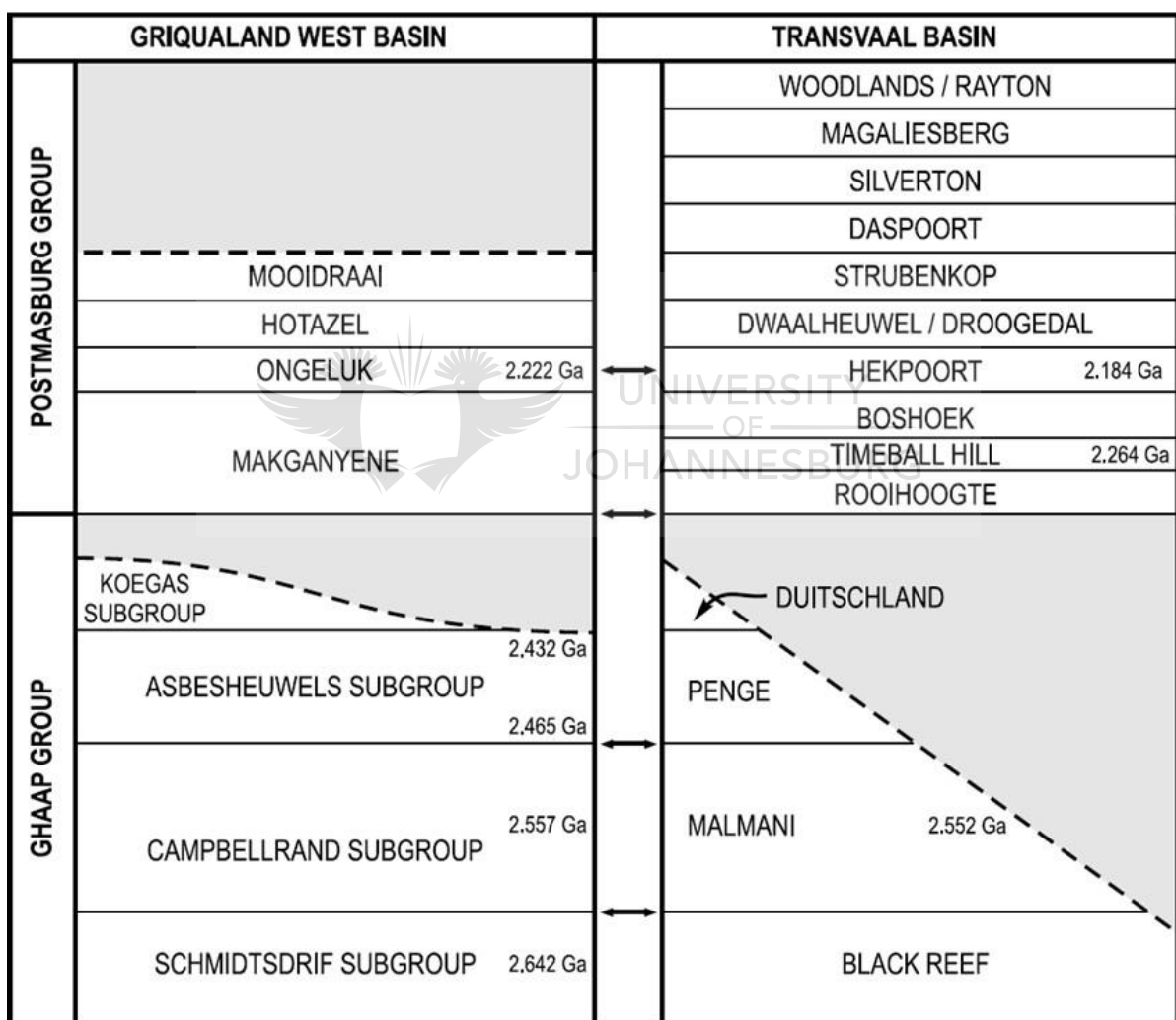


Figure 2.3: Current correlations between subdivisions of the Transvaal Supergroup in the Griqualand West and Transvaal basins (modified after, Moore et al., 2001).

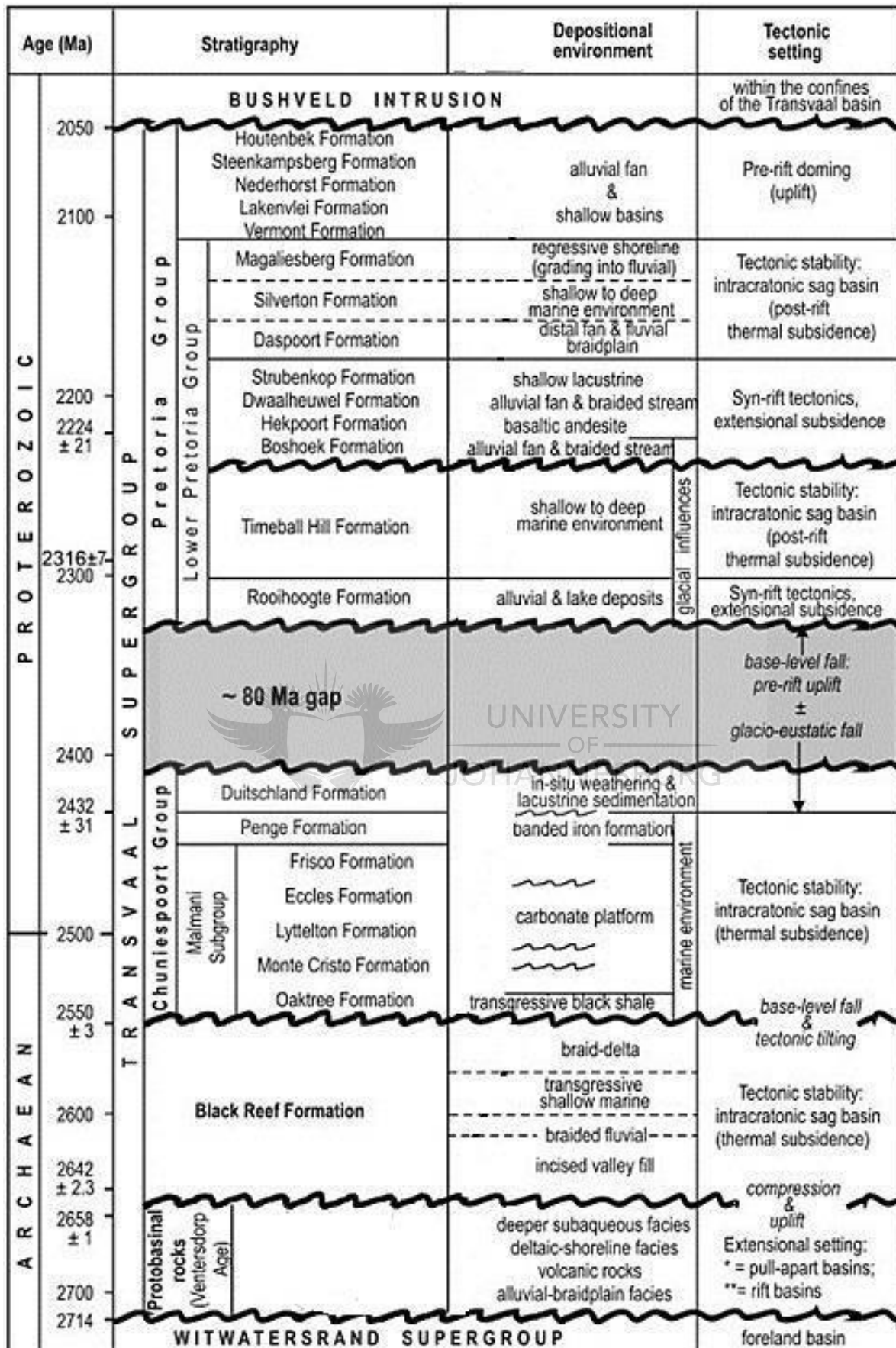


Figure 2.4: Schematic summary figure of stratigraphy, inferred depositional palaeoenvironments, tectonic settings and interpreted sequence stratigraphy for the Transvaal Supergroup within the Transvaal preservational basin (modified after Bose et al., 2012).

## Chapter 3

### The Black Reef Formation

#### 3.1 Introduction

The purpose of this chapter is to provide an overview of the Black Reef as it occurs within the Transvaal basin. Towards achieving this aim, a review of the theories on enrichment of the Black Reef will be conducted. This should allow for an improved understanding of the formation.

#### 3.2 The Black Reef Formation

The Black Reef Formation occurs at the base of the Transvaal Supergroup and is the oldest unit within the Transvaal basin. It consists predominantly of fairly mature quartz arenites, as well as some lesser conglomerate layers and subordinate mudrocks in some places. The Black Reef Formation, which varies from fluvial to shallow marine environments, was deposited on a deeply incised topographical erosional surface in the vast intra-cratonic Transvaal basin on the Kaapvaal Craton (Frimmel, 2014). Within the channels of this erosional surface, large boulder beds, as well as quartzites and conglomerates of the channel facies, have been deposited. The blanket facies conglomerates of the Black Reef occur on the levees of this surface. These two facies both contain the Au and U-bearing pyrite-rich ophiomitic conglomerates, which are very similar to those found within the Witwatersrand reefs (Barton and Hallbauer, 1996; Frimmel, 2014).

The difference between the Black Reef and the Witwatersrand reefs is that the Black Reef experienced very little metamorphism and deformation, and thus falls within the subgreenschist facies (Frimmel, 2014). This formation forms a thin layer that overlies the older basement of the Transvaal basin. This sequence is shown as an upward fining succession with conglomerates forming at the base of the Black Reef Formation then grading into quartz

arenites (which make up the majority) and then into mudrocks at the top of the succession (Johnson et al., 2009). Overall, the Black Reef is a thin siliciclastic fluvial deposit. It generally ranges from 30m to 60m in thickness throughout the basin, with inliers characterised by much larger thicknesses. For example, the Crocodile River dome, Dennilton dome and the Marble Hall inliers of the Black Reef formation reach approximately 280m, 210m and 170m in thickness respectively (Figure 2.2). This suggests that the Black Reef Formation would thicken toward the centre of the Transvaal basin (Hartzer, 1994). The Black Reef has over time been mined intermittently, and these mined or enriched areas are found to occur on the edge of the Transvaal basin which overlies the Wits sediments (Button, 1978). The basal conglomerates in the Black Reef Formation are believed to be the youngest gold bearing conglomerates in South Africa.

The Black Reef shows very similar lithological characteristics to those of the Witwatersrand conglomerates and may suggest a brief regression to a similar sedimentological environment in which the Witwatersrand rocks were deposited. The shale horizons that are often present in the Black Reef Formation usually occur towards the top of the succession. The Black Reef's name is derived from an old mining term of the gold bearing conglomerates mined in the central Transvaal, and was named as such given the dark colour of the rocks that surrounded the conglomerate reefs (De Bever, 1997).

The Black Reef Formation in the study area is found between Springs and Benoni at the Modder East mining operation in the gold rich East Rand gold fields (Figure 3.1).

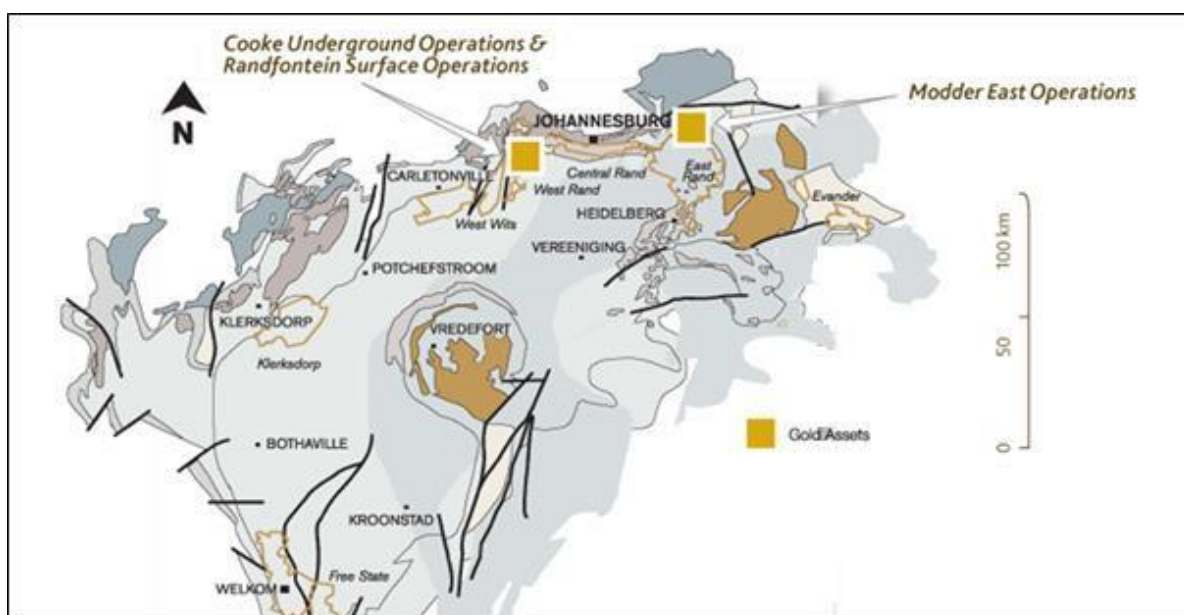


Figure 3.1: Gold One's gold assets , indicating the location of the Modder East mine in the study (Gold One International LTD, 2012)

The Black Reef overlies sediments of the Witwatersrand Supergroup in the study area. It has been suspected that the Ventersdorp lavas within this section were eroded by pre-Transvaal activity (De Bever, 1997). The underlying rocks include quartzitic rocks as well as shales that appear towards the uppermost part of the Witwatersrand sedimentary succession. The Kimberly conglomerate can also form the underlying layer of the Black Reef. The undulating surface on which the Black Reef was deposited has the appearance of erosional channel facies and causes a thickness variation of 1m to 10 m (De Bever, 1997).

The Black Reef Formation in the East Rand gold fields generally consists of two facies: a channel facies (Figure 3.2) and an upper blanket facies (De Bever, 1997). The lower channel facies is a lower or basal conglomerate layer which contains lesser quartzites, as well as some grit layers and lesser carbonaceous shales. This facies is usually where all the economic auriferous resources are located (Figure 3.2).

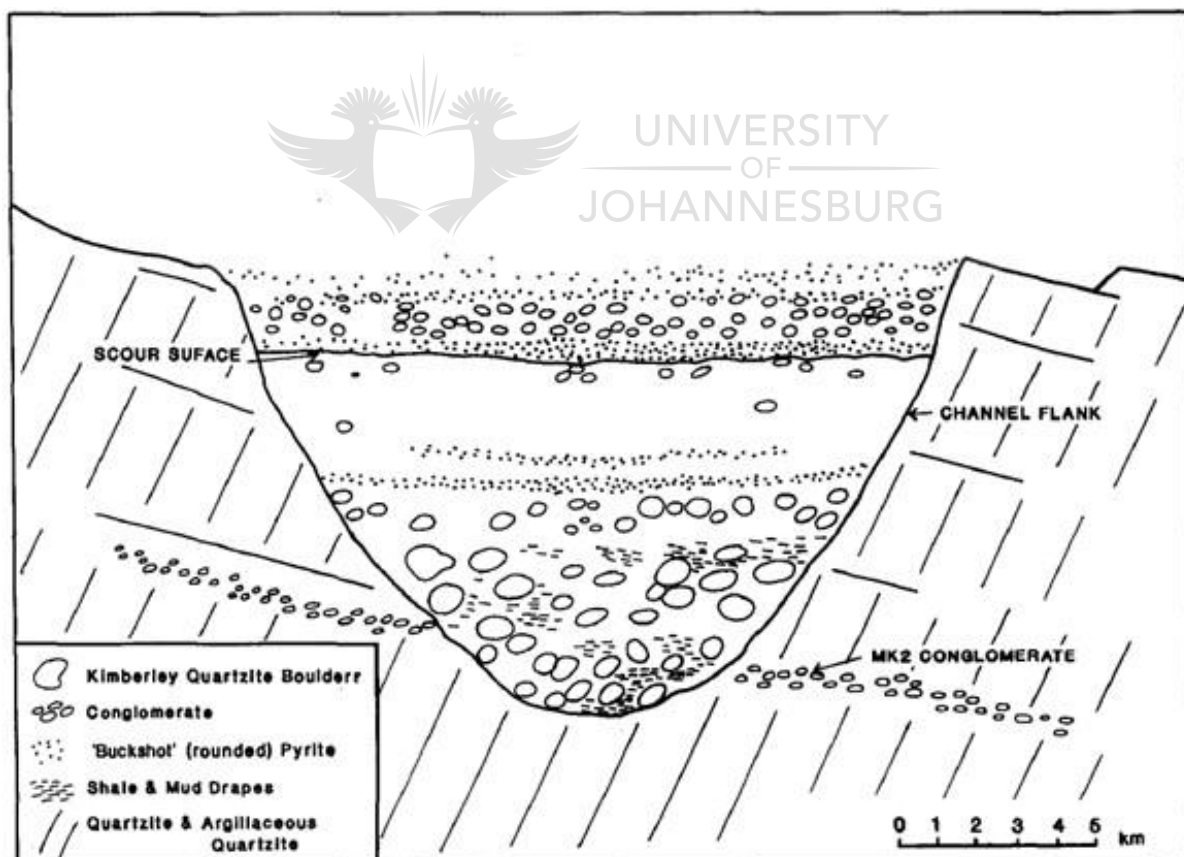


Figure 3.2: Simplified diagram of the Black Reef channel facies (modified after Barton and Hallbauer, 1996).

The second facies of the Black Reef is the upper blanket facies, and is a fairly mature quartzite layer that has some sporadic but very fine grained pyrite within the quartz matrix. This facies gradually grades upwards into a more carbonaceous quartzite and then into a shale and finally transitions into the overlying dolomites. This facies is described as more wide spread and is seen throughout the entire formation. It can vary in thickness but is usually between 7m and 10 m thick (De Bever, 1997; Henry et al., 1990).

The Black Reef depositional environment is thought to have initially been a river system characterised by anastomosing braided river channels in the early stages of its development. These channels were incised and transported sediments, believed to be derived from the Witwatersrand succession in a Southward direction as the dip was slightly southwards for the Transvaal basin in the study area (De Bever, 1997). These channels were actively incising valleys in the sediments they moved over. The Transvaal basin grew larger which led to a marine transgression that ultimately submerged these channel systems. In addition to some destruction of the initial sedimentological features, the active reworking of the channel sediments led to a loss of the primary sedimentological features. The basal conglomerates and quartzites towards the bottom of the formation are believed to be fluvial in origin, whereas the upper or blanket facies (including proto-quartzites and some carbonaceous mud layers and silts) acts as the foreshore and offshore facies (De Bever, 1997). The Buckshot pyrite evident within the basal conglomerates and quartzites was deposited in a stable wave-dominated environment, with the graphite and pyrite muds being formed during times of little sedimentary inflow into the environment (De Bever, 1997).

### **3.3 Theories on enrichment of gold and uranium within the Black Reef.**

The two facies found within the BRQ both contain the Au and U-bearing pyrite-rich oligomictic conglomerates, which are very similar to those found within the Witwatersrand reefs (Barton and Hallbauer, 1996; Frimmel, 2014). With the Black Reef Formation, being low greenschist facies, this leads to the conclusion that the Au did not originate from an external hydrothermal fluid, but rather that it was deposited along with the sediments and later slightly remobilised during lithification of these sediments (Frimmel, 2014). Evidence observed during this study suggests that the gold may be of an in-situ hydrothermal origin. Specifically, there was no evidence of placer gold, as the grains are randomly shaped and

appear to fill voids within the sediments (Frimmel, 2014). The uranium seems to occur within both the detrital uraninite, as well as some brannerite within the Buckshot pyrite leader reef samples. This suggests that it too is affected during the lithification of the sediments (Barton and Hallbauer, 1996). Given that the provenance of the gold and uraninite has not been documented in previous work the source of these metals is still widely unknown.



## Chapter 4

### Sampling at Modder East

#### 4.1 Introduction

Sampling is an essential part of any geometallurgical examination of ore. This chapter will outline the sampling methods used in this study and will give details of this process. The chapter will indicate that the sampling was not conducted in a way that would negatively affect the results.

#### 4.2 Sample Collection

The samples were collected from Gold One's Modder East gold mine, located approximately 30 km outside of Johannesburg, in East Vale, Springs, on the corner of Cloverfield and Outeniqua Roads. This area is situated in the gold-rich East Rand region of Gauteng, South Africa (Figure 1.2). The first sample type was an underground large chip sample that was taken at Modder East operation. This sample was in the form of two large blocks broken directly off the stope face of the Buckshot Pyrite Leader zone (described in Chapter 3). The area was washed down to avoid contamination prior to the extraction of the samples. These two samples (S1, S2) were roughly 30 x 45 cm and 30 x 35 cm respectively in size. The Buckshot Pyrite Leader stope face (from which the samples were removed) is upper most mineable horizon in the underground operations (Figure 4.1).

The next sample type was surface run of mine bulk samples. These samples were taken off the conveyer at the base of the primary crushed that forms part of the metallurgical plant (Figure 1.2 & 1.3). Three separate bulk samples were taken over a three month period. The conveyer belt was stopped and a 1m x 1m block was placed on it. The material within this block was then removed. The conveyer then ran for five minutes after which the entire process was repeated. This was done three times and the material collected constituted one



bulk sample. Three bulk samples were collected overall. The first sample (Sc1) was collected in February, the second (Sc2) was collected in April and the third (Sc3) was collected in June 2013. The bulk samples came in a variety of sizes and none were crushed to any specific size. All sampling was conducted on site at the same location each time.

### **4.3 Underground Locality of Black Reef Samples**

The hanging wall of Black Reef at the Modder East operation consists of a thick quartzite layer that is black in colour. The layer contains quartzite pebbles towards the bottom contact. These quartz pebbles are rounded and slightly elongated. Below this is a conglomerate layer that consisted of again large quartz pebbles as described. Large rounded pyrite grains are also observed in this conglomerate. These pyrite grains, which range from 0.2cm to 1 cm, are occasionally elongated but more often occur as well-rounded grains with a buckshot texture. The matrix between the quartz and pyrite is dark in colour and appeared to be made up of quartz and clay minerals. Below the pyrite conglomerate layer the quartz pebbles are still present but the pyrite grains are much finer grained and appear as stringers with particles smaller than a millimetre. This conglomerate forms the reef known as the buckshot pyrite leader reef. Below this, the thick footwall quartzite as previously described, reoccurs (Figure 4.1). The stope face was just over 1m at  $\pm 120$  cm. The reef varied in thickness at the stope face from between 24cm and 18cm. The footwall and hanging wall are  $\pm 20$ cm and  $\pm 60$ cm respectively. Further description of the Black Reef and more accurate petrography will follow.

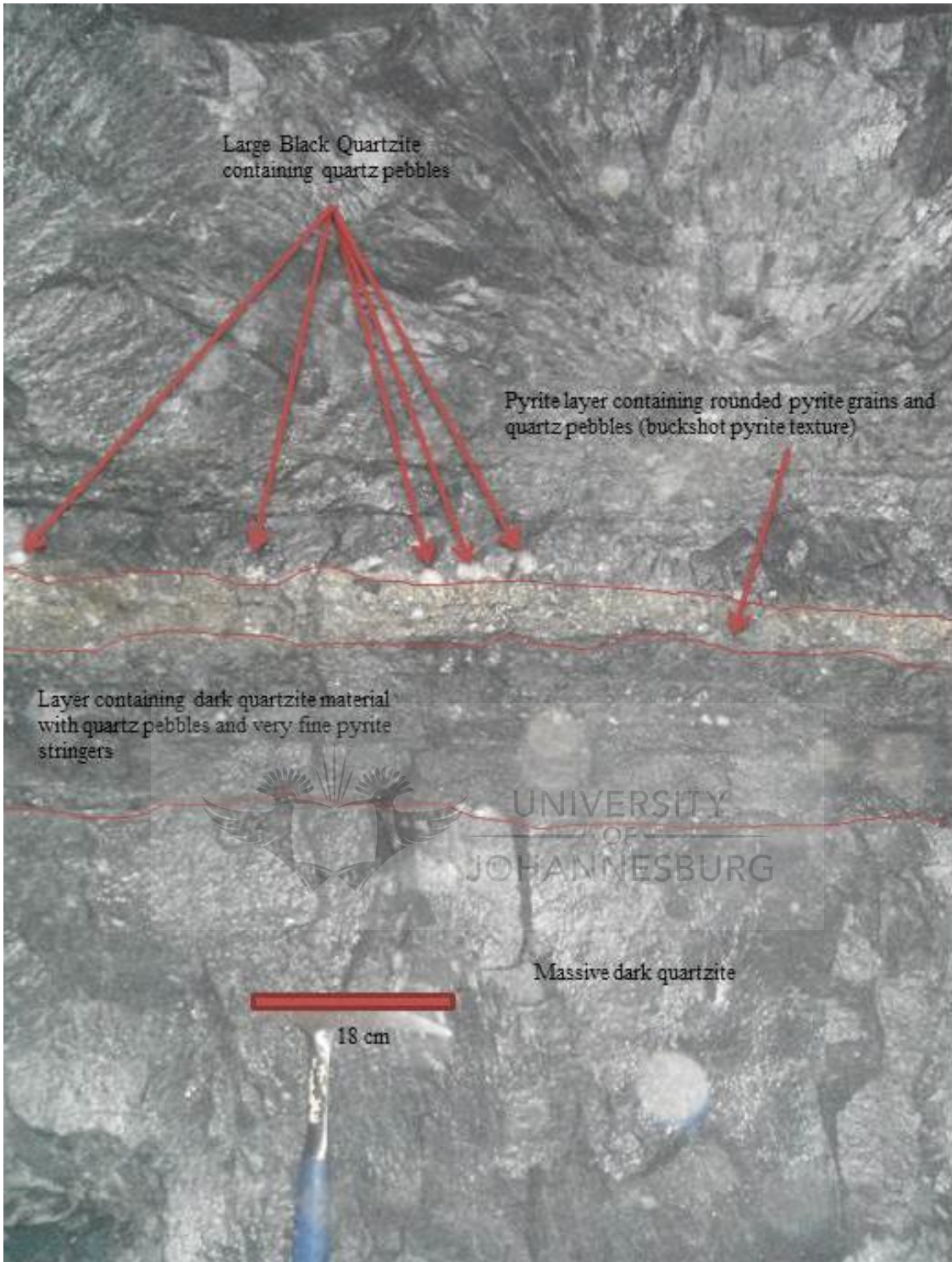


Figure 4.1: Black Reef underground sampling locality at Modder East

## **Chapter 5**

### **Methodology**

#### **5.1 Introduction**

Sample preparation is an essential part of any geometallurgical study as the sample preparation greatly affects the quality of the data that is produced. This chapter will outline all the methods that were employed in preparing the samples for mineralogical and metallurgical test work.

For the mineralogical work thin sections were created and analysed using automated SEM based technology (MLA). 30mm mounts of crushed material were also used in the mineralogical study of this material. For the metallurgical work the run of mine bulk samples had to be correctly blended and crushed in order to provide reliable representative data and avoid effects such as the nugget effect that can occur within this type of sample (Coetzee et al., 2011). Given that the accurate knowledge of mill curves and ideal mill times is essential to commencing with further metallurgical testing, these will also be discussed in this chapter.

#### **5.2 Sample Preparation for Mineralogical Analysis.**

##### **5.2.1 Thin Section Preparation**

One of the large samples (S1) taken from the underground stope face was cut into thin sections which were prepared for use on MLA (images and locations of thin sections made are available in Appendix 1, Figures A1 b-f and Table A1 a). The locations of the thin sections cut from the reef sample were taken from above, within and below the main pyrite layer that occurs within the sample (Figures 4.1 and 5.1).



**Figure 5.1:** Photograph of the slice taken from the S1, slice 3(sl3) and reverse of sl 3 indicating where the thin sections were taken. This was sample taken at the location illustrated in figure 4.1. Also see figure 6.1.

Each of these thin sections were then carbon coated to between 200 and 300 angstrom with 250 angstrom as the ideal thickness, as recommended for use in the MLA (Goodall and Scales, 2007).

The thin sections in this analysis were analysed using the MLA Sparse Phase Liberation function (SPL\_DD\_Lt). This function searches for particles of interest based on the BSE grey level range and then once the particles are found an XBSE analysis is performed on these particles and the directly associated minerals. This function does not provide bulk mineralogy as it isolates the particles that are outlined by the grey level cut offs. A bottom cut level was at 8 for the grey levels in these sections in order to allow the MLA to detect the carbon that was present in the samples (Fandrich et al, 2007). Please note: for table 5.1 and 5.2 dwell time and image size are unit less (Dwell time is on a scale 1, 4, 8 and 16. Image size 100 low resolution 1000 high resolution)

**Table 5.1: SPL\_DD\_Lt setup.**

<b>Specification</b>	<b>Set Limits</b>
Magnification	450x
Image size	500
Dwell time	4
Pixel size	1.3micron
Minimum particle size	4 pixels i.e smaller than 2x2 pixels were ignored (particles smaller than 2.6 micron)
Grey level cut off	150. Anything below BSE level of 150 is ignored.

## **5.2.2 Crushed Material Mounts**

The three surface run of mine bulk samples that were collected from the base of the primary crusher were used to create 30 mm mounts. This material varied in size, ranging between 30cm and 1mm. As such, it was necessary to crush these samples. This was done using a jaw crusher at the University of Johannesburg, to a size passing 3.35 mm, in order to allow for analysis. These bulk samples were then blended and split. (For the sake of clarity, the surface run of mine bulk samples will hitherto be referred to as ‘bulk samples’. These samples are named Sc1, Sc2 and Sc3).

These samples were split initially into 10kg aliquots which were then further split into 1kg aliquots using a rotary splitter at the University of Johannesburg. One of these 1kg aliquots was then split into 16 smaller aliquots, which were used to make sixteen 30mm mounted blocks. This process was repeated for each of the bulk samples to create 48 blocks. These blocks were analysed using the MLA after being carbon-coated to the same angstrom thickness as previously stated (further details to follow in Appendix 1).

The XBSE setup as part of the MLA was identified as the most efficient setup with which to analyse the mounts and attain the bulk modal mineralogy. This Mode uses BSE to identify different grey levels of the materials within the samples and once the grey level is obtained, the x-ray spectra for that mineral is produced. The minerals are classified using a combination of the grey level and x-ray information. The grey level particle separation and the speed of the x-ray analysis make this method suitable for the purposes of this study (Fandrich et al, 2007).

**Table 5.2: XBSE Setup**

<b>Specification</b>	<b>Set Limits</b>
Magnification	350x
Image size	500
Dwell time	4
Pixel size	1.7micron
Minimum particle size	4 pixels i.e. smaller than 2x2 pixels were ignored (particles smaller than 3.4 micron)

### 5.2.3 Minerals Standard File

For MLA analysis a standard file must be created in order to classify the minerals that were identified in the SPL\_DD\_Lt and the XBSE setup. The standard file was initially created during the analysis of the thin sections. Additionally, a list of grey levels and correlating x-ray spectra was created during the initial analysis of the samples. These spectra were compared to the existing standard files within the MLA software and a final file was created to classify and quantify all MLA data produced from the samples (Fandrich et al, 2007).

### 5.3 Mill Tests

Mill tests were conducted in duplicate, using two 1kg aliquots taken from each of the bulk samples. The purpose of this was to observe how long it would take to mill a 1kg sample to 75-80% passing 75  $\mu\text{m}$  as this was the target mill size at Modder East. Each of the samples was milled using a rotating rod mill at the University of Johannesburg. The rod mill contained 6mm x 25mm rods, 8mm x 20mm rods and 6mm x 16mm rods and rotated at an average speed of 73 rpm. Since milling is usually done in the presence of water, an addition of water is required for these tests. The equation "*Water needed= (mass of sample/0.6667) - mass of the sample*" was used for this purpose (Wiese et al, 2005). The relevant volume of water was then added to the sample which was placed into the mill and milled for 10 minutes. The slurry was then removed from the mill and wet sieved into a -75  $\mu\text{m}$  and a +75  $\mu\text{m}$  split using a universal test sieve. This was then dried in an oven at 150°C for approximately 40 to

50 minutes in order to allow for the +75  $\mu\text{m}$  to be dry sieved. This fraction was then placed into a sieve shaker and sieved for 10 minutes in order to get -75 and +75  $\mu\text{m}$  splits. This process was repeated after a further 15 minutes and then a further 25 minutes resulting in a cumulative time of 50 minutes for milling.

At each time interval splits were weighed and plotted to show the mill curve of the samples. This was done in order to determine the optimal mill time to achieve a 75-80% passing 75  $\mu\text{m}$  particle sizes for the 1 kg aliquots of the bulk samples. The aim of this test is to obtain the 75-80% passing 75  $\mu\text{m}$ , as this is the optimal size at the metallurgical plant on site at Modder East. It is essential that this study recreate certain conditions that are achieved at the mine itself.

Two of the 1 kg aliquots from each of the bulk samples were used in order to create a better average overall, as well as to see if there was reproducibility between the samples. Figure 5.2 displays all the mill curves that were plotted.

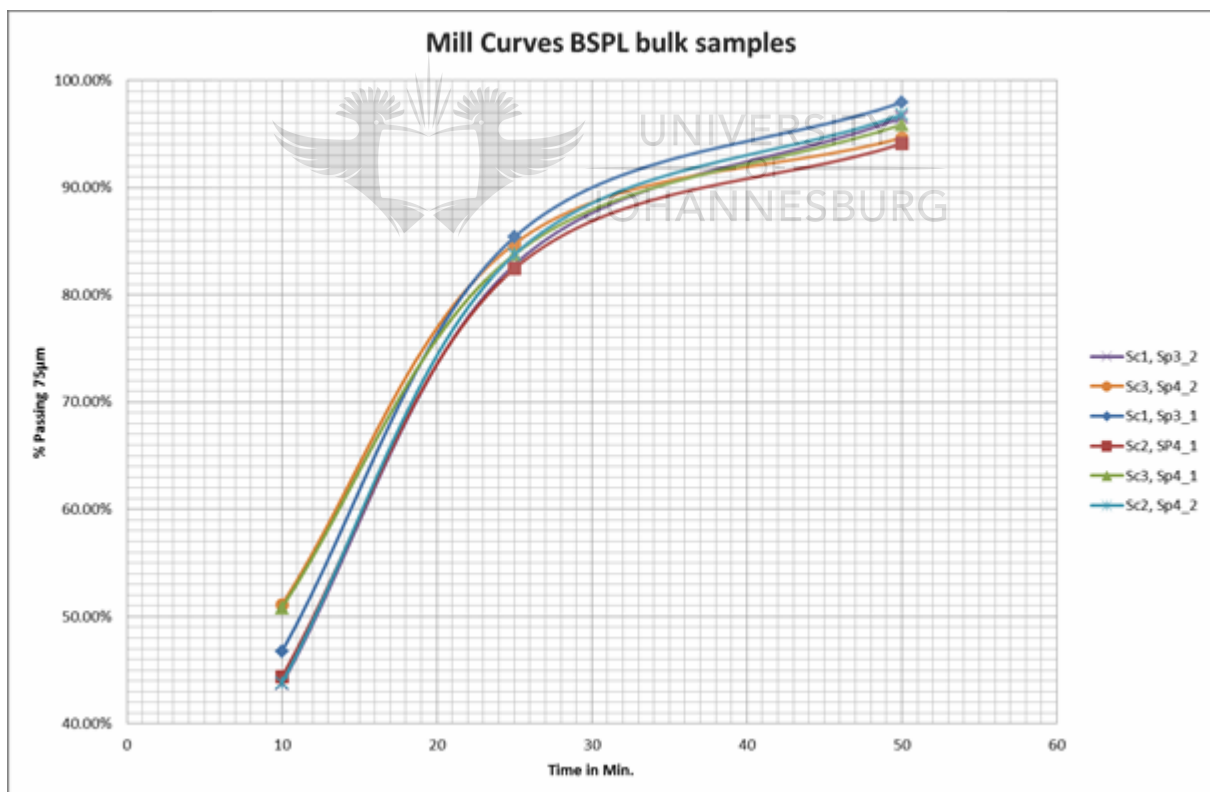


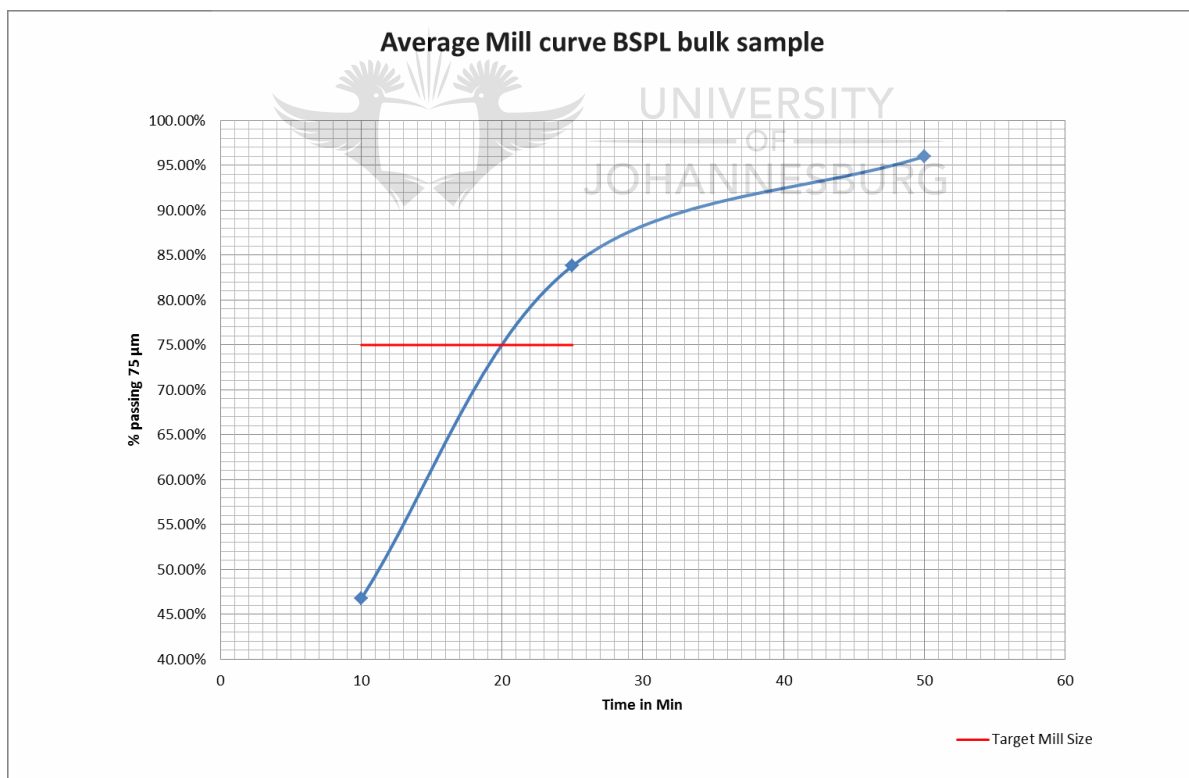
Figure 5.2: Mill curves for samples Sc1, Sc2 and Sc3 (Polynomial curves).

Figure 5.2 demonstrates that the mill curves for the samples are similar and that they produce good reproducibility. It is evident that the samples mill fairly rapidly from between 43% and 51% passing 75  $\mu\text{m}$  at 10 minutes to between 82% to 86% passing at 25 minutes. As the

particles get smaller, and it becomes more difficult to mill a finer size, we see the curve level off. The larger particles may have initially had cracks and fractures which would also allow for easier milling. In Figure 5.3 the average of all the mill curves has been plotted into one line in order to provide the best representative value of the mill curve to achieve a 75% to 80% passing 75  $\mu\text{m}$ . This will provide the ideal mill time to allow for further metallurgical testing.

It is apparent through this plot that in order to achieve a 75%-80% passing particle size, a milling time of between 20 and 23 minutes is required. With regards to any further milling of the bulk samples for metallurgical testing, 21.5 minutes is the milling time required to achieve the desired size. This correlates to a  $\pm 78\%$  passing 75  $\mu\text{m}$ .

All the data from the mill test as well as the images of the equipment used during the mill testing process can be found in Appendix 2 (Tables A2 a, A2 b, Figure A2 a).



**Figure 5.3: Average mill curve for BSPL bulk samples, with a desired mill size indicated by the red line. (Polynomial curve).**



## 5.4 Major and Trace Element Chemistry

The major and trace element chemistry was done in order to observe both the elemental composition of the material as well as the grades of the trace elements relevant to this study. For the major and trace element chemistry assay 6 crushed samples were used for analysis using the methods tabulated in Table 5.3 where the \* indicates the elements that were reported as oxides. Two splits from each sample day were analysed in order to reduce the chance of anomalous gold values, as a result of a possible nugget effect within the sample (Coetzee et al., 2011). The Loss on ignition (LOI) was calculated using gravimetric determination after combustion.

**Table 5.3: Major and trace element chemistry, methods employed for analysis (\* indicates elements reported as an oxide)**

Elements	Method
Au	50 g Fire Assay
Al*, Ca*, Cr*, Cu, Fe*, K*, Mg*, Mn*, Ni, Si*, Ti*, Zn	Zirconium crucible sodium peroxide fusion ICP-OES
As, Co, Pb, Th, U	Zirconium crucible sodium peroxide fusion ICP-MS
Ag, Na*, P*	Four acid digestion ICP-OES
C, S	C,S analyser

Each method was selected as the detection limits for the elements would be within the range of the method chosen. The methods were also chosen for each of the elements analysed as the most accurate measurement for each of the elements will be achieved by the selected method. The analysis of the samples was conducted at the Intertek laboratories.

## 5.5 Grading Analysis

The grading analysis was conducted in order to determine where four elements of interest, Au, U, Th and S, reported in relation to their size fraction after milling (Coetzee et al., 2011). The size fractions that were used were as follows: +212  $\mu\text{m}$ , +106  $\mu\text{m}$ , +75  $\mu\text{m}$ , +53  $\mu\text{m}$ , +25  $\mu\text{m}$ , and -25  $\mu\text{m}$ . However, due to weight constraints the size fractions +212 $\mu\text{m}$ , +106  $\mu\text{m}$

were combined and analysed as one. For each sample a 1kg split was milled and sieved into the various size fractions.

## **5.6 Density Separation**

The density separation was conducted in order to observe whether the elements of interest could be effectively pre-concentrated using a gravity separation method. The density separation concentrates, floats and tails, were analysed for Au, U, Th and S. This test involved a method of heavy liquid separation, performed by placing the milled material from each of the sample collection days into a heavy liquid called LST, which is a concentrated solution of lithium heteropolytungstates in water with a density of 2.95 g/mL at 25°C. The initial step involved in this test work was to remove the -25 µm size fraction through sieving and washing the material. The fraction that was taken out then made up the slimes. The milled material was then mixed into the LST which allowed the heavy minerals to concentrate. This concentration of heavy minerals was then analysed as the sinks and the remaining material that was collected and filtered makes up the floats fraction.

## **5.7 Uranium and Gold Dissolution**

This test was conducted in order to see how gold and uranium would respond to cyanide and acid leaching respectively. Three 10kg aliquots of each of the three bulk samples collected were submitted to SGS. These samples were initially crushed to 3.3mm and then further crushed to 1.7mm. Each sample was once again blended and three 100g representative aliquots were removed for the head analysis for Au and U. These representative aliquots were then milled and assayed for Au and U in triplicate. Thereafter, two 1kg splits from each of the samples were taken and crushed to 80% passing 75 µm. The samples were first leached for uranium using an acid and then for gold using a carbon in leach treatment plan. These samples were preconditioned with lime after the uranium leach to ensure that the gold leach was carried out in alkali conditions, which are required for gold leaching (Stange, 1999).

### 5.7.1 Uranium Dissolution

A 1kg bulk uranium leach was performed on each of the three samples, which were milled to a grind size of 80% passing 75  $\mu\text{m}$ . The conditions for each leach were:

- 50 % solids
- The pH was maintained at 1.2 using sulphuric acid
- The redox potential was maintained at 450mV using the addition of  $\text{MnO}_2$
- Ferric sulphate was then added at 5g/l
- The temperature was maintained at 60°C
- The duration of the leach was 24 hours

For the reporting on each of the samples, solutions were assayed for  $\text{U}_3\text{O}_8$ ,  $\text{Fe}^{2+}$  and  $\text{Fe}^{3+}$  in order to determine the pregnant solution values for these elements. The residues, after leaching, were also assayed for  $\text{U}_3\text{O}_8$ , along with a free acid determination test which was conducted on the final solution. The purpose of this is to determine how much uranium remains in the system after the leaching process has been completed. The uranium dissolution calculation indicates the percentage of the uranium that was recovered during the leach process. The accountability percentage is indicated to account for slight assay errors and is calculated as U head value divided by the average assayed U value expressed as a percentage. If this value falls between 90% and 110% it is considered to be within error and the dissolution calculation is considered accurate. The reagent consumption for  $\text{H}_2\text{SO}_4$  and  $\text{MnO}_2$  was also calculated in order to see how much of this material is used during the leaching process. The average assay is calculated using a weighted formula calculated at SGS based on reliability of assay figures.

### 5.7.2 Gold Dissolution

The gold leach was conducted on three 1 kg representative splits of material that were milled to 80% passing 75  $\mu\text{m}$ . This was the same material that was leached for uranium. The gold leach was conducted after the completion of the U leach. This was a carbon in leach

treatment plan. This is done because leaching of the uranium can lead to higher recoveries during the gold leach. The conditions for each leach were:

- 50% solids
- Precondition for an hour in order to reach the conditions needed for the Au leach.
- The pH was maintained at 10.5-11 using 100g/l of lime.
- Added to the slurry was 5kg/t of NaCN (sodium cyanide)
- Added to the slurry was 20g/l of pre-abraded carbon (Pre-abraded carbon is a normal carbon that is subjected to abrasion, so that it does not break into fines during leaching).
- The overall time for this leach was 24 hours.

For reporting purposes, assays for Au, as well as carbon analysis, were performed on the solution. There was also a residue analysis assay performed for Au in order to observe how much gold remained in the samples after dissolution. The reagent consumption was also analysed for NaCN and CaO (lime) in order to determine how much of the material is used during the leaching process. The solution and carbon percentage is a calculated value of the gold in solution and the gold in carbon divided by the average head Au value. This is in order to account for all the gold within the system: the solid percentage accounts for the gold that has been removed from solution. The Au dissolution calculation provides a percentage of how much of the gold is recovered during this process. The accountability percentage follows the same principles and calculations as discussed in the previous section on the uranium leach. The average assay is calculated using a weighted formula calculated at SGS based on reliability of assay figures.

## **5.8 Flotation**

Flotation was done in order to observe whether or not the minerals of interest would float and to see what recoveries could be attained under the listed conditions. Two 1kg aliquots from each of the bulk samples was used for flotation (six separate flotation samples in total). The floatation cell used was the Denver Flotation machine (Figure 5.4). Each sample was milled, as discussed, to 75%-80% passing 75 $\mu$ m. The six samples were then transferred to the

flotation cell using a minimal amount of water, as the operating cell is a 2.5 litre flotation cell. Once the material has been transferred into the flotation cell, the initial process can begin. With the impeller submerged in the slurry and the air on the machine closed, the impeller speed (according to the size of the sample  $\pm 1$  kg) is set to 1200 rpm. While the slurry was mixing within the cell, samples were taken in order to ascertain the feed details from the slurry before the reagents were added.

For the flotation process, certain reagents need to be added in order to achieve the desired results. Some minerals are required to float and others, such as the non-economic minerals (gangue minerals), need to depress into the slurry. These latter minerals are unwanted in the concentrates. The reagents that were used, based on Wiese et al. (2005), were: Copper sulphate (activator); sodium isobutyl xanthate 'SIBX' (primary collector); senkol 5 (secondary collector); sendep 30D (depressant CMC type); and senfroth XP 200 (frother). These were all supplied by Senmin.

A xanthate collector was used in order to activate the desired minerals such as pyrite, gold and uraninite within the slurry (Bulatovic, 2007). Senkol 5 was used to further target the sulphides that may possibly occur within the slurry, as these can be associated with the minerals of interest in this type of ore body. Sendep 30D is used to depress the naturally floating gangue minerals, which are undesirable in the concentrate (for example, silicates may be present in such minerals). Also added was senfroth, which allows the slurry to more effectively froth during the flotation process.

Each reagent needs to be added after a certain time in order to allow the slurry to condition to the addition of the reagent. The activator, in the form of 4ml of  $\text{CuSO}_4$ , is first added, then after 5 minutes the collectors, 7.50ml of senkol 5 and 4.17ml of SIBX, are added together. After two minutes, the 10ml of depressant (sendep 30D) is added. After a further two minutes 4ml the senfroth XP 200 frother is added and allowed to condition for one minute (Wiese et al., 2005).

After the reagents have been added and conditioned the flotation process can begin. The air valve on the flotation cell is opened and the material begins to froth. Every 15 seconds the material is scraped off and collected. The first concentrate is collected after two minutes, the second after a further four minutes, the third after a further six minutes, and the fourth and final concentrate after a further eight minutes. Thus, the total flotation time is 20 minutes. The mass of the samples, both the wet and dry, are noted. Once these samples were collected

and weighed, it was noted that the values are too low for assay of a single flotation. Thus, the two samples from the same bulk sample were combined in order to achieve the desired weight for the assay and the samples were then assayed for Au, U, Th, and S at the Intertek Laboratories.



**Figure 5.4: Denver flotation cell**

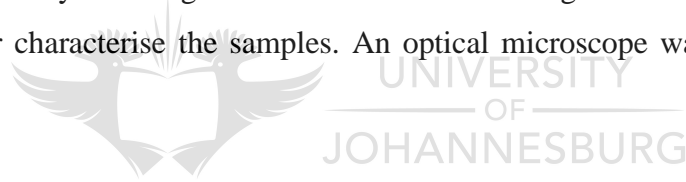
## Chapter 6

### Petrographic Description of Samples

#### 6.1 Introduction

The purpose of this chapter is to discuss the macroscopic and microscopic characteristics of the Black Reef that was analysed in this study. The two large in-situ samples taken, S1 and S2, serve as an effective macroscopic image of the reef section. The cuts that were made from S1 will also aid with the macroscopic description of these samples (Appendix 1). These samples were used to represent the characteristics of the ore which include the basic mineralogy as well as the textures, grain sizes and colour of the samples.

Thin sections were analysed using transmitted and reflected light in order to establish grain sizes and to further characterise the samples. An optical microscope was used towards this end.



#### 6.2 Macroscopic Description of the Black Reef

The two large samples taken from the stope face of the Black Reef indicate three separate layers. The first of these is the massive quartzite layer, which is above the buckshot pyrite layer which in turn overlies the basal layer that is made up of smaller pyrite and quartz grains with more clay material present (Figures 6.1, 6.2, 6.3).

The massive quartzite layer is made up of predominantly massive quartzite matrix with some fine grained pyrite present. These pyrite grains are predominately smaller than 1mm with the largest grains being 1mm in size. Within this layer there are large quartz clasts which usually occur towards the basal contact with the next layer. These clasts range between 0.5cm and 5cm in size. They are well-rounded and are predominantly elongated. The clasts are smoky quartz clasts. The massive quartzite is usually dark in colour and this may be due to the carbonaceous and clay material that is present within this layer (Figures 6.1, 6.2, 6.3).

The next layer is made up of largely well-rounded pyrite clasts that appear detrital. These clasts are between 1 and 0.2 cm. Between the clast, smaller pyrite grains that range between 2mm and less than 1mm in size are evident. These grains also appear well-rounded and detrital. Within this layer large quartz pebbles are also present. These pebbles appear to be sub-rounded to well-rounded clasts and range in size from 4cm to 0.4cm in size. These pebbles are also predominantly smoky to white quartz clasts and are usually well-rounded and elongated. These clasts are fairly well spaced within the pyrite layer. The pyrite layer can be termed buckshot pyrite as the texture of the pyrite grains is fairly distinct (Figures 6.1, 6.2, 6.3).

The basal layer also contains quartz clasts that range from 1 to 0.2 cm in size and appear to be sub to well-rounded clasts. They are again made up of predominantly smoky quartz. These clasts are well spaced within this layer. Pyrite grains also occur within this layer and range from 2 to less than 1 mm in size. These grains are well rounded and also appear to be detrital. These pyrite grains occur within thin layers below the buckshot pyrite layer and give the appearance of pyrite stringers below the main reef section. The remaining material that effectively makes up the groundmass is again dark material with a massive texture as seen above the buckshot layer. However within this layer there appears to be more clay and carbonaceous material present (Figure 6.1, 6.2, 6.3).

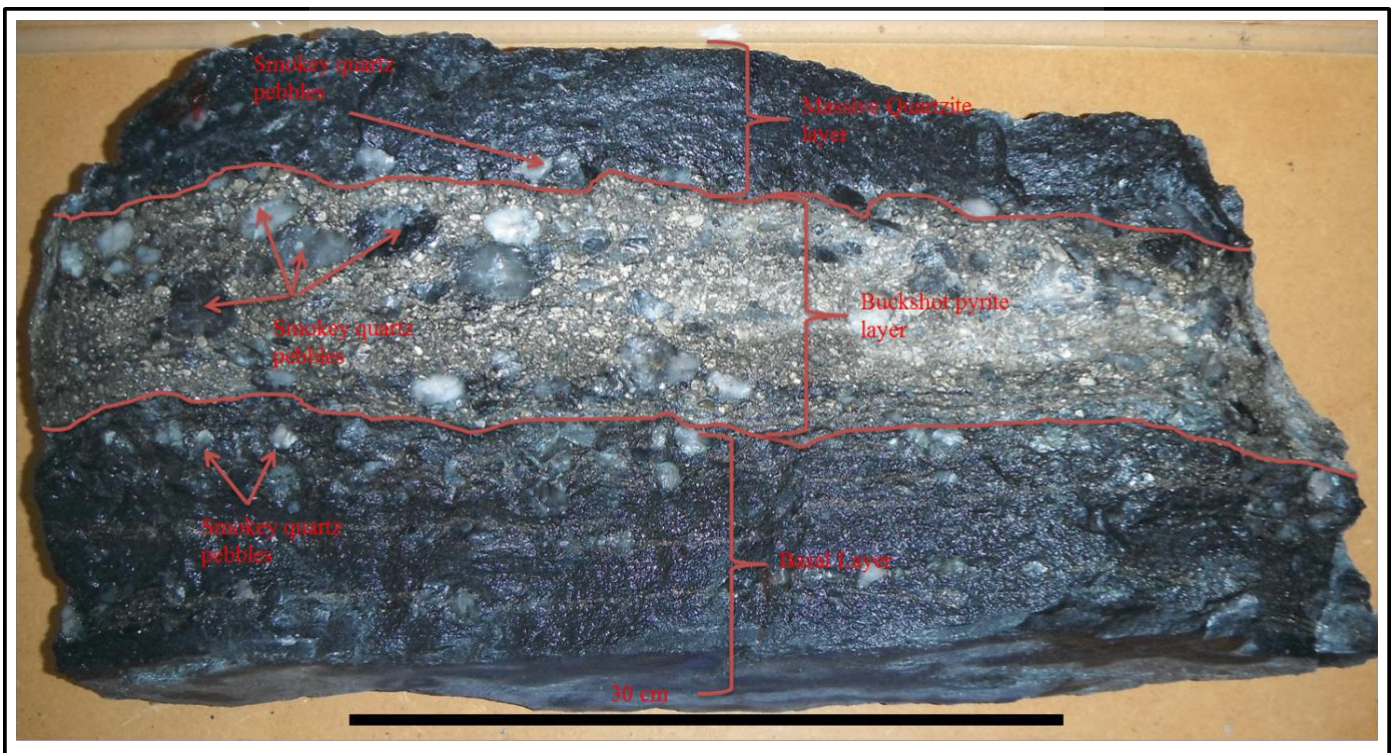


Figure 6.1: BSPL S1, indicating the three layers that make up the Black Reef.





Figure 6.2: BSPL S2, indicating the main composition of the three layers of the Black Reef

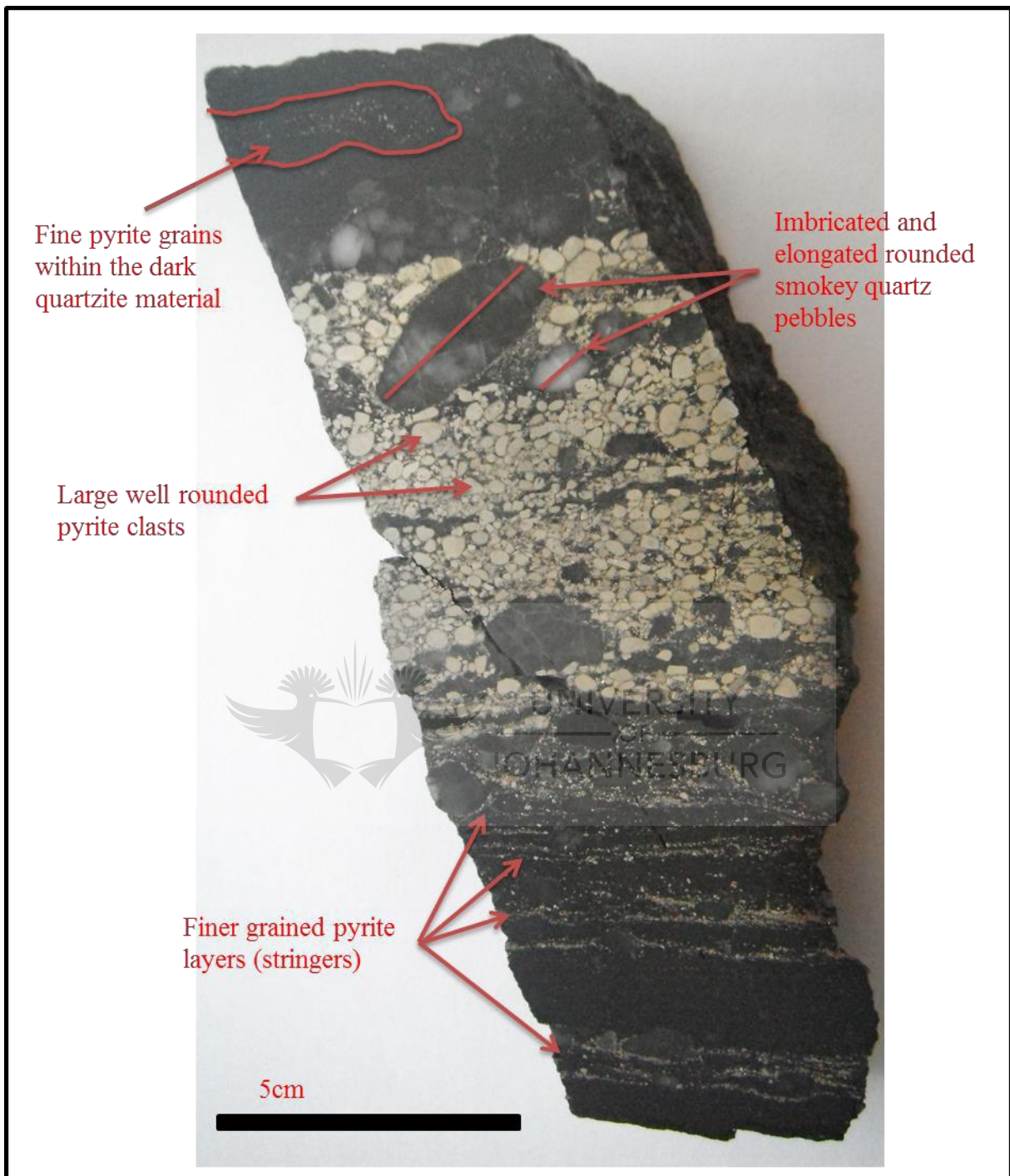


Figure 6.3: BSPL S1, SL 6, indicating the pyrite textures and the imbrication and elongation of the quartzite pebbles

### 6.3 Microscopic Description

Within the microscopic description the three layers that were identified in the macroscopic description also apply.

The first thin section that was cut from above the buckshot pyrite layer indicates very similar features as described within the macroscopic description. Large quartz pebbles can be seen within the section as well as coarse grained quartz that make up the groundmass. The pyrite is very fine grained and is often located on the edges of the larger quartz grains. The majority of the pyrite is less than 1 mm in size and is well rounded detrital grains. We can also see shale clasts that were clear within the macroscopic description. These clast range from 6 to less than 1 mm and they can be seen appearing randomly through the upper massive quartzite layer. Within the slide there are areas seen that are made up of more carbonaceous matter that appear darker than the shale clasts due to the presence of more carbon within the material (Figure 6.4, 6.6). It is indicated under closer inspection that the quartz that makes up the ground mass is mono-crystalline quartz and that the shale clasts are made up of very fine clay materials (Figure 6.5).

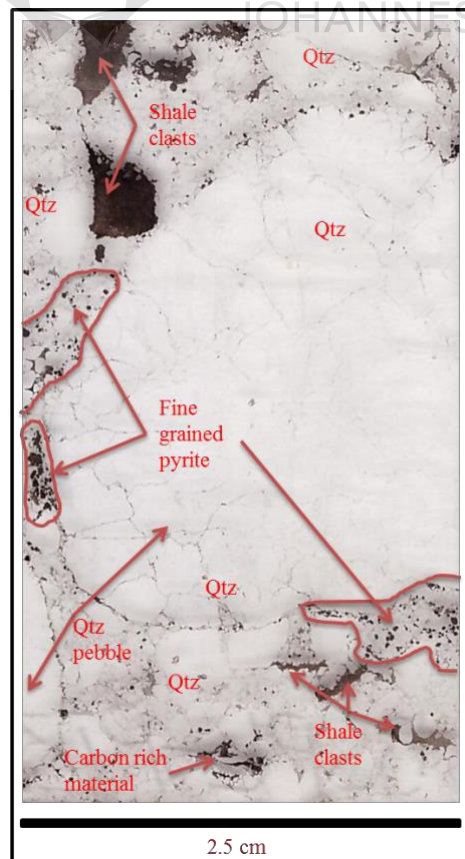


Figure 6.4: Thin section scan: cut from above the BSPL Reef; indicating quartz pebbles, quartz groundmass, fine grained pyrite, shale clasts and carbon rich material.(Thin section cut from S1 figure 6.1, BSPL PT 1)

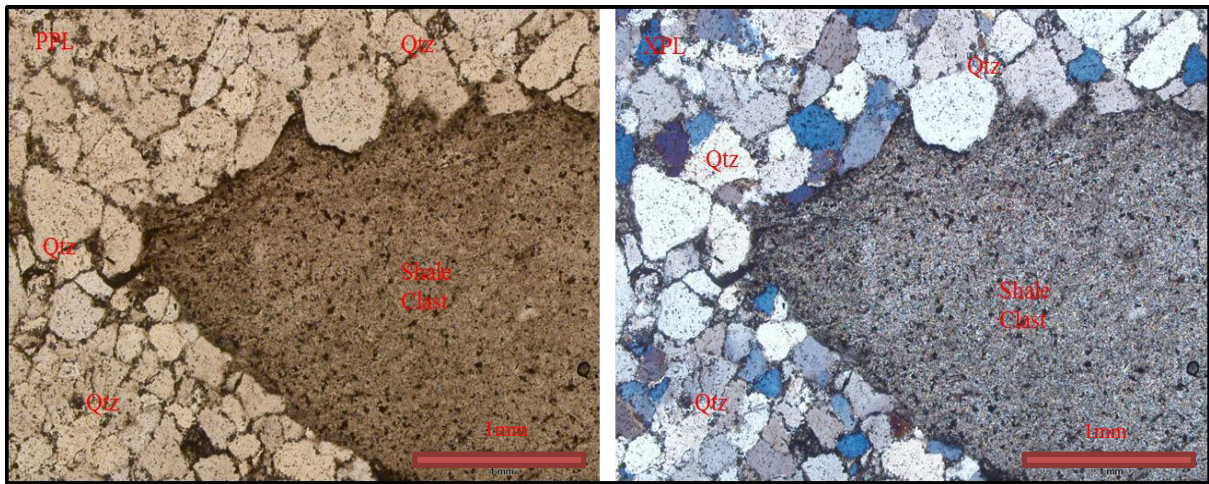


Figure 6.5: PPL(L) and XPL(R) image indicating the mono-crystalline quartz and the fine grained shale clast that occur above the Buckshot reef.(BSPL PR 1 cut from S1)

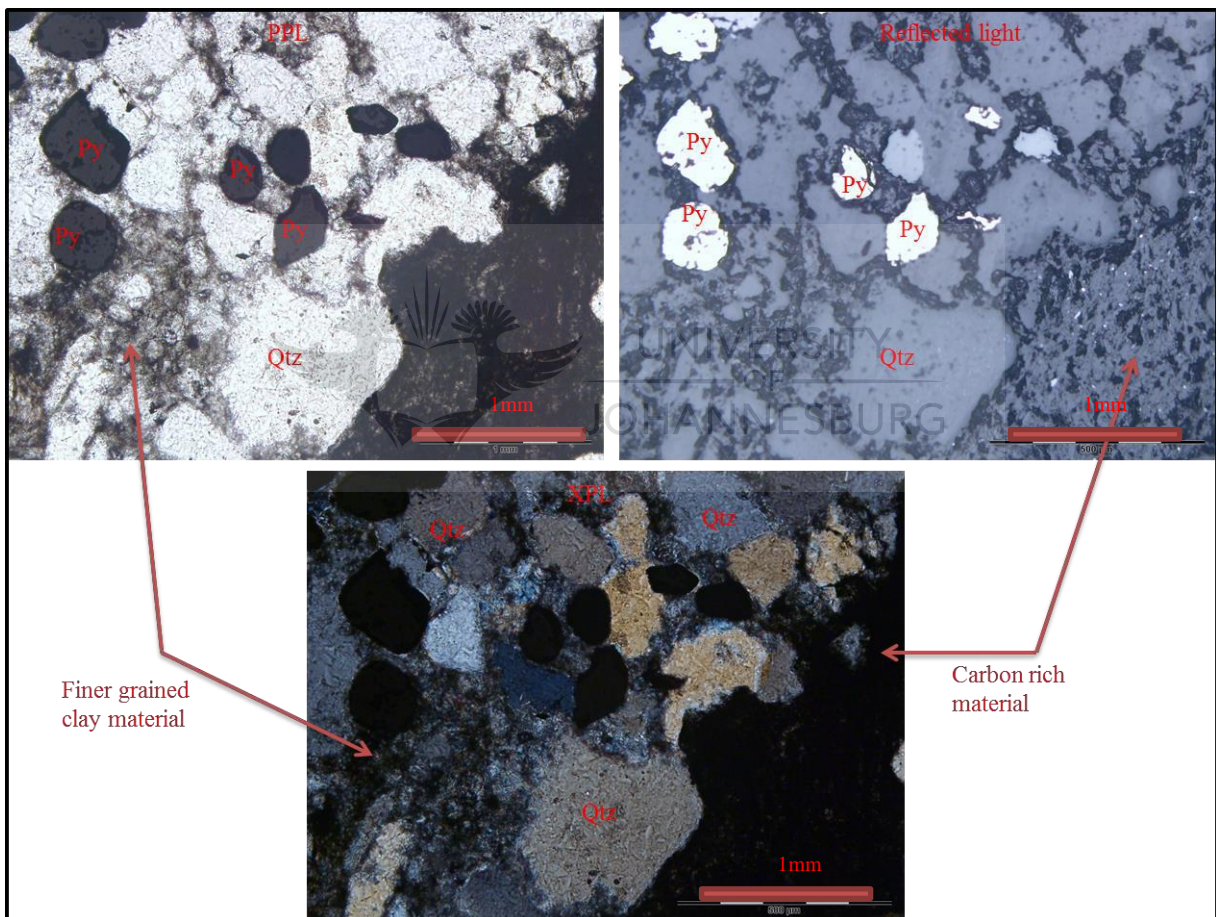


Figure 6.6: XPL(bottom), PPL(top left) and reflected light(top right) images showing the occurrence of the carbon rich material as well as the fin grained rounded pyrite that occur above the buckshot pyrite layer.(BSPL PT 2 cut from S1).

From a thin section that was cut within the buckshot pyrite layer we can see that the pyrite grains are considerably larger within this layer and make up the majority of the clasts found. Rounded and elongated quartz pebbles can still be seen within this layer ranging from 1 to 0.1 mm in size. The majority of the ground mass is also made up of quartz with some clay

clasts still seen. Small black globules are also present within this layer. These are kerogen globules that are present within the buckshot pyrite layer (Figure 6.7).

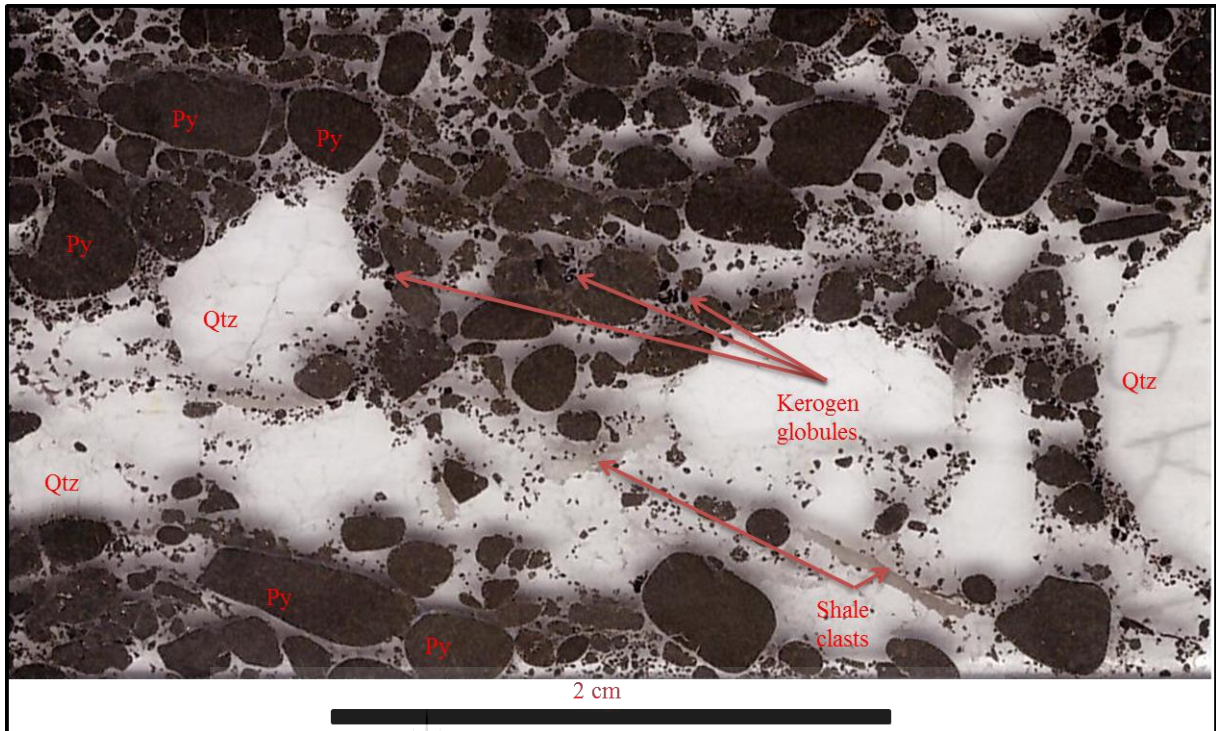


Figure 6.7: Thin section scan using transmitted light: cut from within the buckshot pyrite layer indicating rounded detrital pyrite as well as quartz pebbles, shale clasts and kerogen globules.(BSPL PR 5 cut from S1).

Within this layer a larger grain of the clay material was identified as muscovite. So it can be assumed that along with other clay minerals muscovite makes up part of the mineralogy found within the shale clasts (Figure 6.8).

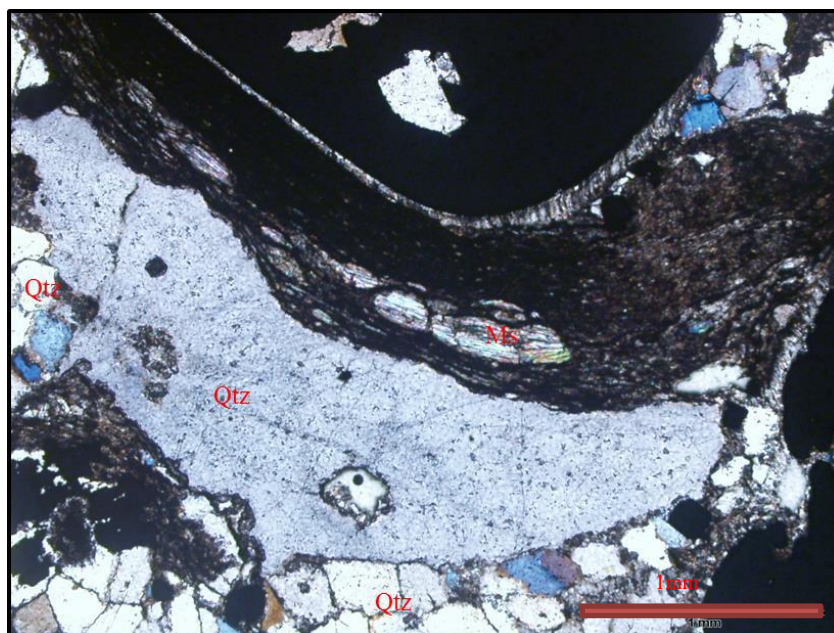


Figure 6.8: XPL image: showing muscovite and quartz ground mass. (BSPL PR 4 cut from S1)

Under reflected light examination of the thin sections gold particles were identified and found within the buckshot pyrite layer. These are angular particles that occur within the ground mass of the buckshot pyrite layer (Figure 6.9 A-D). These particles range from 1  $\mu\text{m}$  to 250  $\mu\text{m}$ . The gold also is found between two rounded pyrite grains (Figure 6.9 B). \*(Further more detailed work for the gold and other minerals was conducted using the MLA and will follow in later chapters.)

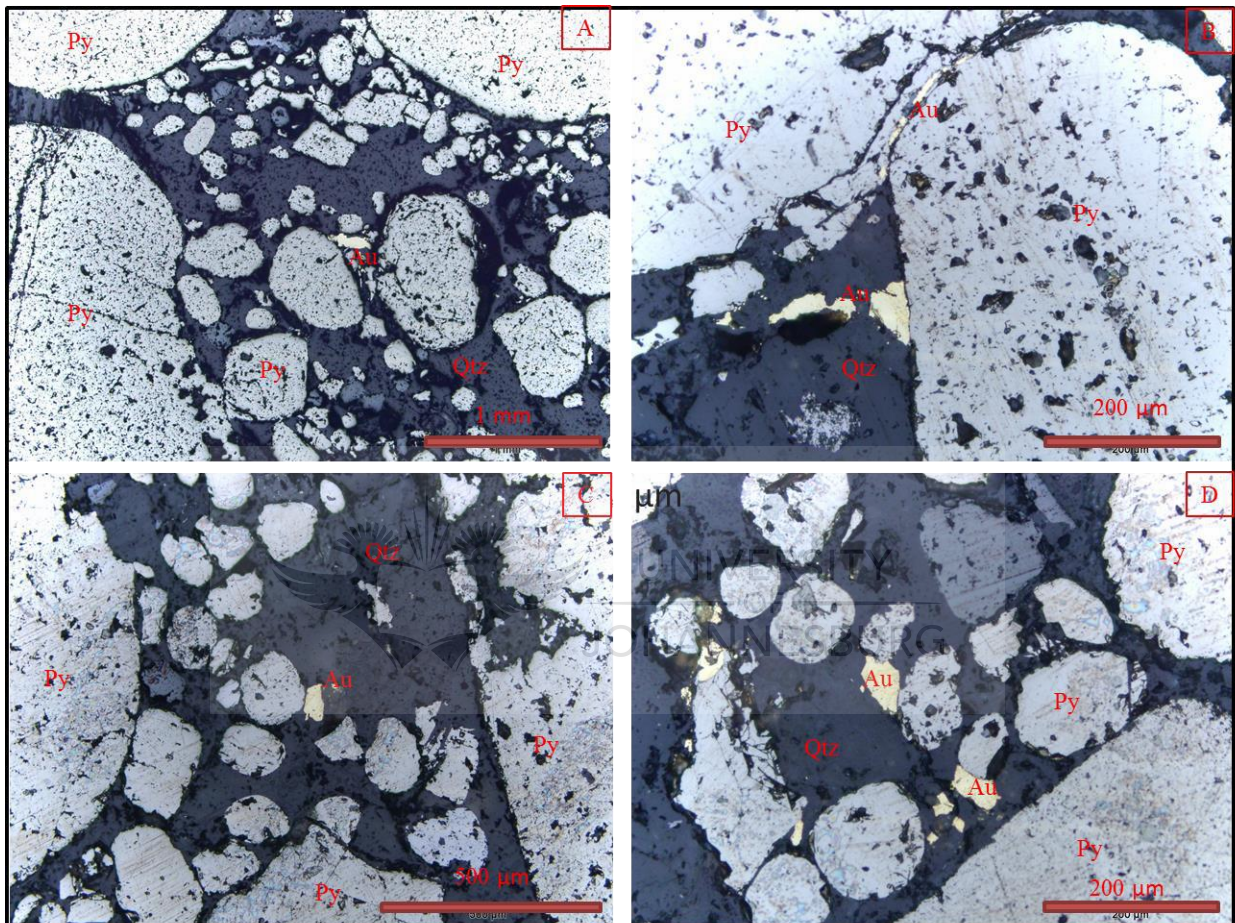
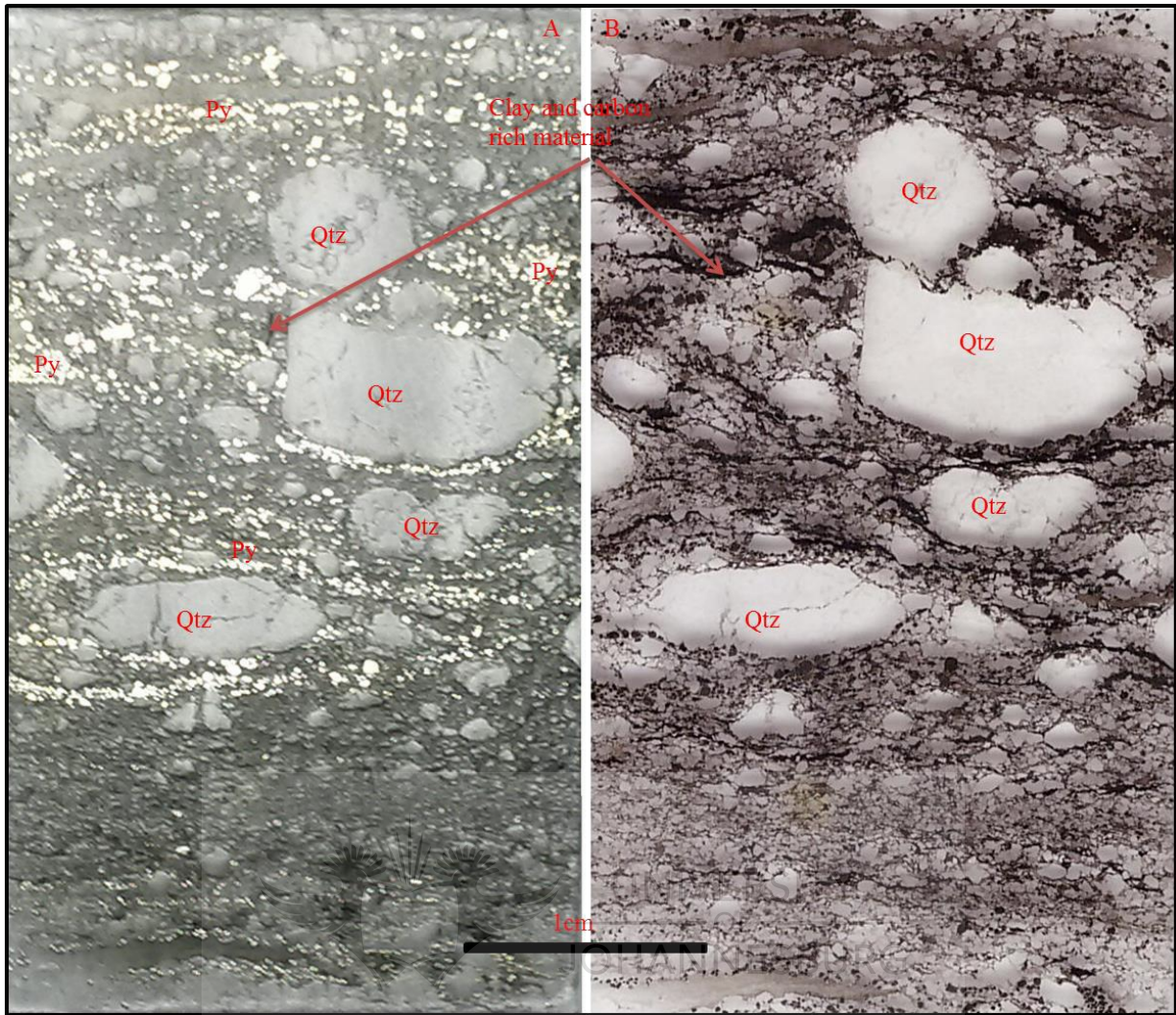


Figure 6.9 A-D: Reflected light images indicating the gold particles found within the buckshot pyrite layer.(BSPL PR 5 cut from S1).

Below the buckshot layer we can see that in general there is more dark clay and carbon rich material appearing in thin section. There are still pyrite grains present within this layer and they are again well rounded and appear detrital in origin. These pyrite grains often occur as thin layers below the main buckshot pyrite layer and give the appearances of stringers. Rounded to sub-rounded elongated quartz clasts are still present but they are slightly smaller in size than within the other two layers discussed.



**Figure 6.10: Photograph (A)(reflected light) and scanned image (B)(Transmitted light) of the same thin section indicating the higher abundances of carbon rich and clay material below the buckshot layer as well as the pyrite and quartz still present.(BSPL PB 7 cut from S1)**

## 6.4 Discussion

Using the descriptions from the macroscopic and microscopic analysis we can see that the samples are made up of three distinct layers. The first layer is the massive quartzite layer that contains quartz pebbles at the base towards the contact between this layer and underlying buckshot pyrite layer. Fine grained pyrite occurs infrequently within this layer. Clay and carbon rich material can be found within this layer which gives it the dark colour that is observed. The next layer is the buckshot pyrite conglomerate that contains similar quartz pebbles to the overlying layer but the large majority of the material is the rounded pyrite

clasts that appear detrital. Within this layer gold particles were observed suggesting that it may be the enriched layer within the Black Reef. Small kerogen globules are also noted within this layer. Below this layer we still see quartz and pyrite present however the grain sizes are much smaller and they are less abundant whereas the clay and carbon rich material is far more abundant than within the other two layers.

Further mineralogical analysis is conducted on these samples using the MLA where more detailed work will be conducted with regards to the modal mineralogy and the occurrences of gold and uranium bearing phases. This will be present in the chapters that follow.





## Chapter 7

### Detailed Mineralogy

#### 7.1 Introduction

This chapter addresses the characteristics, mineral associations and size distribution of the gold and uranium bearing phases found across the BSPL reef, as observed in the MLA analyses on the samples. The MLA Sparse Phase Liberation function was used when analysing thin sections cut from the large slab samples taken from the stope face. The XBSE function was used when analysing the crushed mounts that were created from the bulk samples as previously described. This analysis was conducted in order to determine the modal mineralogy of the bulk samples.

#### 7.2 MLA Standard File



The results for the process used for the creation of the standard file are reflected in Table 7.1. The minerals listed are those found when analysing the thin sections using the Sparse Phase Liberation function. The mineralogy within these samples is fairly basic: 17 minerals were identified throughout the reef section. This standard file is used for all MLA analysis in this study.

#### 7.3 Modal Mineralogy

The modal mineralogy was calculated on the crushed mount samples as representatives of the reef that is processed at the Modder East operation. The modal mineralogy was also calculated from the mount samples using the XBSE setting, which analyses all the material in

the mounts. The purpose of this was to establish the composition of the bulk material with regards to the mineralogy for all three bulk samples (Table 7.2, 7.3, 7.4).

**Table 7.1: MLA Standard file (XBSE\_STD)**

<b>Mineral:</b>	<b>Formula:</b>	<b>Density:</b>	<b>Atomic number(Z):</b>
Quartz	SiO <sub>2</sub>	2.63	10.80
Pyrite	FeS <sub>2</sub>	5.01	20.65
Chromite	(Fe, Mg)Cr <sub>2</sub> O <sub>4</sub>	4.80	19.92
Uraninite	UO <sub>2</sub>	8.73	82.05
Chalcopyrite	CuFeS <sub>2</sub>	4.20	23.54
Kerogen	C <sub>215</sub> H <sub>330</sub> O <sub>12</sub> N <sub>5</sub> S	0.96	5.84
Chlorite	(Mg,Fe) <sub>3</sub> (Si,Al) <sub>4</sub> O <sub>10</sub> (OH) <sub>2</sub> ·(Mg,Fe) <sub>3</sub> (OH) <sub>6</sub>	3.10	11.92
Muscovite	KAl <sub>2</sub> (Si <sub>3</sub> Al)O <sub>10</sub> (OH;F) <sub>2</sub>	2.83	11.33
Pyrophyllite	Al <sub>2</sub> Si <sub>4</sub> O <sub>10</sub> (OH) <sub>2</sub>	2.81	10.58
Gold	Au	19.28	79.00
Galena	PbS	7.40	73.15
Sphalerite	(Zn,Fe)S	4	23.95
Monazite	(Ce, La,Nd,Th)PO <sub>4</sub>	5.15	40.61
Cobaltite	CoAsS	6.23	27.58
Molybdenite	MoS <sub>2</sub>	5.50	31.58
Brannerite	(U, Ca, Y, Ce)(Ti, Fe)O <sub>6</sub>	4.82	39.95
Zircon	ZrSiO <sub>4</sub>	4.65	24.84
Unknown	Fine grained minerals or mineral agglomerates that cannot be resolved by the electron beam (Grouped as Other)	*	*
Invalid	Voids, free surface and clamp metal (Grouped as Other)	*	*

**Table 7.2: Modal mineralogy of the bulk sample Sc1**

<b>Mineral</b>	<b>Wt%</b>	<b>Area%</b>	<b>Particle Count</b>	<b>Grain Count</b>
Quartz	71.90	80.35	323449	331296
Pyrite	21.32	12.50	38117	43754
Chromite	0.45	0.27	1606	1876
Uraninite	0.01	> 0.01	304	489
Chalcopyrite	0.01	0.01	397	520
Kerogen	0.01	0.02	4692	5433
Chlorite	0.31	0.30	4763	7291
Muscovite	3.77	3.92	45495	61572
Pyrophyllite	1.21	1.26	14324	16015
Gold	> 0.01	> 0.01	19	21
Galena	0.01	> 0.01	71	166
Sphalerite	0.02	0.02	310	393
Monazite	> 0.01	> 0.01	33	40
Cobaltite	0.02	0.01	115	133
Molybdenite	> 0.01	> 0.01	2	2
Brannerite	> 0.01	> 0.01	199	244
Zircon	0.07	0.04	885	998
Other	0.89	1.29	25326	49514
Total	100	100	399117	521566

**Table 7.3: Modal mineralogy of the bulk sample Sc2**

<b>Mineral</b>	<b>Wt%</b>	<b>Area%</b>	<b>Particle Count</b>	<b>Grain Count</b>
Quartz	65.73	76.18	309439	323189
Pyrite	28.65	17.42	49426	57912
Chromite	0.14	0.09	653	783
Uraninite	> 0.01	> 0.01	116	160
Chalcopyrite	0.01	0.01	434	572
Kerogen	0.01	0.04	7619	9020
Chlorite	0.37	0.37	5859	11795
Muscovite	3.12	3.36	42319	62710
Pyrophyllite	0.80	0.86	10663	11809
Gold	> 0.01	> 0.01	10	15
Galena	> 0.01	> 0.01	55	66
Sphalerite	0.02	0.01	306	393
Monazite	> 0.01	0.00	47	62
Cobaltite	0.01	0.01	42	51
Molybdenite	0.00	0.00	0	0
Brannerite	> 0.01	> 0.01	99	107
Zircon	0.03	0.02	575	727
Other	1.11	1.63	29590	63277
<b>Total</b>	<b>100</b>	<b>100</b>	<b>386606</b>	<b>545146</b>

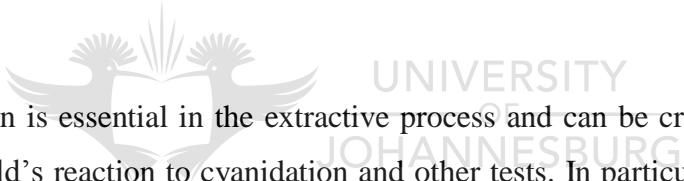
**Table 7.4: Modal mineralogy of the bulk sample Sc3**

<b>Mineral</b>	<b>Wt%</b>	<b>Area%</b>	<b>Particle Count</b>	<b>Grain Count</b>
Quartz	70.13	78.23	447717	481919
Pyrite	21.85	12.78	70034	84978
Chromite	0.27	0.16	1463	1619
Uraninite	> 0.01	> 0.01	144	162
Chalcopyrite	0.01	0.01	470	599
Kerogen	0.02	0.05	14461	16297
Chlorite	0.46	0.43	12586	18819
Muscovite	4.46	4.63	98981	163176
Pyrophyllite	0.70	0.73	16760	19217
Gold	0.01	> 0.01	18	34
Galena	> 0.01	> 0.01	30	53
Sphalerite	0.01	0.01	363	408
Monazite	> 0.01	> 0.01	55	59
Cobaltite	0.01	0.01	74	94
Molybdenite	> 0.01	> 0.01	2	2
Brannerite	> 0.01	> 0.01	138	141
Zircon	0.05	0.03	1029	1111
Other	2.03	2.93	75371	136377
<b>Total</b>	<b>100</b>	<b>100</b>	<b>562082</b>	<b>928158</b>

The largest percentage of the material found within the Black Reef bulk samples is quartz (Tables 7.2-7.4). It is also evident that between 21% and 29% of the material in the samples consists of pyrite. Muscovite, chlorite and pyrophyllite make up a smaller percentage of the material (Tables 7.2-7.4). These minerals are often grouped into clay minerals, and the carbon rich material is likely to contain the kerogen as seen in the modal analysis. The carbon rich areas should contain the clay minerals as well as the kerogen, as previously mentioned. The other minerals identified within the modal mineralogy are found in very small amounts within the Black Reef.

The minerals of interest in this study are the gold and the uranium bearing phases, namely brannerite and uraninite. These minerals are also found in much smaller concentrations within the bulk samples. However, further mineralogical work will be conducted on these minerals as they are of economic importance.

#### **7.4 Gold Mineralogy**



Gold characterisation is essential in the extractive process and can be crucial in determining the nature of the gold's reaction to cyanidation and other tests. In particular, the size and the upgrading and downgrading of the gold are important in the extraction of this precious metal (Petruk, 2000). Gold is found in many different forms in nature: it can occur as native gold, tellurides, electrum and alloys (Kongolo and Mwema, 1998). In this study the gold in question indicated no evidence that the gold was anything other than native gold however in figure 7.1 we see some small concentrations of Ag but not high enough to classify it as electrum. Gold was analysed using the thin sections cut from the large sample S1 using the MLA Sparse Phase Liberation function. The peaks used to identify the gold through the MLA analysis indicated that a large majority of the gold found within the Black Reef is native gold (Figure 7.1).

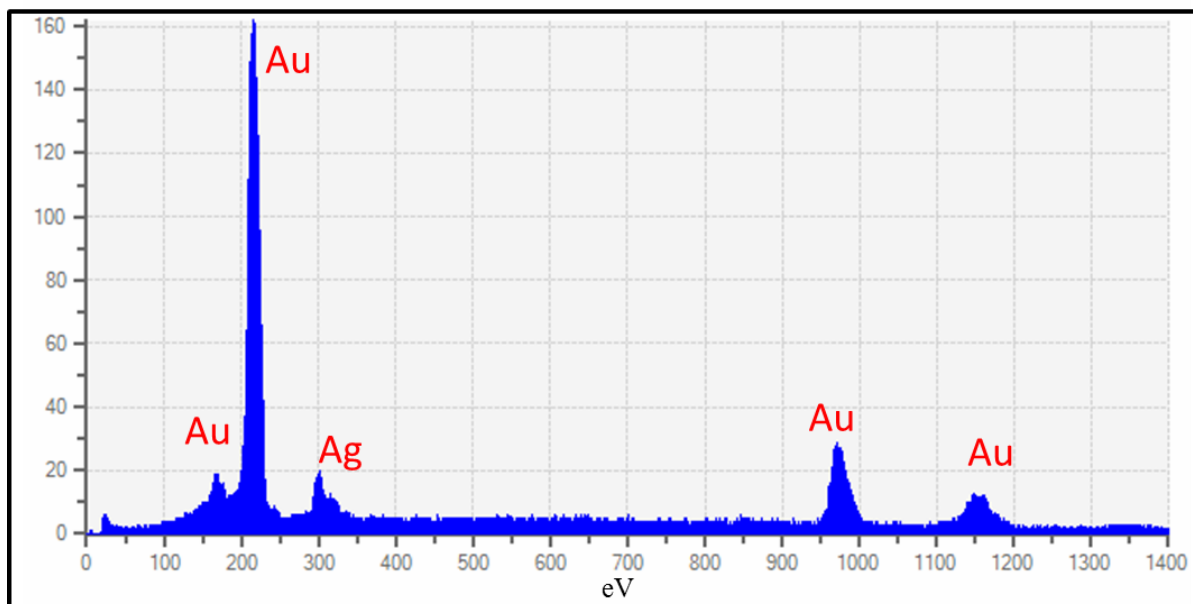


Figure 7.1: Gold EDS peaks from BSPL samples

#### 7.4.1 Gold Occurrence



The gold particles as described in the petrographic chapter were further analysed using the MLA Sparse Phase Liberation function. The samples analysed were again the thin sections cut from the large sample (S1) taken from the underground stope face. This search function yielded effective imaging of the gold particles, and showed two slightly different occurrences of the gold within the BSPL reef. The first and most common occurrence is in the form of discrete particles of gold, which are granular in appearance and show sharp contacts with other minerals. These gold grains are irregularly shaped and vary in size. The dispersion of the gold amongst other minerals provides evidence for the sedimentary remobilization and placement of the gold across the BSPL reef. Additionally, the particles do not show the distinct features observed in placer gold particles. The non-uniform shapes of the grains suggest that they were deposited in the interstitial spaces of the conglomerate matrix after they had been remobilized within the sediments (Figure 7.2, Hallbauer and Utter, 1977, Frimmel, 2014).

Secondly, the gold in the BSPL reef occurs in vein structures in pyrite grains and mineral agglomerates. This occurrence is only observed in a few particles within the BSPL reef (Figure 7.2). The gold within the BSPL reef is mostly coarse grained and is most likely in-situ remobilized native gold (Figure 7.2, 7.3). Given that gold occurs rarely within vein structures, it may have been remobilized during the sedimentation and lithification processes that took place within these rocks (Frimmel, 2014).

#### **7.4.2 Gold Grain size Distribution**

Gold was found to be fairly coarse grained within the Black Reef. The grain size for the gold was analysed in three areas across the Black Reef: above, below and within the buckshot reef (Figure 7.5). Figure 7.4 indicates a size distribution between 2 $\mu$ m and 250 $\mu$ m. This size distribution is an average of all the gold particles found across the Black Reef. The majority of the gold grains are between 10 $\mu$ m and 100 $\mu$ m in size, as indicated by the steep gradient in the curve (Figure 7.4). A comparison of the grains shows that those below and above the reef are finer grained than those within the buckshot reef (Figure 7.5, Appendix 3 Tables A3 a).

Please note: the BSE images contain a sample ID in the bottom left corner this can be looked up in Appendix 1. This ID will refer you to the images Figure A1 b-f for the location of the thin section analysed.

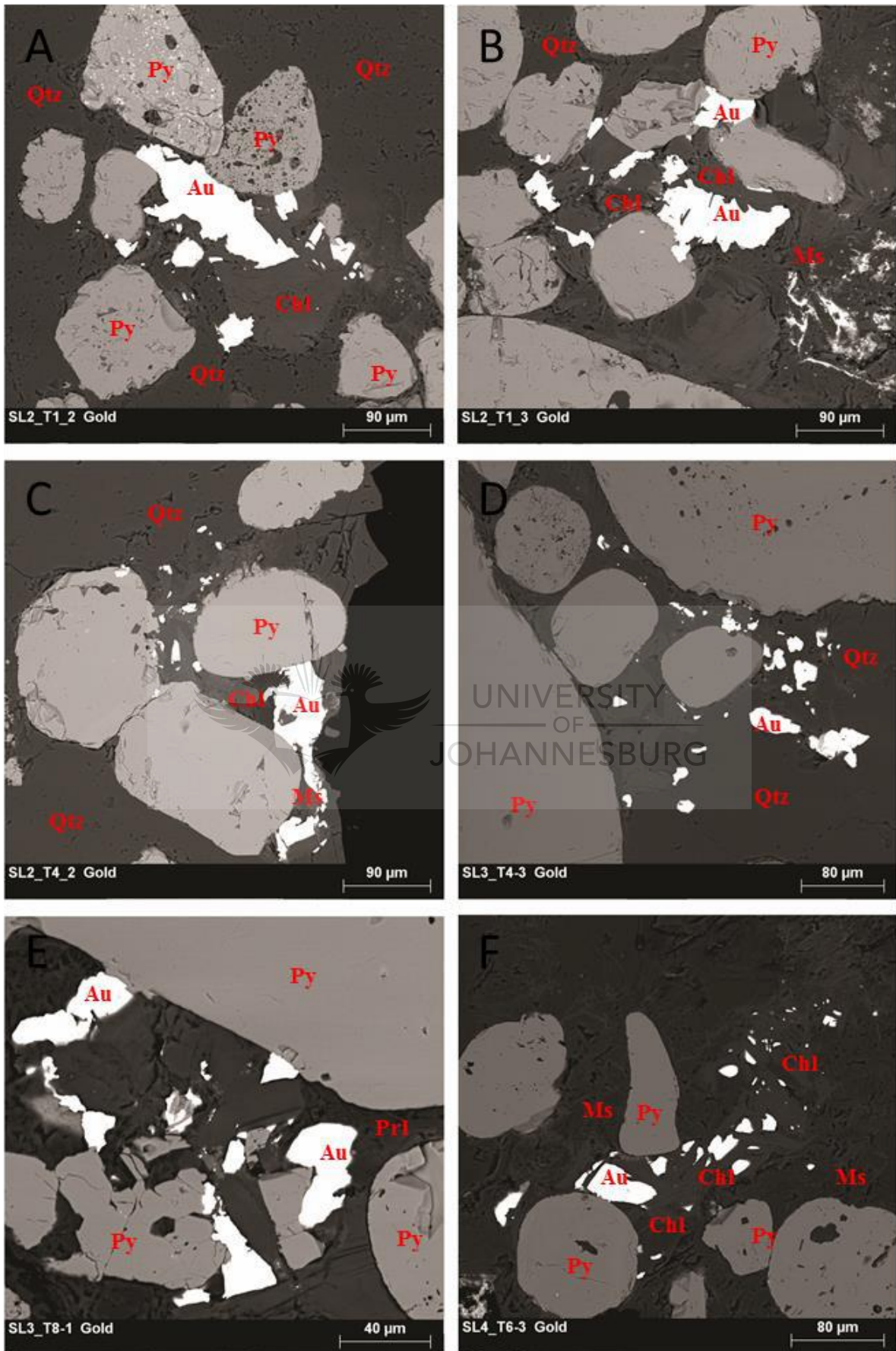


Figure 7.2 A-F: BSE images indicating the discrete gold particles found across the BSPL Reef.

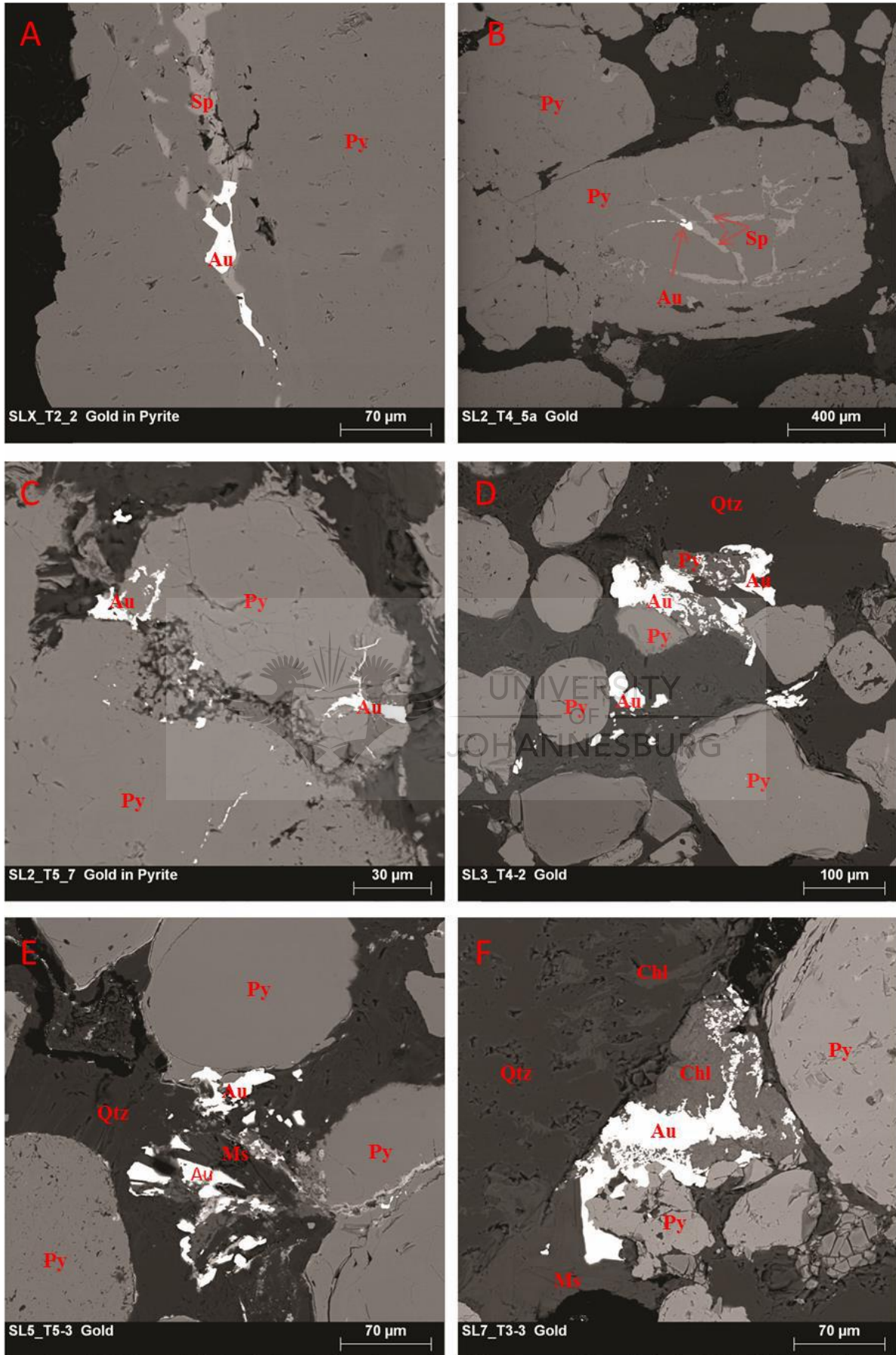
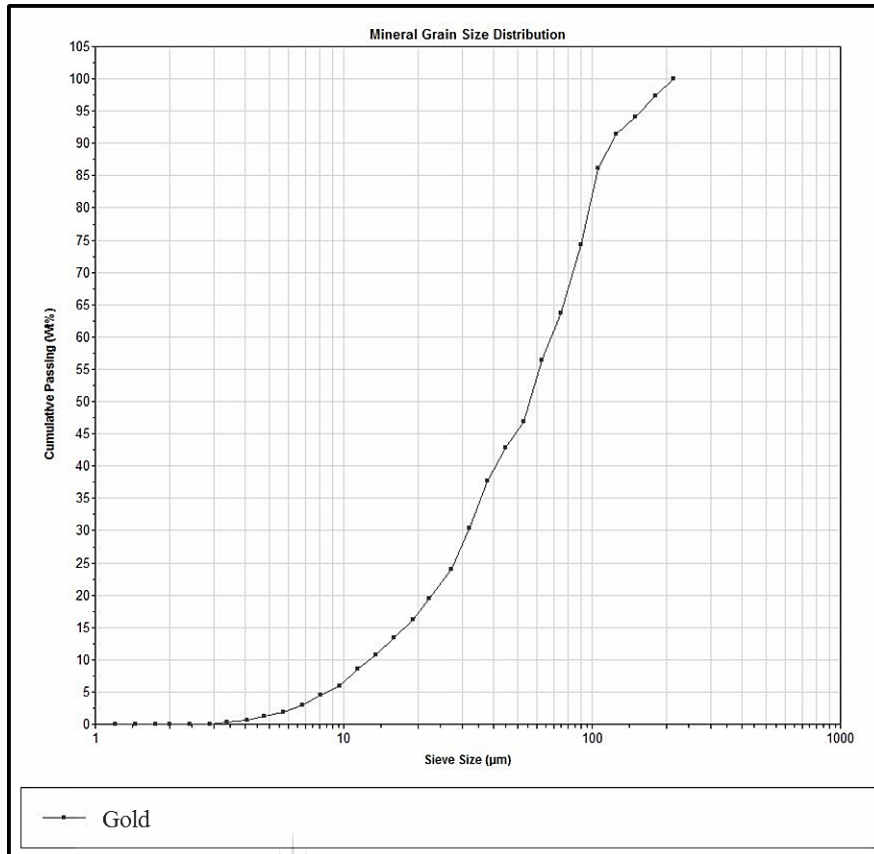
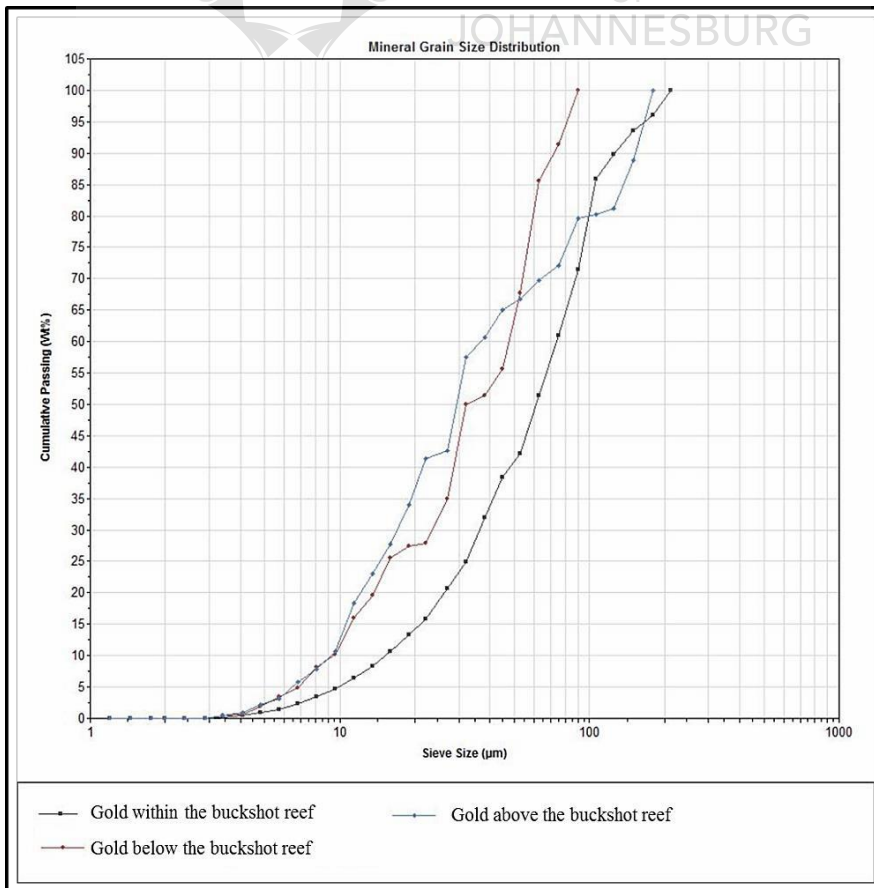


Figure 7.3 A-F: BSE images A-C. They show gold occurring within veins usually within pyrite minerals. D-F indicate mineral agglomerations occurring, providing evidence for remobilization of the gold.





**Figure 7.4: Gold grain size distribution for combined gold grains found above, below and within the buckshot reef**



**Figure 7.5: Gold size distribution indicating the variation of the gold grain sizes above, below and within the buckshot reef.**

### 7.4.3 Gold Associations

The data for these associations was obtained using the dataview software that is used when analysing data from the MLA.

Gold particles were predominantly found within the BSPL reef, and only minor amounts were found above and below the main buckshot pyrite layer (Figures 6.1, 6.2). The gold above the reef shows a strong association to chlorite and quartz, where the latter exists as the main mineral association (Figure 7.6). Pyrite, muscovite and pyrophyllite also show an association with the gold (Figure 7.6). As the gold is largely particulate/in-situ remobilized gold, it will be associated with quartz given that quartz makes up most of the material throughout the reef (as seen in the modal abundance).

Material below the BSPL reef is composed mainly of quartz and clay minerals, with some pyrite stringers. The gold particles below the reef are associated with clay minerals such as muscovite, chlorite and pyrophyllite. In addition, the association with quartz and pyrite indicates a lesser association with the gold found below the reef (Figure 7.6). Within the reef, there is an abundance of quartz, pyrite and clay minerals, as well as some carbon rich material and kerogen globules. The gold within the reef, like that above the reef, is mainly associated with quartz. While pyrite and chlorite clearly show an association to the Au within the reef, this is to a slightly lesser extent. A minor association is evident with the muscovite and pyrophyllite in the buckshot pyrite reef.

It is evident that the gold across the section of the reef gold is associated with five primary minerals: quartz; pyrite; chlorite; muscovite and pyrophyllite (Figure 7.6). This is to be expected as these minerals dominate most of the sample according to data from the modal mineralogy of the bulk samples (Tables 7.2-7.4, Appendix A3 Table Ad-f). Finally, a lesser association of Au with kerogen (the material that makes up the carbon globules) is evident.

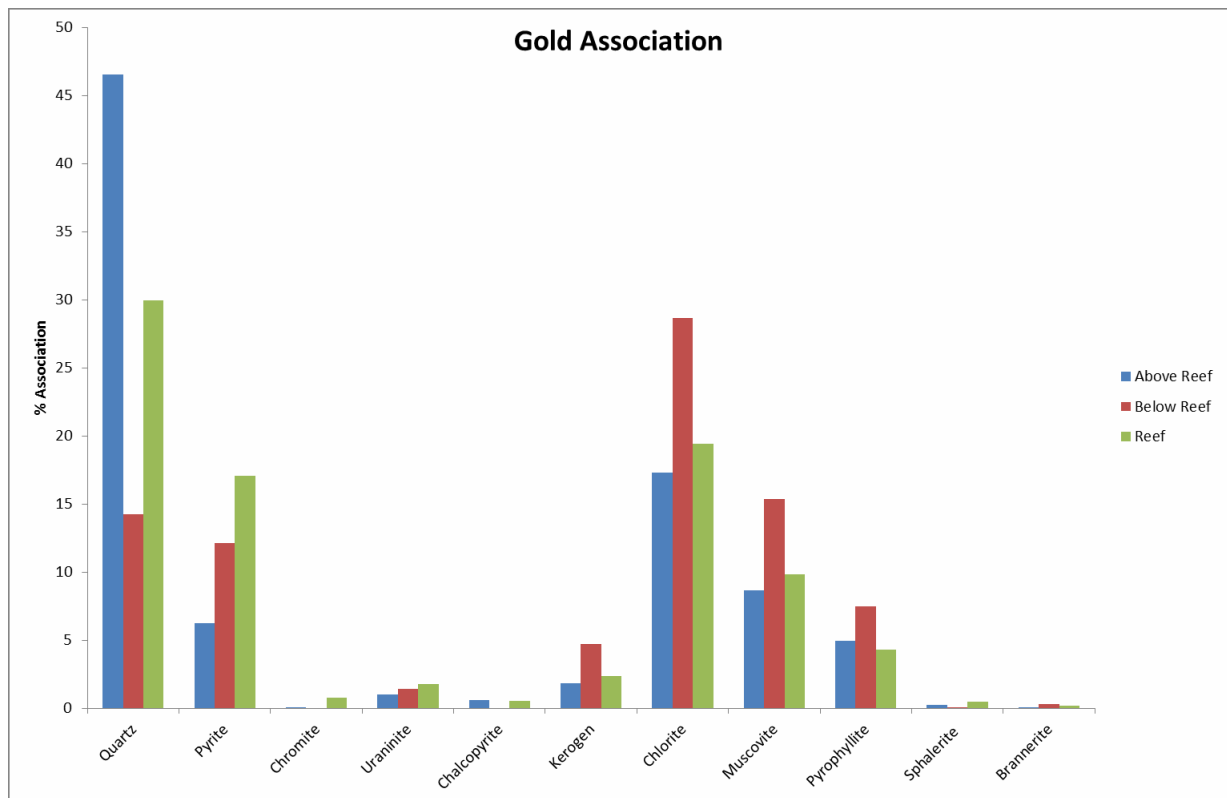
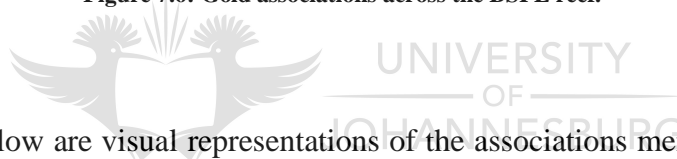


**Figure 7.6: Gold associations across the BSPL reef.**



The images that follow are visual representations of the associations mentioned above. These are BSE images obtained from the MLA, as well as mineral maps of the images that indicate the relation and associations of the gold to the surrounding minerals. The images were taken from thin sections that were cut from the large sample (S1) taken from the stope face. As such, all the images are theoretically in-situ images of the gold.

Figure 7.7 indicates that the most common occurrence of gold is in its association with quartz. This gold grain occurs in a thin section that was cut from the top contact between BSPL reef and the overlying quartzite layer (SL1\_T4: Appendix Figure A1 b). Figure 7.8 indicates gold in association with sphalerite that occurs within a pyrite grain, which most commonly occurs within the buckshot reef. This type of occurrence within vein structures is fairly uncommon within the buck shot pyrite reef, as compared to the previous occurrence. For the sake of clarity, the slide location is included in the figure.

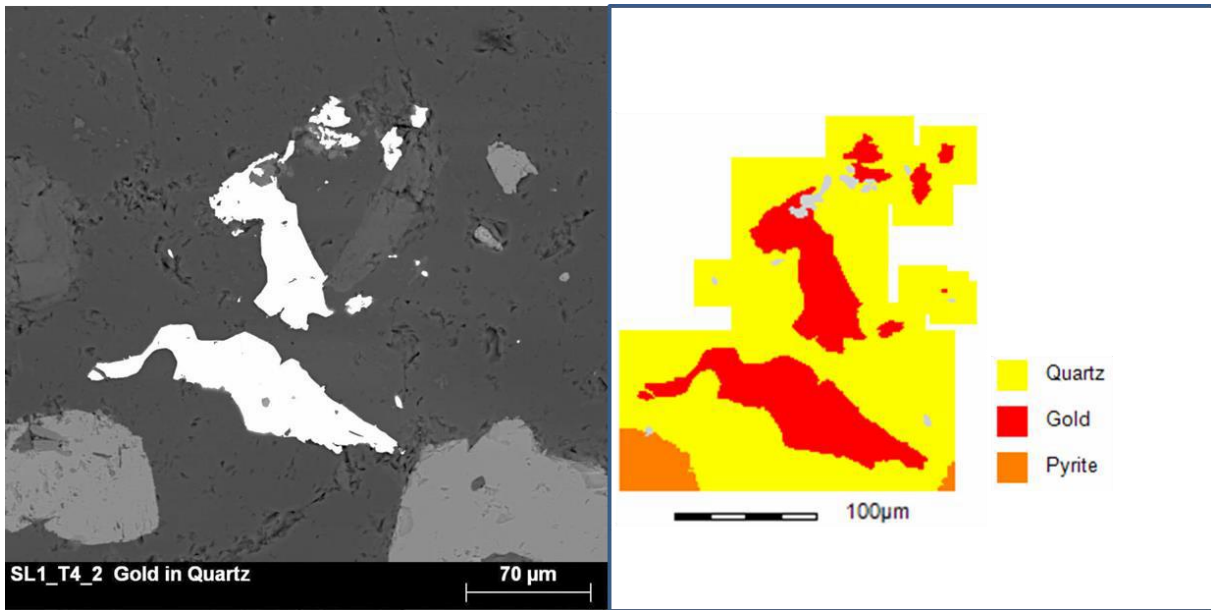


Figure 7.7: BSE image (R), mineral map (L) indicating the associations of the gold with quartz.

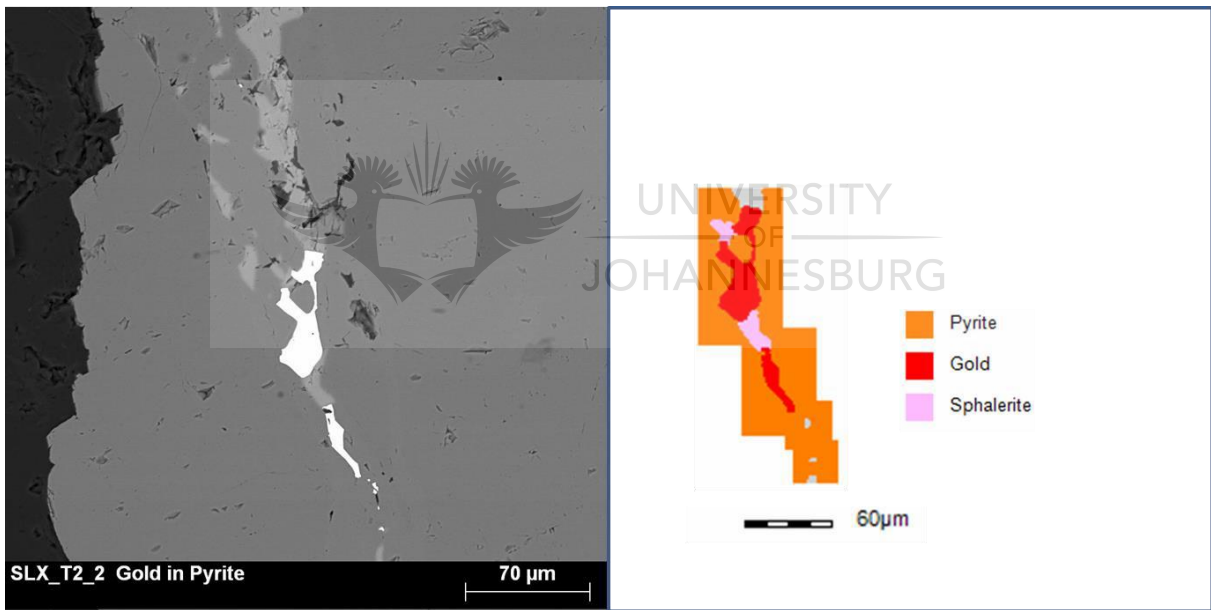


Figure 7.8: BSE image (R), mineral map (L) indicating the associations of the gold with pyrite and sphalerite.

Gold occurs most often between or on the boundary of pyrite grains (Figures 7.9, 7.10) and rarely within, or surrounded by, a pyrite grain. Figure 7.9 indicates other associations between uraninite, muscovite, pyrophyllite and gold and Figure 7.10 indicates the association between gold, chalcopyrite and chlorite specifically. Here, as expected, the gold is evident on a grain boundary of pyrite (Figure 7.10).

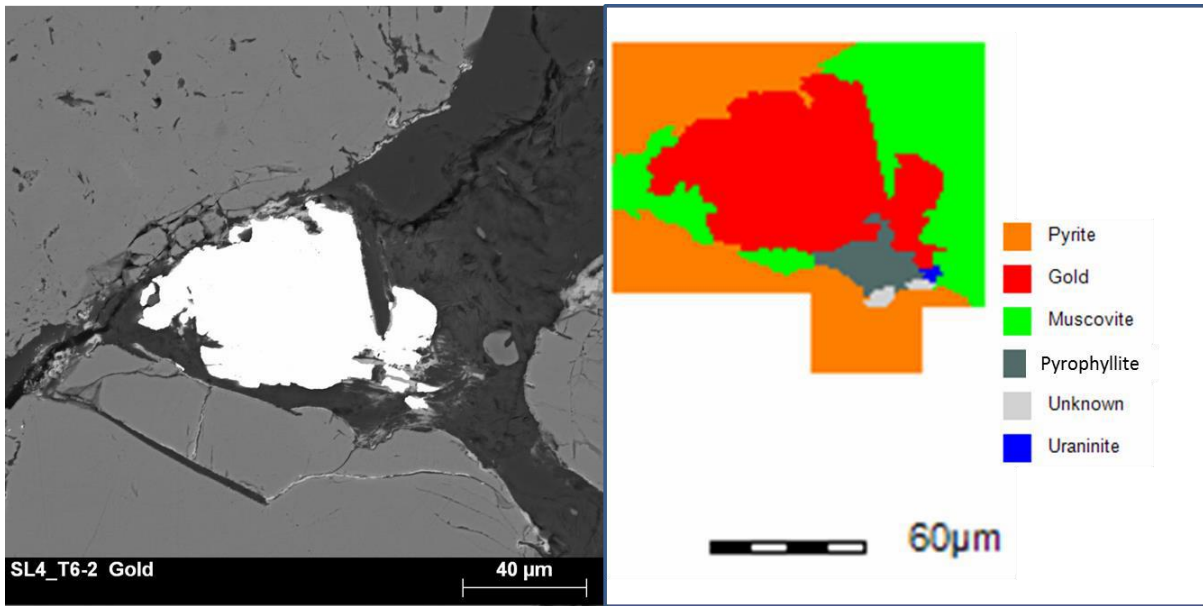


Figure 7.9: BSE image (R), mineral map (L) indicating the associations of the gold with the edges of pyrite grains, as well as muscovite, pyrophyllite and uraninite

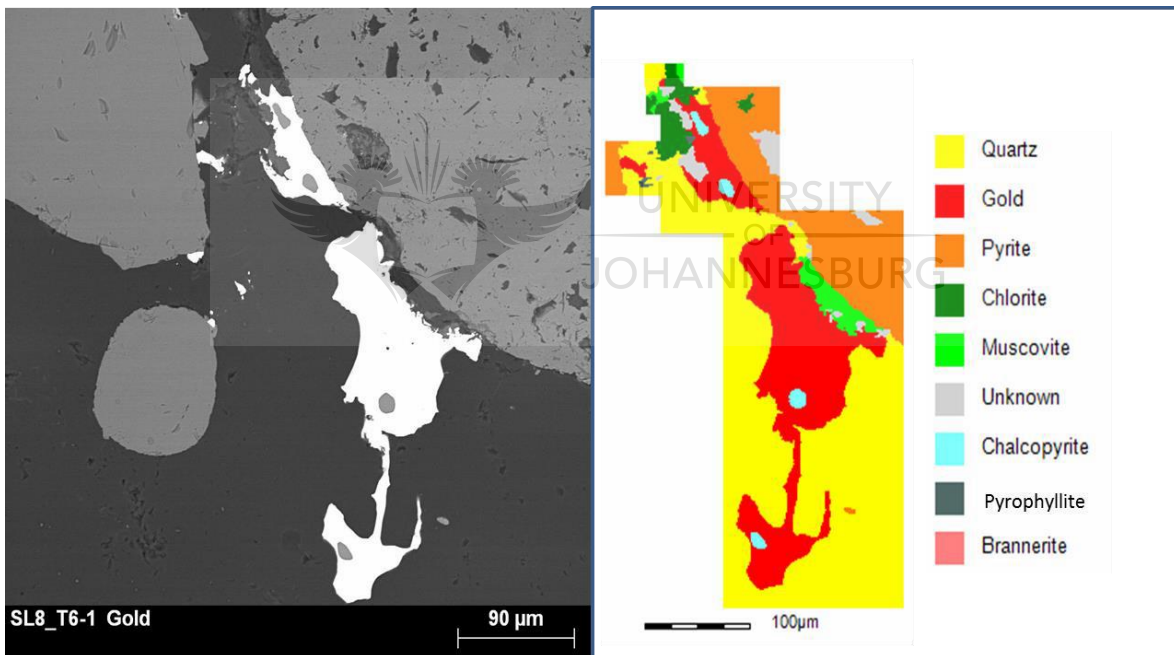


Figure 7.10: BSE image (R), mineral map (L) indicating the associations of the gold with edges of the pyrite grains as well as quartz, muscovite, chalcopyrite and chlorite.

Muscovite, pyrophyllite and chlorite are also commonly associated with the gold within the BSPL reef (Figure 7.6). Figures 7.11, 7.12 and 7.13 indicate these mineral associations with gold within the buckshot pyrite reef.

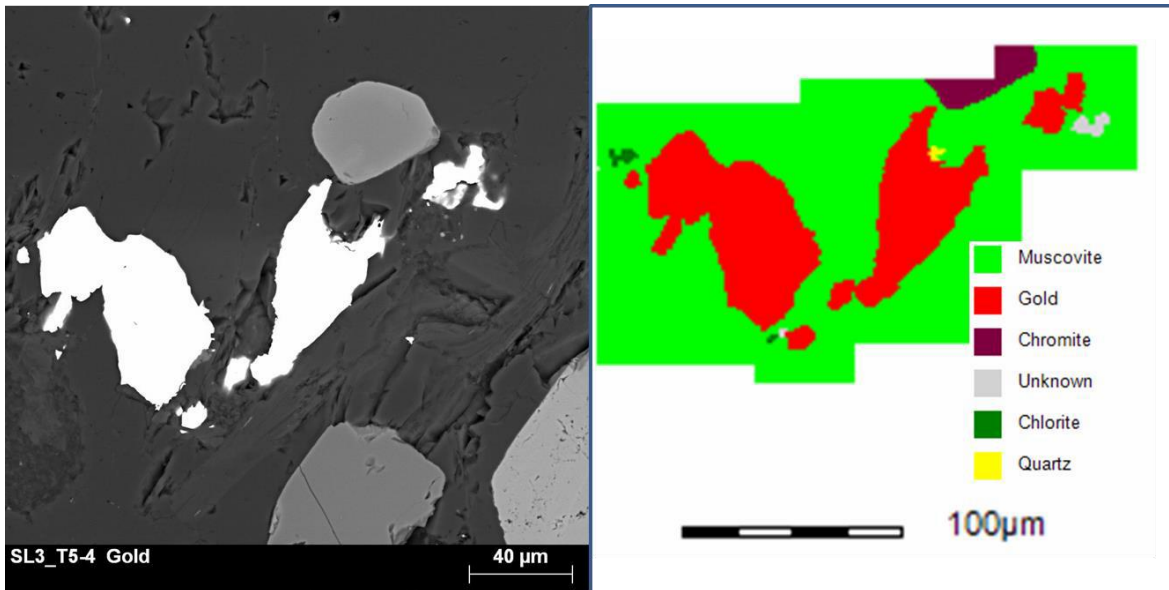


Figure 7.11: BSE image (R), mineral map (L) indicating the associations of the gold with muscovite.

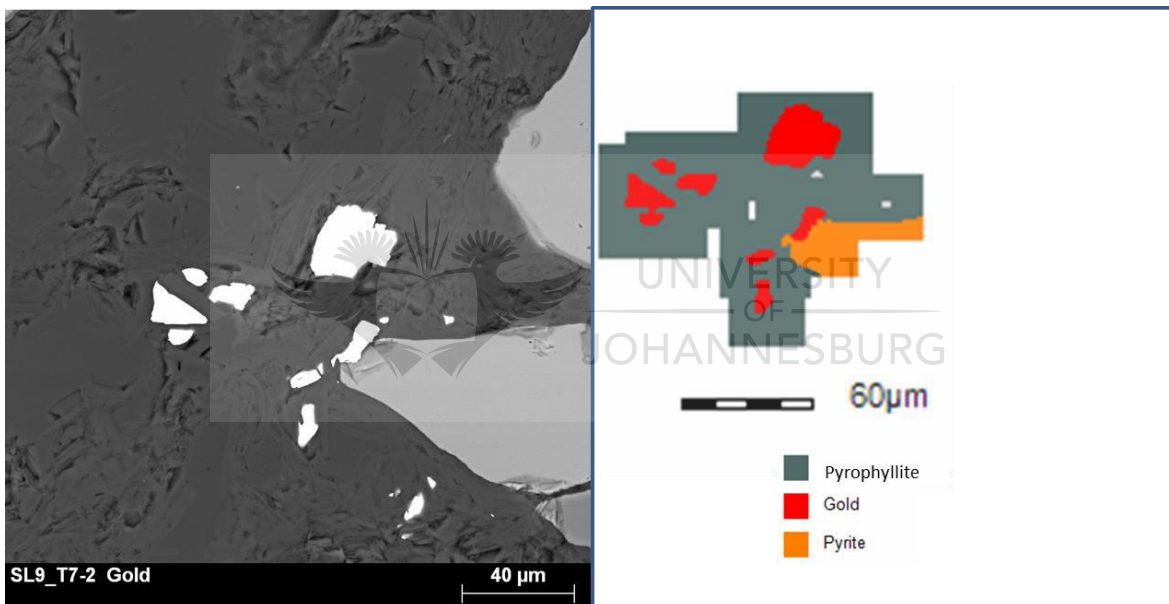


Figure 7.12: BSE image (R), mineral map (L) indicating the associations of the gold with pyrophyllite.

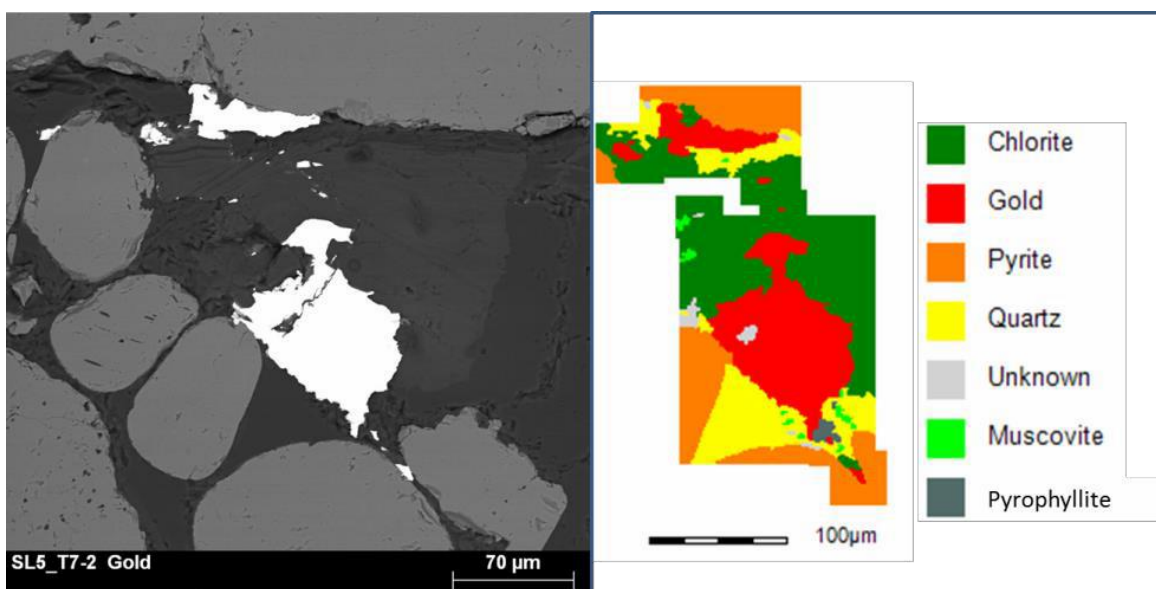


Figure 7.13: BSE image (R), mineral map (L) indicating the associations of the gold with chlorite

Figure 7.14 shows the more complex association of the gold grains found within the BSPL reef. In one instance, the gold grain is associated with muscovite, quartz, chlorite, pyrite and chromite. Figure 7.15 shows the most complex gold association in which gold and uranium appear together, within what appears to be one mineral agglomeration. Gold is also associated with a zircon grain. Again, the BSE image indicates larger gold grains appearing on the boundary of the pyrite grains.

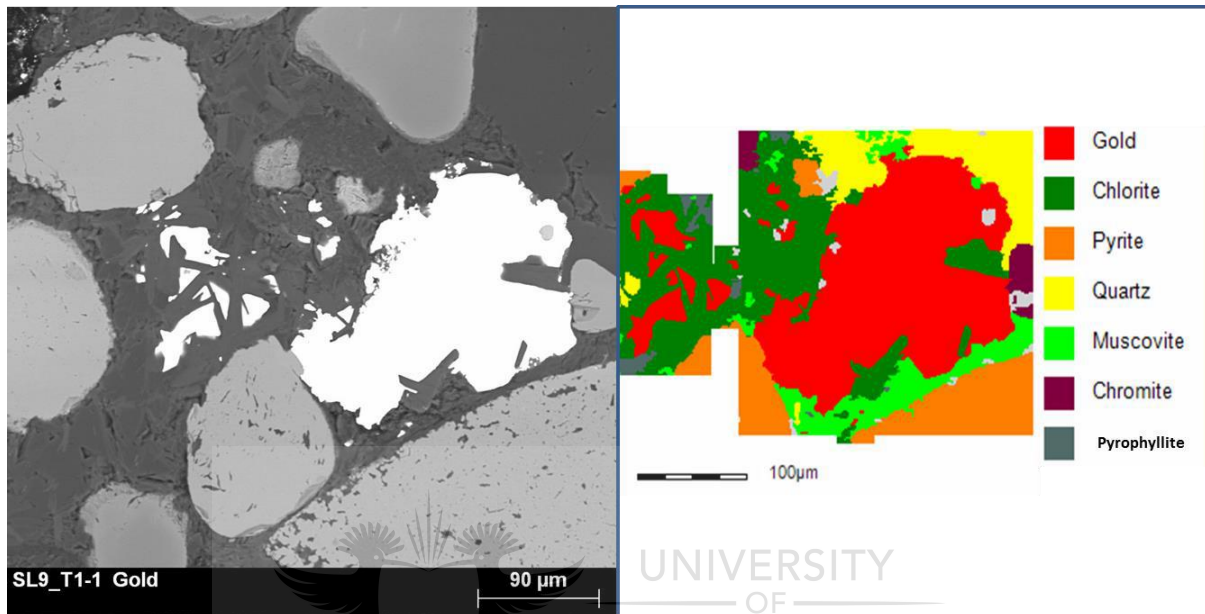


Figure 7.14: BSE image (R), mineral map (L) indicating the more complex associations of the gold within the BSPL Reef.

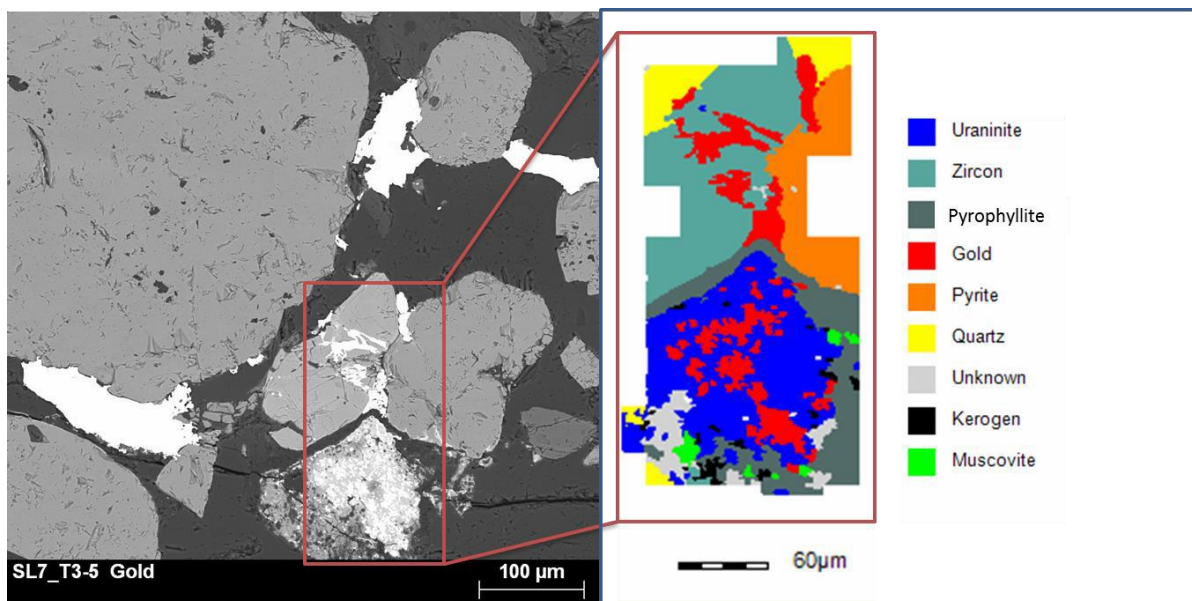


Figure 7.15: BSE image (R), mineral map (L) indicating the more complex associations of the gold within the BSPL Reef.

A further, and lesser, association with gold and kerogen is also evident. In this case, the gold appears within the kerogen, as well as on the boundary of the kerogen globules (Figure 7.16). This association is seen exclusively within the buckshot pyrite reef and not above or below the buckshot layer.

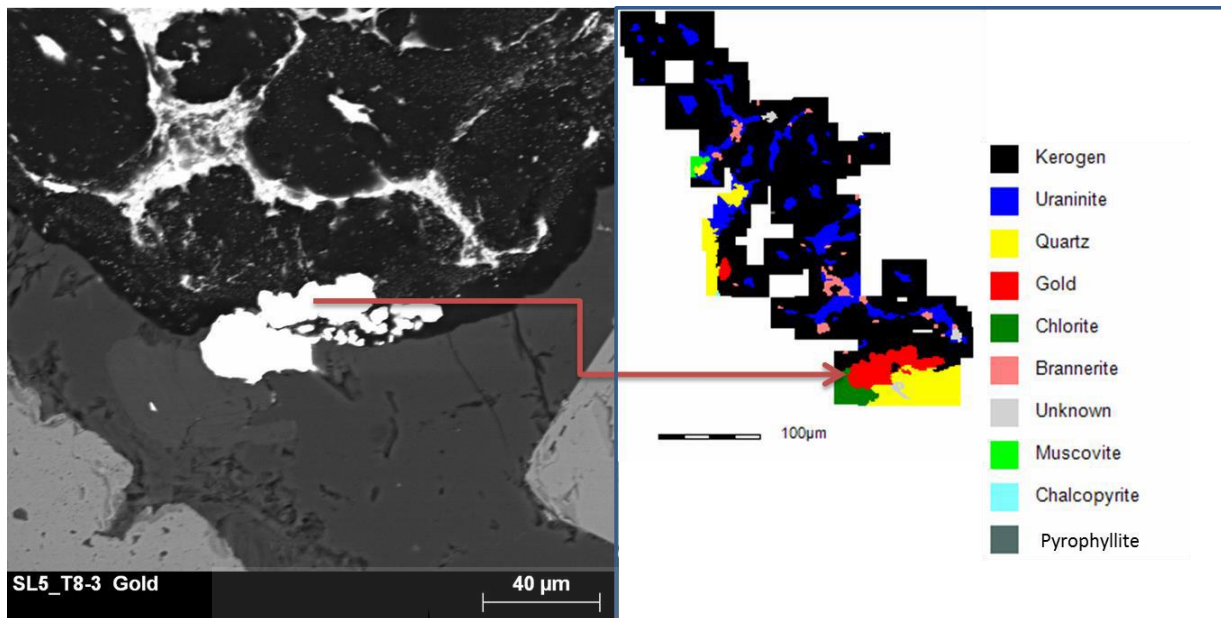


Figure 7.16: BSE image (R), mineral map (L) indicating the association between the kerogen and gold within the BSPL Reef.

It is expected that, for the most part, the gold will be associated with quartz and pyrite as these minerals constitute a large portion of the bulk material within the samples. This is indicated by the modal mineralogy of the bulk samples, which are representatives of the reef itself. The association per modal mineralogy calculation that was conducted divides the percentage association of gold by the average modal mineralogy in wt% of the mineral (Table 7.5).

The purpose of this is to determine which minerals are more significantly associated with the gold. The calculation shows that the gold is significantly associated with uraninite as well as with the carbon material found within the BSPL. Chlorite and chalcopyrite also show a fairly significant association with regards to their modal abundances. However, the low abundance of chalcopyrite renders this association insignificant. Galena, sphalerite and brannerite also show some significance with regards to association to the Au. However, it remains important to consider quartz and pyrite, as these have the highest overall association with the gold within the BSPL reef. Despite their low modal abundance, the clay minerals (muscovite, chlorite and pyrophyllite) are significantly associated with the gold. One of the most



significant associations of the gold is with chlorite, which has a slightly higher modal abundance than some of the other minerals (excluding pyrite and quartz). In table 7.5 the percentages do not total to 100 as the minerals that were not classified during the MLA analysis are not included in the table.

**Table 7.5: Association per modal mineralogy for the associations of gold.**

<b>Mineral</b>	<b>Modal mineralogy wt %</b>	<b>Gold association %</b>	<b>Association per modal mineralogy</b>
Quartz	69.25	30.243	0.437
Pyrite	23.94	11.810	0.493
Chromite	0.29	0.280	0.977
Uraninite	0.01	1.403	140.333
Chalcopyrite	0.01	0.373	37.333
Kerogen	0.01	2.957	221.750
Chlorite	0.38	21.787	57.333
Muscovite	3.78	11.283	2.982
Pyrophyllite	0.90	5.590	6.188
Gold	0.01	0.000	0.000
Galena	>0.01	0.063	19.000
Sphalerite	0.02	0.260	15.600
Cobaltite	0.01	0.010	0.750
Brannerite	>0.01	0.177	147.222
Zircon	0.05	0.090	1.800

## 7.5 Mineralogy of Uranium Bearing Phases

The uranium within a quartzite conglomerate deposit can occur in many different mineral forms, ranging from detrital uraninite to silicate hosted-uranium (Table 7.6; *Bowell et al., 2012*). The uranium located across the Black Reef is hosted within uraninite and brannerite (Table 7.1). These minerals were identified during the MLA analysis as they are very fine grained and thus difficult to observe during petrographic analysis (Figures 7.17, 7.18). It can be calculated from the modal mineralogy of the bulk samples that the uraninite makes up the majority of the uranium bearing phases (88%-90%) while the brannerite makes up the remaining 10% and 12%.

Table 7.6: Chemistry of important ore grade uranium minerals (Bowell et.al. 2012)

Mineral	Formula
Autunite	$\text{Ca}(\text{UO}_2)_2(\text{PO}_4)_2 \cdot 10\text{--}12\text{H}_2\text{O}$
Betafite	$(\text{Ca},\text{U})_2(\text{Nb},\text{Ti})_2\text{O}_6\text{OH}$
Boltwoodite	$\text{HK}(\text{UO}_2)\text{SiO}_4 \cdot 1.5\text{H}_2\text{O}$
Brannerite	$(\text{U},\text{Ca},\text{Y},\text{Ce},\text{La})(\text{Ti},\text{Fe})_2\text{O}_6$
Carnotite	$\text{K}_2(\text{UO}_2)_2(\text{VO}_4)_2 \cdot 1\text{--}3\text{H}_2\text{O}$
Coffinite	$\text{U}(\text{SiO}_4)_{1-x}(\text{OH})_{4x}$
Davidite	$(\text{La},\text{Ce})(\text{Y},\text{U},\text{Fe})(\text{Ti},\text{Fe})_{20}(\text{O},\text{OH})_{38}$
Fourmarierite	$\text{Pb}(\text{UO}_2)_4\text{O}_3(\text{OH})_4 \cdot 4\text{H}_2\text{O}$
Francevillite	$(\text{Ba},\text{Pb})(\text{UO}_2)_2(\text{VO}_4)_2 \cdot 5\text{H}_2\text{O}$
Margaritasite	$(\text{Cs},\text{K},\text{H}_3\text{O})_2(\text{UO}_2)_2(\text{VO}_4)_2 \cdot \text{H}_2\text{O}$
Metatyuyamunite	$\text{Ca}(\text{UO}_2)_2(\text{VO}_4)_2 \cdot 3\text{--}5\text{H}_2\text{O}$
Meta-autunite	$\text{KCa}(\text{H}_3\text{O})_3(\text{UO}_2)_7(\text{PO}_4)_4\text{O}_4 \cdot 6\text{--}8\text{H}_2\text{O}$
Orthobrannerite	$\text{U}_2\text{Ti}_4\text{O}_{12}(\text{OH})_2$
Phosphuranylite	$(\text{H}_3\text{O})_3\text{KCa}(\text{UO}_2)_7[\text{O} \text{PO}_4]_4 \cdot \text{H}_2\text{O}$
Pitchblende	Amorphous $\text{UO}_2$
Saléeite	$\text{Mg}(\text{UO}_2)_2(\text{PO}_4)_2 \cdot 10\text{H}_2\text{O}$
Schoepite	$(\text{UO}_2)_4\text{O}(\text{OH})_6 \cdot 5\text{H}_2\text{O}$
Sklodowskite	$\text{Mg}(\text{UO}_2)_2\text{Si}_2\text{O}_7 \cdot 6\text{H}_2\text{O}$
Torbernite	$\text{Cu}(\text{UO}_2)_2(\text{PO}_4)_2 \cdot 8\text{--}12\text{H}_2\text{O}$
Tyuyamunite	$\text{Ca}(\text{UO}_2)_2(\text{VO}_4)_2 \cdot 5\text{--}8\text{H}_2\text{O}$
Umohoite	$(\text{UO}_2)\text{MoO}_4 \cdot 2\text{H}_2\text{O}$
Uraninite	$\text{UO}_2$
Urano-Iron Oxides	Fe-U-oxide
Uranophane	$\text{Ca}(\text{UO}_2)_2(\text{SiO}_3)(\text{OH})_2 \cdot 5\text{H}_2\text{O}$

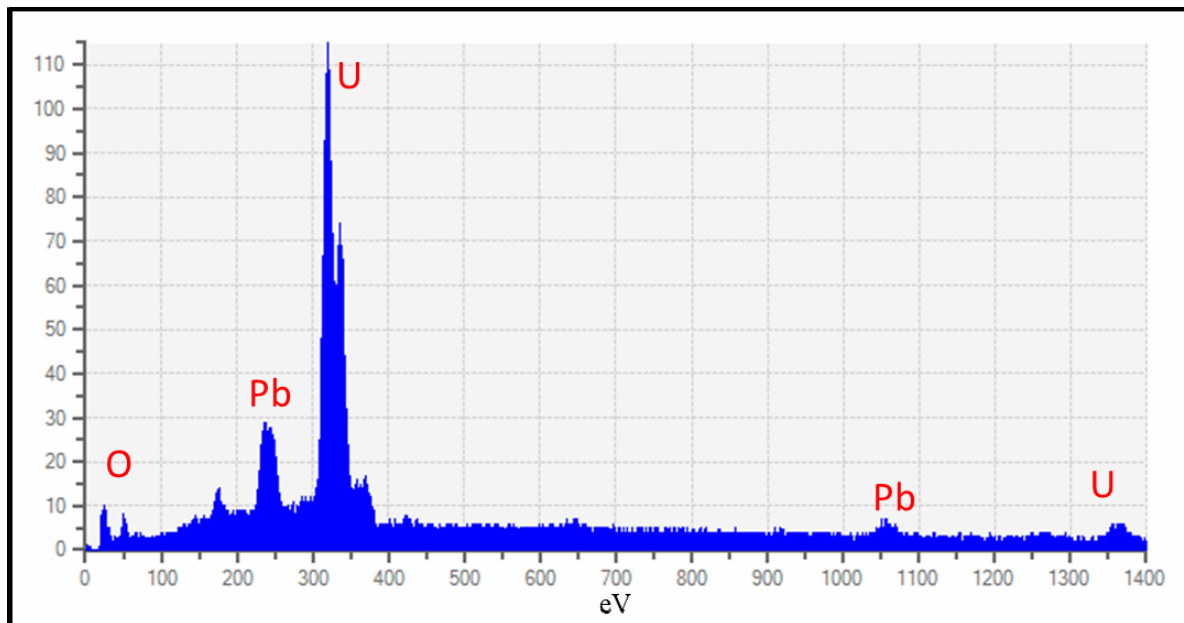


Figure 7.17: Uraninite EDS peaks from BSPL samples

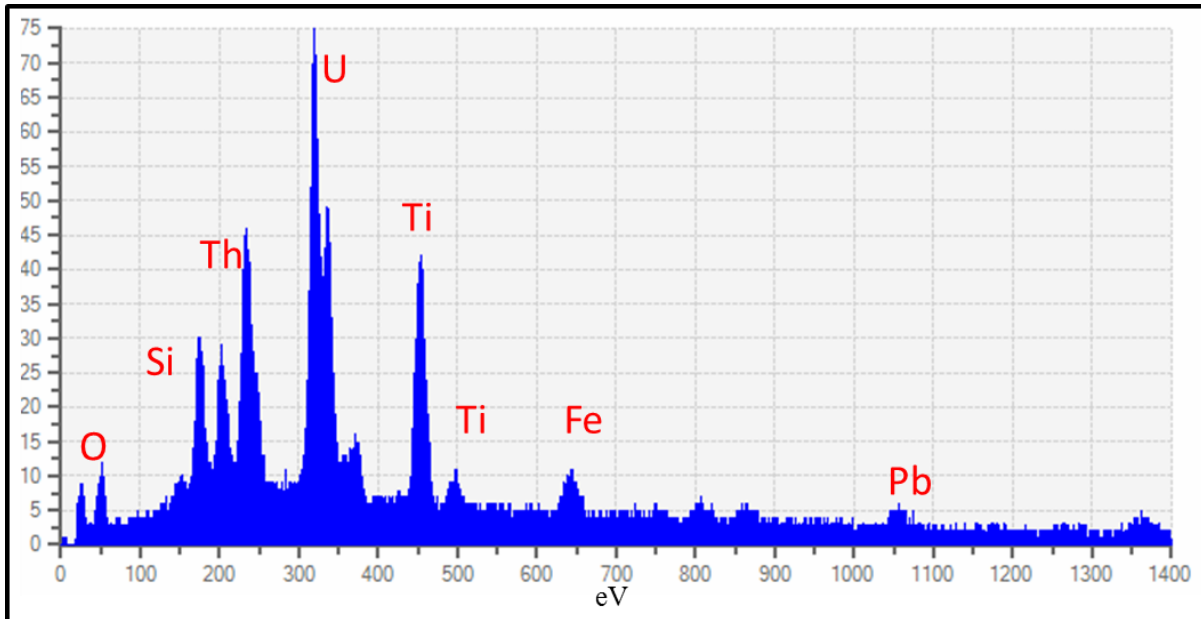


Figure 7.18: Brannerite EDS peaks from BSPL samples

### 7.5.1 Uraninite and Brannerite Occurrence

The uraninite in the BSPL reef occurs in three forms. In the first and most common instance, the uraninite occurs enclosed within a kerogen globule along with other minerals (Figure 7.19 A-F). In the second instance, the kerogen is no longer present and muscovite and chlorite are in association with the uraninite (Figure 7.20 A-D). Thirdly, the uraninite occurs along the grain boundaries of the pyrite grains (Figure 7.20 E-F). This is the least common occurrence.

The brannerite co-occurs with the uraninite and is also observed occurring within the kerogen globules within the buckshot reef (Figure 7.19 A-F). Brannerite, however, appears to not occur as commonly with other minerals such as muscovite and chlorite when not associated to kerogen globules. It was also seen to not occur on the boundary of pyrite grains.

In terms of origin, the uraninite could be detrital (as it formed traps for the kerogen/carbonaceous material that moved through the BSPL reef) or it could have precipitated from the carbonaceous material passing through the black reef. Brannerite is known to be an alteration product of the uraninite. The brannerite, like the uraninite, could have precipitated from the carbonaceous material (Parnell, 1999; Bowell et al., 2012).

## 7.5.2 Uraninite and Brannerite Grain size Distribution

The uraninite grains found in the sparse phase liberation search yielded useful data regarding the size distribution of the particles. The uraninite has a size distribution between  $>2\mu\text{m}$  and  $300\mu\text{m}$ . The majority of the Uraninite grains are between  $>2\mu\text{m}$  and  $90\mu\text{m}$ , indicated by the steep gradient in the curve. This applies to all particles found above, below and within the BSPL reef (Figure 7.21). The comparison conducted on the uraninite grains above, below and within the reef (Figure 7.22) indicated that the grains found above and within the BSPL reef are the finest and coarsest grains, respectively. The grains below the reef are smaller than those within the reef but larger than those above the reef (Figure 7.22). The same analysis conducted for brannerite indicated its size range to be from  $2\mu\text{m}$  to  $150\mu\text{m}$ , with the majority of the grains occurring between  $2\mu\text{m}$  and  $90\mu\text{m}$  in size (Figure 7.23). In a similar trend to the uraninite grains, the brannerite grains above the reef are the finest, whereas the grains below and within the reef appear to be fairly similar (Figure 7.24, Appendix 3 Tables A3 b, A3 c).



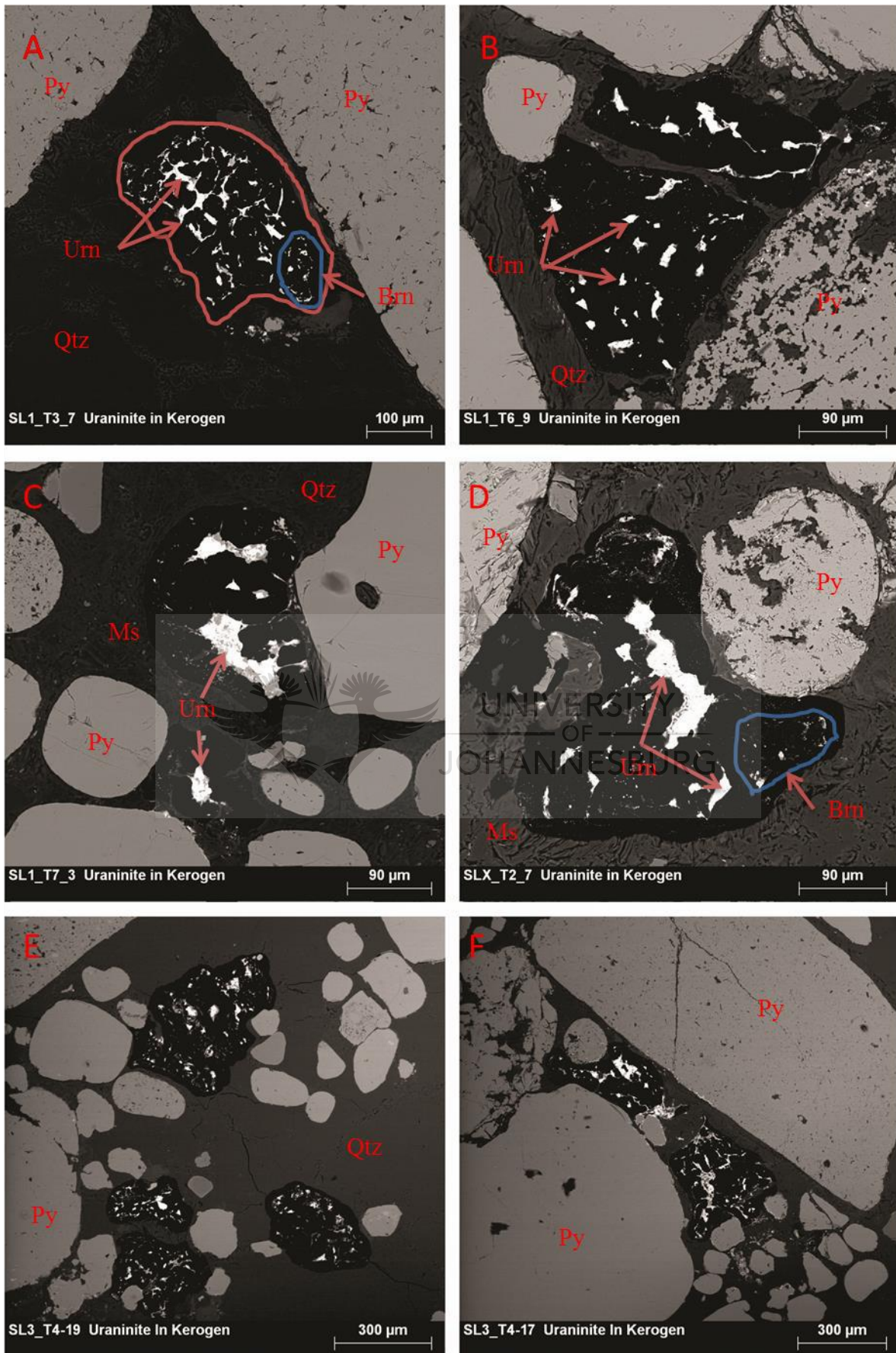


Figure 7.19: BSE images A-F, showing the first type of the uraninite (Urn) and brannerite (Brn) occurrence, where it is completely enclosed by kerogen

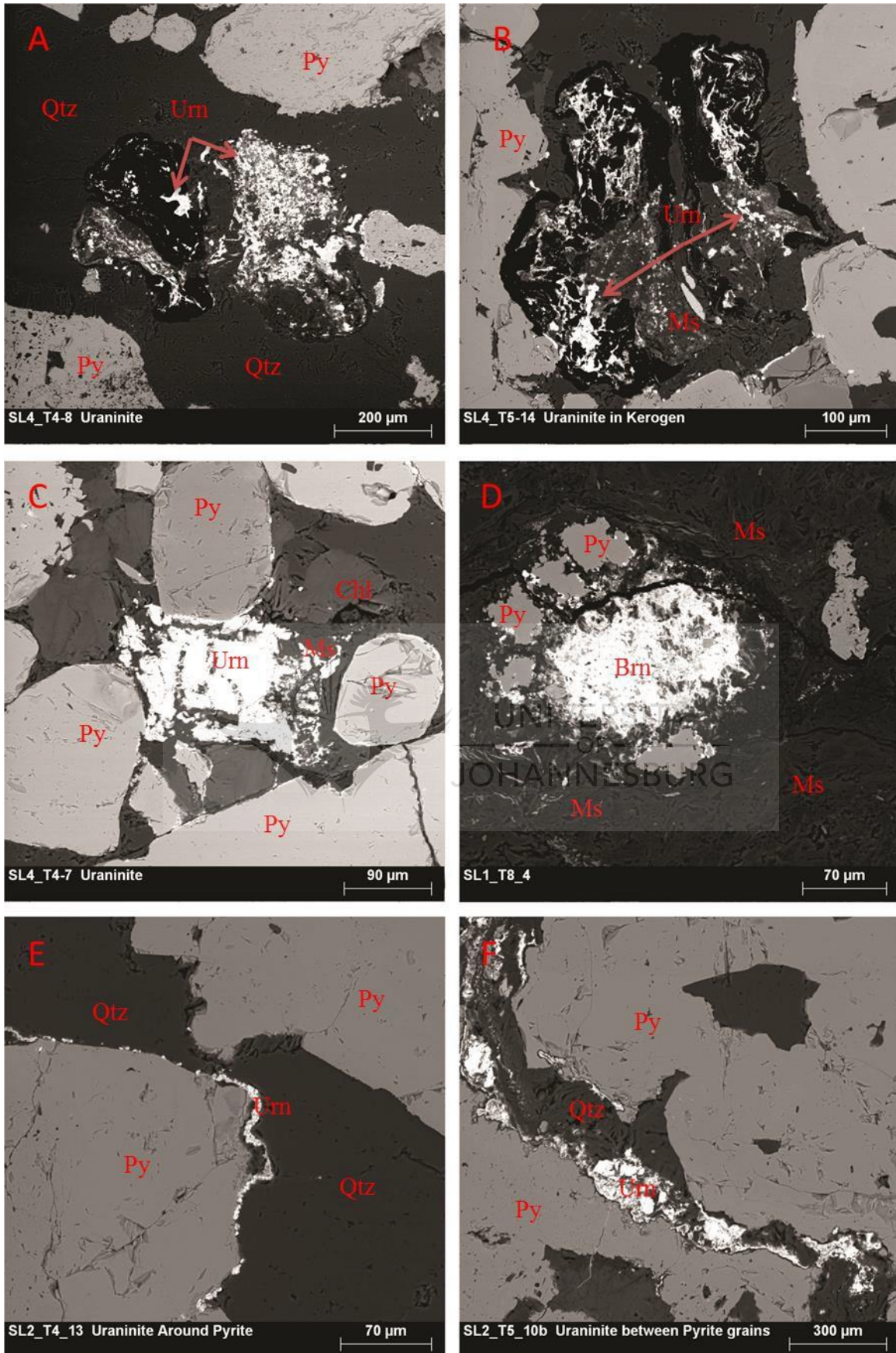
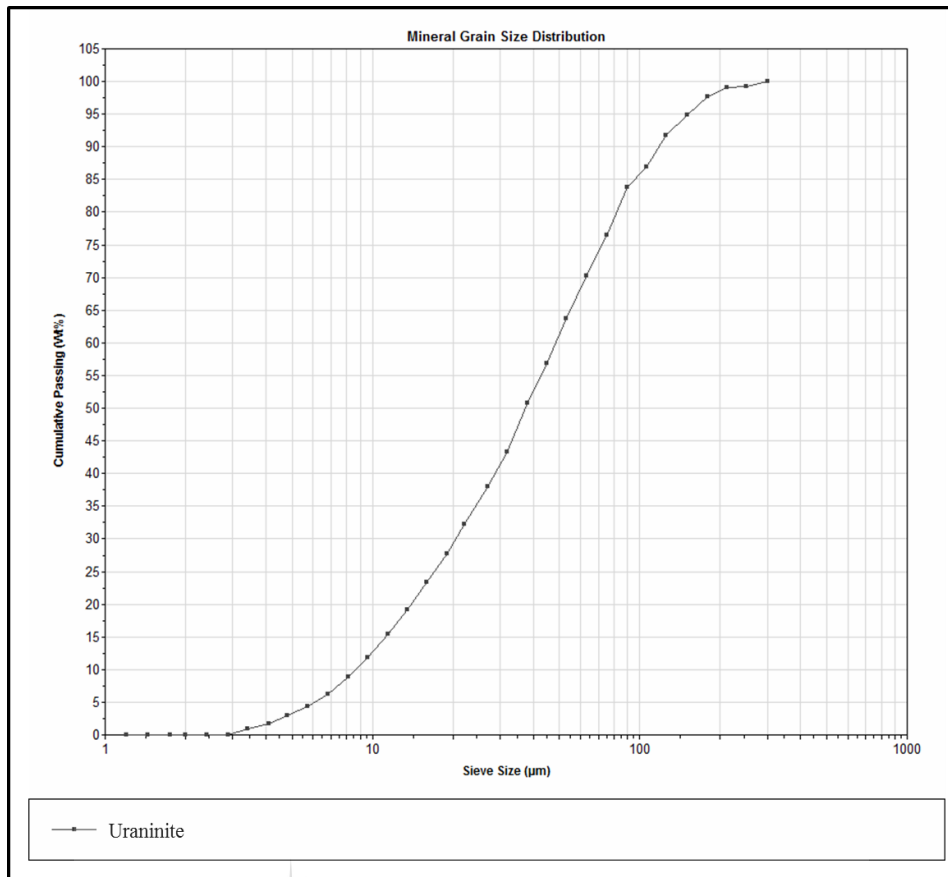
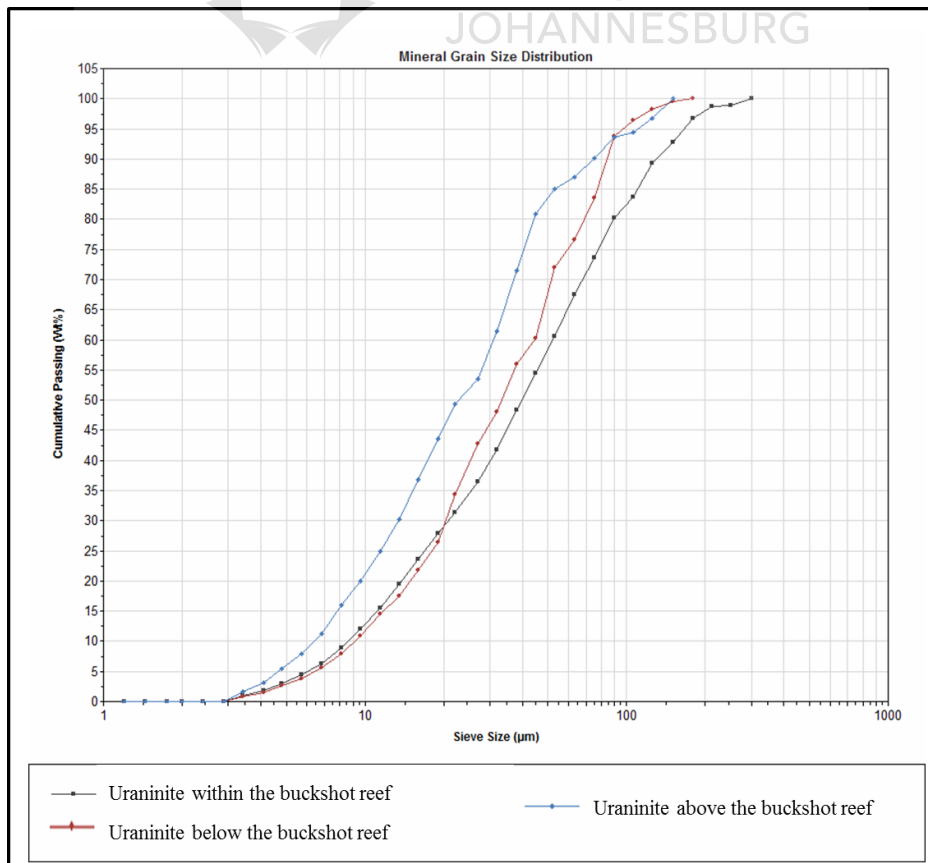


Figure 7.20: BSE Images A-D showing the second type of uraninite and brannerite occurrence, where the uraninite is found within the replacement minerals with the remnant textures of the kerogen can be seen Images E and F, indicating where the uraninite occurs along the pyrite grain boundaries.



**Figure 7.21: Uraninite grain size distribution for all uraninite found above, below and within the buckshot pyrite reef.**



**Figure 7.22: Uraninite size distribution indicating the variation of the uraninite grain sizes above, below and within the buckshot pyrite reef.**

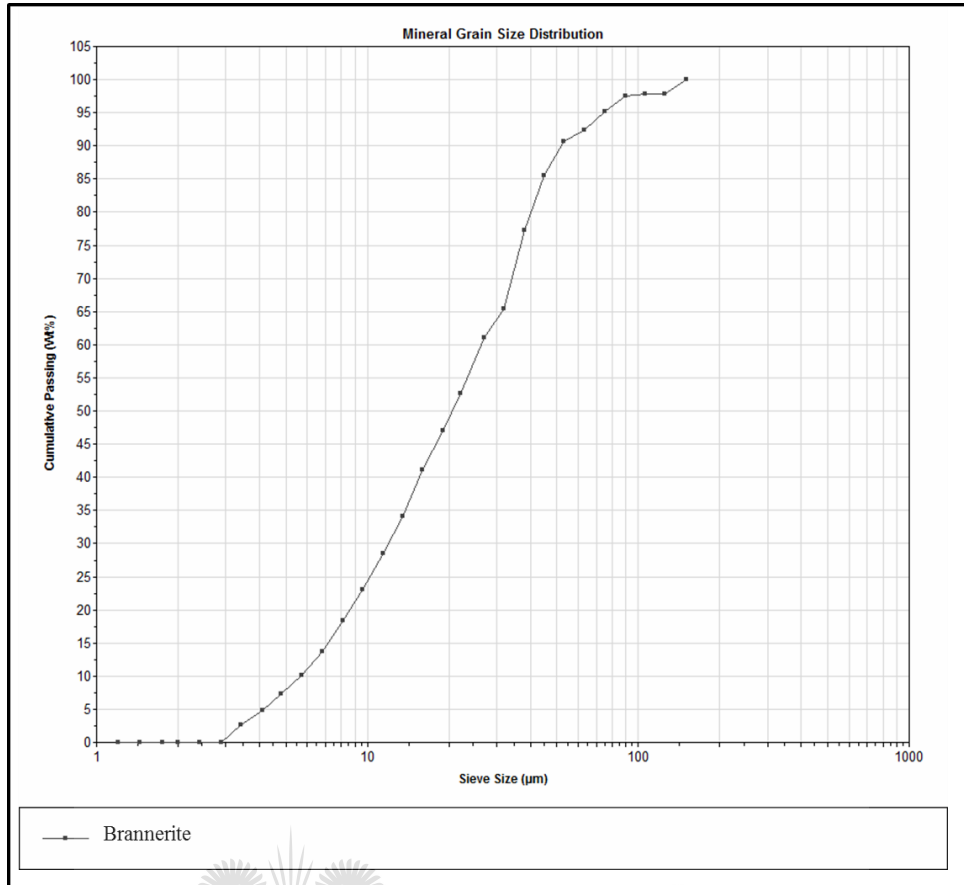


**Figure 7.23: Brannerite grain size distribution for all brannerite found above, below and within the buckshot pyrite reef.**

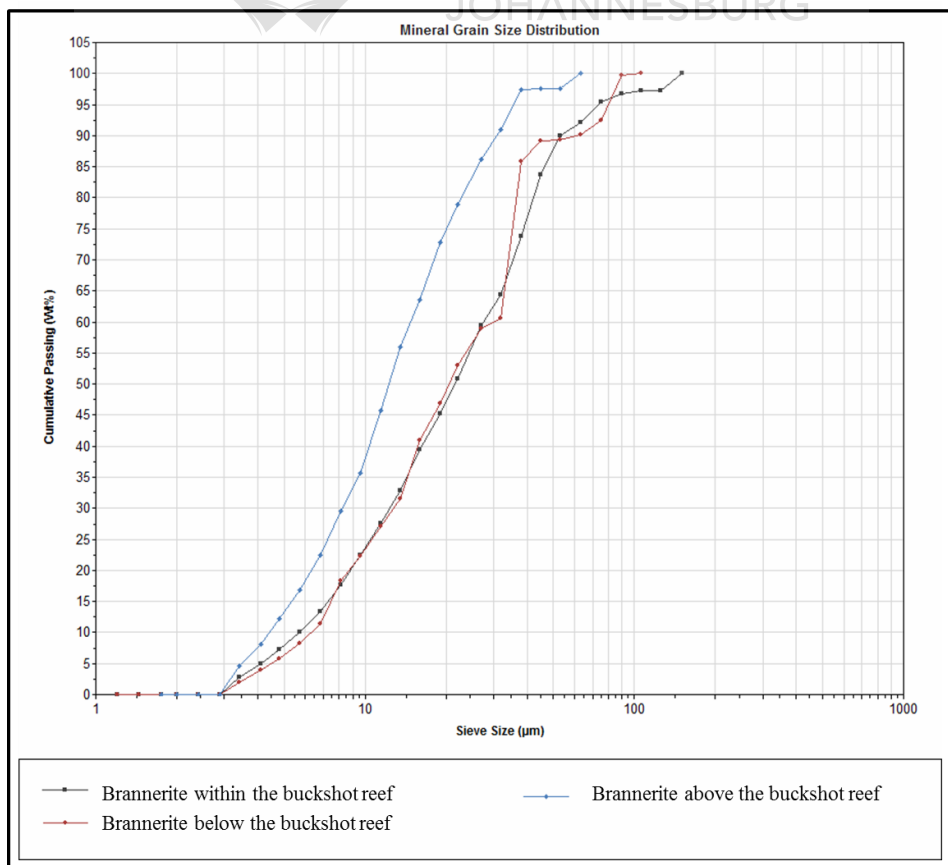


**Figure 7.24: Brannerite size distribution indicating the variation of the brannerite grain sizes above, below and within the buckshot pyrite reef.**



### 7.5.3 Uraninite and Brannerite Associations

The uraninite and brannerite across the buckshot pyrite reef is almost exclusively hosted in carbon-rich material or kerogen globules across the BSPL reef. In addition, the uraninite and brannerite particles that are found within the reef show a strong association to kerogen. The lesser association to muscovite and quartz can be explained by the high abundance of quartz and the relatively high abundance of muscovite in comparison to other minerals (Table 7.2-7.4). While an association with free surface was observed, this can be attributed to a function of the MLA analysis. The reason for this is that the grey levels of the kerogen can often be grouped as a hole/void given the low grey levels of this mineral. Brannerite is seen to be strongly associated to the uraninite and kerogen throughout the samples. The uraninite below the reef shows strong associations with both the kerogen and muscovite (Figure 7.25). This could be explained by the possible replacement of these carbon-rich areas with muscovite and other clay minerals within the samples (Figure 7.25, 7.26, Appendix A3, Table A3 d-f).

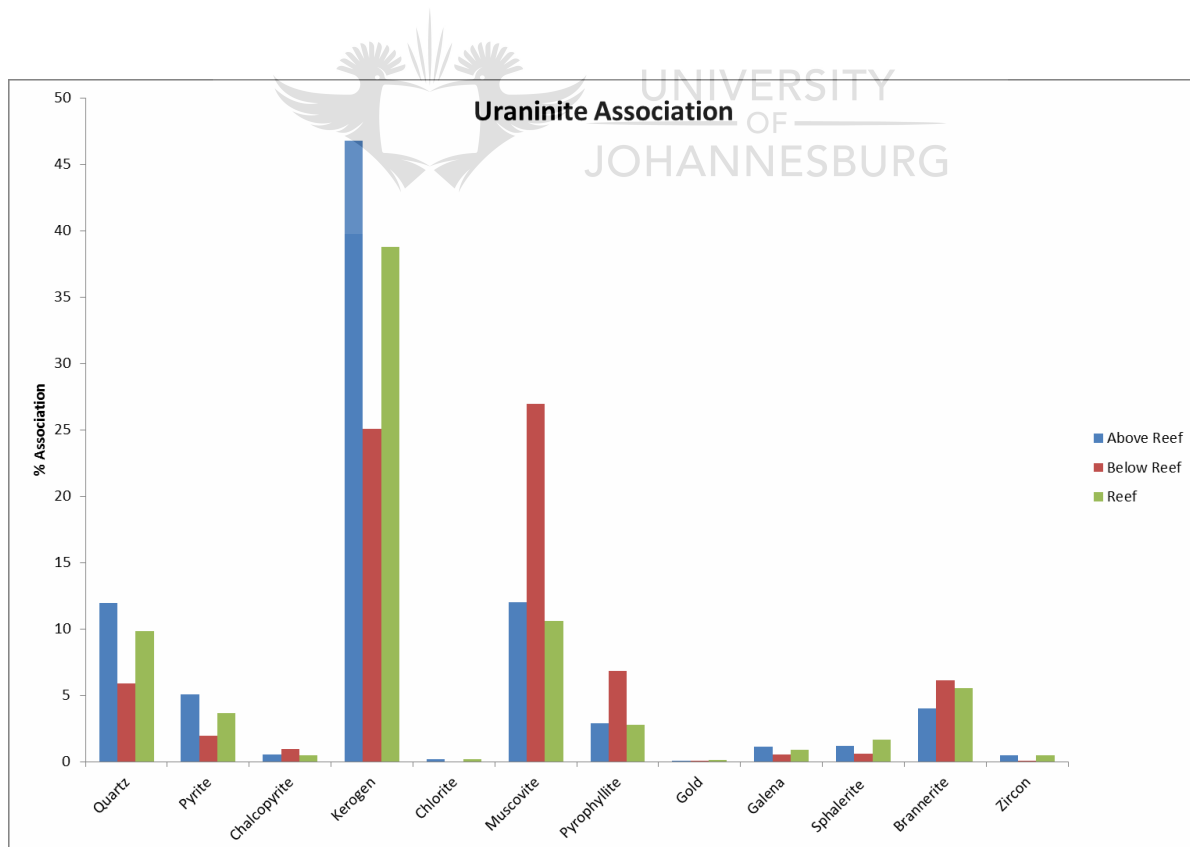
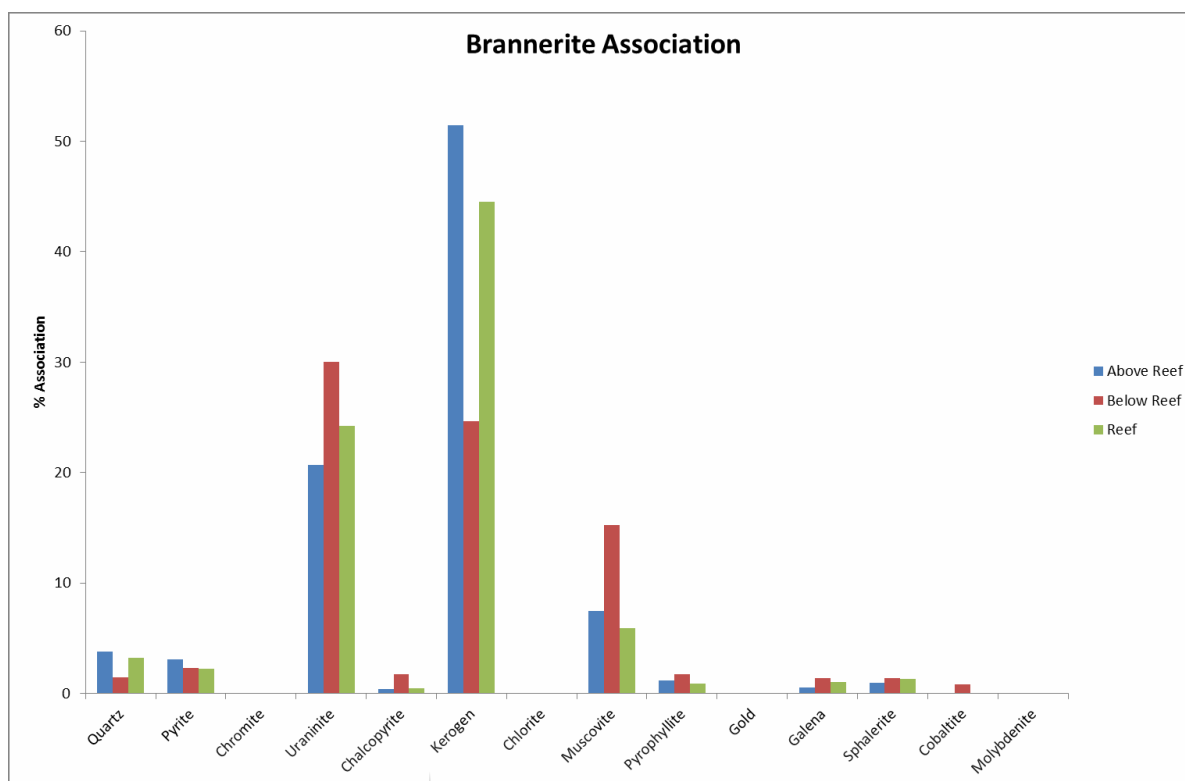


Figure 7.25: Uraninite association across the BSPL Reef.



**Figure 7.26: Brannerite association across the BSPL Reef**

The figures that are visual representations of the associations mentioned above. These images are BSE images obtained from the MLA, as well as mineral maps showing the relation and the association of the uraninite and the brannerite to the surrounding minerals. The uraninite and brannerite have very similar associations and they often occur within the same kerogen globules in the buckshot pyrite reef.

Figures 7.27, 7.28 and 7.29 indicate that the most common association of the uraninite and brannerite is with kerogen, which usually occurs within the BSPL reef (Figure 7.25). An association of the uraninite and brannerite to quartz and muscovite is also observed given that these minerals occasionally appear within the kerogen alongside the uraninite and lesser amounts of brannerite.

Brannerite is often found within the same kerogen globule as uraninite, but there are less particles of brannerite than particles of uraninite. The brannerite particles are also usually smaller than the uraninite particles. These observations are confirmed by the size distribution discussed above as well as by the modal abundances calculated from the bulk samples (Table 7.2-7.4, Figure 7.20-7.22).

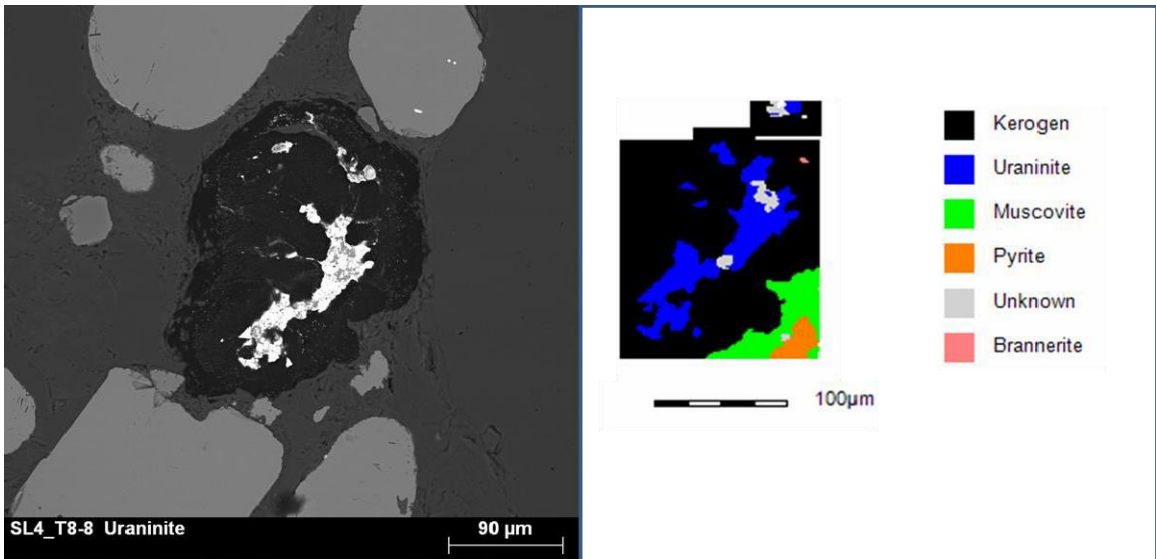


Figure 7.27: BSE image (R), mineral map (L), indicating the uraninite association with kerogen.

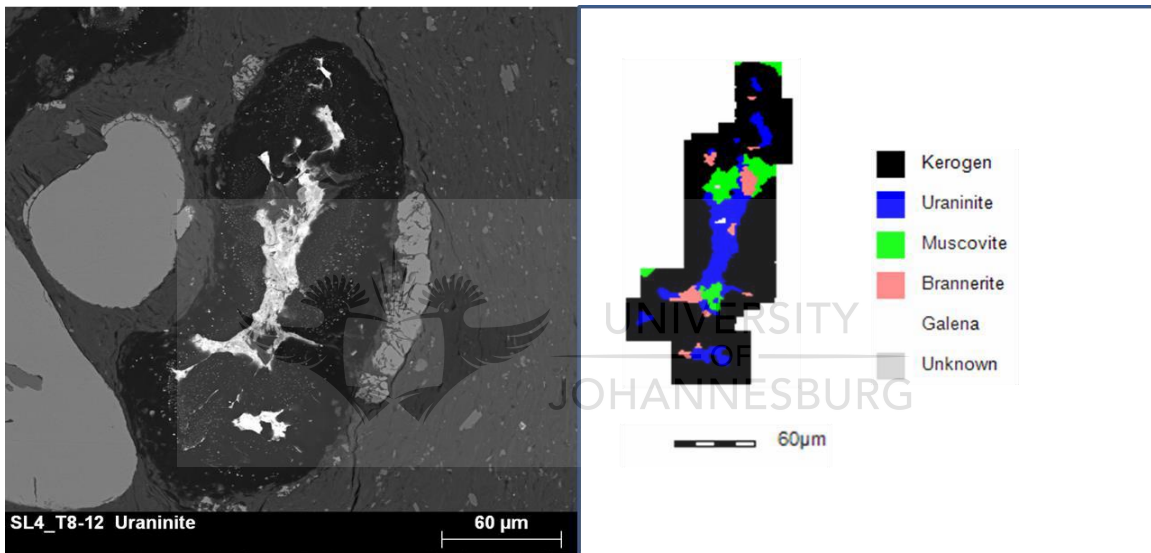


Figure 7.28: BSE image (R), mineral map (L), indicating the uraninite and brannerite association with kerogen, as well as some association with muscovite

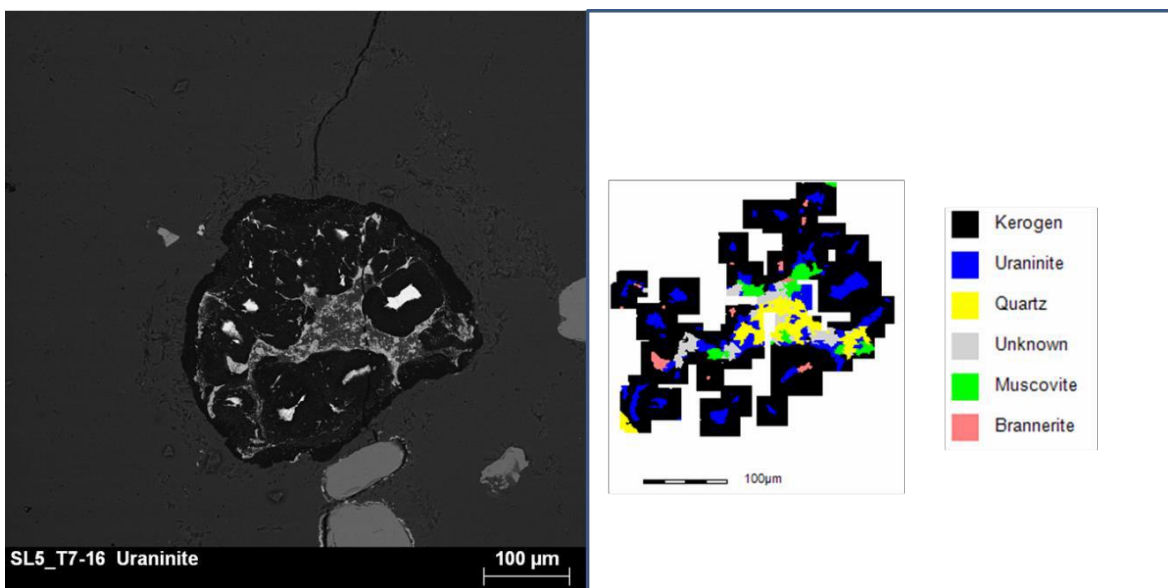
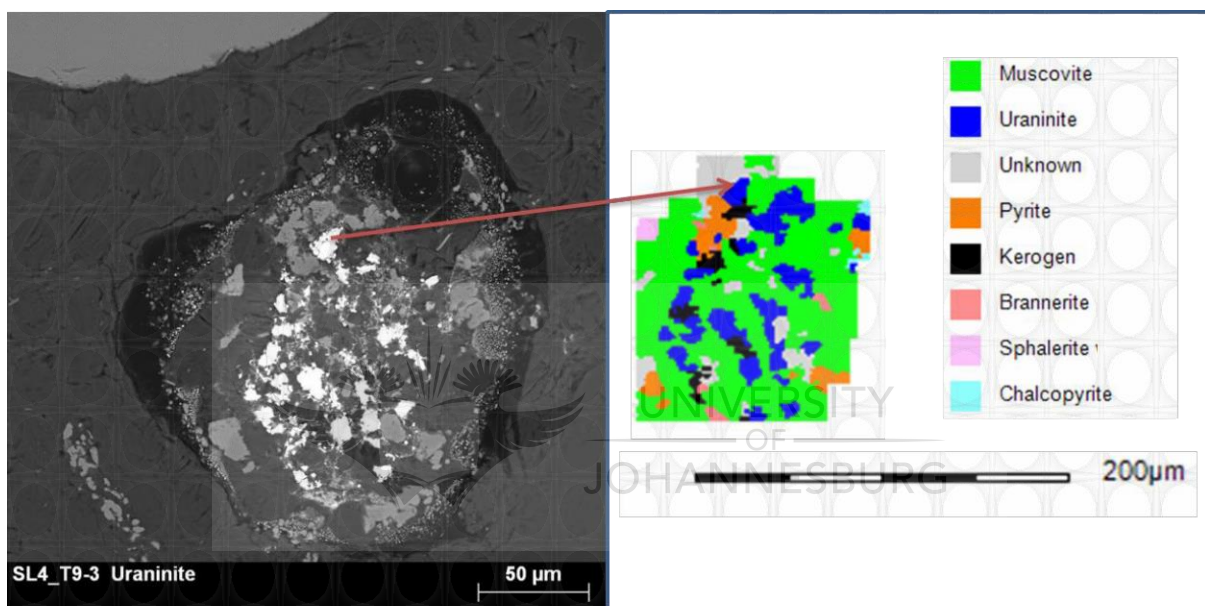
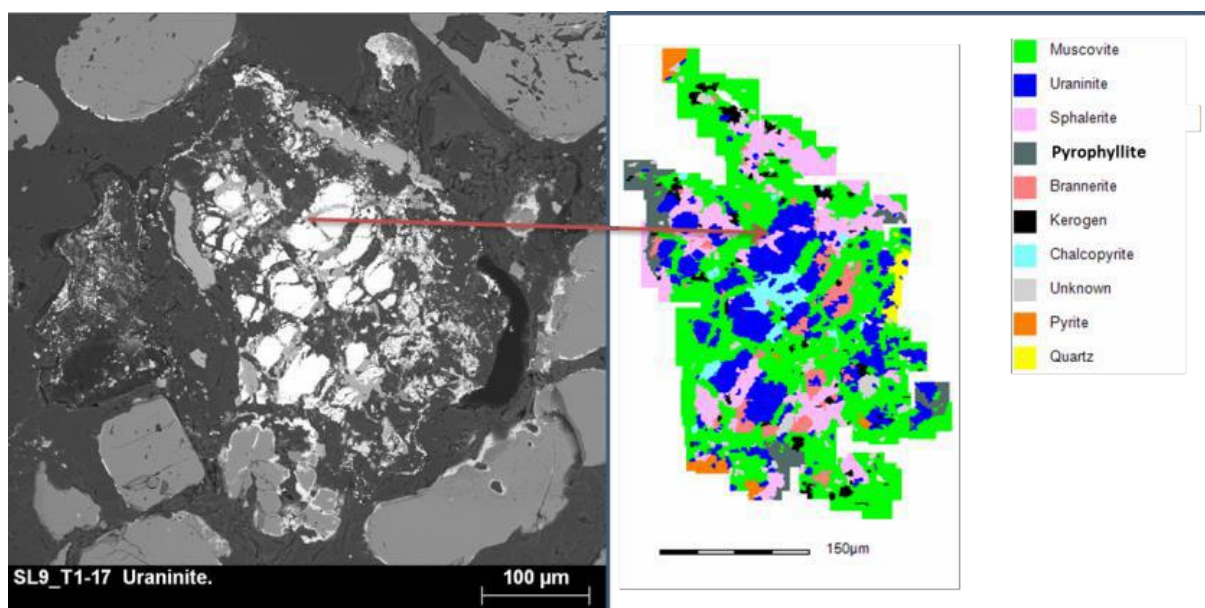


Figure 7.29: BSE image (R), mineral map (L), indicating the uraninite association with kerogen, as well as some association with quartz, muscovite and brannerite.

A further type of occurrence of uraninite is characterised by the possible replacement or remobilisation of the kerogen, which usually leaves behind a structure filled with other minerals. Evidence for this is reflected in images 7.30 and 7.31, in which some kerogen is seen to remain in the BSE image. This mineral found within the kerogen structure is seen to be in association with the uraninite and, in some cases, the brannerite. This poses the question as to whether the uraninite and brannerite formed within the kerogen globules or whether the uraninite and brannerite was detrital, and served as a trap or attracted the kerogen as it was moving up through the sequence (Parnell, 1999). Evidence for this can be seen in Figures 7.30 and 7.31. Sphalerite is also seen occurring within these structures in some cases.



**Figure 7.30: BSE image (R), and mineral map (L), indicating the uraninite association with muscovite which appears to have formed within the remnant kerogen structure.**



**Figure 7.31: BSE image (R), and mineral map (L), indicating the uraninite and brannerite association with muscovite which appears to form within the kerogen remnant structure along with an association with sphalerite**

The uraninite also has some association with pyrite. This association is only seen forming along the boundary of the pyrite grain, which is also closely associated with kerogen (Figure 7.24, 7.32). The most common association of uraninite and brannerite is to kerogen, and brannerite and uraninite often occur within the same kerogen globules. Uraninite and brannerite particles are seen mostly in these forms in the samples (Figure 7.33).

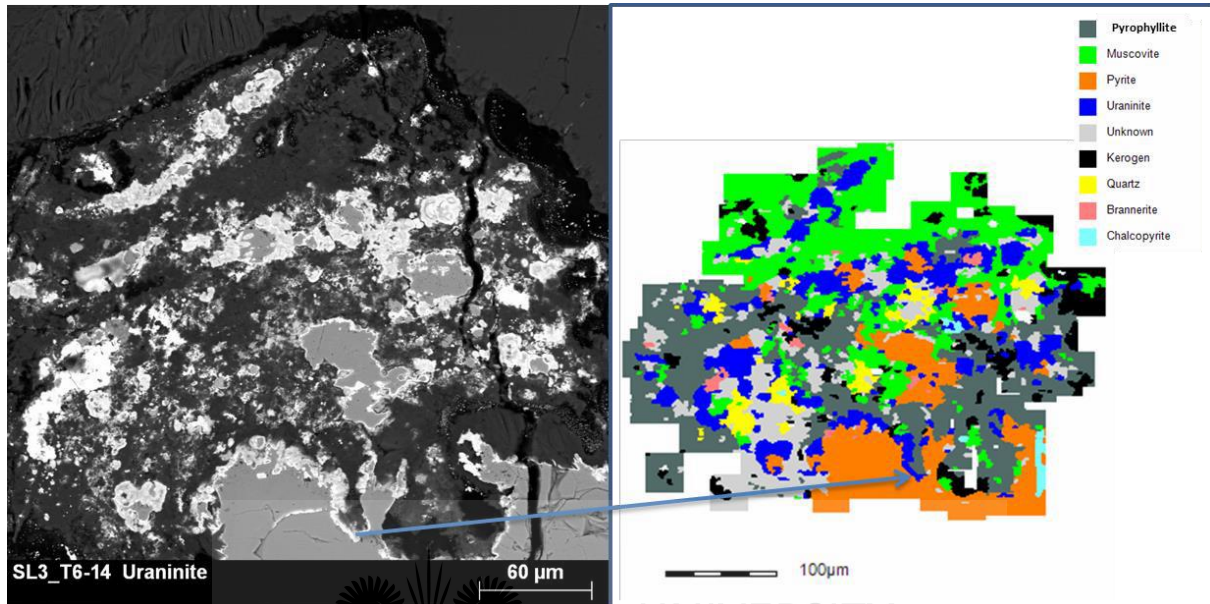


Figure 7.32: BSE image (R), and mineral map (L), indicating the uraninite association with the edge of a pyrite grain.

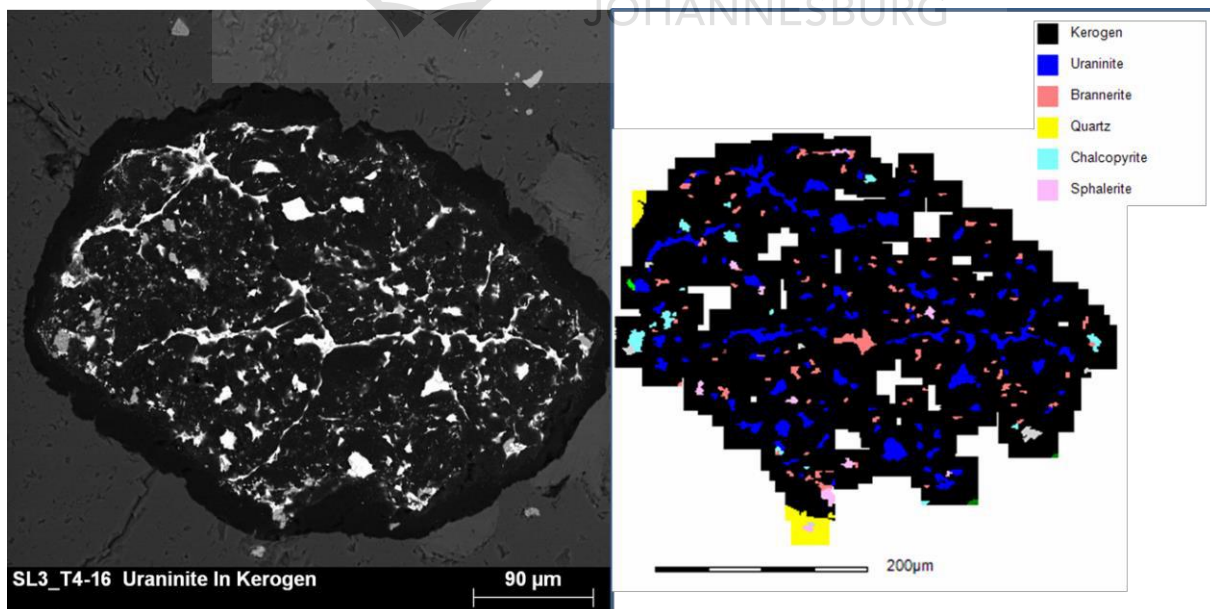


Figure 7.33: BSE image (R), and mineral map (L), indicating the uraninite association with kerogen as well as the occurrence of brannerite within the kerogen.

The association per modal mineralogy calculation conducted for uraninite (Table 7.5, 7.7) indicates that the kerogen or carbon matter in the reef shows a high level of significance with relation to its modal abundance and association to uraninite. This serves as further evidence for the strong association of uraninite and carbon. Brannerite is also significantly associated with the uraninite. This is to be expected as brannerite is known to be an altered product of the uraninite and is often seen in association with uraninite within the kerogen globules (Bowell et al., 2012). Galena, sphalerite, chalcopyrite and gold also show some significant association to uraninite taking into account their modal abundances. The association with muscovite must still be considered significant given the high association between the two within the BSPL reef. Table 7.7 the mineral percentages do not add up to 100 as the unclassified minerals are not included in this table, these minerals are classified as unknown during MLA analysis.

**Table 7.7: Association per modal mineralogy for the associations of uraninite.**

<b>Mineral</b>	<b>Modal mineralogy wt %</b>	<b>Uranium association %</b>	<b>Association per modal mine ralogy</b>
Quartz	69.25	9.227	0.133
Pyrite	23.94	3.543	0.148
Chromite	0.29	0.043	0.151
Uraninite	0.01	0.000	0.000
Chalcopyrite	0.01	0.653	65.333
Kerogen	0.01	36.863	2764.750
Chlorite	0.38	0.120	0.316
Muscovite	3.78	16.523	4.367
Pyrophyllite	0.90	4.167	4.613
Gold	0.01	0.083	12.500
Galena	>0.01	0.857	257.000
Sphalerite	0.02	1.133	68.000
Cobaltite	0.01	0.073	5.500
Brannerite	>0.01	5.230	4358.333
Zircon	0.05	0.347	6.933

## **7.6 Comparison of the Gold and Uranium bearing phases within the BSPL Reef**

It is evident that the gold and uraninite have different associations to certain minerals, and can occasionally occur together in association with kerogen (Figure 7.16). There are, however, more complex textures in which the gold and uraninite appear to have formed a mineral agglomerate (Figure 7.15). This association between the gold and uraninite within the

BSPL reef is very rare. In terms of the size distribution of the gold, uraninite and brannerite (U bearing phase), it is evident that the gold is the coarsest grain on average, while the brannerite is the finest throughout the BSPL reef (Figure 7.34).

From the observations made in this chapter, it can be concluded that both the gold and the uranium bearing phases found within the samples may be detrital in origin and that they are later remobilized during lithification. The irregular shape of the gold particles indicates that the gold has been remobilized during lithification. Additionally, given that the uranium bearing phases have formed traps for the carbon material that encloses them, they could also be detrital in origin. Alternatively, the uranium bearing phases could have precipitated from the carbonaceous material passing through the BSPL reef. A combination of both processes is most likely the case (Parnell, 1999).

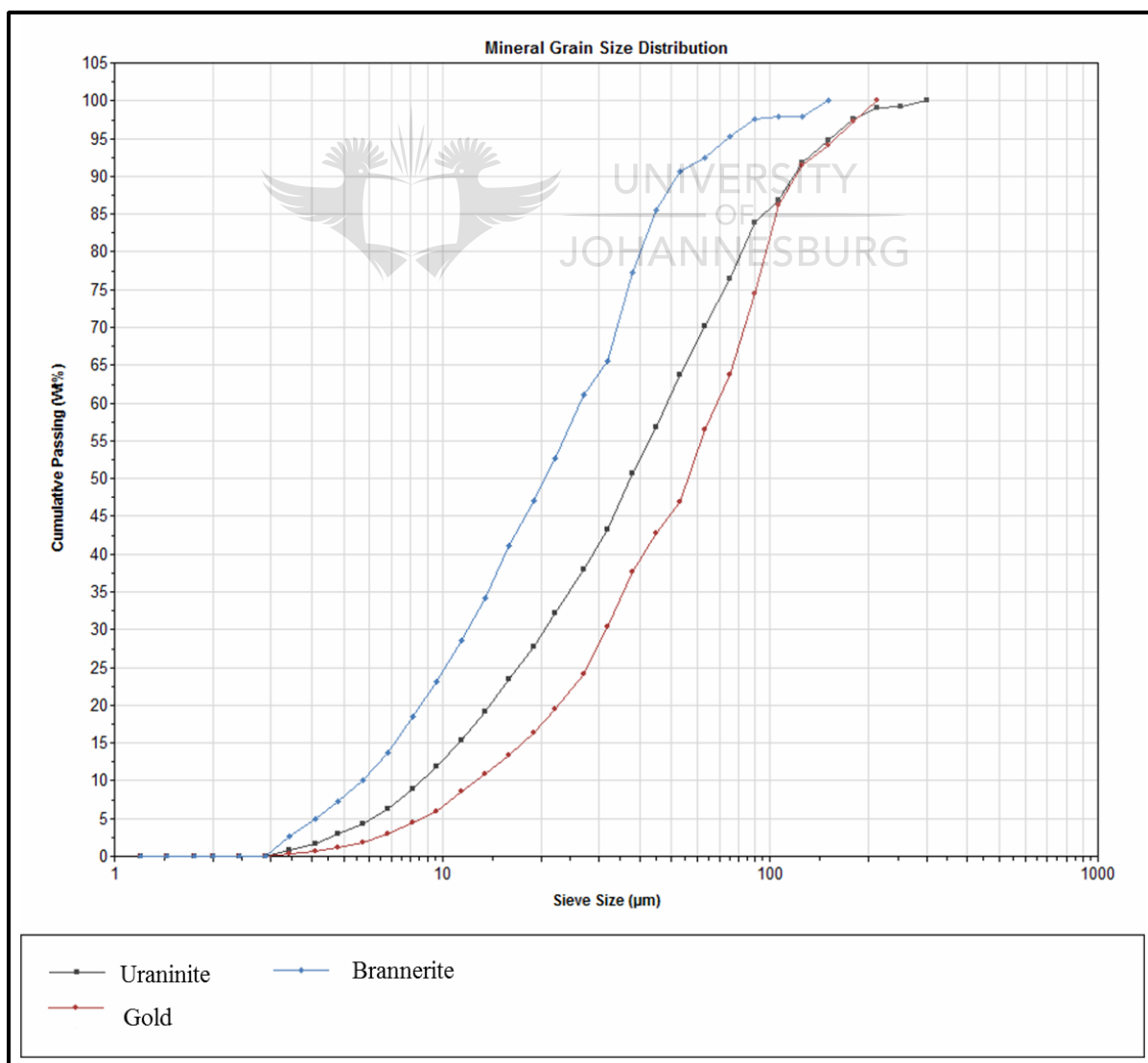


Figure 7.34: Comparison of grain size for gold, uraninite and brannerite.

## Chapter 8

### Major and Trace Element Chemistry, Grading Analysis and Density Separation

#### 8.1 Introduction

This chapter will outline the results for the major and trace element chemistry, grading analysis and density separation test work. The methodologies as well as the processes completed for each test are included in Chapter 5.

Major and trace element chemistry is conducted to determine the bulk chemical composition of the samples with regards to their chemical make-up. This can provide a useful indication as to which minerals host which elements when related to the modal mineralogy, as conducted in Chapter 7. The average grade of the elements of interest (Au, U, Th and S) can also be determined by the assay data attained during this process.

The grading analysis is executed in order to establish where specific elements report with regards to the size fraction within the milled material. This leads to a better understanding of the particles that contain the elements of interest in this study (Au, U, Th and S). This test will therefore indicate if these elements of interest have an association with coarse or fine grained particles within the milled BSPL material (Coetzee et al., 2011).

Density separation testing can indicate whether or not the ore containing the elements of interest can be pre-concentrated using a method of gravity separation. In this study, HLS was conducted. The results of this will determine if this method of pre-concentration will be viable with relation to later extraction of gold and uranium in the BSPL reef (Coetzee et al., 2011).



## 8.2 Major and Trace Element Chemistry

Table 8.1 indicates the major element chemistry conducted across all 6 samples. The major element chemistry considers the bulk composition of the rock with regards to the primary rock forming elements. The major element chemistry indicates that the samples have high SiO<sub>2</sub>, Fe<sub>2</sub>O<sub>3</sub> and Al<sub>2</sub>O<sub>3</sub> compositions relative to the other present elements. Specifically, SiO<sub>2</sub> shows the highest abundance. An analysis of sample collection day two (Sc2) indicates that the Fe<sub>2</sub>O<sub>3</sub> and total S are higher in comparison to the other two sample collection days. This suggests that these samples are more enriched in sulphide minerals such as pyrite. This is justified by the fact that the modal mineralogy reveals pyrite to be a large component within the BSPL reef. The total carbon in all the samples is fairly low (Table 8.1). This assay data confirms the previously discussed modal mineralogy data given that the material is rich in quartz pyrite and muscovite (which are constituted by the elements that report the highest values within the assay data SiO<sub>2</sub>, Fe<sub>2</sub>O<sub>3</sub> and Al<sub>2</sub>O<sub>3</sub>). (The dash indicates that the elements in question is below the detection limits in table 8.1)

**Table 8.1: Major element chemistry of the run of mine bulk samples (Sc1, Sc2 and Sc3).**

Element		Sc1, Sp3-A	Sc1, Sp3-B	Sc2, Sp4-A	Sc2, Sp4-B	Sc3, Sp4-A	Sc3, Sp4-B
SiO <sub>2</sub>	wt%	82.20	79.80	76.00	77.90	82.40	81.20
Al <sub>2</sub> O <sub>3</sub>	wt%	3.35	3.38	2.90	2.91	3.66	3.66
CaO	wt%	–	–	–	–	0.50	0.40
MgO	wt%	0.14	0.13	0.11	0.12	0.36	0.35
Fe <sub>2</sub> O <sub>3</sub>	wt%	8.04	8.20	13.02	13.00	8.01	7.99
K <sub>2</sub> O	wt%	0.60	0.60	0.50	0.50	0.70	0.70
MnO	wt%	0.02	0.02	0.02	0.03	0.03	0.03
Na <sub>2</sub> O	wt%	0.15	0.15	0.11	0.11	0.17	0.17
P <sub>2</sub> O <sub>5</sub>	wt%	–	–	–	–	0.02	0.02
TiO <sub>2</sub>	wt%	0.19	0.18	0.15	0.15	0.22	0.22
Cr <sub>2</sub> O <sub>3</sub>	wt%	0.13	0.13	0.06	0.06	0.09	0.09
LOI	wt%	4.44	4.46	7.01	7.02	4.69	4.67
<b>Total</b>	wt%	100.45	98.28	102.05	101.80	100.85	99.19
S	wt%	5.49	5.54	9.05	9.12	5.05	5.05
C	wt%	0.13	0.16	0.13	0.12	0.30	0.33

The trace element chemistry indicates that the Ni, Zn and As content is relatively high in comparison to the other trace elements. Co, Cu and Pb are lower, ranging between 70ppm and 45ppm, with Ag reporting the lowest ppm. The grades of the elements of interest in this study (Au, U, Th) are expressed in ppm, which is equivalent to gram/tonne (g/t). The gold grades range from 12.7ppm (**Sc3,Sp4-A**) to 7.4ppm (**Sc2,Sp4-B**) with an average grade of 10.1ppm. This represents a fairly high grade across all the samples (Table 8.2). The uranium grades (Table 8.2) are slightly more variable, ranging from 29.6ppm (**Sc2,Sp4-B**) to 56.3ppm

(**Sc1,Sp3-A**). The average grade of the uranium for these samples is 39 ppm. Thorium is similar to gold in that it shows a fairly uniform grade with some slight variation across the samples. The lowest and highest grade is seen in **Sc2,Sp4-B** at 3.6ppm and in **Sc1,Sp3-B** at 5.2 ppm respectively. The average grade of these is 4.4 ppm. This indicates that the grades of the uranium and thorium in these samples are fairly low.

An analysis of sample collection day two (Sc2) indicates that the Fe<sub>2</sub>O<sub>3</sub> and total S are higher in comparison to the other two sample collection days. This finding suggests that these samples are possibly enriched in sulphide minerals, such as pyrite. This is supported by the modal mineralogy (Table 7.2-7.4). It was also noted that the uranium and gold grades are slightly lower in these samples. This suggests that an increased presence of sulphide minerals results in a lower grade of uranium and gold.

**Table 8.2: Trace element chemistry of the run of mine bulk samples (Sc1, Sc2, Sc3).**

Elements		Sc1, Sp3-A	Sc1, Sp3-B	Sc2, Sp4-A	Sc2, Sp4-B	Sc3, Sp4-A	Sc3, Sp4-B
<b>Au</b>	ppm	10.18	11.43	8.66	7.43	12.69	10.34
<b>Ag</b>	ppm	2.10	1.30	0.90	2.20	2.80	1.30
<b>Co</b>	ppm	90	86	77	74	72	68
<b>Cu</b>	ppm	58	53	46	72	59	48
<b>Ni</b>	ppm	200	197	228	228	159	139
<b>Pb</b>	ppm	69	60	69	64	55	100
<b>Zn</b>	ppm	153	132	119	127	120	118
<b>Th</b>	ppm	5	5	4	4	5	4
<b>As</b>	ppm	194	186	267	266	164	161
<b>U</b>	ppm	56	56	31	30	30	31
<b>As/Au</b>	ppm	19.1	16.3	30.8	35.8	12.9	15.6
<b>Au+Ag</b>	ppm	12.3	12.7	9.6	9.6	15.5	11.6

The major and trace element chemistry confirms that the samples are rich in silica and that they are constituted by some clay minerals and by large amounts of pyrite. The combination of the major and trace element chemistry and the modal mineralogy yields useful insight into the bulk modal composition of the BSPL bulk samples (Appendix 4 Table A4 a, A4 b).

### 8.3 Grading Analysis

This section outlines the results of the grading analysis as completed in chapter 5. The assay values for Au, U, Th and S are expressed in Table 8.3 (Appendix 4 Table A4 c).

**Table 8.3: Assay details for the size fractions used in the grading analysis**

ELEMENTS	Au	S	Th	U
UNITS	ppb	ppm	ppm	ppm
<b>SAMPLE NUMBERS</b>				
SC1 sp3_9 +106um	24973	68481	3.93	46.65
SC1 sp3_9 +75um	30420	64225	3.45	46.74
SC1 sp3_9 +53um	9275	55510	3.88	45.53
SC1 sp3_9 +25um	6203	52139	4.15	46.18
SC1 sp3_9 -25um	6906	55261	7.5	84.98
SC2 sp4_9 +106um	11575	62912	3.23	29.92
SC2 sp4_9 +75um	13204	74013	2.6	23.45
SC2 sp4_9 +53um	7241	79598	2.84	24.07
SC2 sp4_9 +25um	3599	78445	4.12	34.65
SC2 sp4_9 -25um	9691	>100000	4.96	43.2
SC3 sp4_9 +106um	25913	46698	4.03	29.36
SC3 sp4_9 +75um	25419	53238	2.67	18.98
SC3 sp4_9 +53um	6692	41969	3.92	29.44
SC3 sp4_9 +25um	7260	42676	4.67	33.13
SC3 sp4_9 -25um	9257	45230	7.01	52.97

### 8.3.1 Grade Reporting by Size Fraction

Gold, the first element of interest, has a fairly even distribution across the 3 intermediate size fractions. Less of the gold appears in the finest and coarsest size fractions. The coarsest and finest size fractions also had the lowest mass percentage, which possibly explains the lack of gold within these size fractions (Figure 8.1-8.3, Table 8.4). For sample masses please refer to Appendix 5 Tables A5 a-d.

**Table 8.4: Gold mass percent per size fraction across all three samples**

Size fraction	Gold mass percentage range
+106 µm	9-15%
+75 µm	18-30%
+53 µm	19-30%
+25µm	25-33%
-25µm	6-12%

Uranium reports primarily to the finer size fractions, with very small amounts reporting to the larger size fractions (Figure 8.1-8.3, Table 8.5).

**Table 8.5: Uranium mass percent per size fraction across all three samples**

Size fraction	Uranium percentage range
+106 $\mu\text{m}$	3-9%
+75 $\mu\text{m}$	7-9%
+53 $\mu\text{m}$	21-28%
+25 $\mu\text{m}$	37-55%
-25 $\mu\text{m}$	9-27%

The Thorium reports as seen in table 8.6 indicating a similar trend to the uranium grading analysis in that the finer size fractions contain more thorium than the coarser size fractions (Figure 8.1-8.3).

**Table 8.6: Thorium mass percent per size fraction across all three samples**

Size fraction	Thorium percentage range
+106 $\mu\text{m}$	3-8%
+75 $\mu\text{m}$	9-8%
+53 $\mu\text{m}$	21-27%
+25 $\mu\text{m}$	38-56%
-25 $\mu\text{m}$	9-28%

The sulphur in these samples is fairly evenly distributed over the various size fractions and follows a similar trend to the mass percentages of the size fractions. The grading analysis is plotted in the Figures 8.1, 8.2, 8.3. The data used to create these plots (Figures 8.1-8.3) are listed in Appendix 5, Tables A5 a-d. This data gives indication on how the gold mass percentage was calculated (portion of the total) as well as the variation between samples.

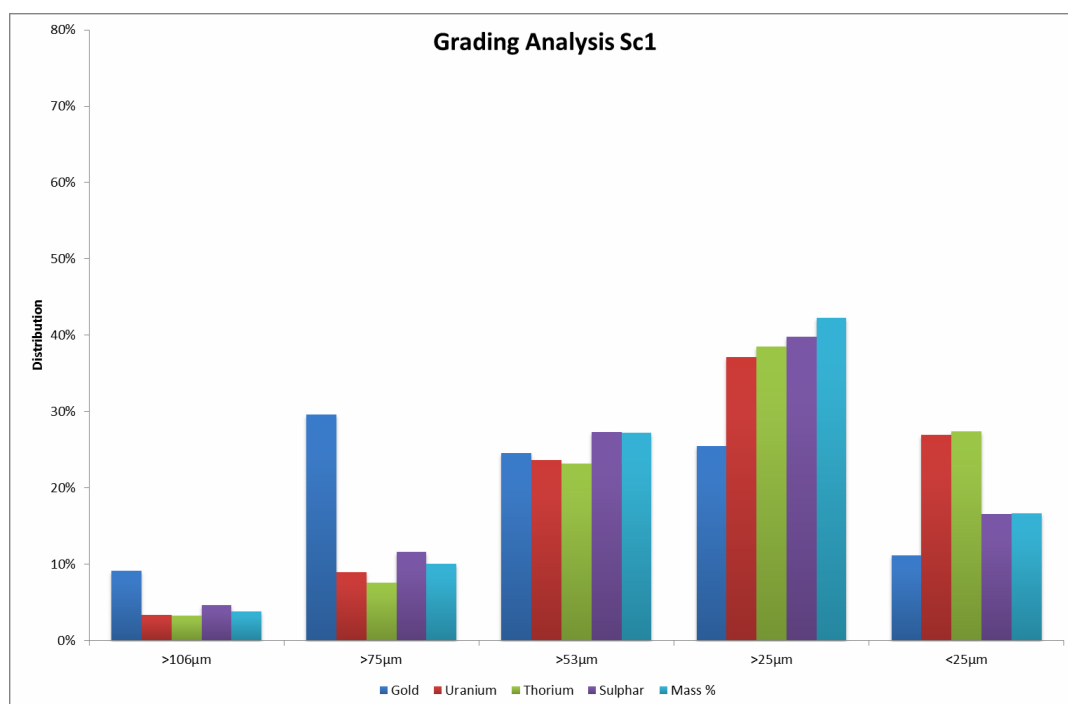


**Figure 8.1: Grading analysis For Sc1 (Sample Collection 1), showing the grade distribution of gold, uranium, thorium and sulphur by size fraction.**

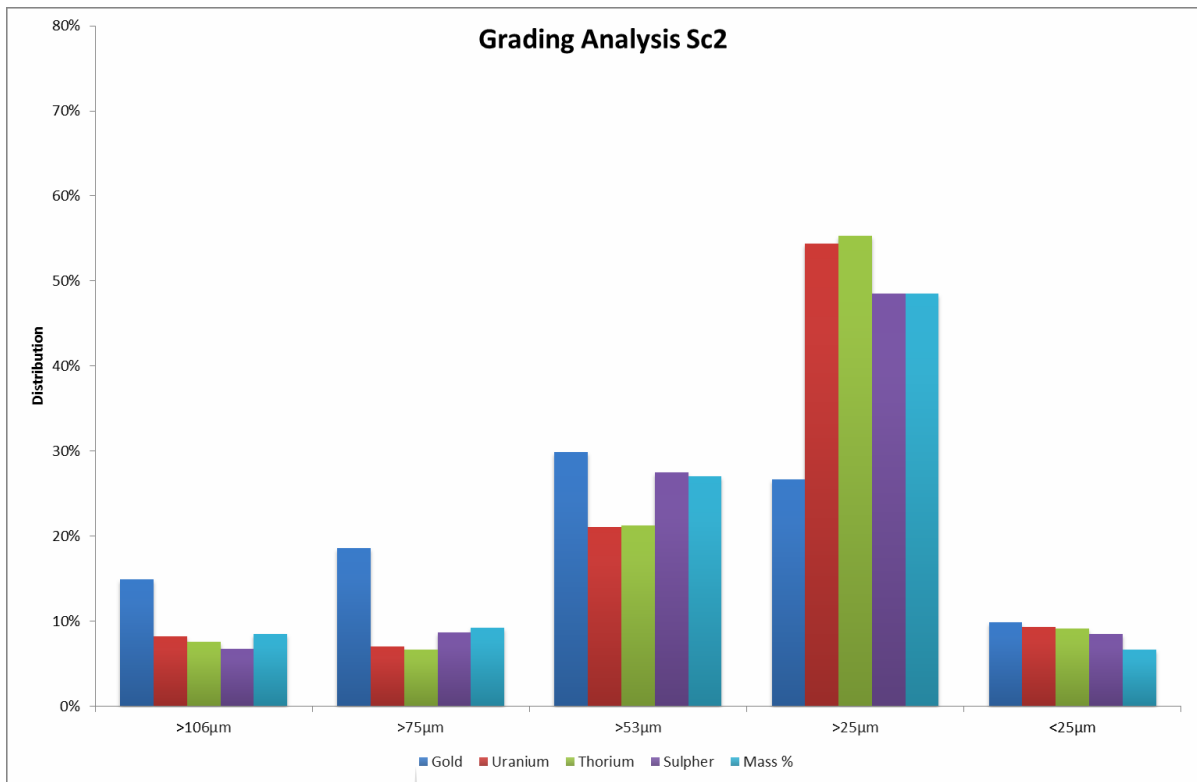


Figure 8.2: Grading analysis For Sc2 (Sample Collection 2), showing the grade distribution of gold, uranium, thorium and sulphur by size fraction.

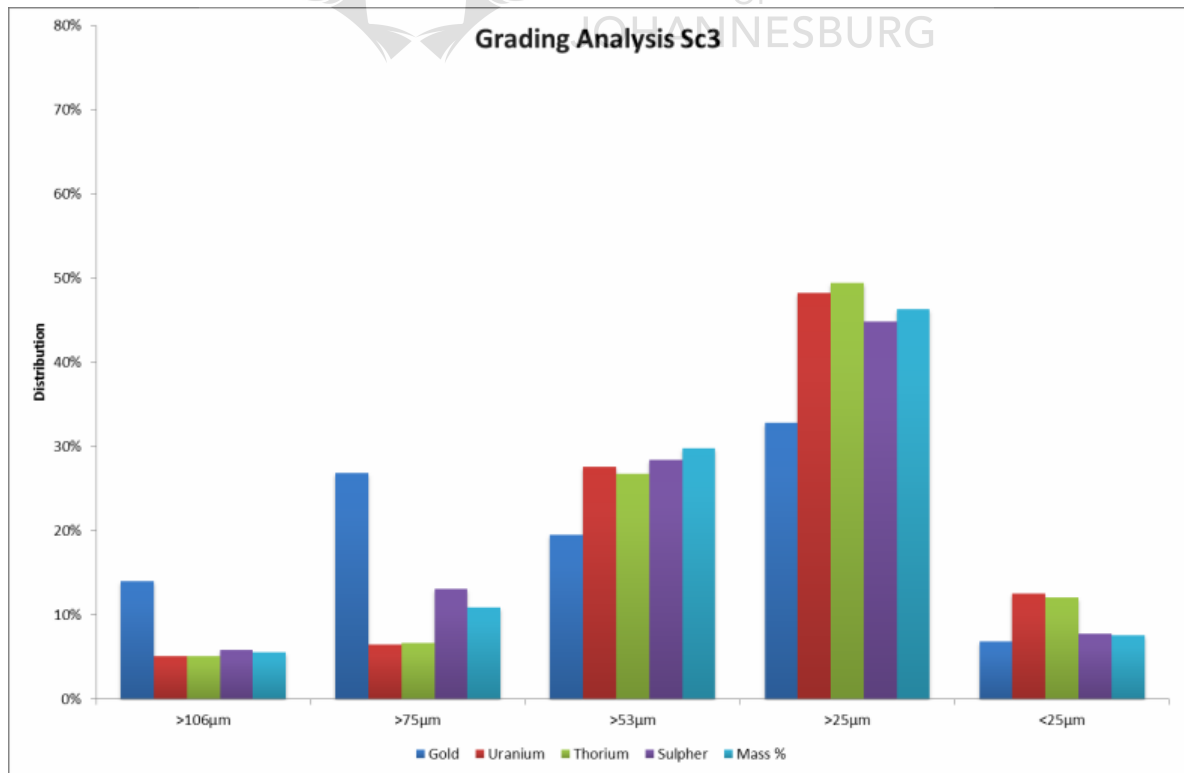


Figure 8.3: Grading analysis For Sc3 (Sample Collection 3), showing the grade distribution of gold, uranium, thorium and sulphur by size fraction.

### 8.3.2 Upgrading and Downgrading Through Sieving.

Upgrading and downgrading through sieving indicates the probable particle sizes for the elements of interest. If an element of interest is upgraded in the coarser size fractions it can be assumed that the element in question is contained in coarser particles within the milled material. The same conclusion applies should the element report to the finer size fraction (in this case, the conclusion would be that the element is contained by finer grained particles). This can also determine the association of the particle containing the element and whether it is associated to coarser or finer grained particles. Figures 8.4 A-D (Appendix 5 Tables A5 a-d) illustrate these points.

Gold (Figure 8.4 A) is significantly upgraded into the coarser size fractions at predominantly +75µm. However, it still shows an upgrade in the +106µm size fractions, with an evident downgrade in the +25µm size fraction. The U (Figure 8.4 B) and Th (Figure 8.4 D) are both significantly upgrade into the +25µm and -25µm size fractions. The sulphur (Figure 8.4C) shows little deviation from the mass percentage, thus suggesting no real upgrade or downgrade. The upgrade and downgrade are relative to the mass percentage of gold in the size fraction.

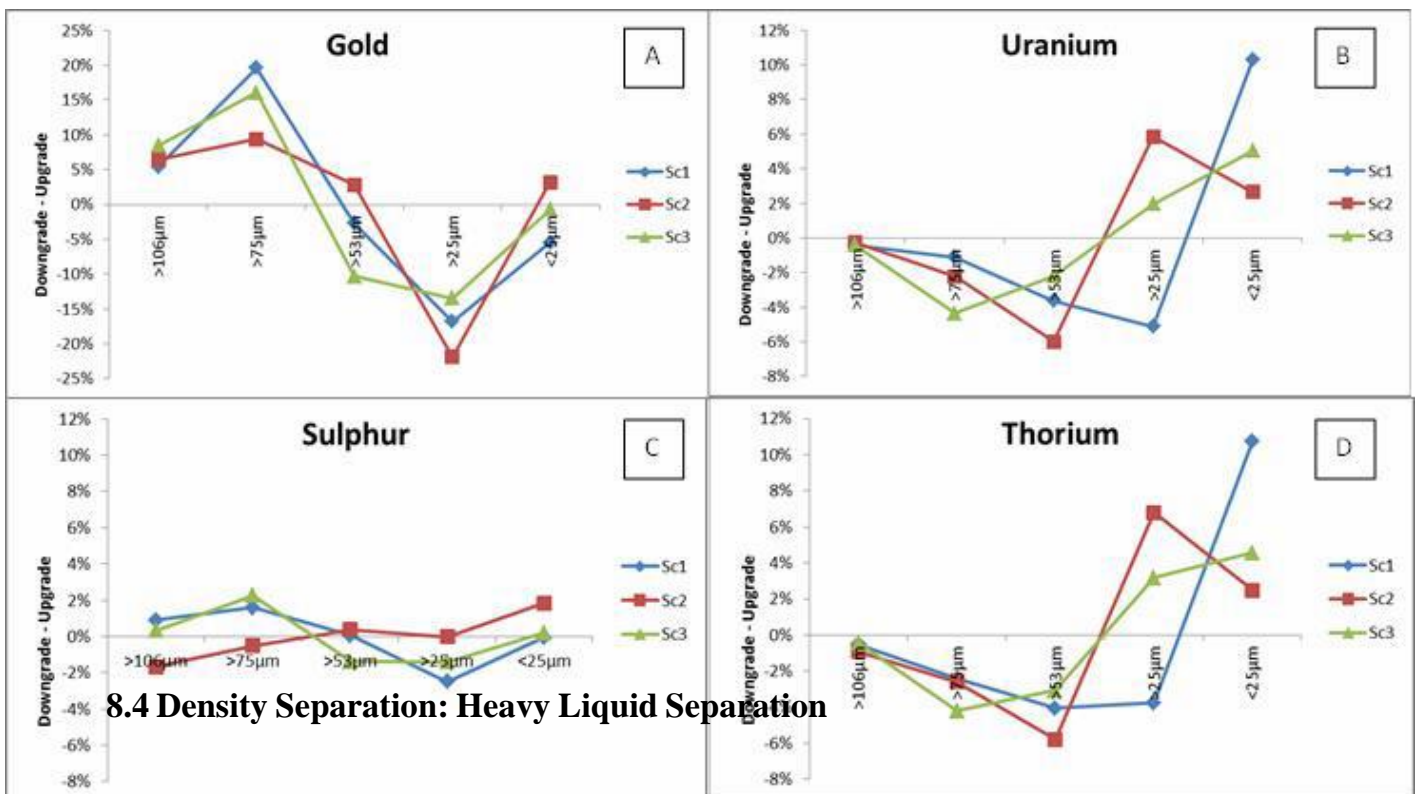


Figure 8.4 A-D: Upgrade - Downgrade of the grading analysis of Au, U, Th and S (Coetzee et al. 2011).

Density separation is an effective method of concentrating minerals that have a high specific density such as gold, and so is often used as a method to pre-concentrate such materials (Kongolo and Mwema, 1998). The method used to separate the dense minerals from the BSPL reef is detailed in Chapter 5.

The heavy mineral concentrates were analysed for Au, U, Th and S. These analyses are graphically represented in Figures 8.5, 8.6 and 8.7. These results indicate that the Au and S report strongly to the sinks fraction, whereas the U and the Th report mainly to the slimes fraction. In the comparison it is evident that the Au and S are effectively concentrated within the sinks fraction, whereas the U and Th are largely lost to the slimes fraction (Figure 8.8). The results of this analysis show that, again, gold may be found in coarser particles that will easily be concentrated in the heavy liquid. The U and Th may then be located within finer particles and can be lost to the slimes fraction as the  $-25\mu\text{m}$  fraction. This size fraction was removed before the material was subjected to the LST as its presence is likely to have negative effects on the heavy liquid separation test (Appendix 4 Table A4 d, Appendix 5 Tables A5 e-h).

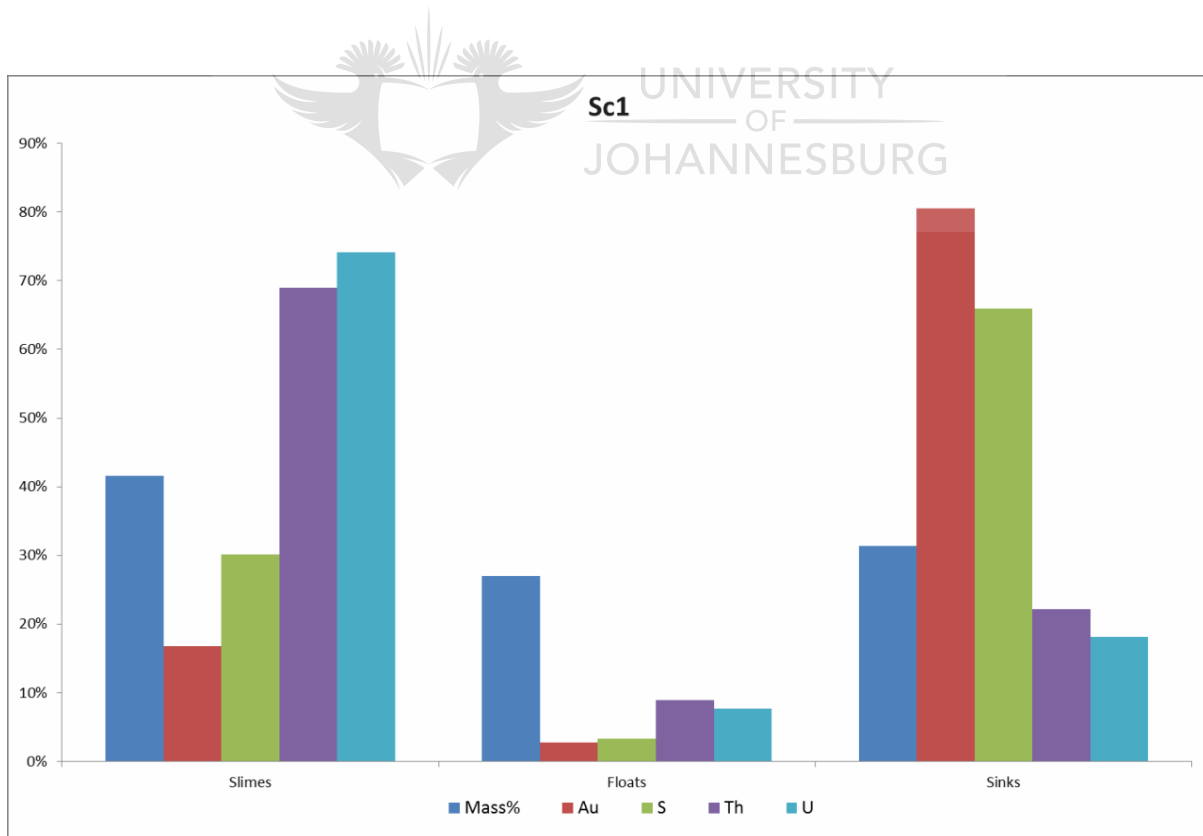


Figure 8.5: Results for HLS for run of mine bulk sample SC1

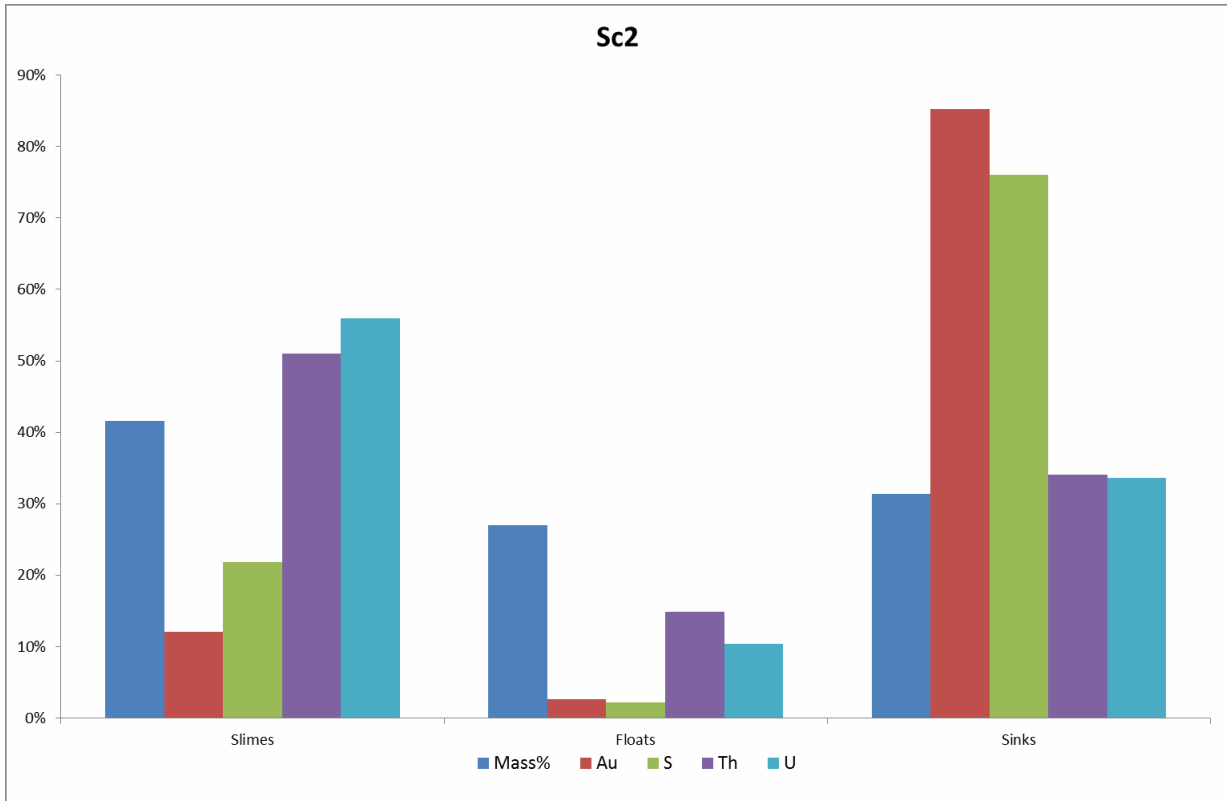


Figure 8.6: Results for HLS for run of mine bulk sample SC2

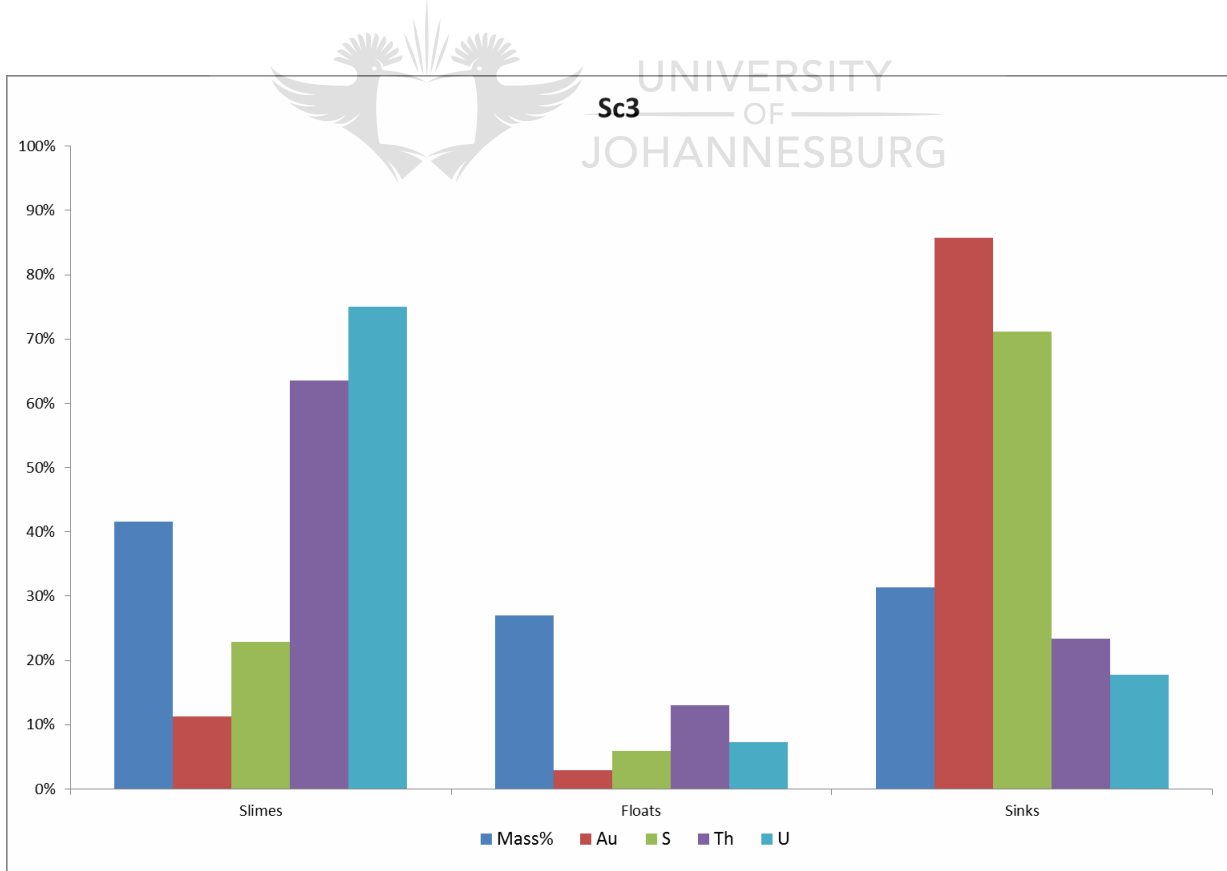


Figure 8.7: Results for HLS for run of mine bulk sample SC2



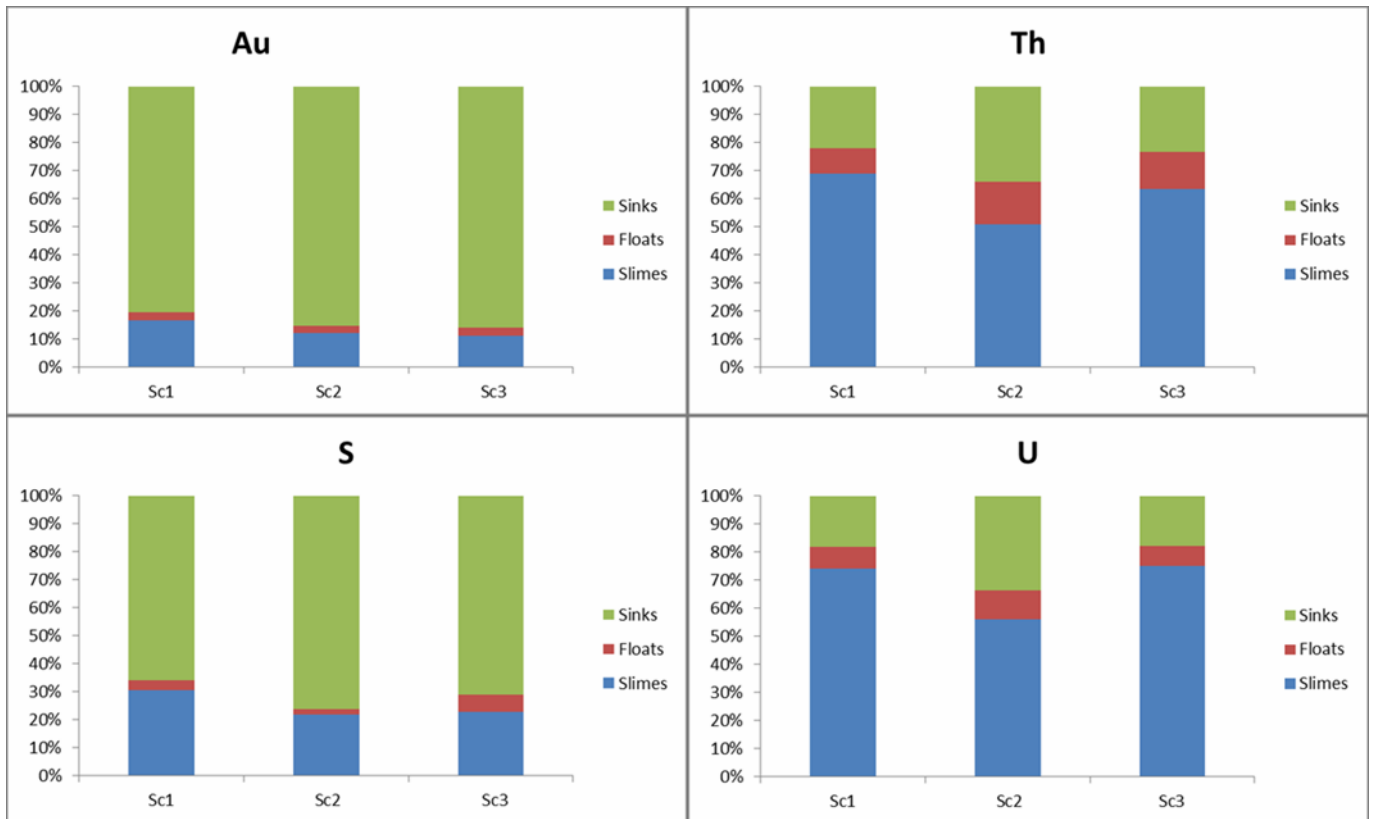


Figure 8.8: Comparison of results of the HLS for Sc1, Sc2, Sc3



## 8.5 Results Summary

The Au occurs mainly in the intermediate size fractions and is upgraded in the coarse fractions. The U and Th prefer to report to the finer size fractions. These observations suggest that the U and Th occur in smaller particles within the reef, whereas the Au can be found in larger particles within it. The S is abundant throughout the reef and is found within all size fractions, as shown in the upgrade downgrade plot for S (Figure 8.4 C). The Au and S behave similarly when subjected to gravity separation using HLS, as does the U and Th. The Au is effectively concentrated using this method while the U and Th report to the slimes fraction, again providing an indication as to their finer particle size in the milled material.

## Chapter 9

### Leaching of Gold and Uranium

#### 9.1 Introduction

Gold and uranium leaching are the primary processes used for the recovery of these two metals. Carbon in leach treatment plants is often used to recover gold and the acid leaching of uranium is usually the most effective method for concentrating this metal (Stange, 1999, Rees, 2000, Venter and Boylett, 2009).

This chapter specifically addresses the results of the uranium and gold dissolution analyses that were performed. The dissolution test work was conducted at SGS using their guidelines and testing methods as outlined in Chapter 5.



#### 9.2 Gold Leach

It is observed from the test results that the Au responds extremely well to the cyanide leaching process, with a 94-99% recovery of the gold across the three samples (Table 9.1). Sc2, the sample with the lowest grade, displayed the lowest recovery at 94.8% (Table 9.1). This, however, is nevertheless a notably high recovery. This may be explained by the higher pyrite content within this bulk samples (Table 7.3). This higher content of pyrite may suggest that some of the gold occurs within the pyrite as vein structures (Figure 7.5 A-C). As such, it is not effectively liberated during the milling process. Sc1 and Sc2 have notably high recoveries. Any lost percentages could be explained by two possible scenarios: the gold may be lost to carbon present within the material (preg-robber); or it may be located within pyrite in vein structures. In the latter case, the gold would be refractory and therefore would not report to the recovered fraction (Rees, 2000). The reagent consumption for NaCN and CaO, as well as the Au in solution, behave similarly across all three samples. From these results it can be concluded that the 'carbon in leach' process is highly effective in recovering the gold

from the run of mine bulk materials. In addition, it can be concluded that the gold within the material is free milling and non-refractory as evidenced by the high recoveries (Rees, 2000).

The head chemistry assays indicate that the gold grades are similar to the original trace element chemistry conducted on the run of mine bulk samples (Table 8.2). This provides an effective indication that the data obtained from this test is comparable to existing data. Finally, the residue assay indicates that only very small amounts of the gold are lost during this test work (Table 9.1).

### **9.3 Uranium Leach**

The uranium leaching results demonstrate that the uranium responds fairly poorly in comparison to the gold: only 60% to 75% of the U is recovered (Table 9.2). This recovery is nevertheless better than those observed in other Witwatersrand uranium deposits (Youlton et al., 2011). Sc2 has the lowest uranium recovery out of the three samples tested: 60.8% of the U is recovered during the leaching process (Table 9.2). Sc2 also shows the highest reagent consumption of H<sub>2</sub>SO<sub>4</sub>. This may be owing to the presence of acid consumers such as carbon in the pulp. In such a case, the uranium would not react with the acid and would therefore not report to the recovered fraction (Venter and Boylett, 2009). The other two samples, Sc1 and Sc3, behave in a fairly similar manner with regards to the grade and reagent consumption. However, the recovery for Sc3 is 9% better than Sc1 (Table 9.2). This may be explained by the slightly higher U ppm count in the pregnant solution or by the slightly higher reagent consumption. Furthermore, the fact that the residue for Sc1 is of the highest grade suggests that some of the U did not react effectively to the leaching process (Table 9.2).

**Table 9.1: Gold dissolution**

Sample ID	Test Description	Reagent addition		Pregnant solution				Au Head			
		NaCN kg/t	CaO kg/t	NaCN ppm	CaO ppm	pH	Au ppm	Average Assay g/t	Au Assay 1	Au Assay 2	Au Calc'd g/t
SC1 - SP 1	CIL	5.0	0.50	3481	123	10.8	0.01	9.44	9.03	10.4	10.4
SC2 - SP 1	CIL	5.0	0.62	3481	146	10.9	0.01	6.59	6.62	6.20	7.21
SC3 - SP 1	CIL	5.0	0.49	3423	56	10.8	0.02	12.3	13.7	12.5	13.4

Sample ID	Residue Assayed g/t	Carbon Au g/t	Reagent consumption		Au Dissolution - Assayed		Au Dissolution - Calc %	Accountability Au %
			NaCN kg/t	CaO kg/t	Soln & Carbon %	Solid %		
SC1 - SP 1	0.31	537	1.45	0.38	106.9	96.7	97.0	110.2
SC2 - SP 1	0.38	441	1.38	0.47	103.6	94.3	94.8	109.3
SC3 - SP 1	0.19	724	1.37	0.43	108.0	98.5	98.6	109.5

**Table 9.2: Uranium dissolution**

Sample ID	Leach Time (hrs)	Reagent addition		Pregnant solution					U Head				
		H <sub>2</sub> SO <sub>4</sub> kg/t	MnO <sub>2</sub> kg/t	U ppm	Fe <sup>2+</sup> mg/l	Fe <sup>3+</sup> mg/l	pH	H <sub>2</sub> SO <sub>4</sub> g/l	Assayed ppm	Head 1 ppm	Head 2 ppm	Head 3 ppm	Calc'd ppm
SC1-SP 1	24	41.7	3.8	41	<30	6480	1.20	24.8	63	63	63	64	62
SC2-SP 1	24	77.2	8.6	20	<30	7780	1.20	20.3	34	34	34	34	33
SC3-SP 1	25	46.3	3.9	42	<30	7340	1.25	23.5	66	66	65	66	60

Sample ID	Residue Assayed ppm	Reagents consumptions H <sub>2</sub> SO <sub>4</sub> kg/t	Dissolution - Assayed		U Dissolution - Calc %	Accountability U %
			Soln %	Solid %		
SC1-SP 1	21.1	16.8	64.7	66.8	66.1	97.9
SC2-SP 1	12.8	56.8	58.1	62.5	60.8	95.6
SC3-SP 1	14.3	21.1	68.9	77.9	75.7	90.9

\* Refer to Chapter 5 for description of tables.

## 9.4 Discussion

The gold responds quite well to the leaching process and can be classified, according to Rees (2000), as free milling gold. In other words, the gold is fairly coarse-grained and reacts well to the milling. This is confirmed by the size distribution of the gold (Figure 7.34). Given that its particles dissolve effectively into solution during leaching, the gold can be effectively recovered during the leaching process. The small losses in the gold leach could be attributed to a lack of effective exposure during milling as provoked by the presence of gold within the pyrite (Figure 7.5 A-C). In such a scenario, the gold would not dissolve into the solution and this fraction would fail to recover (Rees, 2009). In contrast, only 60% to 75% of uranium is recovered, with the remaining U lost during the acid leach process. The lack of recovery could be due a number of factors: firstly, 10-12% percent of the uranium could be in the brannerite mineral phase, which is known not to respond to the leaching process (Table 7.1-7.4, Venter and Boylett, 2009). Secondly, the presence of known acid consumers such as chlorite and muscovite (which are found in these samples in large quantities) may lead to higher reagent consumption in the pregnant solution. As acid consumers, chlorite and muscovite would use up the acid and thus prevent the uranium from dissolving into solution and, by extension, render the recovery of this element unlikely (Table 7.1-7.4, Youlton et al., 2011). The combination of these factors may explain the poor uranium recoveries for these samples. Given this poor recovery and the low grades of uranium found within the BSPL samples it can be concluded that this commodity would be difficult to recover economically from the Modder East mine.

## Chapter 10

### Flotation

#### 10.1 Introduction

While flotation is usually not the preferred method of extraction for gold and uranium, the method is relevant for native gold, which is naturally hydrophobic (Allan and Woodcock 2001). In addition, the method can potentially apply to uranium given the naturally hydrophobic nature of carbon and uranium's strong association to it in the BSPL reef (as observed in the detailed mineralogy, Youlton et al., 2011). Flotation testing was conducted to determine the response of the samples when subjected to the flotation conditions outlined in Wiese et al. (2005). The intersection between the conditions outlined in Wiese et al. with the basic criteria needed for this study qualify these conditions as relevant, despite the fact that the conditions outlined in Wiese et al. pertain to Platinum group minerals. Au, U, Th and S were assayed for this flotation test (original assay details are listed in Appendix Table A4 e). The reagents and methods used in this testing are detailed in Chapter 5.

#### 10.2 Flotation results for Au, U, Th and S

The recovery curves and the average for these four elements are listed in Figures 10.2 and 10.3 respectively. A mass pull curve for the three samples is depicted in Figure 10.4 (Appendix A6 a-g). The results indicate that the gold and sulphur report largely to the first concentrate and that they are extremely well-floated over the entire process, with very little amounts of gold and sulphur reporting to the tails fraction (Figure 10.1). Up to 80% of the U reports to the concentrates in the flotation and 20-30% reports to the tails (Figure 10.1). The thorium does not respond as well, with up to 40% reporting to the tails fraction. With regards to the recovery curves, the Au and S respond quickly during the flotation process, whereas the U and Th respond gradually over time (Figure 10.2).

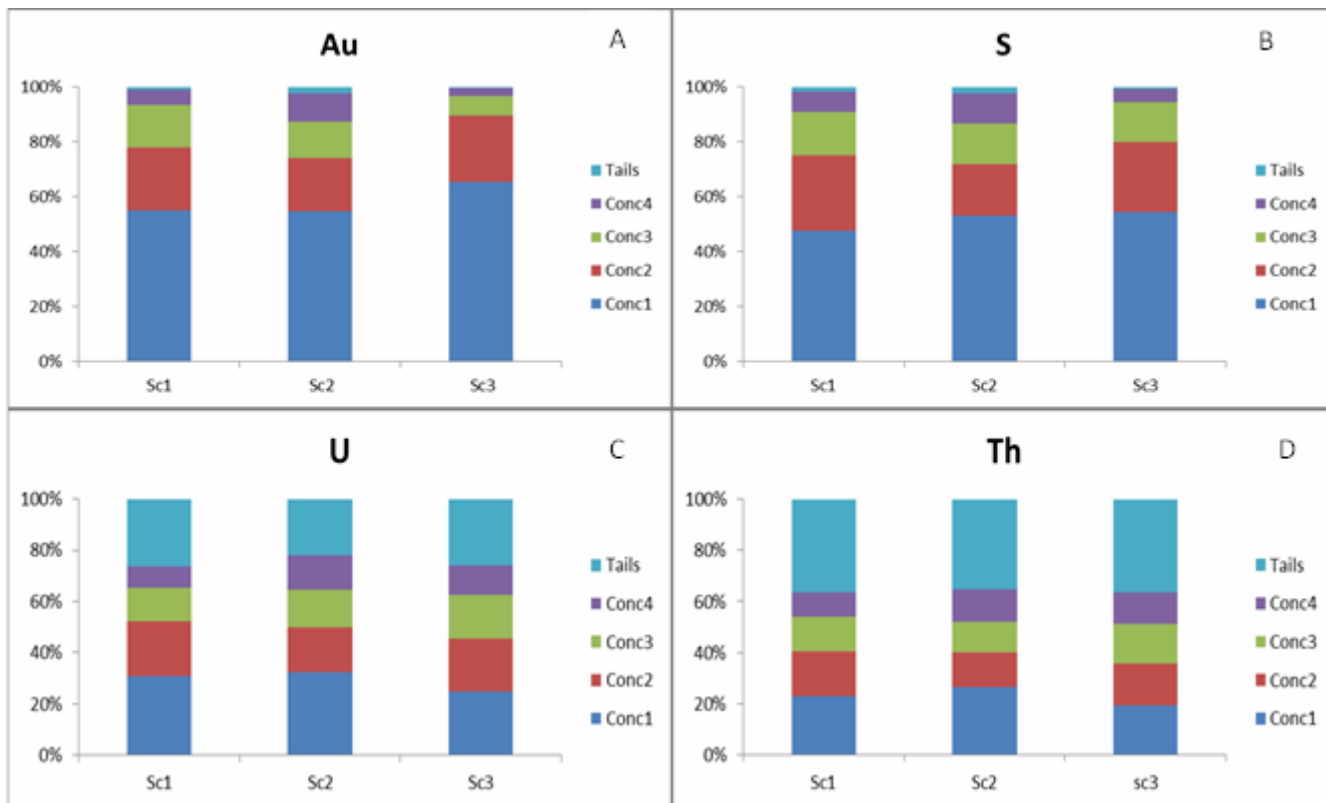


Figure 10.1: Flotation concentrates mass percentages. (Appendix A6 a-g)

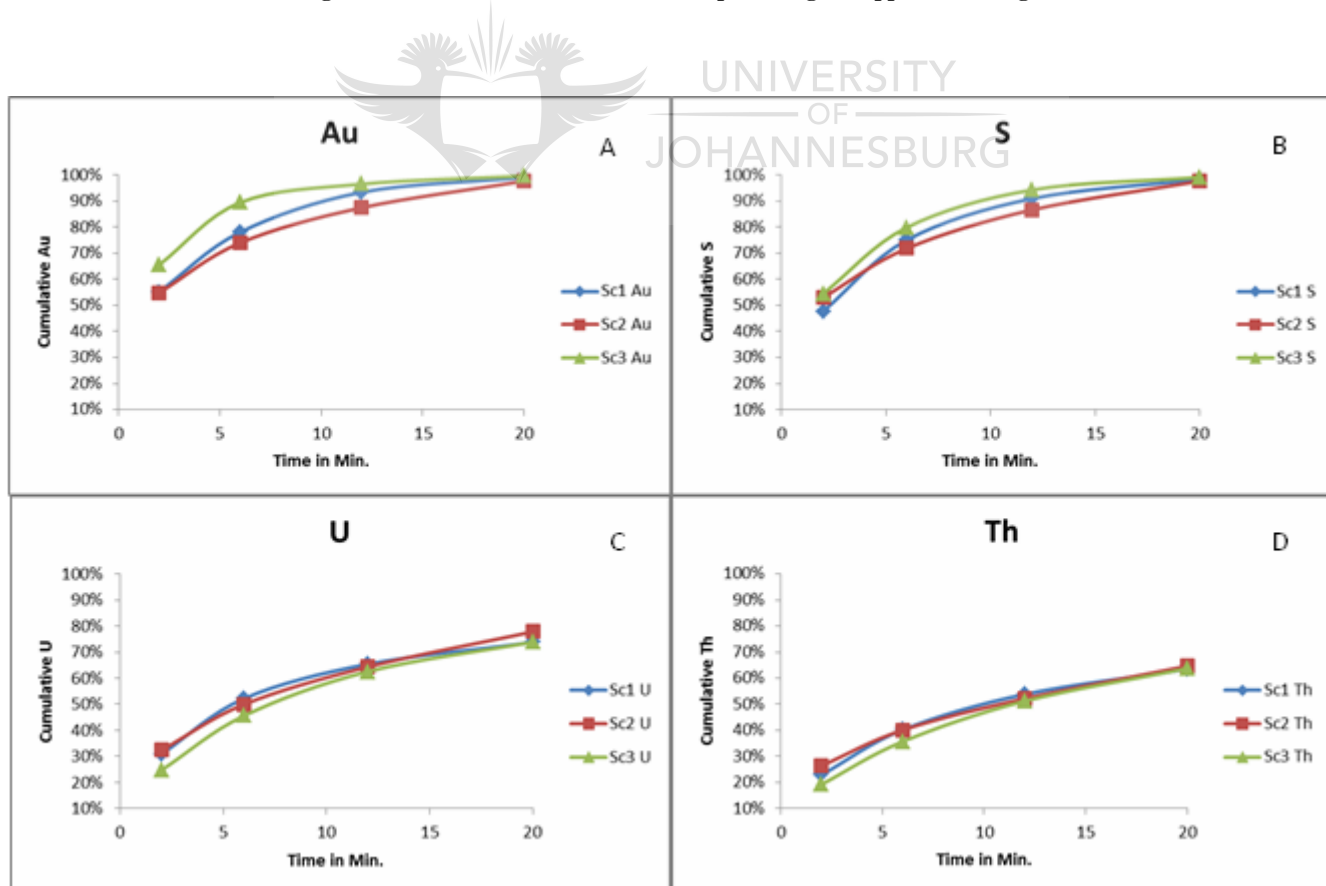


Figure 10.2: Cumulative recovery over time for Au, S, U and Th. (Appendix A6 a-g)

When analysed in combination, it is apparent that the Au and the S respond much quicker than the U and Th. This result is expected as Au and S are known to float more effectively than the U and Th (Figure 10.3, Rees, 2000).

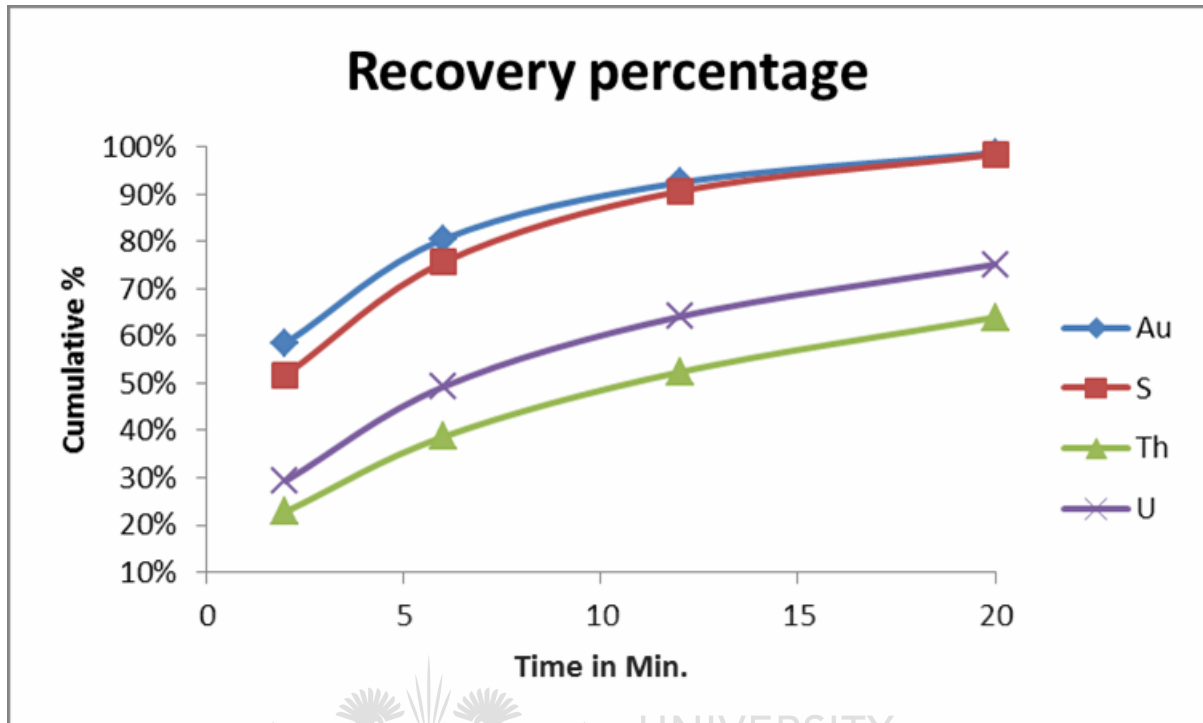


Figure 10.3: Average recovery curves for Au, S, Th and U (Appendix A6 a-g).

With regards to the mass pull figure, sample Sc2 indicates a higher mass pull in comparison to Sc1 and Sc3. This may be as a result of higher pyrite content within the sample (Tables 7.2-7.4).

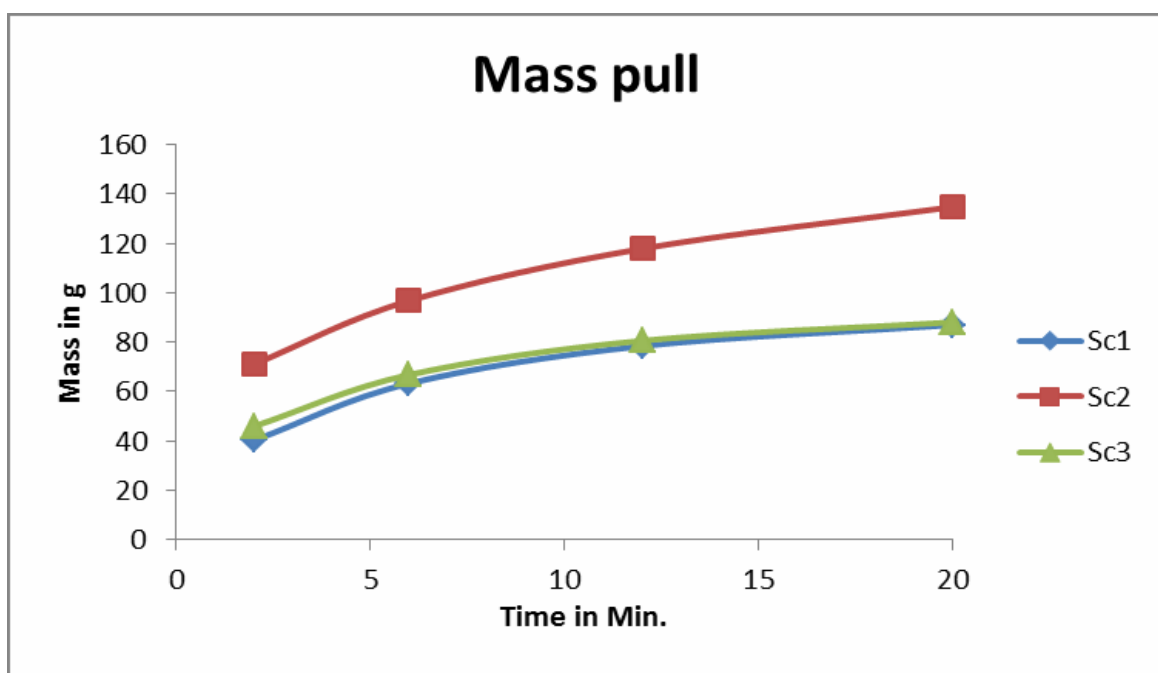


Figure 10.4: Mass pull for samples Sc1, Sc2 and Sc3 (Appendix A6 a-g)



### 10.3 Discussion

The gold and sulphur respond very well and relatively quickly under the flotation conditions as outlined in Chapter 5. These elements report largely to the first concentrate during flotation. The uranium and thorium, however, respond gradually over the flotation time. This could possibly be due to the entrainment of these elements which occurs as a result of their small particle size. Moreover, the recovery curves mirror the mass pull (Figure 7.39; Lloyd, 1981). However, uraninite is known to float with the addition of a xanthate collector, (Lloyd, 1981) and carbon in the form of kerogen (which is closely associated with U and Th) is naturally hydrophobic (Lloyd, 1981). It is likely that this combination of factors would cause some of the U and Th to report to the concentrates (Youlton et al., 2011).



# Chapter 11

## Discussion and Conclusions

### 11.1 Introduction

The purpose of this chapter is to discuss, summarize and conclude the data presented in this study, especially with regards to mineralogy, recovery and processing of the desired elements (Au, U and Th). This data and mineralogy can aid in the recovery and understanding of the desired minerals found within the Black Reef.

### 11.2 Mineralogy of the Ore

The mineralogy of the ore body plays a significant role in the recovery and performance of the ore when subjected to various extractive methods. The mineral form that the desired elements take can greatly affect how these elements perform when subjected to various extractive processes.

It can be concluded that the BSPL samples are largely conglomerates made up of three separate layers. The first of these is a massive quartzite layer with some large quartz pebbles at the basal contact, with some finer grained pyrite also present in small amounts. Below this layer is the pyrite conglomerate later, which constitutes the main part of the reef. This is where the buckshot pyrite texture is observed. This layer contains some carbon in the form of kerogen globules as well as clay material, which is found in the interstitial matrix of the buckshot pyrite grains. This clay material is largely made out of three minerals: muscovite (as the most abundant of the clay minerals), chlorite (as the least abundant) and pyrophyllite. Through the use of a microscope, it was discovered that gold particles are present in this later. As such, this layer is likely to be the richest throughout the reef section. The layer below this, where finer grained pyrite is present, is made up of more clay and carbon rich material than the layers above. The pyrite grains in question appear as stringers within this layer.

This mineralogy of the BSPL reef is comparable to that of the Witwatersrand conglomerate reefs, given that both have high pyrite and quartz contents. The Black Reef, however, contains less feldspar and more clay minerals than the Witwatersrand conglomerate reefs. The conglomerates found within the Black Reef are therefore expected to be less mature than those found within the Witwatersrand reefs (Hallbauer and Utter, 1977). There has also been less deformation within the Black Reef than within the Witwatersrand rocks (Frimmel, 2014).

The detailed studies conducted with the use of the MLA focused on the gold and uranium bearing minerals in the BSPL reef.

### **11.2.1 Gold Mineralogy**

Gold can naturally occur in many different forms, with native gold as the most common occurrence. Alloys and tellurides as well as electrum are also common occurrences of gold in nature (Kongolo and Mwema, 1998).

In this study, there was no evidence to suggest that the gold in question was anything other than native gold. As the peaks used to identify the gold in the MLA analysis showed only Au peaks with no significant quantities of Ag, it can be concluded that a large majority of the gold found within the BSPL is native gold (Figure 7.1). Gold was observed under the microscope using reflected light as well as through using the MLA. These processes showed that the gold particles are larger than the other elements of interest (Figure 6.9). This potentially means that it would be relatively easy to liberate and target the gold through extractive methods such as leaching (Coetzee et al., 2011).

The gold within the reef is associated with five dominant minerals: quartz; pyrite; chlorite; muscovite and pyrophyllite. This association of gold is expected as these minerals make up the majority of the bulk modal composition of the sample (Table 7.2-7.4).

The gold particles are often irregular in shape and do not appear to be rounded placer gold particles, such as those described in Hallbauer and Utter (1977). The combination of the grain description and the lack of evidence for the entry of hydrothermal fluids into the Black Reef Formation (Frimmel, 2014) suggests that the gold within the Black Reef is in-situ remobilized native gold (Frimmel, 2014). This explains why the gold is found in irregular

shaped, discrete particles within the conglomerate matrix and occasionally within vein structures (which are usually observed within pyrite particles (Figure 7.4, 7.5)). The particles were largely found to be fairly coarse grained, and coarser than the uranium bearing mineral phases, when analysed by the MLA.

### **11.2.2 Uraninite and Brannerite Mineralogy**

The uranium hosted within the Black Reef occurs in two mineral forms: brannerite, and uraninite, which is the more common occurrence of uranium within the BSPL (Table 7.2). A complex mineralogy of the uranium is often seen within the pebble-bed conglomerate deposits. The Uranium ranges from extremely fine-grained to refractory uranium within these types of deposits (Bowell et al., 2011). These minerals were identified during the sparse phase search conducted on the MLA since the particle sizes were small and therefore difficult to identify using a conventional microscope.

An association between these minerals and kerogen was noted. This type of relationship can also be seen within Witwatersrand uranium ores (Youlton et al., 2011). The association of the uraninite and brannerite to kerogen could be as a result of these minerals trapping the carbonaceous material as it moves through the Black Reef Formation. This process is better known as radiolytic polymerization, which essentially causes the carbon to be attracted to, and trapped by, the uranium bearing minerals. The uraninite and brannerite can then move into solution within the carbon, thus creating the disseminated uraninite and brannerite found within the kerogen globules (Parnell, 1999). The reverse of this process could also explain the association in question: in such a case, the uranium would have been in solution within the carbonaceous material as it moved into the Black Reef, following which the uranium bearing phases precipitated from the carbonaceous material (Parnell, 1999; Youlton et al., 2011).

### **11.3 Major and Trace Element Chemistry, Size distribution and HLS**

Department studies, which involves major and trace element chemistry assays and the grade by size departments of minerals, is essential to understanding the behaviour of the ore during

metallurgical processing. Methods of pre-concentration, such as heavy liquid separation or gravity concentration, need to be analysed in order to determine the effectiveness of these procedures in terms of concentrating the desired materials. This effectiveness must be established before the process of removing the gangue minerals from the desired minerals that need to be recovered can begin (Butcher et al., 2000; Chryssoulis, 2001; Coetzee et al., 2011). In this study, it was found that the run of mine bulk samples are generally silica-rich, and that they consist of a large percentage of pyrite (Fe and S). The Fe is typically above 8wt% and the total S is generally above 5%. The combination of this finding and the modal mineralogy suggests that the pyrite content within the reef is relatively high. The silica component within the BSPL reef is largely comprised of quartz, which makes up the bulk modal mineralogy. The kerogen observed in the reef accounts for the 0.1-0.3wt% total carbon in the bulk material. This is again comparable to the reefs of the Witwatersrand Supergroup, but it is important to note that the carbon content within the Black Reef is higher than the average carbon content found within Witwatersrand reefs such as the Vaal Reef (Hallbauer and Utter 1977).

### **11.3.1 Gold Grade, Size Department and HLS performance.**



Gold characterization is essential in the extractive process and can be crucial in determining how the gold will react to further testing. The factors of size as well as the upgrading and downgrading of the gold are important in the extraction of this precious metal (Petruk, 2000).

The gold found within the BSPL bulk samples ranges from 7.4g/ton to 12.6g/ton, which is higher than the global average of 1-5 g/ton found in auriferous reefs around the world (Mudd, 2007). The samples of this study indicated that the gold mainly reported to the size fractions below the target mill size of 75 $\mu$ m, with only 10-15% observed larger than 75 $\mu$ m. With regards to the upgrade and downgrade of the samples, the gold is significantly upgraded in the coarser size fractions, with a significant downgrade in the finer size fractions. This confirms the size range that was attained using the MLA (Figure 7.2). This suggests that the gold is coarse-grained and has been either liberated, or was attached to coarse-grained material following the milling process. The Au is not mirrored by the S, which was analysed for in the same test. This result is unexpected given the findings of previous studies based on the Witwatersrand reefs (Mnogma, 2012).

Gold can be pre-concentrated using methods that involve density separation by gravity (Petruk, 2000). In this study, the gold was effectively pre-concentrated using a heavy liquid separation. The same test when applied to sulphur indicated a comparison between the gold and sulphur, which suggests that the two elements are associated. This finding is comparable to many of the studies based on the Witwatersrand reefs (Mngoma, 2012). In contrast, the testing performed on the size department showed no clear correlation between Au and S.

An anomalous result was noted with regards to the Au, S and Fe content in the original trace element chemistry assay (Table 8.1). As the Fe and S concentrations increased (assuming these elements were obtained from the pyrite as the modal mineralogy suggested) the Au showed an evident decrease in abundance. In other words, the lowest Au values showed the highest Fe and S values. Therefore, as the pyrite content increases the gold content decreases. This is unexpected, as gold is closely associated to the quantity of pyrite in many of the Witwatersrand's reefs (Minter, 1976).

### **11.3.2 Uranium and Thorium Grade, Size Department and HLS performance.**

The uranium found in the samples ranges in concentration from 29ppm to 56ppm or g/ton (Table 8.1). This is a fairly low abundance in comparison to other sandstone or quartzite-hosted uranium deposits, as well as in comparison to other quartz-pebble conglomerates that occur within the Witwatersrand rocks (Bowell et al., 2011; Youlton et al., 2011). Thorium ranges between 3.5ppm and 5.2ppm or g/ton, which also fairly low within this type of deposit (Youlton et al., 2011).

The department of these samples is a fine-grained department, as the majority of the uranium and thorium is found in the finer size fractions, with less than 10 % reporting to the +75 $\mu$ m size fractions. The uranium and thorium are also significantly upgraded into the finer size fractions (Figure 8.4). This is common within these types of deposits, especially where there is a large abundance of pyrite and quartz (Bowell et al., 2011). A mirrored trend, with regards to the uranium, is also observed in the thorium. This may be due to the solid solution that occurs between the U and Th, where there is a variable concentration of Th in U-bearing minerals (FrondeL, 1907).

Two methods can be employed in order to pre-concentrate uranium ores: 1. Radiometric sorting of the ore, which is used to concentrate finer particles of uranium-bearing phases, or 2. Scrubbing and screening the ore (Bowell et al., 2011). While these methods were not employed in this study, U and Th in the gold pre-concentrates were tested for. The fact that the tests showed the majority of the U and Th reporting to the slimes fraction during the heavy liquid testing ruled this method out as an effective means of concentrating the U and Th (Figure 8.8).

#### **11.4 Geometallurgical Testing**

Geometallurgical testing is crucial in ascertaining how the ore will perform when subjected to recovery processes as implemented in the mining industry. First, the bulk samples that need to be subjected to other processes need to be milled. The reason for this is that the ore first has to be broken down into finer particles so that processes such as leaching and flotation can be effective (Walters and Kojovic, 2006; Alruiz et al., 2009).

The target size for the milling of the BSPL bulk samples was 75-80% passing 75 $\mu$ m, since this was the required mark used at the Modder East operation processing plant. On average, one kilogram of the BSPL bulk samples took approximately 21.5 minutes to reach the target mill size of between 75-80% passing 75 $\mu$ m. This short milling time is a result of the sedimentary origin of the minerals in the BSPL reef (as described in Chapter 6) which ultimately makes the samples softer in comparison to other ore bodies. In contrast, igneous-hosted PGMs can take up to 40 minutes to reach the outlined size (Dzvinamurungu et al., 2013). The milling time for all the samples was very similar with regards to the reaction to milling. This kind of uniformity means that a mine could apply the same milling time to all the ore fed into the milling and recovery plant, which would allow for cost effective and simple milling requirements.

### 11.4.1 Gold Metallurgical Performance

Globally, cyanide leaching methods, including carbon in-pulp and carbon in-leach treatment plans, have been the primary means of recovering gold from ore. While attempts to develop less toxic means of gold extraction have been made in response to the negative environmental effects of cyanide, none of these has proved as effective as the cyanide related processes (Rees, 2000). In this study, all three submitted samples showed a very high recovery: between 94% and 99%. Therefore, the gold in this sample can be classified as non-refractory or free milling gold, as outlined in Rees (2000). The recovery also reconfirms that the gold is in-situ remobilized and fairly coarse. In addition, the high percentage of recovery with the gold leach indicates that the gold is well-exposed in the crushed and milled material (as it is the exposed surface that reacts with acid during the leaching process). Such results should therefore be expected at the mine when calculating recoveries within the Black Reef ore. The 1-6% loss in gold recoveries could be attributed to the absorbing of gold by the carbon present in the material during the leaching process. Such materials (known as preg-robbbers) could account for the up to 6% loss in gold recoveries (Rees, 2000). In addition to the preg-robbbers the loss in gold recoveries could also be attributed to the gold lock within pyrite grains thus making it refractory and unrecoverable.

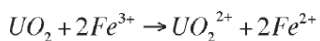
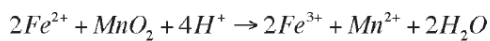
In general, flotation is not a widely used method of extraction for recovering gold from materials. Nevertheless, flotation was used as a method of extraction in this study. This decision was informed by the fact that the reef contains significant amounts of pyrite (as evident in the modal mineralogy) and that the association of gold to pyrite is common within Witwatersrand reefs. The hypothesis was that flotation might therefore offer an alternative method of extraction. The results (97-99% gold and sulphur recoveries) indicated that the gold and sulphur in the flotation process showed patterns that mirrored each other. However, this study also found that gold is generally not contained within pyrite minerals, which means that the performance in the flotation process cannot be attributed entirely to its entrainment within the sulphide minerals. Having acknowledged this, it is also important to note that gold is known to float when exposed to flotation conditions such as those emulated in this study. In addition, evidence of existing literature suggests that native gold in some ores is naturally hydrophobic and will therefore float effectively during the flotation process (Allan and Woodcock, 2001). Given the above findings and observations, an argument could be made for flotation as an alternative to cyanide leaching of the ore.



## 11.4.2 Uranium Metallurgical Performance

The leaching process of uranium is highly dependent on which uranium hosting minerals occur within a specific reef (Venter and Boylett, 2009). In the case of this study, two uranium bearing minerals were identified: uraninite and brannerite. Acid leaching of uranium is generally the most popular process for extracting uranium from ore. Tetravalent uranium, like that found in the uraninite, must be oxidized to the hexavalent form in order for dissolution to occur. This is achieved by the reaction with  $Fe^{3+}$  (Equation 7.1) which allows the uranium to oxidise and form  $Fe^{2+}$ .

**Equation 7.1: Reaction showing the oxidization of uraninite. (Adapted from Venter and Boylett 2009).**



Brannerite, which can be considered refractory uranium, does not respond well to this process (Venter and Boylett, 2009). The testing showed that between 60% and 75% of the uranium was recovered using the methods outlined by SGS. The lack of 100% recovery in this instance could be attributed to the percentage of uranium found within the brannerite and other refractory phases within the BSPL samples, as well as to acid consuming minerals in the BSPL samples (Venter and Boylett, 2009; Youlton et al., 2011). The 60-75% recovery is nevertheless relatively high in comparison to the recoveries seen within some Witwatersrand reefs. However, the grade seen in the Black Reef is far lower than that seen in the Witwatersrand reefs (Lloyd, 1981).

While the uranium flotation results of this study are not as impressive as the gold recovery, the recovery of the uranium is notable with up to 80% recovery. This could be as a result of the fact that carbon will float when exposed to the flotation conditions, given its hydrophobic nature. Furthermore, the high uranium-kerogen association facilitates the flotation of the uranium as entrained material (Youlton et al., 2011). Moreover, Lloyd (1981) maintains that uraninite can be recovered if it is effectively activated with the addition of a xanthate collector. This may also be the source of the U and Th that report to the concentrates during flotation.

### 11.4.3 Implications for Recovery based on Metallurgical Performance

Geometallurgy and the extraction of ore is by no means a new field and has been used in metal recovery for a long time. However, mining companies have only recently started to invest significantly in understanding the role that mineralogy and other factors can play in the extraction of precious metals (Alruiz et al., 2009). The gold found in this study is very similar to the conglomeratic gold that occurs within the Witwatersrand ores between the interstitial vacancies that occur within the matrix of a conglomerate (Petruk, 2000). This means that the gold would be present in areas that are readily breakable during the crushing and milling of the ore. With regards to this in-situ gold study, while it was not clearly evident as to how the gold was liberated, the leach testing found that the gold was free milling (as classified in Rees, (2000). The presence of carbon and chalcopyrite in the samples could be detrimental during the leaching process. The carbon may reabsorb the gold within the material. This would lead to the loss of the gold to the tailings. As noted earlier, this process (known as preg-robbing) frequently occurs during the leaching process (Rees, 2000). The presence of chalcopyrite would also affect the leaching process as it can often consume the cyanide thus reducing the potential for gold recovery (Vaughan, 2004). These factors, therefore, needed to be considered when leaching the gold from the Modder East samples. However, the large recovery percentages as evident in the testing of the samples suggest that these are insignificant factors in the calculation of gold recovery. The testing and processing of the gold indicated that the gold is not necessarily dependant on the pyrite or found locked within the pyrite, as is the case with the Witwatersrand reefs and other reefs of this kind. However, the samples still responded extremely well when subjected to the outlined flotation conditions. This suggests that the native gold within these samples may be hydrophobic (Allan and Woodcock, 2001; Teague et al., 1999). Thus, it can be said that there are two viable options for the recovery of the gold. With regards to flotation, further testing needs to be conducted in order to determine what other minerals may float and report to the concentrates during flotation. This needs to be studied so that potential problems associated with flotation may be identified. Such issues could include the occurrence of gangue minerals within the concentrates. These specific minerals could possibly have an effect in the later processing of the metals in question (Teague et al., 1999).

With regards to the pre-concentration of the gold, the HLS results demonstrate that the gravity method would be effective in concentrating the gold as a large portion of the gold

reports to the sinks. However, some losses remain, as seen in the slimes and floats. This needs to be considered when employing the pre-concentration step in the processing of the gold.

The results of the uranium leaching are fairly poor in comparison with the Au recoveries. This can be attributed to the percentage of brannerite: as a refractory ore mineral in the context of uranium, its presence renders a certain percentage of uranium unrecoverable. These factors in the recovery need to be considered as part of the calculations when mining and processing uranium, so that the viability of uranium leaching may be established (Youlton et al., 2011). It is likely that the thorium would follow the same trend, given that it is found in a solid solution with the uranium bearing minerals (FrondeI, 1907). Therefore, considering the grades of the U and the Th, as well as the percentage of brannerite in the samples, the processing of the uranium and thorium from these samples could prove problematic.

## 11.5 Conclusions and Recommendations

Youlton et al., (2011) and Coetzee et.al. (2011) illustrate the importance of identifying all the characteristics of the ore through detailed studies. The careful identification of the geometallurgical characteristics of the metals targeted during mining can prove valuable in establishing more productive and cost effective ways to extract the economic minerals.

The following conclusions were considered notable with regards to this study:

- The samples taken from the Modder East mine are silica rich quartzite conglomerates that contain a notable layer of buckshot pyrite. This is the main ore containing horizon within the Black Reef samples.
- The in-situ MLA analysis indicated that gold is fairly simple conglomeritic gold as described by Petruk, (2000) and occurs in the interstitial spaces within the conglomerate matrix. It was also indicated through analysis that the large majority of the gold found within the samples is native gold.

- The gold is fairly coarse grained in-situ remobilized gold as determined by the shape and size of the gold grains found within the BSPL samples. This observation leads to the conclusion that the gold was deposited at the same time as the rest of the sediments and then later remobilized by the lithification process. As such, the Black Reef Formation can be classified as sub-green schist facies rocks (Frimmel, 2011).
- The gold relevant to this study can be effectively concentrated using simple gravity methods as indicated by the heavy liquid separation results.
- As the leach testing conducted on the samples indicated recoveries of over 94%, it can be concluded that the gold is effectively leached and available to move into the cyanide solution. The high recoveries suggest that the gold is free milling and non-refractory (Rees, 2000).
- The results of this study indicate that the gold can be easily recovered using traditional methods such as direct cyanidation (as employed at Modder East processing plant). Since almost all of the gold reports to the concentrates, it can be said that a potential alternative to cyanidation is flotation. Flotation also effectively concentrates the sulphur in the samples, as expected. However a high pyrite content within the concentrate will make the concentrate low grade and will have to be further processed.
- Uranium that occurs within the Black Reef is found to be in two mineral forms: uraninite and brannerite.
- From the analysis of the uranium bearing phases it can be concluded that the uranium within these samples could have been either deposited as detrital uraninite and brannerite, or it could have precipitated out of the carbonaceous material that moved into the Black Reef Formation. It could also be a combination of these two methods (Parnell, 1999; Youlton et al., 2011).
- The uranium is fairly low grade, ranging between 30 g/ton and 60g/ton, which is not viable with regards to mining of this material (Bowell et al., 2012). The percentage of brannerite that hosts the uranium renders the uranium refractory and unrecoverable, resulting in a loss of uranium during processing (Youlton et al., 2011).
- The study recorded that only 60% to 75% of the uranium is recovered during the leaching process and that this recovery occurs at low grades. As such, it can be concluded that uranium is a difficult metal to obtain economically, even if other pre-

concentration methods such as radiometric sorting or the scrubbing of the ore are employed (Bowell et al., 2011).

- While uranium and thorium are successfully upgraded during flotation, however low grades are likely to render the concentration and recovery of both uranium and thorium expensive.
- As the majority of the U and Th reported to the finer size fractions, the most effective method of concentrating the U and Th would be size screening in this study.

Considering the decent gold recoveries indicated in this study, the recommendation is that the Black Reef ore should be milled to between 75% and 80% passing 75 $\mu$ m. As the results of the study show, this would lead to the effective exposure of the gold during the cyanide leaching process. Should recoveries reflect lower than 94%, an investigation should be conducted to determine whether or not there have been problems during the extraction process or whether or not the mineralogy of the ore has changed.

It is also recommended that further investigation be carried out with regards to employing pre-concentration of the gold, as a small percentage was seen to be lost during the HLS testing. The recommendation is for alternative methods to be evaluated and employed before considering the introduction of a pre-concentration method in the extraction of the gold within the Black Reef.

The bright phases within the samples were analysed using the SPL\_Lt and the XBSE routines that are available on the MLA. This identification and classification of the phases proved to be an effective and time-efficient process that ultimately leads to important conclusions regarding the size distribution, occurrence and associations of the gold, uranium and thorium bearing mineral phases. As such, it is recommended that any further investigation of this kind should be conducted using the MLA technology.

Further investigation is also recommended with regards to the flotation of the gold and uranium within the Black reef as other potentially problematic phases may also report to the concentrates during flotation (Bulatovic, 2007). The results of this study demonstrate that the U and Th mirror the mass pull of the flotation testing, which means that the recoveries of these fine grained uranium bearing minerals could be attributed to entrainment during flotation. Therefore, further investigation regarding uranium flotation within the Black Reef needs to be conducted.

As the evidence of this study does not pinpoint a definite source of the uranium hosted within the Black Reef, further investigation is recommended to determine the precise source of the uranium bearing mineral phases in the Black Reef. Finally, as this study has shown that the uranium grades in the Reef are fairly low, a further investigation should be conducted into the economic viability of pre-concentrating the uranium.



## References:

- Allan, G.C. and Woodcock, J.T. (2001). A review of the flotation of native gold and electrum. *Minerals Engineering*, **14**, pp. 932-962.
- Alruiz, O.M., Morrell, S., Suazo, C.J. and Naranjo, A. (2009). A novel approach to the geometallurgical modelling of the Collahuasi grinding circuit. *Minerals Engineering*, **22**, pp. 1060-1067.
- Barton, E.S. and Hallbauer, D.K. (1996). Trace-element and U-Pb isotope compositions of pyrite types in the Proterozoic Black Reef, Transvaal Sequence, South Africa: Implications on genesis and age. *Chemical Geology*, **133**, pp. 173-199.
- Bose, P.K., Eriksson, P.G., Sarkar, S., Wright, D.T., Samantha, P., Mukhopadhyay, S., Mandal, S., Banerjee, S. and Altermann, W. (2012). Sedimentation patterns during the Precambrian: A unique record? *Marine and Petroleum Geology*, **33**, pp. 34-68.
- Bowell, R.J., Grogan, J., Hutton-Askenny, M., Brough, C., Penman, K. and Sapsford, D.J. (2011). Geometallurgy of uranium deposits. *Minerals Engineering*, **24**, pp. 1305-1313.
- Bulatovic, S.M. (2007). *Handbook of flotation Reagents, Chemistry, Theory and Practice: Flotation of sulphide ores*. Elsevier science and Technology Books. **Volume 2**, pp. 1-17.
- Butcher, A.R., Helms, T.A., Gottlieb, P., Bateman, R., Ellis, S., and Johnson, N.W. (2000). Advances in the quantification of gold deportment by QEMSCAN. Seventh Mill Operators Conference, Kalgoorlie, WA. AusIMM. pp. 267-271.
- Button, A. (1978). Correlation of the Gondwana formation based on stratigraphic trends in the Witwatersrand basin. *Transactions of the Geological society of South Africa*, **81**, pp. 109-114.
- Coetzee, L.L., Theron, S.J., Martin, G.J., David, J., van der Merwe, T. and Stanek, A. (2011). Modern gold deportments and its application to industry. *Minerals Engineering*, **24**, pp.565-575.
- Chryssoulis, S.L. (2001). Using mineralogy to optimize recovery by flotation. *Journal of Minerals, Metals and Materials Society*, **53**, pp. 48-50.
- De Bever, N.J., (1997). An Overveiw of the Early Proterozoic, Auriferous Black Reef Placer in the Transvaal Basin. M.Sc Thesis, Faculty of Science, Rhodes University, Supervisor : Prof John Moore. pp 118.

- De Wit, M.J., De Ronde, C.E.J., Tredoux, M., Roering, C., Hart, R.J., Armstrong, R.A., Green, R.W.E., Peberdy, E. and Hart, R.A. (1992). Formation of an Archaean continent. *Nature*, **357**. pp. 553-562.
- Dominy, S.C., Xie, Y. and Plattern, I.M. (2008). Characterisation of in-situ gold particle size and distribution for sampling protocol optimisation. Ninth International Congress for Applied Mineralogy, Brisbane, QLD. pp. 175-185.
- Dzvinamurungu, T., Viljoen, K.S., Knoper, M.W., and Mulaba-Bafubiandi, A. (2013) Geometallurgical characterisation of Merensky Reef and UG2 at the Marikana Mine, Bushveld Complex, South Africa. *Minerals Engineering*, **52**. pp. 74-81.
- Eriksson, P.G., Altermann, W., Catuneanu, R., van der Merwe, R. and Bumby, A.J.(2001) Major influences of the evolution of the 2.67-2.1 Ga Transvaal Basin, Kaapvaal craton. *Sediment geology*, **141-142**. pp. 205–231.
- Fandrich, R. Gu, Y. Burrows, D., and Moeller, K.. (2007). Modern SEM-based mineral liberation analysis. *International Journal of Mineral Processing*, **84(1-4)**. pp. 310–320.
- Frimmel, H.E. (2014). A giant Mesoproterozoic crustal gold-enrichment episode: possible causes and consequences for exploration. Society of economic geologists, special publication, **18**. Pp. 209-234.
- FrondeL, C. (1907). Systematic mineralogy of uranium and thorium. U.S. Geological Survey. Bulletin **1064**. Washington, U.S. Government print office, 1958.
- Goodall, W.R. and Scales, P.J. (2007). An overview of the advantages and disadvantages of the determination of gold mineralogy by automated mineralogy. *Minerals Engineering*, **20**. pp. 504-517.
- Gold One International (2013). [www.gold1.co.za](http://www.gold1.co.za). Accessed: 14 October 2013.
- Hallbauer, D.K. and Utter, T. (1977). Geochemical and morphological characteristics of gold particles from recent river deposits and the fossil placers of the Witwatersrand. *Mineral Deposita*, **12**. pp. 293-306.
- Hartzer, F.J. (1994). Geology of the Transvaal inliers in the Bushveld Complex. Ph.d. thesis (unpubl.), Rand Afrikaans University Johannesburg, 368 pp.
- Henry, G., Clendenin, C.W. and Charlesworth, E.G. (1990). Depositional facies of the black reef Quartzite formation in the Eastern Transvaal, Geological Society of South Africa, **90**. pp. 230-233
- Johnson, M.R., Anhaeusser, C.R. and Thomas, R.J. (2009). The Geology of South Africa (Eds). Geological Society of South Africa, Johannesburg Council for Geoscience, Pretoria, 691pp
- Kongolo, K. and Mwema, M.D. (1998). The extractive metallurgy of gold. *Hyperfine Interactions*, **111**. pp. 281-289.



- Lloyd, P.J.D. (1981). The Flotation of gold, uranium, and pyrite from Witwatersrand ores. *Journal of the South African institute of mining and Metallurgy*, February 1981, pp. 41-47.
- Minter, W.E.L, (1976). Detrital Gold, Uranium and Pyrite concentrations related to sedimentology in the Precambrian Vaal reef Placer, Witwatersrand, South Africa. *Economic Geology*, **71**. pp. 157-176.
- Moore, J.M, Tsikos, H. and Polteau, S. (2001). Deconstructing the Transvaal supergroup, South Africa: implications for Palaeoproterozoic paleoclimate models. *Journal of African Earth Sciences*, **33**. pp. 437-444.
- Mnogma, L., (2012). A gold, uranium and thorium department analysis of Witwatersrand ore from cooke section, rand uranium Randfontein. M.Sc thesis. Department of Geology. University of Johannesburg.
- Mudd, G.M. (2007). Global trends in gold mining: Towards quantifying environmental and resource sustainability. *Resources Policy*, **32**, Issues 1–2. pp. 42-56.
- Parnell, J. (1999). Petrographic evidence for the emplacement of carbon into the Witwatersrand conglomerates under high fluid pressure. *Journal of Sedimentary Research*, **69**. pp. 164-170.
- Petruk, W. (2000). *Applied mineralogy in the mining industry*. 1<sup>st</sup> ed, Amsterdam; New York, Elsevier. 124 pp.
- Poujol, M., Robb, L. J., Anhaeusser, C.R. and Gericke, B. (2003). A review of the geochronological constraints on the evolution of the Kaapvaal Craton, South Africa. *Precambrian Research*, **127**. pp. 181-213.
- Rees, K.L. (2000). The leaching and absorption behaviour of gold ores. Ph.D. Thesis. Department of Chemical Engineering. The University of Melbourne. 289 pp.
- Stange, W. (1999). The process design of gold leaching and carbon in pulp circuits. *The Journal of the South African institute of Mining and Metallurgy*, **43**. pp. 13-26
- Teague, A.J., Van Deventer, J.S.J. and Swaminathan, C. (1999). A conceptual model for gold flotation. *Mineral Engineering*, **12**. pp. 1001-1019.
- Walters, S. and Kojovic, T. (2006). Geometallurgical mapping and mine modelling (GeM111), the way of the future. In: *Proceedings of SAG 2006*, Vancouver, pp.411–425.
- Wiese, J., Harris, P. and Bradshaw, D. (2005). The influence of the reagent suite on the flotation of ores from the Merensky reef. *Minerals Engineering*, **18**. pp. 189-198.
- Vaughan, J.P. (2004). The process mineralogy of gold: The classification of ore types. *Journal of Minerals, Metals and Materials Society*, **56**, number 7. pp. 46-48.

Venter, R. and Boylett, M. 2009. The evaluation of various oxidants used in acid leaching of uranium. Hydrometallurgy Conference 2009, The Southern African Institute of Mining and Metallurgy, **109**. pp. 445-456

Youlton, B.J., Coetzee, L.L., Scott, L.M., O'Connell, J., O'Connell, R. and Kinnaird, K.A. (2011). Uranium deportment studies: Beyond the assay. ALTA Uranium Conference Proceedings, Perth Western Australia. pp 43-55.



## Appendix 1:

### Sample Preparation

Further details of sample preparation for the bulk samples and images for thin section preparation, that were analyzed using the MLA.

#### Bulk samples:

- Sample collection day 1 (**SC1**) weight: 46kg
  - This was crushed to a size passing 3.35 mm
  - It was then blended for 10 minutes in a rotary blender
  - This was then split into 10 kg splits, with the remains of 6kg using the Jones riffler. (**SC1, Sp1-Sp4**)
    - One of these 10kg splits was once again split into 1kg aliquots using a Rotary riffler. (**Sc1, Sp3, 1-10**)
    - One of these 1 kg aliquots was then split again into 8 splits of about 125g. (**Sc1, Sp3\_3, A-H**)
    - Then split D was again split into 8 (**Sc1, Sp3\_3, D, a-h**)
    - **a** and **e** of these splits were combined and split into 8 using Rotary micro riffler, and this was also done for **c** and **g** resulting in 16 equal splits. These resulting 16 splits were used to create 30 mm mounted blocks that will be analyzed by the MLA, which were labeled as **Sc1, Sp3\_3, 1-16**
- This process was repeated for sample collection days 2 and 3 (**Sc2, Sc3**) with the only difference that split 4 (**Sp4**) of the ten kilo splits was used.
  - **Sc2** 52 kg
  - **Sc3** 48.6 kg

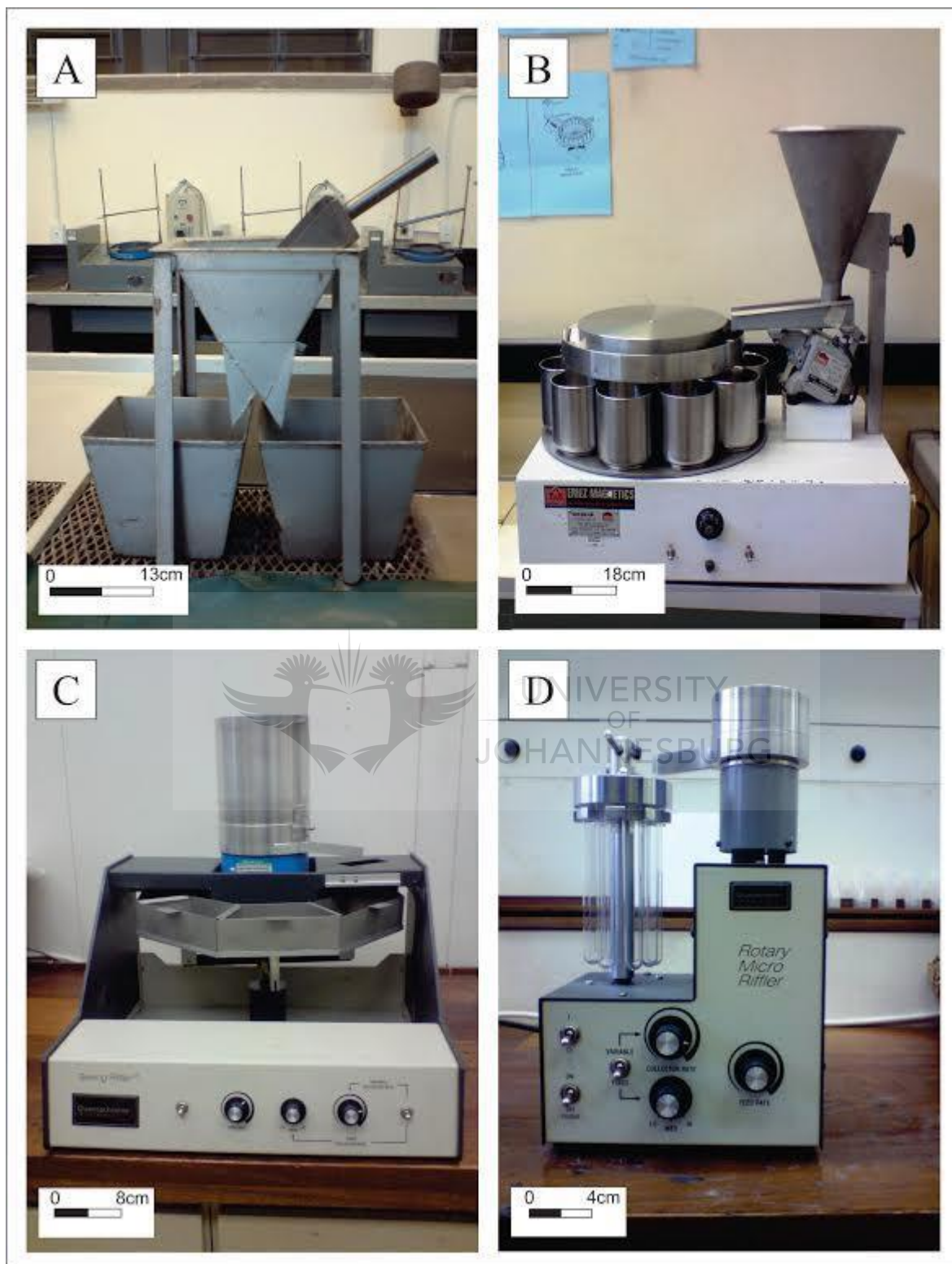


**Figure A1 a:** Splitters used in the preparation of the bulk samples. Splitter A (Jones riffler) was used to create the 10 kg splits. Splitter B (Rotary riffler, 10 sections) was used to create the 1 kg splits. The next two splitters C and D (rotary riffler and micro rotary micro riffler 8 sections) were used to create the smaller splits that were used to create the mounts. Picture courtesy of Derek Rose PhD Candidate at university of Johannesburg, 2013

### Thin section Preparation:

Thin sections were prepared from the large sample, **S1**, which is indicated in Figure 6.1 in Chapter 6. Slices between, 1.5 to 2 cm thick, where cut. Nine slices where cut from this sample. Slice 6 (S1 sl6) was polished for use in hand sample descriptions. Sample names are as follows **BSPL S1 SI-1 T-1** for the first slice and first thin section of that slice. In the figures below are pictures of the slices made and the location of the thin sections cut, as well as the sample names of the thin sections. There was also a sample S1 X that was made and is listed Table A1 a, but photographs of this slice were not recorded, but the location within the reef was. Nine thin sections were also made with the purpose of transmitted and reflected light microscopy. Three were made from above the pyrite layer, three within the pyrite layer and three below the pyrite layer. This was done to add to the description and mineral identification. .

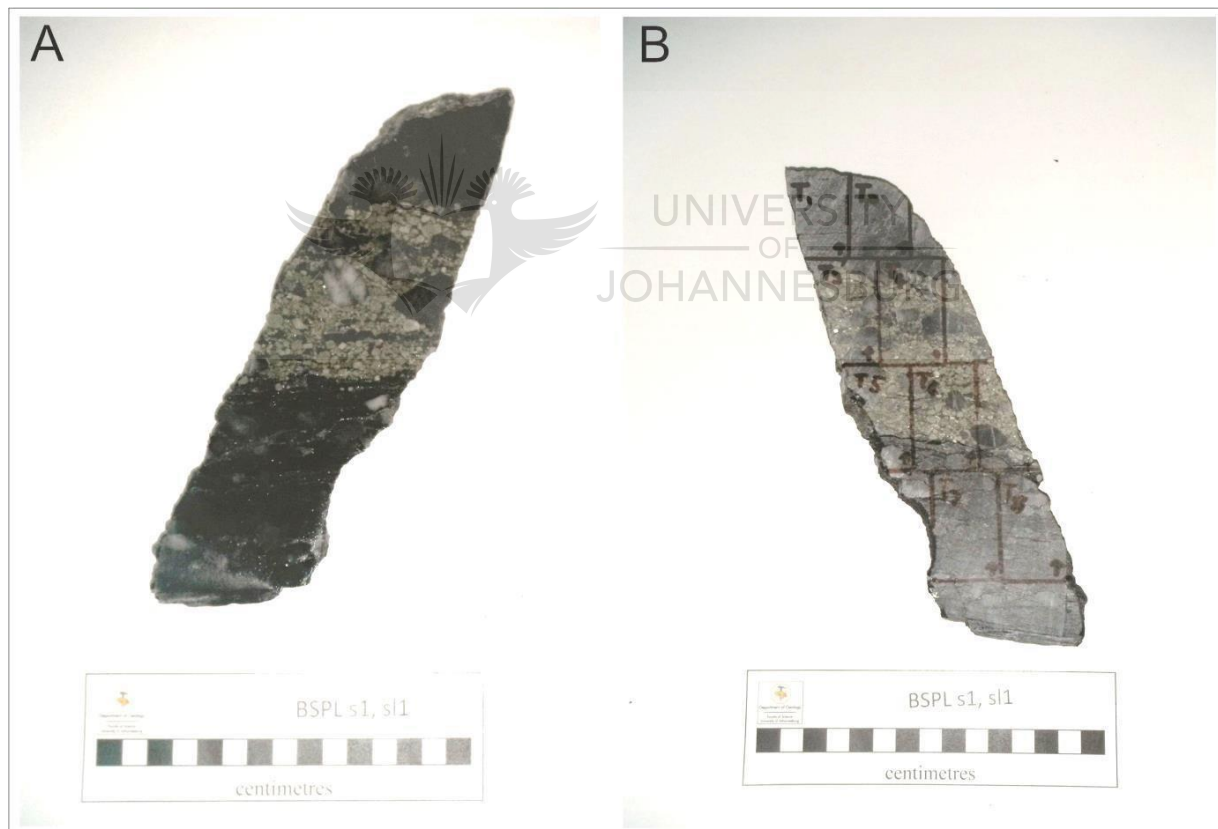


Figure A1 b: Photographs of BSPL s1, sl 1(A) and the reverse (B)

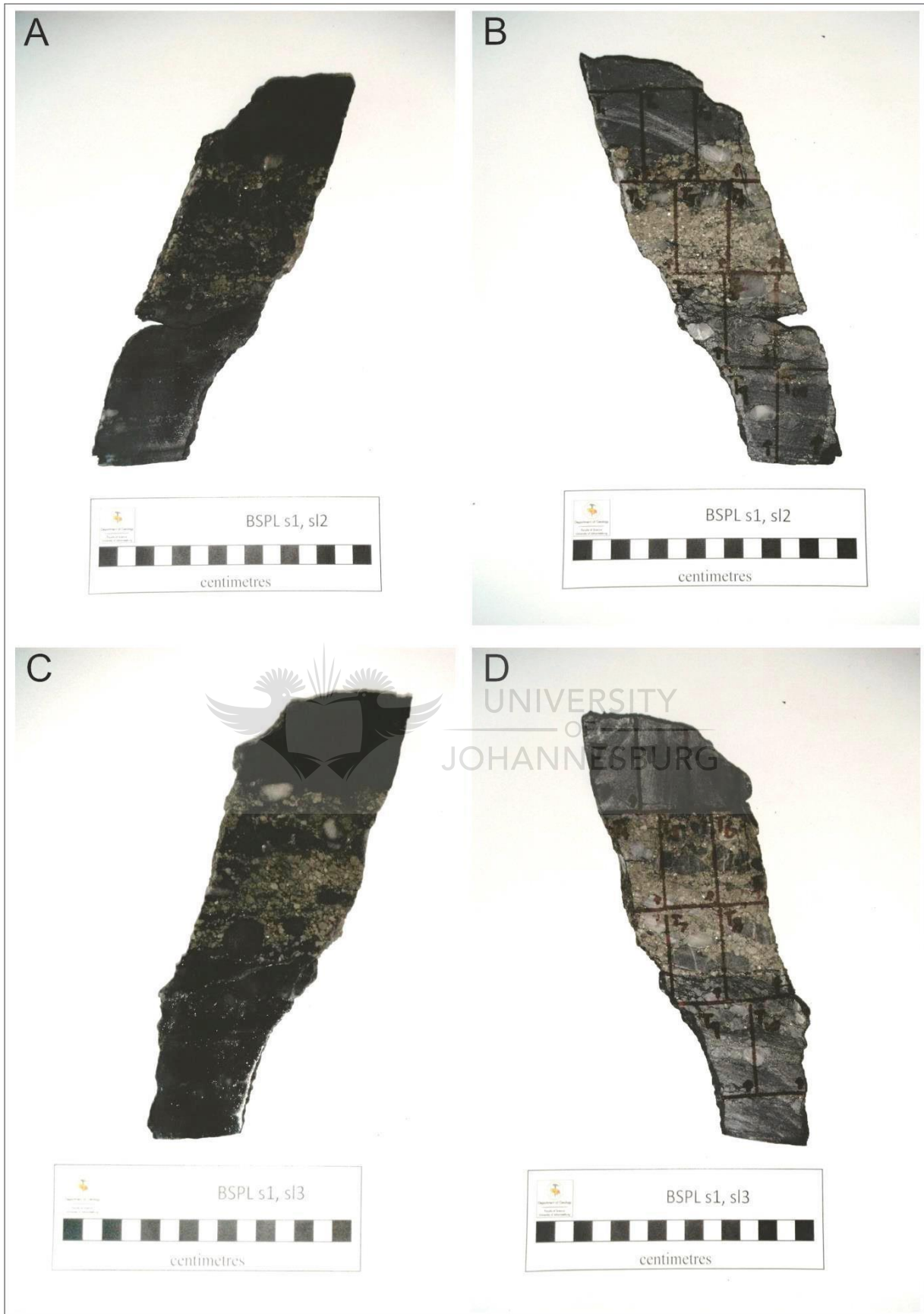


Figure A1 c: Photographs of BSPL s1, s2-3(A-C) and the reverse (B-D)

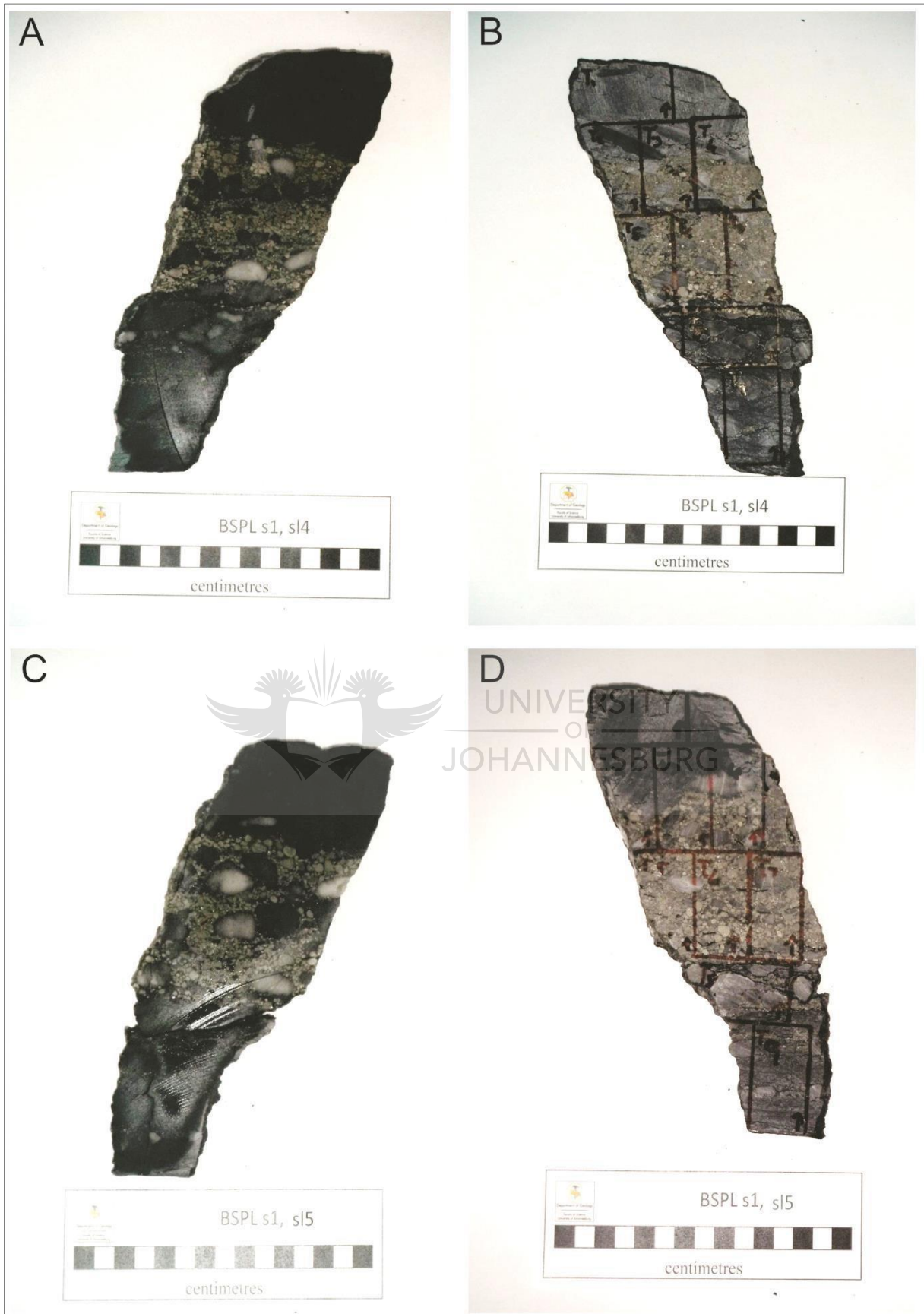


Figure A1 d: Photographs of BSPL s1, s4-5(A-C) and the reverse (B-D)

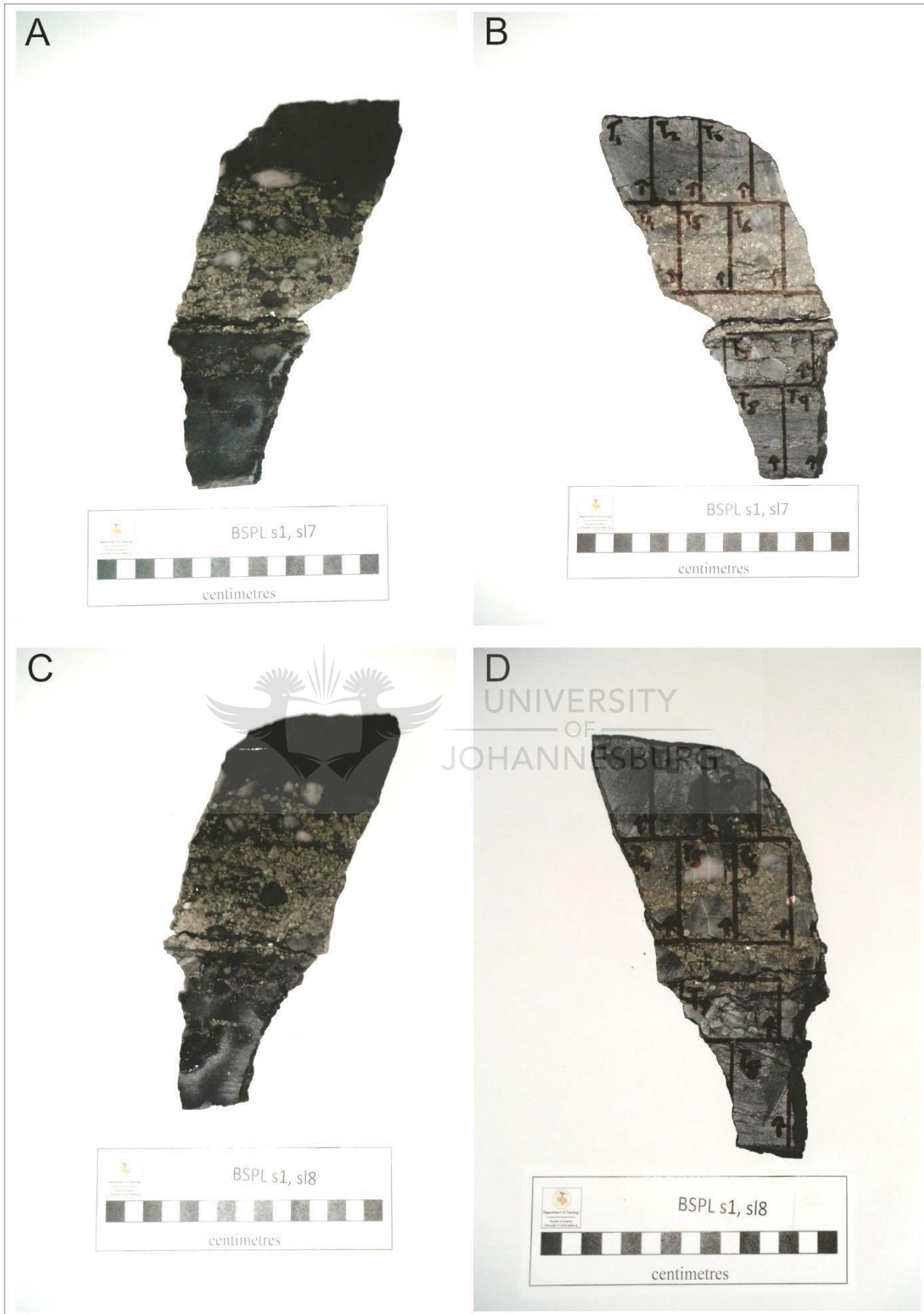


Figure A1 e: Photographs of BSPL s1, s7-8 (A-C) and the reverse (B-D)



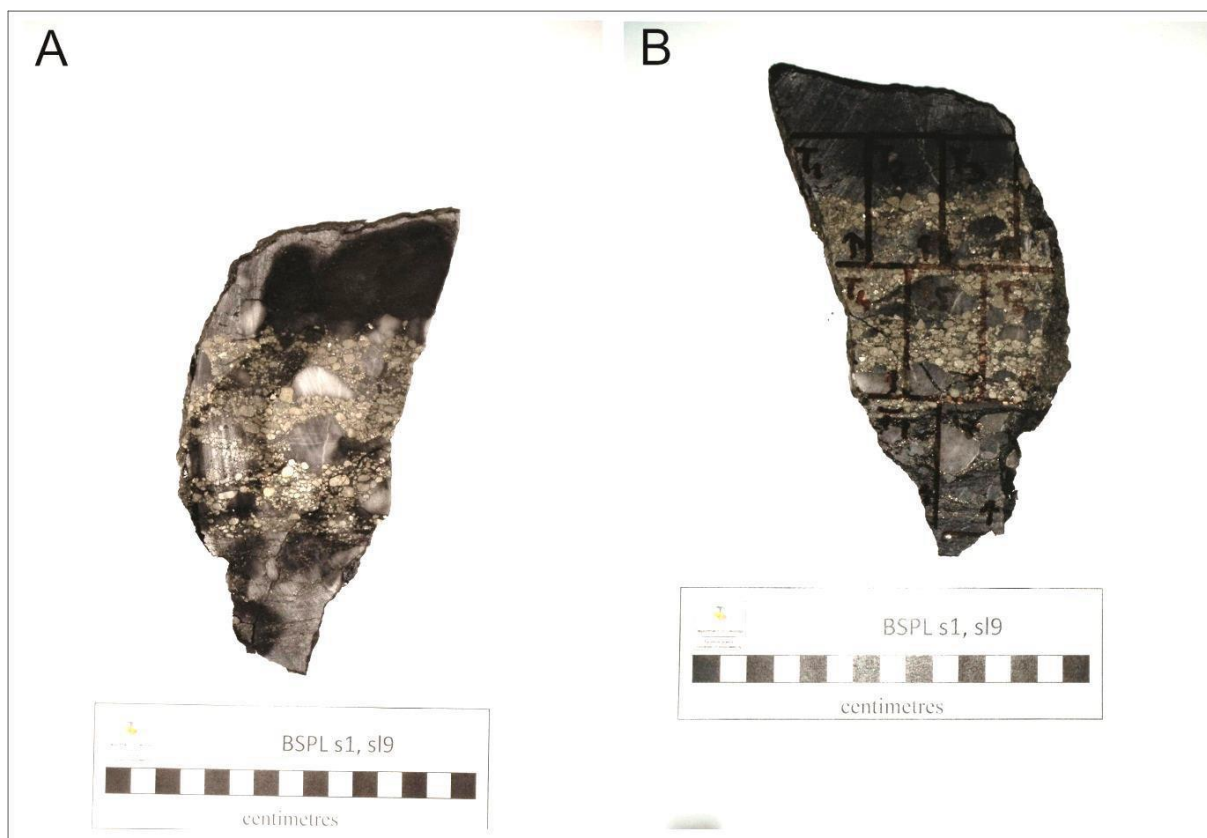


Figure A1 f: Photographs of BSPL s1, s19(A) and the reverse (B)

Table A1 a: Thin section names with reference to previous photographs indicating location within the slices

Slice 1	Slice x	Slice 2	Slice 3	Slice 4
BSPL s1, sl-1, T-1	BSPL s1, sl-1, T-2	BSPL s1, sl-2, T-1	BSPL s1, sl-3, T-1	BSPL s1, sl-4, T-1
BSPL s1, sl-1, T-2	BSPL s1, sl-x, T-2	BSPL s1, sl-2, T-2	BSPL s1, sl-3, T-2	BSPL s1, sl-4, T-2
BSPL s1, sl-1, T-3	BSPL s1, sl-x, T-3	BSPL s1, sl-2, T-3	BSPL s1, sl-3, T-3	BSPL s1, sl-4, T-3
BSPL s1, sl-1, T-4	BSPL s1, sl-x, T-4	BSPL s1, sl-2, T-4	BSPL s1, sl-3, T-4	BSPL s1, sl-4, T-4
BSPL s1, sl-1, T-5		BSPL s1, sl-2, T-5	BSPL s1, sl-3, T-5	BSPL s1, sl-4, T-5
BSPL s1, sl-1, T-6		BSPL s1, sl-2, T-6	BSPL s1, sl-3, T-6	BSPL s1, sl-4, T-6
BSPL s1, sl-1, T-7		BSPL s1, sl-2, T-7	BSPL s1, sl-3, T-7	BSPL s1, sl-4, T-7
BSPL s1, sl-1, T-8		BSPL s1, sl-2, T-8	BSPL s1, sl-3, T-8	BSPL s1, sl-4, T-8
BSPL s1, sl-1, T-9		BSPL s1, sl-2, T-9	BSPL s1, sl-3, T-9	BSPL s1, sl-4, T-9
		BSPL s1, sl-2, T-10	BSPL s1, sl-3, T-10	
Slice 5	Slice 7	Slice 8	Slice 9	Petrography
BSPL s1, sl-5, T-1	BSPL s1, sl-7 T-1	BSPL s1, sl-8 T-1	BSPL s1, sl-9 T-1	BSPL PT-1
BSPL s1, sl-5, T-2	BSPL s1, sl-7 T-2	BSPL s1, sl-8 T-2	BSPL s1, sl-9 T-2	BSPL PT-2
BSPL s1, sl-5, T-3	BSPL s1, sl-7 T-3	BSPL s1, sl-8 T-3	BSPL s1, sl-9 T-3	BSPL PT-3
BSPL s1, sl-5, T-4	BSPL s1, sl-7 T-4	BSPL s1, sl-8 T-4	BSPL s1, sl-9 T-4	BSPL PR-4
BSPL s1, sl-5, T-5	BSPL s1, sl-7 T-5	BSPL s1, sl-8 T-5	BSPL s1, sl-9 T-5	BSPL PR-5
BSPL s1, sl-5, T-6	BSPL s1, sl-7 T-6	BSPL s1, sl-8 T-6	BSPL s1, sl-9 T-6	BSPL PR-6
BSPL s1, sl-5, T-7	BSPL s1, sl-7 T-7	BSPL s1, sl-8 T-7	BSPL s1, sl-9 T-7	BSPL PB-7
BSPL s1, sl-5, T-8	BSPL s1, sl-7 T-8	BSPL s1, sl-8 T-8	BSPL s1, sl-9 T-8	BSPL PB-8
BSPL s1, sl-5, T-9	BSPL s1, sl-7 T-9			BSPL PB-9

## Appendix 2

### Mill test Data

In this appendix is the data that was obtained during the mill testing that was elaborated in Chapter 5. Images of the equipment used are also displayed within this appendix.

**Table A2 a: Data used to plot mill curves obtained during mill testing.**

Sample ID	Mass of sample	Amount of water		Mass(g) of -75 $\mu$ m fraction after 10mins	Mass(g) of +75 $\mu$ m fraction after 10mins
		required for 66.67% solids(ml)			
Sc1, Sp3_1	948.4	474.12		443.2	497.8
Sc2, Sp4_1	980.3	490.07		435.0	553.0
Sc3, Sp4_1	1035.4	517.62		526.2	488.8
Sc1, Sp3_2	960.8	480.32		419.8	534.6
Sc2, Sp4_2	978.8	489.32		428.8	539.6
Sc3, Sp4_2	1004.4	502.12		513.2	468.2

Sample ID	Mass(g) of -75 $\mu$ m fraction after 15mins	Mass(g) of +75 $\mu$ m fraction after 15mins	Mass(g) of -75 $\mu$ m fraction after 25mins	Mass(g) of +75 $\mu$ m fraction after 25mins
	(cum. Time 25mins)	(cum. Time 25mins)	(cum. Time 50mins)	(cum. Time 50mins)
Sc1, Sp3_1	809.8	132.6	929.0	7.8
Sc2, Sp4_1	808.2	157.2	922.4	28.6
Sc3, Sp4_1	867.4	143.0	992.8	12.5
Sc1, Sp3_2	795.6	155.4	927.4	15.0
Sc2, Sp4_2	819.8	141.0	947.6	13.2
Sc3, Sp4_2	851.4	122.4	950.6	14.8

**Table A2 b: Percentage passing 75  $\mu$ m , loss during the mill testing process percentage, grams**

Sample ID	%passing -75 $\mu$ m	%passing -75 $\mu$ m	%passing -75 $\mu$ m	loss during	loss during
	10 mins.	25 mins.	50 mins.	testing(g)	testing(%)
Sc1, Sp3_1	46.73%	85.39%	97.95%	11.6	1.22%
Sc2, SP4_1	44.37%	82.44%	94.09%	29.3	2.99%
Sc3, Sp4_1	50.82%	83.77%	95.89%	30.1	2.91%
Sc1, Sp3_2	43.69%	82.81%	96.52%	18.4	1.92%
Sc2, Sp4_2	43.81%	83.76%	96.81%	18.0	1.84%
Sc3, Sp4_2	51.10%	84.77%	94.64%	39.0	3.88%



Figure A2 a: A: Rotary mill, B: Sieve shaker, C: Filter press, D: Oven used to dry samples. In each photograph a 30 cm ruler is used for scale.

## Appendix 3

### Grain Size Distribution and Mineral Association data

The size distribution graphs in this study used data obtained from the MLA as well as the association matrix that is created by the DATA view software. The data used to create the graphs and figures within chapter 7 can be found within this appendix.

**Table A3 a: Gold grain size distribution.**

Sieve Size in $\mu\text{m}$	Reef Cum. Passing Wt%	Below Cum. Passing Wt%	Above Cum. Passing Wt%	Combined Cum. Passing Wt%
212.00	100.00	100.00	100.00	100.00
180.00	96.07	100.00	100.00	97.32
150.00	93.63	100.00	88.85	94.13
125.00	89.73	100.00	81.13	91.46
106.00	85.94	100.00	80.28	86.16
90.00	71.40	100.00	79.65	74.38
75.00	60.99	91.34	72.13	63.76
63.00	51.43	85.55	69.81	56.40
53.00	42.21	67.72	66.75	46.93
45.00	38.34	55.60	65.04	42.84
38.00	31.91	51.44	60.65	37.63
32.00	24.96	50.00	57.44	30.40
27.00	20.72	34.96	42.62	24.03
22.00	15.87	27.93	41.41	19.47
19.00	13.35	27.49	34.06	16.26
16.00	10.62	25.59	27.72	13.45
13.50	8.32	19.62	22.96	10.82
11.40	6.50	15.93	18.30	8.53
9.60	4.75	10.16	10.73	5.94
8.10	3.42	8.10	7.91	4.50
6.80	2.29	4.85	5.77	3.01
5.70	1.49	3.50	3.18	1.89
4.80	0.94	1.82	2.24	1.18
4.10	0.51	0.70	0.98	0.62
3.40	0.20	0.40	0.42	0.27
2.90	0.00	0.00	0.00	0.00
2.40	0.00	0.00	0.00	0.00
2.00	0.00	0.00	0.00	0.00
1.75	0.00	0.00	0.00	0.00
1.45	0.00	0.00	0.00	0.00
1.20	0.00	0.00	0.00	0.00

**Table A3 b: Uraninite grain size distribution**

Sieve	Reef	Below	Above	Combined
Size in µm	Cum. Passing Wt%	Cum. Passing Wt%	Cum. Passing Wt%	Cum. Passing Wt%
300.00	100.00	100.00	100.00	100.00
250.00	98.97	100.00	100.00	99.27
212.00	98.66	100.00	100.00	99.04
180.00	96.68	100.00	100.00	97.63
150.00	92.84	99.63	100.00	94.82
125.00	89.28	98.25	96.68	91.81
106.00	83.65	96.45	94.47	86.90
90.00	80.16	93.81	93.66	83.79
75.00	73.59	83.59	90.22	76.42
63.00	67.52	76.56	87.05	70.21
53.00	60.52	71.90	85.01	63.72
45.00	54.43	60.22	80.93	56.86
38.00	48.39	55.96	71.49	50.73
32.00	41.79	48.06	61.37	43.27
27.00	36.50	42.83	53.50	37.94
22.00	31.43	34.41	49.34	32.22
19.00	27.83	26.41	43.53	27.75
16.00	23.63	21.87	36.83	23.41
13.50	19.48	17.56	30.20	19.14
11.40	15.54	14.53	24.93	15.42
9.60	11.98	10.94	20.03	11.87
8.10	8.99	7.89	16.09	8.91
6.80	6.32	5.67	11.29	6.30
5.70	4.40	3.82	7.98	4.36
4.80	2.94	2.57	5.43	2.91
4.10	1.74	1.54	3.16	1.72
3.40	0.92	0.81	1.64	0.90
2.90	0.00	0.00	0.00	0.00
2.40	0.00	0.00	0.00	0.00
2.00	0.00	0.00	0.00	0.00
1.75	0.00	0.00	0.00	0.00
1.45	0.00	0.00	0.00	0.00
1.20	0.00	0.00	0.00	0.00

**Table A3 c: Brannerite grain size distribution**

Sieve	Reef	Below	Above	Combined
Size in µm	Cum. Passing Wt%	Cum. Passing Wt%	Cum. Passing Wt%	Cum. Passing Wt%
150.00	100.00	100.00	100.00	100.00
125.00	97.19	100.00	100.00	97.88
106.00	97.19	100.00	100.00	97.88
90.00	96.81	99.78	100.00	97.55
75.00	95.36	92.45	100.00	95.24
63.00	92.15	90.21	100.00	92.45
53.00	89.96	89.25	97.55	90.63
45.00	83.73	89.20	97.55	85.52
38.00	73.86	85.92	97.40	77.20
32.00	64.43	60.61	90.98	65.50
27.00	59.36	58.92	86.12	61.13
22.00	50.83	53.01	78.93	52.60
19.00	45.22	46.87	72.85	47.01
16.00	39.39	41.02	63.49	41.17
13.50	32.91	31.53	55.97	34.17
11.40	27.54	27.00	45.75	28.50
9.60	22.42	22.35	35.74	23.04
8.10	17.71	18.36	29.59	18.42
6.80	13.45	11.37	22.40	13.64
5.70	10.11	8.32	16.88	10.14
4.80	7.32	5.83	12.20	7.33
4.10	4.89	3.96	8.08	4.90
3.40	2.77	1.95	4.57	2.71
2.90	0.00	0.00	0.01	0.00
2.40	0.00	0.00	0.01	0.00
2.00	0.00	0.00	0.00	0.00
1.75	0.00	0.00	0.00	0.00
1.45	0.00	0.00	0.00	0.00
1.20	0.00	0.00	0.00	0.00

**Table A3 d: Association matrix BSPL Reef**

Mineral	Quartz	Pyrite	Chromite	Uraninite	Chalcopyrite	Kerogen	Chlorite	Muscovite	Pyrophyllite	Gold	Galena	Sphalerite	Monazite	Cobaltite	Molybdenite	Brannerite	Zircon	Clamp Metal	Unknown	Free Surface	Total
Quartz	0.00	6.86	0.15	10.03	0.23	7.41	1.26	5.77	2.92	1.73	0.86	1.52	0.08	0.87	0.02	0.71	1.67	0.06	16.77	41.08	100.00
Pyrite	9.39	0.00	0.06	5.61	0.66	2.97	1.48	8.12	3.01	1.38	1.23	1.76	0.08	0.08	0.04	0.74	0.67	0.16	7.25	55.31	100.00
Chromite	10.64	3.02	0.00	3.69	0.05	1.42	3.58	10.63	3.39	3.47	0.30	0.14	0.00	0.25	0.00	0.73	1.40	0.08	9.03	48.18	100.00
Uraninite	9.82	3.63	0.05	0.00	0.47	38.75	0.18	10.61	2.78	0.12	0.91	1.64	0.00	0.01	0.04	5.56	0.50	0.01	7.48	17.43	99.99
Chalcopyrite	5.31	11.10	0.02	9.60	0.00	30.98	0.27	8.52	2.81	0.65	3.55	2.06	0.00	0.27	0.10	2.35	0.08	0.05	4.85	17.44	100.01
Kerogen	4.54	1.30	0.01	24.01	0.87	0.00	0.09	7.18	2.29	0.09	3.99	1.66	0.00	0.00	0.06	6.12	0.23	0.01	5.02	42.51	99.98
Chlorite	12.48	10.78	0.51	1.94	0.12	1.43	0.00	6.31	4.49	11.58	0.41	7.11	0.02	0.86	0.01	0.10	0.48	0.16	5.99	35.21	99.99
Muscovite	6.41	6.73	0.19	12.04	0.47	13.29	0.71	0.00	4.25	0.64	1.39	2.20	0.04	0.48	0.02	1.45	1.69	0.04	12.57	35.40	100.01
Pyrophyllite	8.42	5.67	0.13	7.73	0.33	9.88	1.19	11.29	0.00	0.62	2.08	2.40	0.05	0.41	0.00	0.52	1.08	0.04	14.32	33.82	99.98
Gold	29.96	17.04	0.79	1.77	0.54	2.34	19.43	9.82	4.31	0.00	0.06	0.47	0.00	0.03	0.00	0.18	0.20	0.08	10.44	2.56	100.02
Galena	5.44	5.27	0.02	5.27	1.09	40.57	0.25	7.61	4.90	0.03	0.00	1.18	0.00	0.00	0.09	1.36	0.76	0.00	4.05	22.09	99.98
Sphalerite	10.96	9.33	0.02	8.56	0.59	16.35	5.84	13.13	6.49	0.17	1.05	0.00	0.00	0.08	0.02	1.57	0.02	0.01	7.06	18.73	99.98
Monazite	23.25	13.45	0.00	0.00	0.00	0.14	0.52	5.80	4.25	0.00	0.00	0.09	0.00	0.00	0.00	0.04	0.08	0.00	6.64	45.75	100.01
Cobaltite	49.09	2.95	0.25	0.30	0.58	0.13	5.26	18.98	7.29	0.09	0.00	0.60	0.00	0.00	0.00	0.02	0.00	0.02	7.82	6.62	100.00
Molybdenite	11.44	11.50	0.00	12.70	1.19	29.38	0.68	5.75	0.67	0.00	2.61	0.97	0.00	0.00	0.00	2.45	0.00	0.00	3.12	17.54	100.00
Brannerite	3.24	2.27	0.04	24.24	0.49	44.50	0.04	5.89	0.90	0.05	1.05	1.33	0.00	0.00	0.04	0.00	0.00	0.00	3.74	12.17	99.99
Zircon	16.21	4.73	0.21	4.79	0.03	3.64	0.45	13.82	3.98	0.11	1.05	0.04	0.00	0.00	0.00	0.01	0.00	0.03	5.71	45.20	100.01
Clamp Metal	1.07	1.87	0.01	0.09	0.04	0.33	0.30	0.53	0.17	0.00	0.00	0.04	0.00	0.01	0.00	0.01	0.02	0.00	25.64	68.06	98.19
Unknown	25.88	5.52	0.14	8.69	0.25	10.09	0.69	12.53	7.28	0.66	0.77	1.22	0.03	0.16	0.01	0.94	0.67	1.28	0.00	23.21	100.02

**Table A3 e: Association matrix below BSPL reef**

Mineral	Quartz	Pyrite	Chromite	Uraninite	Chalcopyrite	Kerogen	Chlorite	Muscovite	Pyrophyllite	Gold	Galena	Sphalerite	Monazite	Cobaltite	Molybdenite	Brannerite	Zircon	Clamp Metal	Unknown	Free Surface	Total
Quartz	0.00	1.86	0.02	5.92	0.20	2.91	0.26	2.38	0.99	0.59	0.37	0.38	0.04	0.45	0.00	0.32	0.54	0.19	58.82	23.76	100.00
Pyrite	2.29	0.00	0.02	3.05	1.77	2.86	0.42	8.78	1.40	1.14	4.57	0.49	0.03	0.13	0.02	0.68	0.10	0.04	5.46	66.76	100.01
Chromite	5.14	5.60	0.00	7.77	0.00	3.17	0.00	18.46	3.21	0.00	0.00	0.00	0.05	1.04	0.00	0.00	0.02	4.61	10.97	39.98	100.02
Uraninite	5.90	1.96	0.02	0.00	0.94	25.09	0.00	26.96	6.81	0.06	0.54	0.59	0.19	0.21	0.01	6.11	0.09	0.02	12.79	11.70	99.99
Chalcopyrite	1.68	9.43	0.00	8.26	0.00	13.28	0.13	28.98	8.30	0.00	1.43	1.25	0.00	0.48	0.00	3.28	0.28	0.00	6.44	16.76	99.98
Kerogen	2.15	1.74	0.01	24.12	1.16	0.00	0.04	12.12	2.43	0.21	2.08	0.70	0.02	0.04	0.02	4.56	0.19	0.01	7.89	40.52	100.01
Chlorite	3.33	5.11	0.00	0.05	0.14	0.54	0.00	17.00	6.13	28.65	0.04	0.10	0.01	0.05	0.00	0.00	0.00	0.27	11.41	27.19	100.02
Muscovite	1.68	4.47	0.03	19.25	2.54	12.38	0.73	0.00	3.27	0.72	0.84	0.77	0.06	0.47	0.01	2.18	0.84	0.04	16.25	33.47	100.00
Pyrophyllite	2.12	2.14	0.03	19.27	2.85	7.75	0.77	10.67	0.00	1.26	1.29	1.17	0.15	0.59	0.02	0.73	0.37	0.14	18.76	29.92	100.00
Gold	14.22	12.15	0.00	1.41	0.00	4.69	28.65	15.37	7.50	0.00	0.12	0.06	0.00	0.00	0.00	0.27	0.00	0.00	12.78	2.80	100.02
Galena	3.69	21.97	0.00	5.11	1.45	23.44	0.04	9.07	4.52	0.16	0.00	0.33	0.00	0.00	0.00	2.27	0.89	0.00	13.52	13.55	100.01
Sphalerite	5.76	7.05	0.00	10.29	2.86	13.44	0.35	19.09	9.42	0.06	0.38	0.00	0.00	0.27	0.00	5.35	0.02	0.00	9.03	16.64	100.01
Monazite	0.89	0.76	0.00	5.05	0.00	1.94	0.03	2.39	3.75	0.00	0.00	0.00	0.00	0.00	0.00	0.04	0.09	0.00	5.35	79.70	99.99
Cobaltite	21.24	5.04	0.17	3.58	3.47	1.31	0.32	39.69	8.07	0.02	0.00	0.69	0.00	0.00	0.05	2.43	0.16	0.00	6.84	6.93	100.01
Molybdenite	0.00	23.58	0.00	4.18	0.35	15.39	0.00	32.74	18.41	0.00	0.00	0.00	0.00	2.56	0.00	0.00	0.00	0.00	0.16	2.64	100.01
Brannerite	1.49	2.30	0.00	30.06	1.77	24.62	0.00	15.28	1.77	0.06	1.38	1.41	0.00	0.84	0.00	0.00	0.00	0.05	12.78	6.19	100.00
Zircon	6.59	1.09	0.00	1.30	0.82	2.95	0.00	17.45	2.33	0.00	1.02	0.01	0.08	0.04	0.00	0.00	0.00	0.00	4.17	62.15	100.00
Clamp Metal	0.95	0.17	0.05	0.06	0.00	0.15	0.32	0.32	0.38	0.00	0.00	0.00	0.00	0.00	0.00	0.03	0.00	0.00	19.58	78.00	100.01
Unknown	59.14	1.44	0.01	5.04	0.30	3.93	0.29	8.70	3.35	0.31	0.76	0.19	0.04	0.06	0.00	0.97	0.11	0.92	0.00	14.44	100.00

**Table A3 f: Association matrix above BSPL reef**

Mineral	Quartz	Pyrite	Chromite	Uraninite	Chalcopyrite	Kerogen	Chlorite	Muscovite	Pyrophyllite	Gold	Galena	Sphalerite	Monazite	Cobaltite	Molybdenite	Brannerite	Zircon	Clamp Metal	Unknown ree	Surface	Total
Quartz	0.00	2.94	0.16	3.11	0.22	3.09	0.63	3.16	1.13	2.03	0.71	0.60	0.26	0.37	0.00	0.20	3.39	0.06	16.72	61.23	100.01
Pyrite	11.53	0.00	0.06	5.06	1.35	1.87	1.00	7.31	2.24	0.48	1.64	0.89	0.03	0.04	0.01	0.62	0.56	0.17	6.43	58.71	100.00
Chromite	23.37	2.80	0.00	2.55	0.00	0.83	1.73	14.14	0.91	0.15	0.17	0.00	0.00	0.06	0.00	0.38	0.25	0.00	6.98	45.70	100.02
Uraninite	11.96	5.04	0.06	0.00	0.55	46.75	0.18	12.00	2.91	0.07	1.12	1.17	0.00	0.00	0.01	4.02	0.45	0.01	7.56	6.13	99.99
Chalcopyrite	7.35	3.54	0.00	4.14	0.00	25.38	0.04	8.07	4.36	0.14	1.09	1.28	0.00	0.00	0.01	0.59	2.80	0.01	4.24	36.97	100.01
Kerogen	5.75	0.84	0.01	22.13	1.17	0.00	0.20	9.25	2.00	0.06	2.62	1.15	0.00	0.00	0.02	4.67	0.22	0.00	5.90	44.00	99.99
Chlorite	9.44	4.88	0.18	0.80	0.05	2.81	0.00	10.55	4.14	10.30	0.05	1.80	0.08	0.70	0.00	0.03	0.30	0.72	5.48	47.67	99.98
Muscovite	7.24	4.37	0.22	7.43	0.64	11.96	1.22	0.00	2.59	0.82	0.41	1.39	0.24	0.14	0.00	0.90	3.93	0.06	10.56	45.88	100.00
Pyrophyllite	7.80	4.03	0.04	5.23	0.77	8.60	1.55	8.38	0.00	1.01	0.86	1.77	0.01	0.00	0.00	0.40	0.50	0.00	13.40	45.63	99.98
Gold	46.55	6.24	0.05	1.03	0.58	1.84	17.28	8.66	4.96	0.00	0.01	0.25	0.00	0.00	0.00	0.08	0.07	0.32	10.23	1.84	99.99
Galena	10.14	9.84	0.01	7.40	0.65	30.20	0.04	3.21	2.23	0.00	0.00	0.42	0.00	0.00	0.00	0.60	0.80	0.00	3.98	30.47	99.99
Sphalerite	12.57	7.62	0.00	8.59	1.60	18.06	3.51	18.50	7.71	0.13	0.70	0.00	0.00	0.00	0.00	1.41	0.14	0.00	8.53	10.94	100.01
Monazite	24.79	0.58	0.00	0.20	0.00	0.01	0.49	11.82	0.09	0.00	0.00	0.00	0.00	0.00	0.00	0.00	0.91	0.00	1.57	59.56	100.02
Cobaltite	71.26	1.60	0.06	0.00	0.00	0.00	6.39	8.56	0.13	0.00	0.00	0.00	0.00	0.00	0.00	0.00	0.00	0.00	4.35	7.65	100.00
Molybdenite	0.01	0.08	0.00	0.04	0.03	0.51	0.00	0.06	0.00	0.00	0.00	0.01	0.00	0.00	0.00	0.00	0.00	0.00	0.01	99.25	100.00
Brannerite	3.79	3.12	0.04	20.68	0.43	51.46	0.06	7.45	1.21	0.03	0.57	1.00	0.00	0.00	0.00	0.00	0.00	0.04	5.10	5.02	100.00
Zircon	25.23	1.72	0.02	1.36	0.46	1.27	0.20	14.56	0.85	0.02	0.35	0.05	0.07	0.00	0.00	0.00	0.00	0.01	12.15	41.69	100.01
Clamp Metal	0.31	0.21	0.00	0.01	0.00	0.01	0.09	0.08	0.00	0.00	0.00	0.00	0.00	0.00	0.00	0.02	0.01	0.00	12.36	86.72	99.82
Unknown	35.80	1.68	0.05	2.43	0.12	3.82	0.42	5.25	2.18	0.24	0.29	0.53	0.03	0.03	0.00	0.28	2.09	3.73	0.00	41.02	99.99



## Appendix 4

### Chemical Assay Data

All the original copies of the assay data as reported by Intertek laboratories are contained within this appendix. These include the major and trace element chemistry assay, grading analysis assay, HLS Assay and the flotation assay. Also included are details of the abbreviations used within the assay processes.

Method Code descriptions (Intertek Genalysis Perth):

- **/CALC**: No digestion or other pre-treatment undertaken. Results determined by calculation from other reported data.
- **/CSA**: Induction furnace Analysed by infrared spectrometry.
- **4A/OE**: Multi-acid digest including hydrofluoric, nitric, perchloric and hydrochloric acids in Teflon tubes. Analysed by inductively coupled plasma optical (atomic) emission spectrometry.(ICP-OES)
- **4AH/OE**: Modified (for higher precision) Multi-acid digest including hydrofluoric, nitric, perchloric and hydrochloric acids in Teflon tubes. Analysed by ICP-OES.
- **4A/MS**: Multi-acid digestion including hydrofluoric, nitric, perchloric and hydrochloric acids in Teflon tubes. Analysed by inductively coupled plasma mass spectrometry.(ICP-MS)
- **4AH/MS**: Modified (for higher precision) Multi-acid digest including hydrofluoric, nitric, perchloric and hydrochloric acids in Teflon tubes. Analysed by ICP-MS.
- **FA50/AA**: 50g lead collection fire assay. Analysed by flame atomic absorption spectrometry.
- **FA25/OE**: 25g lead collection fire assay in new pots. Analysed by ICP-OES.
- **FP1/MS**: Sodium peroxide fusion (zirconia crucibles) and hydrochloric acids to dissolve the melt. Analysed by ICP-MS.

- **FP1/OE:** Sodium peroxide fusion (zirconia crucibles) and hydrochloric acid to dissolve the melt. Analysed by ICP-OES.
- **LOI/GR:** Loss on ignition. Gravimetric determination

**Table A4 a: Major element chemistry assay for run of mine bulk samples**

	SiO2	Al2O3	CaO	MgO	Fe2O3	K2O	MnO	Na2O	P2O5	TiO2	Cr2O3	LOI-1000	S	C
UNITS	%	%	%	%	%	%	%	%	%	%	%	%	%	%
DETECTION	0.3	0.02	0.2	0.02	0.02	0.1	0.004	0.004	0.015	0.02	0.01	0.01	0.01	0.01
METHOD	FP1/OE	FP1/OE	FP1/OE	FP1/OE	FP1/OE	FP1/OE	FP1/OE	4A/OE	4A/OE	FP1/OE	FP1/OE	LOI/GR	/CSA	/CSA
<b>SAMPLE NUMBERS</b>														
Sc1, Sp3-A	82.2	3.35	X	0.14	8.04	0.6	0.02	0.15	X	0.19	0.13	4.44	5.49	0.13
Sc1, Sp3-B	79.8	3.38	X	0.13	8.20	0.6	0.02	0.15	X	0.18	0.13	4.46	5.54	0.16
Sc2, Sp4-A	76.0	2.90	X	0.11	13.02	0.5	0.02	0.11	X	0.15	0.06	7.01	9.05	0.13
Sc2, Sp4-B	77.9	2.91	X	0.12	13.00	0.5	0.03	0.11	X	0.15	0.06	7.02	9.12	0.12
Sc3, Sp4-A	82.4	3.66	0.5	0.36	8.01	0.7	0.03	0.17	0.02	0.22	0.09	4.69	5.05	0.3
Sc3, Sp4-B	81.2	3.66	0.4	0.35	7.99	0.7	0.03	0.17	0.02	0.22	0.09	4.67	5.05	0.33
<b>CHECKS</b>														
Sc1, Sp3-A	83.5	3.38	X	0.13	8.13	0.6	156	1529	X	0.19	1366	4.47	5.46	0.14
<b>STANDARDS</b>														
OREAS 183								296	X					
OREAS 193	42.7	3.07	0.4	20.27	19.53	X	3159			0.05	9555			
OREAS 97													6.63	0.06
ST517														
<b>BLANKS</b>														
Control Blank	X	X	X	X	X	X	X	X	X	X	X		X	X
Control Blank								X	X					
Control Blank	X	X	X	X	X	X	X			X	X			
Acid Blank								X	X					
Acid Blank	X	X	X	X	X	X	X			X	X			

**Table A4 b: Trace element chemistry assay for run of mine bulk samples**

	Au	Ag	Co	Cu	Ni	Pb	Zn	Th	As	U
UNITS	ppm	ppm	ppm	ppm	ppm	ppm	ppm	ppm	ppm	ppm
DETECTION	0.005	0.5	1	20	20	20	20	0.1	20	0.1
METHOD	FA50/AA	4A/OE	FP1/MS	FP1/OE	FP1/OE	FP1/MS	FP1/OE	FP1/MS	FP1/MS	FP1/MS
<b>SAMPLE NUMBERS</b>										
Sc1, Sp3-A	10.178	2.1	90	58	200	69	153	5	194	56.3
Sc1, Sp3-B	11.43	1.3	86	53	197	60	132	5.2	186	55.9
Sc2, Sp4-A	8.66	0.9	77	46	228	69	119	3.7	267	31.4
Sc2, Sp4-B	7.433	2.2	74	72	228	64	127	3.6	266	29.6
Sc3, Sp4-A	12.689	2.8	72	59	159	55	120	4.5	164	30.3
Sc3, Sp4-B	10.344	1.3	68	48	139	100	118	4.4	161	30.6
<b>CHECKS</b>										
Sc1, Sp3-A	11.267	2	84	52	195	59	136	4.6	190	53.2
<b>STANDARDS</b>										
OREAS 183		X								
OREAS 193			485	40	19101	X	201	0.5	X	0.5
OREAS 97										
ST517	5.205									
<b>BLANKS</b>										
Control Blank	X	X	X	X	X	X	X	X	X	0.2
Control Blank		X								
Control Blank			X	X	X	X	X	0.2	X	0.2
Acid Blank		X								
Acid Blank			X	X	X	X	X	X	X	X

Table A4 c: Grading analysis assay

ELEMENTS	Au	Au-Rp1	S	S-Rp1	Th	U
UNITS	ppb	ppm	ppm	%	ppm	ppm
DETECTION	1	0.005	50	0.01	0.01	0.01
METHOD	FA25/OE	FA25/OE	4A/OE	/CSA	4A/MS	4A/MS
<b>SAMPLE NUMBERS</b>						
SC1 sp3_9 >106um	24973		68481		3.93	46.65
SC1 sp3_9 <106>75um	30420	27.855	64225		3.45	46.74
SC1 sp3_9 <75>53um	9275		55510		3.88	45.53
SC1 sp3_9 <53>25um	6203		52139		4.15	46.18
SC1 sp3_9 >25um	6906		55261		7.50	84.98
SC2 sp4_9>106um	11575		62912		3.23	29.92
SC2 sp4_9<106>75um	13204		74013		2.60	23.45
SC2 sp4_9<75>53um	7241		79598		2.84	24.07
SC2 sp4_9<53>25um	3599		78445		4.12	34.65
SC2 sp4_9>25um	9691		>100000	11.86	4.96	43.20
SC3 sp4_9>106um	25913		46698		4.03	29.36
SC3 sp4_9<106>75um	25419		53238		2.67	18.98
SC3 sp4_9<75>53um	6692		41969		3.92	29.44
SC3 sp4_9<53>25um	7260		42676		4.67	33.13
SC3 sp4_9>25um	9257		45230		7.01	52.97
<b>CHECKS</b>						
SC2 sp4_9<53>25um	4001		79771		4.08	35.02
<b>STANDARDS</b>						
AMIS0167			8233		49.29	470.95
AMIS0307	430					
AMIS0029			15340		93.53	880.2
OxP116	14894					
ST463	9412					
OREAS 98				15.87		
<b>BLANKS</b>						
Control Blank	X		X		X	0.01



UNIVERSITY  
OF  
JOHANNESBURG

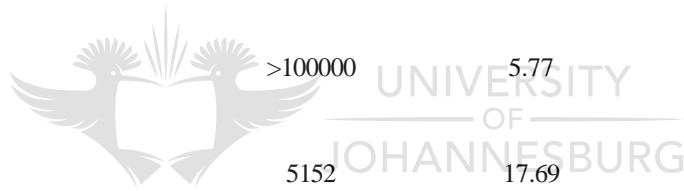
**Table A4 d: Assay for heavy liquid separation testing**

ELEMENTS	Au	S	Th	U
UNITS	ppb	ppm	ppm	ppm
DETECTION	1	50	0.01	0.01
METHOD	FA25/OE	4A/OE	4A/MS	4A/MS
<b>SAMPLE NUMBERS</b>				
Sc1, Sp3-4 Slimes	4352	40701	8.45	99.98
Sc1, Sp3-4 Floats	1103	6808	1.69	15.99
Sc2, Sp4-4 Slimes	3364	68747	6.51	59.18
Sc2, Sp4-4 Floats	607	5524	1.56	9.02
Sc3, Sc4-4 Slimes	3755	33167	8.12	65.64
Sc3, Sc4-4 Floats	971	8767	1.69	6.45
<b>CHECKS</b>				
Sc2, Sp4-4 Slimes	3378	69294	6.41	59.71
<b>STANDARDS</b>				
AMIS0167		7449	48.04	462.43
AMIS0278	264			
AMIS0085		3439	53.52	266.68
<b>BLANKS</b>				
Control Blank	X	X	X	X
Control Blank	X	X	0.03	0.15



Table A4 e: Flotation assay

ELEMENTS	Au	Au-Rp1	S	S-Rp1	Th	Th-Rp1	U	U-Rp1
UNITS	ppb	ppb	ppm	%	ppm	ppm	ppm	ppm
DETECTION	1	1	50	0.01	0.01	0.01	0.01	0.01
METHOD	FA25/OE	FA25/OE	4A/OE	4AH/OE	4A/MS	4AH/MS	4A/MS	4AH/MS
<b>SAMPLE NUMBERS</b>								
Sc1 Sp3 Conc1	102795		>100000	41.41	7.9	8.05	143.48	148.49
Sc1 Sp3 Conc2	74239		>100000	41.34	10.43	10.64	172.09	180.52
Sc1 Sp3 Conc3	76096		>100000	36.73	12.5		163.34	
Sc1 Sp3 Conc4	49408		>100000	30.16	15.64	15.08	182.11	178.77
Sc1 Sp3 Feed	15616		60661	6.34	4.85		49.88	
Sc1 Sp3 Tails		691	5727	0.54	4.83		46.61	
Sc2 Sp 4Conc1	43999		>100000	44.07	3.66		46.28	
Sc2 Sp 4Conc2	42636		>100000	43.27	5.27		69.42	
Sc2 Sp 4Conc3	36566		>100000	41.45	5.63		69.35	
Sc2 Sp 4Conc4	34422		>100000	38.52	7.3		81.09	
Sc2 Sp 4Feed	8435		87972	9.22	3.44	3.44	31.32	28.61
Sc2 Sp 4Tails		1282	13897	1.32	3.32	3.04	21.45	20.39
Sc3 Sp 4Conc1	126565		>100000	41.54	4.11		42.19	
Sc3 Sp 4Conc2	101715		>100000	42.53	7.73		78.12	
Sc3 Sp 4Conc3	45583		>100000	36.51	11.02		96.27	
Sc3 Sp 4Conc4	36532		>100000	22.59	16.39	16.66	118.1	122.62
Sc3 Sp 4Feed	12577		53407	5.17	3.86		24.7	
Sc3 Sp 4Tails		332	3249	0.29	3.39	2.98	19.49	18.51
<b>CHECKS</b>								
Sc2 Sp 4Conc2			>100000		5.77		77.8	
<b>STANDARDS</b>								
OREAS 922			5152		17.69		3.68	
CCU-1d				31.4				
GBM908-11				28.76				
MP-1b				14.06				
MPL-5				1.2				
ST463		9669						
ST517		5377						
ST403		1950						
ST 502	48520							
AMIS0133	302042							
AMIS0167						48.13		479.39
OREAS 100a						52.11		142.53
MPL-5						92.23		10.4
GBM908-11						0.97		0.65
<b>BLANKS</b>								
Control Blank			X		X		X	
Control Blank			X		X		X	
Control Blank				X				
Control Blank				X				
Control Blank		X						
Control Blank	X							
Control Blank						0.02		0.14
Control Blank						X		X



## Appendix 5

### Grading Analysis, Density Separation data

Within this appendix is the data used for the plots created in Chapter 8 regarding the grading analysis and density separation tests that were conducted.

**Table A5 a: Gold data, grading analysis**

Size fractions	Weights (g)	g/ton	Actual amount of gold (g)	element %	mass %	Up/Downgrade
SC1 sp3_9 >106um	34.8	24.973	0.000869060	9.18%	3.78%	5.39%
SC1 sp3_9 <106>75um	92.2	30.420	0.002804724	29.61%	10.02%	19.59%
SC1 sp3_9 <75>53um	250.8	9.275	0.002326170	24.56%	27.26%	-2.70%
SC1 sp3_9 <53>25um	389.0	6.203	0.002412967	25.48%	42.28%	-16.80%
SC1 sp3_9 >25um	153.2	6.906	0.001057999	11.17%	16.65%	-5.48%
<b>Total</b>	<b>920.0</b>		<b>0.009470921</b>	<b>100.00%</b>	<b>100.00%</b>	
SC2 sp4_9 >106um	80.2	11.575	0.000928315	14.94%	8.46%	6.48%
SC2 sp4_9 <106>75um	87.6	13.204	0.001156670	18.61%	9.24%	9.38%
SC2 sp4_9 <75>53um	256.8	7.241	0.001859489	29.92%	27.08%	2.84%
SC2 sp4_9 <53>25um	460.4	3.599	0.001656980	26.67%	48.56%	-21.89%
SC2 sp4_9 >25um	63.2	9.691	0.000612471	9.86%	6.67%	3.19%
<b>Total</b>	<b>948.2</b>		<b>0.006213925</b>	<b>100.00%</b>	<b>100.00%</b>	
SC3 sp4_9 >106um	53.4	25.913	0.001383754	14.00%	5.53%	8.47%
SC3 sp4_9 <106>75um	104.6	25.419	0.002658827	26.89%	10.83%	16.06%
SC3 sp4_9 <75>53um	287.8	6.692	0.001925958	19.48%	29.81%	-10.33%
SC3 sp4_9 <53>25um	446.8	7.260	0.003243768	32.81%	46.28%	-13.47%
SC3 sp4_9 >25um	72.8	9.257	0.000673910	6.82%	7.54%	-0.72%
<b>Total</b>	<b>965.4</b>		<b>0.009886217</b>	<b>100.00%</b>	<b>100.00%</b>	

**Table A5 b: Uranium Data, grading analysis**

Size fractions	Weights(g)	g/ton	Actual amount of U(g)	element %	mass %	Up/Downgrade
SC1 sp3_9 >106um	34.8	46.65	0.000162342	3.36%	3.78%	-0.42%
SC1 sp3_9 <106>75um	92.2	46.74	0.000430943	8.92%	10.02%	-1.11%
SC1 sp3_9 <75>53um	250.8	45.53	0.001141892	23.62%	27.26%	-3.64%
SC1 sp3_9 <53>25um	389.0	46.18	0.001796402	37.17%	42.28%	-5.12%
SC1 sp3_9 >25um	153.2	84.98	0.001301894	26.93%	16.65%	10.28%
<b>Total</b>	<b>920.0</b>		<b>0.004833473</b>	<b>100.00%</b>	<b>100.00%</b>	
SC2 sp4_9>106um	80.2	29.92	0.000239958	8.18%	8.46%	-0.27%
SC2 sp4_9<106>75um	87.6	23.45	0.000205422	7.01%	9.24%	-2.23%
SC2 sp4_9<75>53um	256.8	24.07	0.000618118	21.08%	27.08%	-6.00%
SC2 sp4_9<53>25um	460.4	34.65	0.001595286	54.41%	48.56%	5.86%
SC2 sp4_9>25um	63.2	43.20	0.000273024	9.31%	6.67%	2.65%
<b>Total</b>	<b>948.2</b>		<b>0.002931808</b>	<b>100.00%</b>	<b>100.00%</b>	
SC3 sp4_9>106um	53.4	29.36	0.000156782	5.11%	5.53%	-0.42%
SC3 sp4_9<106>75um	104.6	18.98	0.000198531	6.47%	10.83%	-4.36%
SC3 sp4_9<75>53um	287.8	29.44	0.000847283	27.61%	29.81%	-2.20%
SC3 sp4_9<53>25um	446.8	33.13	0.001480248	48.24%	46.28%	1.96%
SC3 sp4_9>25um	72.8	52.97	0.000385622	12.57%	7.54%	5.03%
<b>Total</b>	<b>965.4</b>		<b>0.003068466</b>	<b>100.00%</b>	<b>100.00%</b>	

**Table A5 c: Thorium data, grading analysis**

Size fractions	Weights(g)	g/ton	Actual amount of Th (g)	element %	mass %	Up/Downgrade
SC1 sp3_9 >106um	34.8	3.93	0.000136764	3.26%	3.78%	-0.52%
SC1 sp3_9 <106>75um	92.2	3.45	0.000318090	7.59%	10.02%	-2.43%
SC1 sp3_9 <75>53um	250.8	3.88	0.000973104	23.22%	27.26%	-4.04%
SC1 sp3_9 <53>25um	389.0	4.15	0.001614350	38.52%	42.28%	-3.77%
SC1 sp3_9 >25um	153.2	7.50	0.001149000	27.41%	16.65%	10.76%
<b>Total</b>	<b>920.0</b>		<b>0.004191308</b>	<b>100.00%</b>	<b>100.00%</b>	
SC2 sp4_9>106um	80.2	3.23	0.000259046	7.56%	8.46%	-0.90%
SC2 sp4_9<106>75um	87.6	2.60	0.000227760	6.65%	9.24%	-2.59%
SC2 sp4_9<75>53um	256.8	2.84	0.000729312	21.28%	27.08%	-5.80%
SC2 sp4_9<53>25um	460.4	4.12	0.001896848	55.36%	48.56%	6.80%
SC2 sp4_9>25um	63.2	4.96	0.000313472	9.15%	6.67%	2.48%
<b>Total</b>	<b>948.2</b>		<b>0.003426438</b>	<b>100.00%</b>	<b>100.00%</b>	
SC3 sp4_9>106um	53.4	4.03	0.000215202	5.10%	5.53%	-0.43%
SC3 sp4_9<106>75um	104.6	2.67	0.000279282	6.62%	10.83%	-4.22%
SC3 sp4_9<75>53um	287.8	3.92	0.001128176	26.74%	29.81%	-3.07%
SC3 sp4_9<53>25um	446.8	4.67	0.002086556	49.45%	46.28%	3.17%
SC3 sp4_9>25um	72.8	7.01	0.000510328	12.09%	7.54%	4.55%
<b>Total</b>	<b>965.4</b>		<b>0.004219544</b>	<b>100.00%</b>	<b>100.00%</b>	

**Table A5 d: Sulphur data, grading analysis**

Size fractions	Weights(g)	g/ton	Actual amount of S (g)	element%	mass %	Up/Downgrade
SC1 sp3_9 >106um	34.8	68481	2.3831388	4.68%	3.78%	0.89%
SC1 sp3_9 <106>75um	92.2	64225	5.9215450	11.62%	10.02%	1.59%
SC1 sp3_9 <75>53um	250.8	55510	13.9219080	27.31%	27.26%	0.05%
SC1 sp3_9 <53>25um	389.0	52139	20.2820710	39.79%	42.28%	-2.49%
SC1 sp3_9 >25um	153.2	55261	8.4659852	16.61%	16.65%	-0.04%
<b>Total</b>	<b>920.0</b>		<b>50.9746480</b>	<b>100.00%</b>	<b>100.00%</b>	
SC2 sp4_9>106um	80.2	62912	5.0455424	6.78%	8.46%	-1.68%
SC2 sp4_9<106>75um	87.6	74013	6.4835388	8.71%	9.24%	-0.52%
SC2 sp4_9<75>53um	256.8	79598	20.4407664	27.47%	27.08%	0.39%
SC2 sp4_9<53>25um	460.4	78445	36.1160780	48.54%	48.56%	-0.02%
SC2 sp4_9>25um	63.2	100000	6.3200000	8.49%	6.67%	1.83%
<b>Total</b>	<b>948.2</b>		<b>74.4059256</b>	<b>100.00%</b>	<b>100.00%</b>	
SC3 sp4_9>106um	53.4	46698	2.4936732	5.87%	5.53%	0.34%
SC3 sp4_9<106>75um	104.6	53238	5.5686948	13.10%	10.83%	2.27%
SC3 sp4_9<75>53um	287.8	41969	12.0786782	28.42%	29.81%	-1.39%
SC3 sp4_9<53>25um	446.8	42676	19.0676368	44.86%	46.28%	-1.42%
SC3 sp4_9>25um	72.8	45230	3.2927440	7.75%	7.54%	0.21%
<b>Total</b>	<b>965.4</b>		<b>42.5014270</b>	<b>100.00%</b>	<b>100.00%</b>	

**Table A5 e: Au data for HLS including mass % calculation**

ELEMENTS	Au		Actual amount of Au (g)	Actual amount of Au (%)	Assay gold value in g/ton.	Expected amount of Au (g)
UNITS	ppb	G/ton	weight (g)	Mass %		
<b>SAMPLE NUMBERS</b>						
Sc1, Sp3-4 Slimes	4352	4.35	189.4	0.000824	16.76%	41.61%
Sc1, Sp3-4 Floats	1103	1.10	122.8	0.000135	2.75%	26.98%
Sinks+ Floats				0.000960		
Sc1, Sp3-4 Au sinks	27680	27.68	143.0	0.003958	80.49%	31.41%
<b>Total</b>			<b>455.2</b>			
Sc2, Sp4-4 Slimes	3364	3.36	108.8	0.000366	12.05%	28.83%
Sc2, Sp4-4 Floats	607	0.61	132.6	0.000080	2.65%	35.14%
Sinks+ Floats				0.000446		
Sc2, Sp4-4 Au sinks	19046	19.05	136.0	0.002590	85.30%	36.04%
<b>Total</b>			<b>377.4</b>			
Sc3, Sc4-4 Slimes	3755	3.76	164.0	0.000616	11.34%	34.79%
Sc3, Sc4-4 Floats	971	0.97	162.4	0.000158	2.90%	34.45%
Sinks+ Floats				0.000774		
Sc3, Sc4-4 Au sinks	32106	32.11	145.0	0.004655	85.75%	30.76%
<b>Total</b>			<b>471.4</b>			



**Table A5 f: S data for HLS**

ELEMENTS		S					
UNITS	ppm	G/ton	weight(g)	Actual		Expected amount of S(g)	Assayed S value in g/ton.
				Actual amount of S(g)	amount of S(%)		
<b>SAMPLE NUMBERS</b>							
Sc1, Sp3-4 Slimes	40701	40701	189.4	7.7087694	30.71%	25.10428	55150
Sc1, Sp3-4 Floats	6808	6808	122.8	0.8360224	3.33%		
Sinks+ Floats				8.5447918			
Sc1, Sp3-4 S sinks		115801	143.0	16.5594882	65.96%		
Total			455.2				
Sc2, Sp4-4 Slimes	68747	68747	108.8	7.4796736	21.82%	34.28679	90850
Sc2, Sp4-4 Floats	5524	5524	132.6	0.7324824	2.14%		
Sinks+ Floats				8.2121560			
Sc2, Sp4 S sinks		191725	136.0	26.0746340	76.05%		
Total			377.4				
Sc3, Sc4-4 Slimes	33167	33167	164.0	5.4393880	22.85%	23.8057	50500
Sc3, Sc4-4 Floats	8767	8767	162.4	1.4237608	5.98%		
Sinks+ Floats				6.8631488			
Sc3, Sc4-4 S sinks		116845	145.0	16.9425512	71.17%		
Total			471.4				

**Table A5 g: Th Data for HLS**

ELEMENTS		Th					
UNITS	ppm	G/ton	weight (g)	Actual		Expected amount of Th(g)	Assayed Value of Th in G/ton.
				Actual amount of Th(g)	amount of Th (%)		
<b>SAMPLE NUMBERS</b>							
Sc1, Sp3-4 Slimes	8.45	8.45	189.4	0.001600430	68.94%	0.00232152	5.1
Sc1, Sp3-4 Floats	1.69	1.69	122.8	0.000207532	8.94%		
Sinks+ Floats				0.001807962			
Sc1, Sp3-4 Th sinks		3.59	143.0	0.000513558	22.12%		
Total			455.2				
Sc2, Sp4-4 Slimes	6.51	6.51	108.8	0.000708288	51.00%	0.001388832	3.68
Sc2, Sp4-4 Floats	1.56	1.56	132.6	0.000206856	14.89%		
Sinks+ Floats				0.000915144			
Sc2, Sp4-4 Th sinks		3.48	136.0	0.000473688	34.11%		
Total			377.4				
Sc3, Sc4-4 Slimes	8.12	8.12	164.0	0.001331680	63.48%	0.00209773	4.45
Sc3, Sc4-4 Floats	1.69	1.69	162.4	0.000274456	13.08%		
Sinks+ Floats				0.001606136			
Sc3, Sc4-4 Th sinks		3.39	145.0	0.000491594	23.43%		
Total			471.4				

**Table A5 h: U data for HLS**

ELEMENTS		U						Assay value of U in G/ton.
UNITS	ppm	G/ton	weight (g)	Actual amount of U(g)	Actual amount of U (%)	Expected amount of U(g)		
<b>SAMPLE NUMBERS</b>								
Sc1, Sp3-4 Slimes	99.98	99.98	189.4	0.018936212	74.15%	0.02553672	56.1	
Sc1, Sp3-4 Floats	15.99	15.99	122.8	0.001963572	7.69%			
Sinks+ Floats				0.020899784				
U sinks		32.42613	143	0.004636936	18.16%			
Total			455.2					
Sc2, Sp4-4 Slimes	59.18	59.18	108.8	0.006438784	55.94%	0.0115107	30.5	
Sc2, Sp4-4 Floats	9.02	9.02	132.6	0.001196052	10.39%			
Sinks+ Floats				0.007634836				
U sinks		28.499	136	0.003875864	33.67%			
Total			377.4					
Sc3, Sc4-4 Slimes	65.64	65.64	164	0.01076496	75.00%	0.01435413	30.45	
Sc3, Sc4-4 Floats	6.45	6.45	162.4	0.00104748	7.30%			
Sinks+ Floats				0.01181244				
U sinks		17.5289	145	0.00254169	17.71%			
Total			471.4					



## Appendix 6

### Flotation Data

Within this appendix is the data used to create the plots that are depicted within Chapter 10 regarding flotation.

**Table A6 a: Flotation calculations for Au**

	Au		Actual amount		
	ppb	G/ton	Mass in g	of Au in g	Mass%
Sc1 Sp3 Conc1	102795	102.795	80.4	0.008264718	55.14%
Sc1 Sp3 Conc2	74239	74.239	46.2	0.003429842	22.88%
Sc1 Sp3 Conc3	76096	76.096	30.2	0.002298099	15.33%
Sc1 Sp3 Conc4	49408	49.408	17.2	0.000849818	5.67%
Sc1 Sp3 Feed	15616	15.616	210	0.00327936	
Sc1 Sp3 Tails	691	0.691	210	0.00014511	0.97%
total C1,C2,C3,C4 tails			384	0.014987587	100.00%
Sc2 Sp 4Conc1	43999	43.999	142.2	0.006256658	54.77%
Sc2 Sp 4Conc2	42636	42.636	51.4	0.00219149	19.18%
Sc2 Sp 4Conc3	36566	36.566	42.2	0.001543085	13.51%
Sc2 Sp 4Conc4	34422	34.422	33.8	0.001163464	10.18%
Sc2 Sp 4Feed	8435	8.435	211.4	0.001783159	
Sc2 Sp 4Tails	1282	1.282	210	0.00026922	2.36%
total C1,C2,C3,C4 tails			479.6	0.011423917	100.00%
Sc3 Sp 4Conc1	126565	126.565	91.8	0.011618667	65.47%
Sc3 Sp 4Conc2	101715	101.715	41.8	0.004251687	23.96%
Sc3 Sp 4Conc3	45583	45.583	27.6	0.001258091	7.09%
Sc3 Sp 4Conc4	36532	36.532	15	0.00054798	3.09%
Sc3 Sp 4Feed	12577	12.577	215.4	0.002709086	
Sc3 Sp 4Tails	332	0.332	210	0.00006972	0.39%
total C1,C2,C3,C4 tails			386.2	0.017746145	100.00%

**Table A6 b: Flotation calculations for S**

S						
	%	G/ton	Mass in g	Actual amount of S in g	Mass%	
Sc1 Sp3 Conc1	41.41	414100	80.4	33.29364	47.69%	
Sc1 Sp3 Conc2	41.34	413400	46.2	19.09908	27.36%	
Sc1 Sp3 Conc3	36.73	367300	30.2	11.09246	15.89%	
Sc1 Sp3 Conc4	30.16	301600	17.2	5.18752	7.43%	
Sc1 Sp3 Feed	6.34	63400	210	13.314		
Sc1 Sp3 Tails	0.54	5400	210	1.134	1.62%	
total C1,C2,C3,C4 tails			384	69.8067	100.00%	
Sc2 Sp 4Conc1	44.07	440700	142.2	62.66754	53.02%	
Sc2 Sp 4Conc2	43.27	432700	51.4	22.24078	18.82%	
Sc2 Sp 4Conc3	41.45	414500	42.2	17.4919	14.80%	
Sc2 Sp 4Conc4	38.52	385200	33.8	13.01976	11.02%	
Sc2 Sp 4Feed	9.22	92200	211.4	19.49108		
Sc2 Sp 4Tails	1.32	13200	210	2.772	2.35%	
total C1,C2,C3,C4 tails			479.6	118.19198	100.00%	
Sc3 Sp 4Conc1	41.54	415400	91.8	38.13372	54.49%	
Sc3 Sp 4Conc2	42.53	425300	41.8	17.77754	25.40%	
Sc3 Sp 4Conc3	36.51	365100	27.6	10.07676	14.40%	
Sc3 Sp 4Conc4	22.59	225900	15	3.3885	4.84%	
Sc3 Sp 4Feed	5.17	51700	215.4	11.13618		
Sc3 Sp 4Tails	0.29	2900	210	0.609	0.87%	
total C1,C2,C3,C4 tails			386.2	69.98552	100.00%	

**Table A6 c: Flotation calculations for Th**

	Th		Actual amount		
	ppm	G/ton	Mass in g	of Th in g	Mass%
Sc1 Sp3 Conc1	7.9	7.9	80.4	0.00063516	22.87%
Sc1 Sp3 Conc2	10.43	10.43	46.2	0.000481866	17.35%
Sc1 Sp3 Conc3	12.5	12.5	30.2	0.0003775	13.59%
Sc1 Sp3 Conc4	15.64	15.64	17.2	0.000269008	9.68%
Sc1 Sp3 Feed	4.85	4.85	210	0.0010185	
Sc1 Sp3 Tails	4.83	4.83	210	0.0010143	36.51%
total C1,C2,C3,C4 tails			384	0.002777834	100.00%
Sc2 Sp 4Conc1	3.66	3.66	142.2	0.000520452	26.38%
Sc2 Sp 4Conc2	5.27	5.27	51.4	0.000270878	13.73%
Sc2 Sp 4Conc3	5.63	5.63	42.2	0.000237586	12.04%
Sc2 Sp 4Conc4	7.3	7.3	33.8	0.00024674	12.51%
Sc2 Sp 4Feed	3.44	3.44	211.4	0.000727216	
Sc2 Sp 4Tails	3.32	3.32	210	0.0006972	35.34%
total C1,C2,C3,C4 tails			479.6	0.001972856	100.00%
Sc3 Sp 4Conc1	4.11	4.11	91.8	0.000377298	19.23%
Sc3 Sp 4Conc2	7.73	7.73	41.8	0.000323114	16.47%
Sc3 Sp 4Conc3	11.02	11.02	27.6	0.000304152	15.50%
Sc3 Sp 4Conc4	16.39	16.39	15	0.00024585	12.53%
Sc3 Sp 4Feed	3.86	3.86	215.4	0.000831444	
Sc3 Sp 4Tails	3.39	3.39	210	0.0007119	36.28%
total C1,C2,C3,C4 tails			386.2	0.001962314	100.00%

**Table A6 d: Flotation calculations for U**

	U		Actual amount		
	ppm	G/ton	Mass in g	of U in g	Mass%
Sc1 Sp3 Conc1	143.48	143.48	80.4	0.011535792	30.89%
Sc1 Sp3 Conc2	172.09	172.09	46.2	0.007950558	21.29%
Sc1 Sp3 Conc3	163.34	163.34	30.2	0.004932868	13.21%
Sc1 Sp3 Conc4	182.11	182.11	17.2	0.003132292	8.39%
Sc1 Sp3 Feed	49.88	49.88	210	0.0104748	
Sc1 Sp3 Tails	46.61	46.61	210	0.0097881	26.21%
total C1,C2,C3,C4 tails			384	0.03733961	100.00%
Sc2 Sp 4Conc1	46.28	46.28	142.2	0.006581016	32.39%
Sc2 Sp 4Conc2	69.42	69.42	51.4	0.003568188	17.56%
Sc2 Sp 4Conc3	69.35	69.35	42.2	0.00292657	14.40%
Sc2 Sp 4Conc4	81.09	81.09	33.8	0.002740842	13.49%
Sc2 Sp 4Feed	31.32	31.32	211.4	0.006621048	
Sc2 Sp 4Tails	21.45	21.45	210	0.0045045	22.17%
total C1,C2,C3,C4 tails			479.6	0.020321116	100.00%
Sc3 Sp 4Conc1	42.19	42.19	91.8	0.003873042	24.73%
Sc3 Sp 4Conc2	78.12	78.12	41.8	0.003265416	20.85%
Sc3 Sp 4Conc3	96.27	96.27	27.6	0.002657052	16.97%
Sc3 Sp 4Conc4	118.1	118.1	15	0.0017715	11.31%
Sc3 Sp 4Feed	24.7	24.7	215.4	0.00532038	
Sc3 Sp 4Tails	19.49	19.49	210	0.0040929	26.14%
total C1,C2,C3,C4 tails			386.2	0.01565991	100.00%

**Table A6 e: Flotation combine calculations**

Sample	Au Mass%	S Mass%	Th Mass%	U Mass%
Sc1 Sp3 Conc1	55.14%	47.69%	22.87%	30.89%
Sc1 Sp3 Conc2	22.88%	27.36%	17.35%	21.29%
Sc1 Sp3 Conc3	15.33%	15.89%	13.59%	13.21%
Sc1 Sp3 Conc4	5.67%	7.43%	9.68%	8.39%
Sc1 Sp3 Tails	0.97%	1.62%	36.51%	26.21%
total C1,C2,C3,C4 tails	100.00%	100.00%	100.00%	100.00%
Sc2 Sp 4Conc1	54.77%	53.02%	26.38%	32.39%
Sc2 Sp 4Conc2	19.18%	18.82%	13.73%	17.56%
Sc2 Sp 4Conc3	13.51%	14.80%	12.04%	14.40%
Sc2 Sp 4Conc4	10.18%	11.02%	12.51%	13.49%
Sc2 Sp 4Tails	2.36%	2.35%	35.34%	22.17%
total C1,C2,C3,C4 tails	100.00%	100.00%	100.00%	100.00%
Sc3 Sp 4Conc1	65.47%	54.49%	19.23%	24.73%
Sc3 Sp 4Conc2	23.96%	25.40%	16.47%	20.85%
Sc3 Sp 4Conc3	7.09%	14.40%	15.50%	16.97%
Sc3 Sp 4Conc4	3.09%	4.84%	12.53%	11.31%
Sc3 Sp 4Tails	0.39%	0.87%	36.28%	26.14%
total C1,C2,C3,C4 tails	100.00%	100.00%	100.00%	100.00%

**Table A6 f: Flotation recovery vs. time**

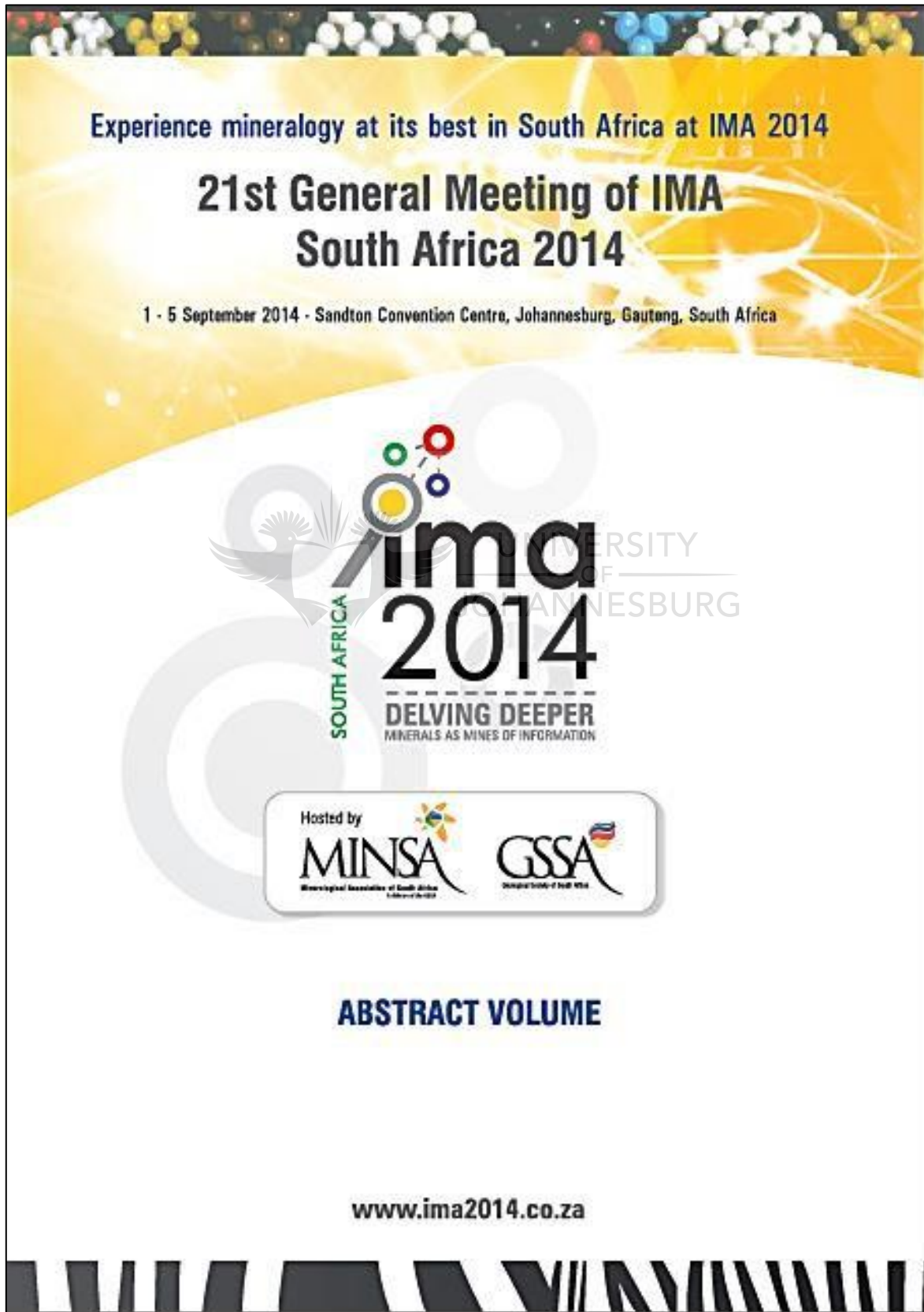
Elements		Au	Au	S	S	Th	Th	U	U
Sample	Time floated min.	Mass%	cummulative. %	Mass%	cummulative. %	Mass%	cummulative. %	Mass%	% cummulative
Sc1 Sp3 Conc1	2	55.14%	55.14%	47.69%	47.69%	22.87%	22.87%	30.89%	30.89%
Sc1 Sp3 Conc2	6	22.88%	78.03%	27.36%	75.05%	17.35%	40.21%	21.29%	52.19%
Sc1 Sp3 Conc3	12	15.33%	93.36%	15.89%	90.94%	13.59%	53.80%	13.21%	65.40%
Sc1 Sp3 Conc4	20	5.67%	99.03%	7.43%	98.38%	9.68%	63.49%	8.39%	73.79%
Sc1 Sp3 Tails		0.97%		1.62%		36.51%		26.21%	
total C1,C2,C3,C4 tails		100.00%		100.00%		100.00%		100.00%	
Sc2 Sp 4Conc1	2	54.77%	54.77%	53.02%	53.02%	26.38%	26.38%	32.39%	32.39%
Sc2 Sp 4Conc2	6	19.18%	73.95%	18.82%	71.84%	13.73%	40.11%	17.56%	49.94%
Sc2 Sp 4Conc3	12	13.51%	87.46%	14.80%	86.64%	12.04%	52.15%	14.40%	64.35%
Sc2 Sp 4Conc4	20	10.18%	97.64%	11.02%	97.65%	12.51%	64.66%	13.49%	77.83%
Sc2 Sp 4Tails		2.36%		2.35%		35.34%		22.17%	
total C1,C2,C3,C4 tails		100.00%		100.00%		100.00%		100.00%	
Sc3 Sp 4Conc1	2	65.47%	65.47%	54.49%	54.49%	19.23%	19.23%	24.73%	24.73%
Sc3 Sp 4Conc2	6	23.96%	89.43%	25.40%	79.89%	16.47%	35.69%	20.85%	45.58%
Sc3 Sp 4Conc3	12	7.09%	96.52%	14.40%	94.29%	15.50%	51.19%	16.97%	62.55%
Sc3 Sp 4Conc4	20	3.09%	99.61%	4.84%	99.13%	12.53%	63.72%	11.31%	73.86%
Sc3 Sp 4Tails		0.39%		0.87%		36.28%		26.14%	
total C1,C2,C3,C4 tails		100.00%		100.00%		100.00%		100.00%	

**Table A6 g: Average Flotation recovery vs. time**

Average					
	Time floated min.	Au	S	Th	U
Conc1	2	58.46%	51.73%	22.82%	29.34%
Conc2	6	80.47%	75.59%	38.67%	49.24%
Conc3	12	92.45%	90.62%	52.38%	64.10%
Conc4	20	98.76%	98.39%	63.96%	75.16%

## Appendix 7

### Published Conference Abstract





### Laser modification of mineral surface properties

Kotova O<sup>1</sup>, Leonenko N<sup>2</sup>, Gazaleeva G<sup>3</sup>

1 - Institute of geology Komi SC UB RAS \*kotova@geo.komisc.ru

2 - Institute of Mining of Far-Eastern Branch of RAS 3 - Uralmekhanobr OJSC, Russia

Ores with complex material composition and low contrast of physical-chemical and technological properties of valuable components are the basis of the raw minerals base of Russia. Energy influences are considered as an efficient method of intensification of raw mineral processing and applied to increase the contrast of mineral properties and efficient disintegration of fine mineral complexes.

The aim of the present work is an experimental study of mechanisms of laser influence on the phase composition, structural, chemical and technological properties of materials for the development of processing technologies of bauxite ores, red muds and gold-containing tailings.

Electron microscopy was the basic investigation method. X-ray methods were used for the analysis of the phase composition.

New experimental data on the laser influence on the phase composition, geometrical and technological properties of bauxite minerals, red muds and gold-containing tailings are presented. The mechanisms of formation of micro- and nanophases on mineral surfaces are influenced by the energy. The change of surface atom state, concentration of metals, agglomeration of titanium minerals and formation of new phases occurred under the laser influence on bauxite and red mud. The mechanism of agglomeration of gold is also presented.

Acknowledgements: The work was supported by the projects of RAS Programs: 12-M-35-2055; 12-III-A-08-020 & RFBR: 13-05-00586

### A geometallurgical examination of gold, uranium and thorium in the Black Reef quartzite formation

McLoughlin A<sup>1</sup>, Blignaut L, Viljoen F

Geology Department, University of Johannesburg \*mcloughlinandrew49@gmail.com

The Black Reef quartzite formation forms part of the Transvaal Supergroup. It has significant concentrations of gold and uranium. This mineralization occurs predominantly in the BSPL (buck shot pyrite leader) reef of the Black Reef formation. In the present study we examine for the first time ever, the nature of the gold and uranium mineralization in the reef using Mineral Liberation Analyzer (MLA) technology. Samples were taken from Gold One International's operation at Modder East in Johannesburg's gold rich East Rand region. The size distribution and mineral association of gold and uranium are critical during metallurgical processing of the ore. Thin sections of the samples were analyzed to determine the size distribution and mineral association of gold and uranium within the reef. Gold is primarily associated with quartz, pyrite, muscovite and chlorite, and lower levels of association are also observed in the case of pyrophyllite, uraninite and kerogen. The association of the gold is very similar to that found within the Witwatersrand reefs as the same strong association between quartz and pyrite is also observed. The size distribution for gold found in these samples varies with position above, within and below the BSPL reef, with smaller grains of gold encountered above the reef (2-90  $\mu\text{m}$  in size). Gold within buckshot pyrite reef is much larger, varying in size from 2 micron to 200 micron. Gold from below the reef can vary in size up to 180 micron. This pattern is repeated for uraninite, with similar size distribution curves observed although the uraninite is much finer than the gold. The uraninite is markedly associated with kerogen globules but also does occur in association with quartz, muscovite, pyrophyllite, sphalerite and chalcopyrite on a much lesser scale. The characteristics of the uranium are similar to those found in the carbon seams of the Witwatersrand reefs.

